

Production of a fusogenic oncolytic virus: In-depth process development and process intensification

Dissertation

zur Erlangung des akademischen Grades

**Doktoringenieurin / Doktoringenieur
(Dr.-Ing.)**

von M.Sc. Sven Göbel

geb. am 09.11.1994 in Stuttgart

genehmigt durch die Fakultät für Verfahrens- und Systemtechnik der Otto-
von-Guericke-Universität Magdeburg

Gutachter:

Prof. Dr.-Ing. Udo Reichl

Dr. Ingo Jordan

Assoc. Prof. Dr. Alexander (Sandy) Douglas

Promotionskolloquium am 07.11.2024

“We are prone to overestimate how much we understand about the world and to underestimate the role of chance in events.”

Daniel Kahneman

Göbel, Sven:

Production of a fusogenic oncolytic virus:

In-depth process development and process intensification

PhD thesis, Max Planck Institute Magdeburg, 2024.

Abstract

Oncolytic virotherapy is an elegant approach to cancer therapy, leveraging viruses to selectively infect and destroy cancer cells, sparing healthy tissues. While the oncolytic virus (OV) directly targets the tumor, effectiveness is further enhanced by simultaneous stimulation of the body's immune system with an anti-tumor response. This strategy offers hope for treating otherwise untreatable types of cancer. However, often highly concentrated dose inputs in the range of 10^8 - 10^{11} infectious virions/injection are required to achieve a therapeutic effect and delivery to tumor sites. Therefore, development of robust OV production processes are crucial to generate highly concentrated virus inoculum. Various OV platforms currently under investigation rely on anchorage-dependent cell types due to their historical use in commercial viral vaccine production. However, the use of adherent cell cultures has multiple drawbacks, including low virus yields, increased batch variation, and limited scalability, especially for fusogenic OVs that cause syncytia formation and bystander cell death. Alternatively, the use of suspension cell lines may be more advantageous, but the low availability of GMP-compliant continuous suspension cells further complicates the development of commercially viable products for virotherapy. To overcome these challenges, the project aimed to (i) identify suitable substrates that allowed for rapid growth and high virus titers in a tightly controlled production system, and (ii) establish transferable batch and perfusion processes for large-scale production of a novel fusogenic OV.

A broad range of suspension cell lines were screened to develop a highly efficient and scalable batch production process for a novel hyper-fusogenic hybrid of vesicular stomatitis virus and Newcastle disease virus (rVSV-NDV). Small-scale cultivations (15–50 mL) were used to optimize critical upstream processing parameters (multiplicity of infection (MOI), temperature, pH, adaptation, aggregation) for four promising cell substrates (AGE1.CR.pIX, BHK-21, HEK293, CCX.E10). Not only the cell line, but also the culture medium played a pivotal role for the peak virus titer and the stability of virus particles in the supernatant. The identification of an optimal MOI for each cell line was

critical to achieve high infectious virus titers, while increased cell-to-cell contact had no detectable effect on rVSV-NDV yield. Virus adaptations resulted in similar virus yields, however onset of virus release was drastically reduced. Best conditions were transferred to 1 L and 3 L stirred tank bioreactors (STR) or 10 L orbitally shaken bioreactors, resulting in a 100-fold increase in virus yield (up to 4.2×10^8 TCID₅₀/mL), when compared to production in adherent cell cultures without loss of oncolytic potency.

Next, process intensification methods were evaluated by increasing cell concentrations in perfusion mode. Initial optimization studies focusing on MOI, viable cell concentration (VCC) at time of infection, media, and usage of supplements were carried out in shake flasks using a high cell density (HCD) semi-perfusion strategy. Improved virus titers (43-56-fold), cell-specific virus yields (CSVY) (5-28-fold), and volumetric virus productivities (VVP) (6-18-fold) were observed after infection at $>20 \times 10^6$ cells/mL. Subsequently, continuous perfusion processes were implemented using an acoustic settler or membranes as cell retention devices (CRDs) coupled to bioreactors. Depending on the cell substrate, VCCs up to 15.0 - 45.9×10^6 cells/mL and rVSV-NDV titers of up to 7.1×10^9 TCID₅₀/mL ($>1,000$ -fold increase compared to production in adherent cultures) were achieved without loss of oncolytic potency. CSVYs obtained for these HCD cultivations were up to 2-fold higher compared to batch cultivations, resulting in space-time-yield (STY) increases of $>460\%$ and comparable VVPs. Modification of a traditional membrane-based ATF set-up by utilization of a hollow-fiber membrane with a large internal lumen (0.75 mm) combined with a high flow rate (1.5 L/min) hampered syncytia formation and prevented complete blockage. However, rVSV-NDV was retained by the membrane ($>97\%$ at 18 h post infection). Transition to tangential flow depth filtration (TFDF) perfusion allowed continuous virus harvesting and clarification with a high reduction of solution turbidity ($>95\%$), despite the fusogenic OV causing large multi-nucleated syncytia. Implementation of this novel, closed, single-use perfusion system substantially simplified process operations and constitutes a cornerstone for integrated, sustainable and economical OV production up to 2000 L. Taken together, this work paves the way for the establishment of an efficient large-scale manufacturing process, in either batch or perfusion mode that provides sufficient amounts of highly potent virus material to allow for phase I clinical trials in cancer patients.

Kurzfassung

Die Entwicklung effizienter Produktionsverfahren für onkolytische Viren (OV) spielt eine entscheidende Rolle für die klinische Anwendung und den Erfolg der Virotherapie. Obwohl derzeit viele verschiedene OV-Plattformen untersucht werden, basiert die Herstellung solcher Viren hauptsächlich auf adhärennten Zellkulturen, die viele Herausforderungen mit sich bringen. Bevor eine Produktion im Industriemaßstab in Betracht gezogen bzw. optimiert werden kann, muss zuerst ein Zellsubstrat identifiziert werden, welches ein schnelles Zellwachstum und eine hohe Virusausbeute in einem stringent kontrollierten Produktionssystem ermöglicht. Allerdings sind GMP-konforme kontinuierliche Suspensionszelllinien nur begrenzt verfügbar, was die Entwicklung kommerziell nutzbarer Produkte weiter erschwert. In dieser Arbeit wurden sämtliche Hürden auf dem Weg zu einem optimierten Batch- und Perfusionsprozesse chronologisch betrachtet, um schließlich die effiziente Produktion eines fusogenen OV in verschiedenen Kultivierungssysteme zu etablieren.

Im ersten Teil dieses Projekts wurde ein breites Spektrum von Suspensionszelllinien verschiedener Wirtsspezies untersucht, um ein effizientes und skalierbares Batch-Produktionsverfahren für ein neuartiges hyperfusogenes Hybrid-Virus aus vesikulären Stomatitis und dem Newcastle Disease Virus (rVSV-NDV) zu entwickeln. Kultivierungen im kleinen Maßstab (15-50 ml) wurden zur Optimierung kritischer Upstream-Prozessparameter (Multiplizität der Infektion (MOI), Temperatur, pH-Wert, Virus-Adaptation, Zellaggregation) für vier vielversprechende Zellsubstrate (AGE1.CR.pIX, BHK-21, HEK293, CCX.E10) verwendet. Nicht nur die Zelllinie, sondern auch das Kulturmedium spielte eine entscheidende Rolle für hohe Virustiter und die Stabilität der Viruspartikel im Überstand. Die Identifizierung einer optimalen MOI für jede Zelllinie war entscheidend, um hohe infektiöse Virustiter zu erreichen, während ein erhöhter Zell-zu-Zell-Kontakt keine nachweisbaren Auswirkungen auf die rVSV-NDV-Ausbeute hatte. Virusadaptierungen führten zu ähnlichen Virusausbeuten, jedoch wurde der Beginn der Virusfreisetzung beschleunigt. Die besten Bedingungen wurden in 1 L und 3 L Rührbioreaktoren oder 10 L geschüttelte Bioreaktoren übertragen. Damit wurde eine 100-

fache Steigerung des Virustiters (bis zu $4,2 \times 10^8$ TCID₅₀/ml) im Vergleich zur Produktion in adhärennten Zellkulturen ohne Beeinträchtigung der onkolytischer Potenz erreicht.

Als nächstes wurden Methoden zur Prozessintensivierung durch Erhöhung der Zellkonzentrationen im Perfusionsmodus evaluiert. Erste Optimierungsstudien, die sich auf die MOI, die Lebendzellkonzentration (VCC) zum Zeitpunkt der Infektion, Medien und die Verwendung von Zusätzen konzentrierten, wurden in Schüttelkolben unter Verwendung einer Semi-Perfusionsstrategie mit hoher Zelldichte (HCD) durchgeführt. Nach der Infektion mit $>20 \times 10^6$ Zellen/mL wurden verbesserte Virustiter (43- bis 56-fach), zellspezifische Virusausbeuten (CSVY) (5-28-fach) und volumetrische Virusproduktivitäten (VVP) (6-18-fach) beobachtet. Anschließend wurden kontinuierliche Perfusionsprozesse unter Verwendung eines akustischen Filters oder von Membranen als Zellrückhaltevorrichtungen (CRDs), die an Bioreaktoren gekoppelt sind, implementiert. Je nach Zellsubstrat wurden Konzentrationen von bis zu $15,0-45,9 \times 10^6$ Zellen/ml und rVSV-NDV-Ausbeuten von bis zu $7,1 \times 10^9$ TCID₅₀/ml (>1.000 -fache Steigerung im Vergleich zu adhärennten Zellkulturen) ohne Verlust der onkolytischen Potenz erreicht. Die zellspezifischen Virusausbeuten, die bei diesen HCD-Kulturen erzielt wurden, waren im Vergleich zu früheren Batch-Kulturen bis zu 2-mal höher, was zu Raum-Zeit-Ausbeutesteigerungen von $>460\%$ und vergleichbaren volumetrischen Virusproduktivitäten führte. Die Modifizierung eines herkömmlichen membranbasierten ATF-Aufbaus durch Verwendung einer Hohlfasermembran-Membran mit einem großen internem Durchmesser (0,75 mm) in Kombination mit einer hohen Durchflussrate (1,5 L/min) beeinträchtigte die Synzytienbildung und verhinderte eine vollständige Blockierung der Membran. Allerdings wurde rVSV-NDV von der Membran zurückgehalten ($>97\%$ bei 18 h nach Infektion). Der Übergang zur TFDF-Perfusion ermöglichte eine kontinuierliche Virusernte und Klärung mit einer starken Verringerung der Trübung der Lösung ($>95\%$), obwohl das fusogene rVSV-NDV die Ausbildung großer Synzytien verursachte. Die Implementierung dieses neuartigen, geschlossenen Einweg-Perfusionsystems vereinfacht die Prozessabläufe erheblich und bildet einen Grundstein für künftige Entwicklungen in Richtung integrierter, nachhaltiger und wirtschaftlicher Prozesse bis zum 2000-Liter-Maßstab.

Insgesamt ebnet unser Projekt den Weg für die Etablierung eines effizienten großtechnischen Herstellungsprozesses, entweder im Batch- oder im Perfusionsmodus, der ausreichende Mengen an hochwirksamem Virusmaterial für eine klinische Phase 1 Studie an Krebspatienten liefert.

Declaration

DeepL and ChatGPT were used to improve readability and language of this PhD thesis. After using this tool, the author reviewed and edited the content as needed and takes full responsibility for the content of the publication.

Magdeburg, 17.06.2024

Sven Göbel

Contents

Danksagung	III
Abstract	V
Kurzfassung	VII
Declaration	X
Contents	IX
List of Abbreviations	XIII
List of Symbols	XIV
List of Figures	XV
List of Tables	XVI
Abstract	3
Kurzfassung	6
Declaration	9
Contents	10
List of Abbreviations	12
List of Symbols	13
List of Figures	14
List of Tables	15
1. Introduction	1
2. Theoretical background	4
2.1. Virotherapy	5
2.1.1. Mechanism of action	8
2.1.2. Fusogenic oncolytic viruses	10
2.1.3. Design of rVSV-NDV	11
2.2. Cell culture-based virus production	17

2.3. Production of OVs	18
2.4. Process intensification strategies	21
2.4.1. From batch cultures to intensified processes.....	22
2.4.2. Cell retention devices	26
2.4.3. Application of bio-capacitance	35
3. Manuscripts.....	39
3.4. First Manuscript.....	40
3.5. Second Manuscript	41
3.6. Third Manuscript	42
3.7. Fourth Manuscript	43
4. Conclusions.....	44
5. Outlook.....	50
Bibliography	53
List of publications.....	61
Declaration of Honor	66

List of Abbreviations

AS	acoustic settlers
ATF	alternating tangential flow filtration
CRD	cell retention device
DF	depth filtration
DIP	defective interfering particles
F	fusion protein
G	glycoprotein
HCD	high cell density
HF	hollow-fiber
HN	hemagglutinin-neuraminidase protein
IFN	interferon
L	large protein
M	matrix protein
mAb	monoclonal antibody
MOI	multiplicity of infection
MVA	modified vaccinia Ankara virus
NDV	Newcastle disease virus
NP	nucleocapsid protein
OV	oncolytic virus
P	phosphoprotein
pi	post infection
RV	reactor-volume
rVSV-NDV	recombinant Vesicular stomatitis virus-Newcastle disease virus
STR	stirred tank bioreactor
TFDF	tangential flow depth filtration
TFF	tangential flow filtration
VBB	virus-based biopharmaceuticals
VSV	Vesicular stomatitis virus

List of Symbols

CSPR	cell-specific perfusion rate	pL/cell/d
CSVY	cell-specific virus yields	virions/cell
CVSPR	cell-volume-specific perfusion rate	pL/ μm^3 /d
STY	space-time-yield	virions/RV/d
VCC	viable cell concentration	cells/mL
VCV	viable cell volume	%
VVP	volumetric virus productivity	virions/L/d

List of Figures

Figure 1.: Clinical landscape of oncolytic viruses	7
Figure 2.: Mechanism of action of OVs in tumor cells	9
Figure 3.: Schematic representation of Newcastle disease virus	12
Figure 4.: Schematic representation of vesicular stomatitis virus	14
Figure 5.: Construction of the hybrid rVSV-NDV virus	16
Figure 6.: Overview of critical process parameters	22
Figure 7.: Schematic representation of virus production processes	24
Figure 8.: Cell retention devices and their connections to a bioreactor vessel	26
Figure 9.: Schematic illustration of an ATF setup with a hollow-fiber unit	29
Figure 10.: Schematic illustration of an acoustic settler setup	31
Figure 11.: Scheme of the TFDF setup for perfusion cultivations	35
Figure 12.: Overview of the publications	40

List of Tables

Table 1.: Overview of the production of several clinical grade OVs

19

1. Introduction

Cancer as a disease has the ability to invade nearly any organ or tissue within the body, leading to immense suffering for both the individuals afflicted and society as a whole. Despite decades of intensive research, cancer persists as a major global health threat with severe epidemiological and financial burdens. Cancer immunotherapy is quickly changing the landscape of medical oncology by harnessing the patient's immune system as the basis for the therapy. Oncolytic viruses (OVs) have recently earned their place as virotherapy, a subset of cancer immunotherapy. OVs generally comprise replication-competent viruses that are either inherently tumor-specific or have been genetically engineered to replicate preferentially in tumor cells [1, 2]. OVs can be further genetically modified to insert transgenes into the viral genome, promoting antitumor immunity (OV vector). With the first OV vector gaining U.S. and EU licensing in 2015 [3], and a myriad of other OV platforms in development stages, regulatory authorities have started to establish criteria for the evaluation of these novel therapeutic interventions. This includes the development robust and efficient manufacturing processes that conform to regulatory requirements for drug development. In particular, a subset of OV vector platforms that induce syncytia formation in infected cells pose additional challenges to the manufacturing process [4]. Design and identification of a potent OV is the first milestone for treatment of patients. To achieve cost-effective production for clinical applications at relevant dosages (10^8 – 10^{11} infectious particles per dose), manufacture of OVs at high titers with sufficient yields is an obligation that is often overlooked during early research and development stages [5]. Establishing high-yield manufacturing processes while taking into account process complexity, culture medium, stability of infectious virions, production times, and small footprints can be a high hurdle. Though established, OV production in static anchorage-dependent cell cultures poses major challenges that complicate scale-up: Limited monitoring of pH, dissolved oxygen (DO), and restricted harvesting options. This can be circumvented, when using suspension cells as they allow for various scale-up possibilities from laboratory to industrial scale [6]. However, not all continuous cell lines are equally susceptible and suitable for the production of a target virus. Thus, comprehensive screenings with a wide range of hosts derived from

different species and/or tissues have to be performed to identify an ideal candidate fulfilling the following criteria: i) susceptibility to the respective OV, ii) robust growth in chemically-defined medium with doubling times below 30 h (preferably in suspension), iii) high infectious virus titers, and iv) regulatory requirements [7, 8]. Additionally, the choice of medium plays a critical role in facilitating the development of clinical-grade manufacturing processes. Dependence on serum components, such as fetal calf serum, raises production and purification costs, result in batch-to-batch variation and increase the risk of unwanted adventitious contaminations [9].

Shifting from static cultures to suspension cell lines can already enable the establishment of a high volume batch processes with high yields. Further optimization can be achieved by careful balancing of technical process parameters and infection conditions.

For process intensification, high cell density (HCD) cultivations in perfusion mode using a cell retention device (CRD) are a viable option for various cell culture-based biopharmaceutical applications. For influenza A virus and modified vaccinia Ankara virus (MVA), significantly higher titers, cell-specific virus yields (CSVYs), and volumetric virus productivities (VVPs) were achieved using perfusion mode compared to batch cultivations or processes using parental adherent cell lines [10-16]. Similar results may be reached, when applying intensified perfusion strategies for the manufacturing of OVs. Various CRDs are available that bring their distinct benefits and challenges. Choosing an efficient, scalable, and GMP-compliant CRD that ideally supports a continuous harvest is thus crucial and has to be evaluated empirically with respect to cell, product, and process requirements [17].

This work summarizes the comprehensive endeavors made to establish an efficient process for the suspension cell culture-based production of a fusogenic hybrid of vesicular stomatitis virus and Newcastle disease virus (rVSV-NDV) and to provide guidance for establishment of other OV platforms. Initially, suitable cell substrates were identified that allowed for rapid growth and high virus titers in a tightly controlled production system (Manuscript 1). Next, an optimized and transferable batch process was developed using a novel GMP-compliant cell line (CCX.E10), considering ease of scale-up and compliance with GMP requirements (Manuscript 3). As a follow-up to the first manuscript, process intensification methods were established for all three

identified cell substrates. Using shake flasks as a small-scale screening model in semi-perfusion mode, process conditions in HCD were optimized. Identified culture conditions were subsequently transferred to full perfusion cultivations in STRs employing an acoustic settler for cell retention and an automated process control strategy (Manuscript 2). Finally, an intensified perfusion process using a tangential flow depth filtration membrane with prospects for large-scale production was set-up (Manuscript 4).

2. Theoretical background

This chapter is partially based on the following publication [18]:






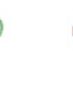




Göbel S*, Pelz L, Reichl U, & Genzel Y (2022). Chapter 5b Upstream Processing for Viral Vaccines—Process Intensification. In L. C. Amine Kamen (Ed.), *Bioprocessing of Viral Vaccines* (Vol. 1, pp. 79–137). Taylor & Francis Group.

2.1. Virotherapy

Historically, the surgical excision of a tumor was synonymous with cancer therapy. Scientific discoveries in the 19th and 20th century led to the development of new treatments, which are classified today as radiotherapy (1895), chemotherapy (1942), and immunotherapy (1957) [1]. Until today, no treatment or treatment combination is applicable to every tumor type or tumor stage, resulting in a growing skepticism about the future of cancer therapy. Nonetheless, clinical reports describing tumor regressions coinciding with natural infections accumulated in the mid-1900s [1, 19, 20]. This led to the accidental discovery and exploration of viruses for therapeutic treatment, e.g. virotherapy as a subset of immunotherapy. In the 1950s, researchers posed the question whether wild-type viruses could be specifically used to kill tumor cells. As a result, first clinical research was conducted using a variety of viruses including hepatitis B virus [21], West Nile virus [22], adenovirus adenoidal-pharyngeal-conjunctival virus [23], measles virus [2], and mumps virus [24]. While clinical efficacy and resulting tumor regression was observed for many viruses, effects were often transient and associated with severe side effects (severe encephalitis, necrosis) or death [1]. The administered therapeutic material was non-attenuated viruses from infectious body fluids or tissue samples from patients with ongoing infections [1, 19]. Together with their intrinsic viral pathogenicity and regulatory barriers of using non-attenuated pathogens as well as major breakthroughs in the development of chemotherapeutics, scientific interest in virotherapy in the 1970s and 1980s decelerated. Approaching the year 2000, progress in the field of genetic engineering allowed the adaptation or engineering of wild-type viruses to eliminate their pathogenicity [25]. These advancements led the clinical translation of many new and diverse viruses for virotherapy. Many reviews cover the landscape of current clinical trials of virotherapy [2, 5, 20, 26, 27]. To date, a total of four OV products have been approved by regulatory agencies for clinical treatment. From RigVir (picornavirus) for treatment of melanoma in 2004 in Latvia [28], H101 (adenovirus) for nasopharyngeal carcinoma in 2005 in China [29], Talimogene Laherparepvec (T-Vec, herpes simplex virus) for advanced inoperable melanoma in 2015 in the US and the European Union [30], and Delytact (herpes simplex virus) for malignant glioma in Japan in 2021 [31]. As of 2024, over 180 clinical trials at various stages of development are investigating OVs (Figure 1 b, ClinicalTrials.gov 2024).

Both DNA and RNA viruses have been investigated as potential candidates for OV development, with DNA viruses being used to a greater extent (Figure 1c) [27]. The main driver behind their use is the larger genome and the associated higher capacity to encode transgenes, which can further increase therapeutic activity without impairing viral replication. Although the small genome size of RNA viruses limits their capacity to encode large transgenes, they can cross the blood-brain barrier and target tumor cells in the central nervous system [32]. While there is no standard method for selecting the type of OV, some viruses exhibit a natural tropism and predilection for specific tumor cells, whereas others require genetic modification [27]. The natural diversity of virus families, who have evolved specificities for different cell types results in a great variety of virus types being used for therapeutic development. Currently, viruses from nine different families are investigated in clinical trials [20]. Figure 1a shows the 10 most commonly used virus types from the *Adenoviridae* (adenovirus), *Picornaviridae* (coxsackievirus, seneca valley virus, poliovirus), *Herpesviridae* (herpesvirus), *Paramyxoviridae* (measles virus, Newcastle disease virus), *Reoviridae* (reovirus), *Poxviridae* (vaccinia virus), and *Rhabdoviridae* (vesicular stomatitis virus) family. Greater specificity to the respective tumor cells and/or efficacy can be achieved by genetic engineering. As a result, today's virotherapy is a well-tolerated clinical treatment with reduced side effects (fever, flu symptoms, rare toxicities) [20].

a

	Herpesvirus	Adenovirus	Vaccinia virus	Reovirus	Coxsackievirus	Seneca Valley virus	Poliovirus	Measles virus	Newcastle disease virus	Vesicular stomatitis virus
Model										
Genome	dsDNA 150 kb	dsDNA 36 kb	dsDNA 190 kb	dsRNA 123 kb	ss(+)RNA 28 kb	ss(+)RNA 7 kb	ss(-)RNA 7.5 kb	ss(-)RNA 16 kb	ss(-)RNA 15 kb	ss(-)RNA 11 kb
Capsid symmetry	Icosahedral	Icosahedral	Complex	Icosahedral	Icosahedral	Icosahedral	Icosahedral	Icosahedral	Helical	Helical
Virion	Enveloped	Naked	Complex coats	Naked	Naked	Naked	Naked	Enveloped	Enveloped	Enveloped
Replication site	Nucleus and cytoplasm	Nucleus and cytoplasm	Cytoplasm	Cytoplasm	Cytoplasm	Cytoplasm	Cytoplasm	Cytoplasm	Cytoplasm	Cytoplasm
Methods of entry	HVEM, nectin-1, nectin 2	CAR, CD46	Receptor-mediated endocytosis	JAM-A	CAR/ICAM1/DAF	Endocytosis	CD155	SLAM, CD46	Sialic acid	LDLR
Blood-brain barrier penetration	-	-	-	+	-	+	+	-	+	-
Advantages	Large genome to insert large fragments and multiple transgenes; drug to shut-off	Feasibility of manufacturing high viral titers; ease of genome manipulation; inherently potent lytic activity	Fast, efficient spreading virus; high-speed life cycle; up to 40kd large gene fragment insertion; enough knowledge due to smallpox	Good adaptability for intravenous injection; displaying no dose-limiting toxicity	Good adaptability for intravenous injection	Nonpathogenic in human	Clinical trial experience	Clinical trial experience	Nonpathogenic in human	High-speed life cycle; nonpathogenic in human
Disadvantages	Pathogenicity; ubiquitous nAbs	Extensive tissue tropism	Pathogenicity	Rarely gene-editing	Pathogenicity; ubiquitous nAbs	Clinical trials were not entirely satisfactory	Highly pathogenic in neurons of the human	Pathogenicity	Rarely gene-editing	Clinical trials were not entirely satisfactory; rarely gene-editing

dsDNA double-stranded DNA, dsRNA double-stranded RNA, ssRNA single-stranded RNA, HVEM herpesvirus entry mediator, CAR coxsackie adenovirus receptor, JAM-A junctional adhesion molecule A, ICAM1 Inter cellular adhesion molecule 1, DAF decay-accelerating factor, SLAM signaling lymphocytic activation molecule, LDLR low-density lipoprotein receptor, nAbs neutralizing antibodies

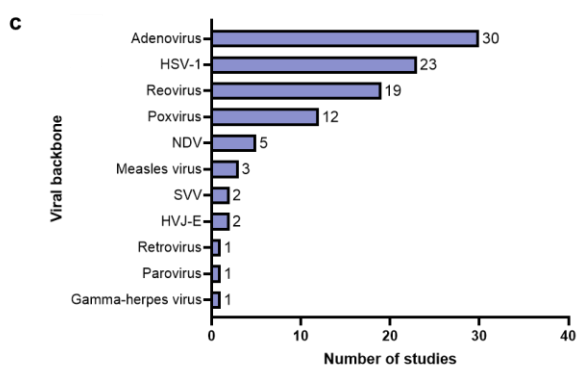
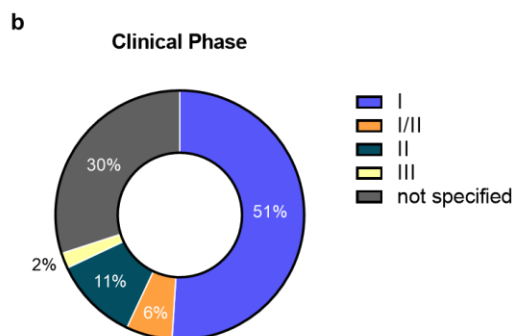


Figure 1 Clinical landscape of oncolytic viruses. a Features of oncolytic viruses used in clinical trials. **b** Distribution of oncolytic viruses by clinical stage from 2020. **b** Virus types used in 2020 in clinical trials. Figure adapted and taken from [25] (a; Free use under CCABY 4.0) and [27] (b+c; license acquired).

Although many clinical trial results support a general efficacy of OV, the very high efficacy expectation set by preclinical models of current OV is often not confirmed [2]. Translation of pre-clinical efficacy to patient populations is a multifactorial challenge with many aspects including route and schedule of administration, type and stage of cancer, optimal combination therapy, resistance against antibody neutralization, improving tumor specificity remaining to be elucidated [20]. Moreover, optimal dosing regimens are a pivotal factor, yet, often limited by low yields obtained from outdated

production processes, as discussed in Chapter (2.3). By careful combination of genetic engineering strategies, combination therapies and technological advances in virus production, next-generation OV's can be dosed at higher concentrations and designed for higher efficiency against diseases with unmet medical needs.

2.1.1. Mechanism of action

In contrast to conventional treatments using brute-force approaches such as chemotherapy or radiotherapy, OV's offer an alternative approach as they can precisely infect and destroy tumor cells. This tumor selectivity is driven by several factors, ultimately resulting in a preferential replication of the OV within the tumor cells (Figure 2). Expression of specific cellular receptors on tumors mediates OV-specific recognition and consequently improves OV infection [32]. Genetic modification of surface proteins to detect tumor-specific cellular receptors can further improve infection efficiency, as shown for OV's directly targeted towards overexpressed epidermal growth factor receptors [32]. Moreover, tumor cells have several intrinsic properties, which enhance the replication of OV's. As they sustain chronic proliferation by deregulation of growth-promoting signals and their metabolism is forced into constant glycolysis, it is advantageous for the OV's to use the cell machinery of the tumor cell for their replication [32, 33]. Dysfunctional immune responses caused by mutations within the tumor cells lead to antiviral interferon type I (IFN) signaling deficiencies, favoring viral replication. On the other hand, normal healthy cells have a functioning interferon system that effectively limits viral replication (Figure 2) [32, 34]. Following tumor cell lysis, OV's spread to neighboring cells, self-amplifying oncolysis until susceptible tumor cells deplete or immune responses attenuate virus replication [35].

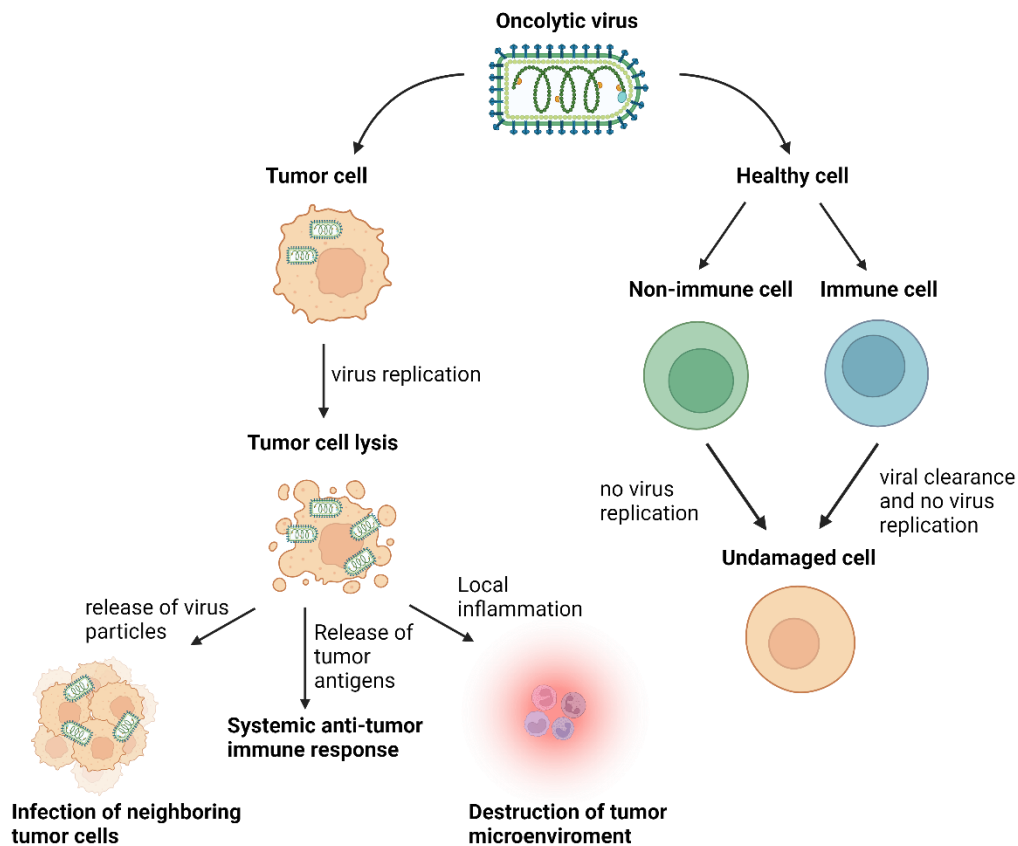


Figure 2 Mechanism of action of OVs in tumor cells. While OVs possess the ability to infect both normal and tumor cells, the intrinsic malfunctions in cancer cells confer a selective advantage for viral replication. In healthy cells (immune and non-immune cell types), OVs are not replicated due to the presence of antiviral type I interferon (IFN) signaling and other regulatory mechanisms. On the other hand, after infection of tumor cells, OVs can replicate, causing tumor cell lysis and the release of new viruses that can subsequently infect adjacent tumor cells. Secondary immune and antiviral responses are enhanced by release of various signaling molecules. Figure adapted from [32]. Created with BioRender.com.

Breaking the immunological tolerance of tumor cells is the second crucial mechanism of action of OVs. Following oncolytic cell death, tumor cells release tumor-associated antigens that promote an adaptive immune response, mediating tumor regression at distant sites not directly exposed to the virus [32, 36]. In addition, a variety of signaling molecules including cytokines (such as type I interferons, tumor necrosis factor- α , and interleukin-12), cellular damage-associated molecular patterns, and viral pathogen-

associated molecular patterns are released (Figure 2). These molecules promote the maturation of antigen-presenting cells and can activate antigen- and/or virus-specific CD8⁺ T cell responses. Once activated, CD8⁺ T cells become cytotoxic effector cells and migrate to tumor sites, where they exert anti-tumor immunity through antigen recognition and elimination [32, 36]. Lastly, upon detection of OV infection, dendritic cells undergo activation and transition to a mature state [32]. Through the secretion of cytokines and chemokines, these activated DCs stimulate innate immune responses by NK cells and macrophages. Additionally, activated DCs play a crucial role in initiating adaptive immunity by priming antigen-specific T cells [32, 37]. Here, viral antigens next to costimulatory molecules and inflammatory cytokines are presented on MHC molecules, effectively overcoming tumor-associated immunosuppression [32, 37].

2.1.2. Fusogenic oncolytic viruses

Fusion of the viral and cell membrane is a critical first step in the life cycle of some enveloped viruses to facilitate entry and replication. This is mainly supported by fusogenic membrane glycoproteins on the viral surface, also referred to as fusion proteins. These fusion proteins interact with receptors and co-receptors on target cell membranes, instigating specific fusion processes dictated by their protein structure [38, 39]. While the primary role of fusion proteins is to facilitate this process, their expression on the cell surface of infected cells can also cause fusions between non-infected and infected cells [38, 40]. Over time, regions of non-viable, multinucleated giant cells (up to 100 nuclei), known as syncytia, are formed [39, 41]. OVs displaying these fusogenic phenotypes have distinct advantages over their non-fusogenic counterparts, as an increased intratumoral spread can be achieved via this “bystander effect”. As a result, only few mature virions are released into the surrounding healthy tissue or into systemic circulation. Additionally, the fusion of infected cells and neighboring tumor cells enables individual virions to eradicate large numbers of tumor cells as they merge into the expanding syncytium [39, 42]. Rather than replicating to high virus titers, this mechanism permits multiple rounds of replication without exposure to neutralizing antibodies, thus promoting the development of a safe therapeutic agent [39]. Compared to non-fusogenic OV's, tumor cell death via syncytia

formation stimulates a particular immunogenic response [39, 41, 43-45]. While the exact mechanism of cell death associated with syncytia formation is not yet elucidated, several observations suggest a heterogeneous process [39] involving necrosis [41], apoptosis [46], and autophagy [46-48]. This results in the release of a broad range of tumor antigens, which facilitates their cross-presentation by dendritic cells to cytotoxic T cells [39, 48]. Combined with the enhanced tumor immunogenicity, fusogenic OV's could confer long lasting immunity [39, 47].

2.1.3. Design of rVSV-NDV

2.1.3.1. Newcastle disease virus

Newcastle disease virus (NDV) is an enveloped single-stranded, negative-sense RNA virus within the *Avulavirus* genus of the *Paramyxoviridae* family [49]. It is a pleomorphic membrane-enveloped virus with a spherical shape ranging 150-400 nm in diameter [50]. Its genome encodes six proteins (Figure 3): nucleocapsid protein (NP), large protein (L), phosphoprotein (P), matrix protein (M), hemagglutinin-neuraminidase protein (HN), and fusion protein (F). NP, L, and P constitute the protein subunits of the nucleocapsid and are associated with the RNA genome. Here, NP is responsible for RNA-binding, while P and L form the viral polymerase, catalyzing the transcription and replication of the virus within the host cell cytoplasm [50]. The M protein is involved in viral assembly and links both the viral membrane and the nucleocapsid. Attachment to sialic acid receptors outside of the host cell membrane is mediated by the HN protein. Moreover, it is responsible for cleaving of sialic acid residues from the surface of virions and infected cells [50]. The F protein promotes the fusion of the viral envelope with the host cell plasma to permit the penetration of NDV into host cells. Following viral entry, both, transcription and replication, occur in the cytoplasm. Detailed descriptions of the viral replication cycle of NDV are published in the literature and will not be discussed further in this thesis [50-53].

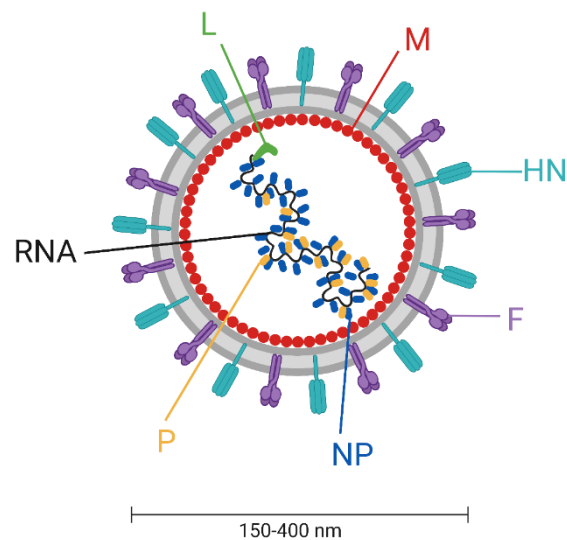


Figure 3 Schematic representation of Newcastle disease virus. The nucleocapsid protein (NP), large protein (L), phosphoprotein (P), matrix protein (M), hemagglutinin-neuraminidase protein (HN), and fusion protein (F) are shown. Created with BioRender.com.

NDV is highly contagious and can lead to severe respiratory, enteric, or neurological symptoms in infected poultry populations. Here, the virulence is further classified into three categories (velogenic, mesogenic, or lentogenic) and influenced by factors such as the cleavage site of the F protein and the structure of the HN protein [39]. NDV's replication cycle is very rapid, producing maximal yields within 12 h post infection (hpi) [51]. Infections in humans remain asymptomatic, as NDV is highly sensitive to type I IFNs, which are the human's first line of antiviral defence, well before the onset of the adaptive immune system [36, 54, 55]. However, as for other OVVs, this IFN sensitivity confers tumor cell specificity as tumor cells with dysfunctional immune responses facilitate the replication of the virus. NDV-mediated apoptosis of tumor cells initiates innate immune system activation characterized by elevated cytokine production and enhanced antigen presentation. Consequently, this converts the immunosuppressive tumor microenvironment into a pro-inflammatory state, resulting in robust anti-tumor immune responses [36]. Altomonte et al. achieved an exogenous protease-independent fusion activity of NDV by introducing a multibasic cleavage and activation site (rNDV/F3aa) into the fusion protein [56]. This resulted in enhanced tumor cell killing by formation of large intratumoral syncytia. Subsequent modification of this vector by introducing a single amino acid substitution (leucine to alanine at position 298, L289A) in the fusion protein, further increased fusogenicity [39, 56]. Although several

preclinical studies demonstrated a high efficacy of NDV against human and rodent tumor cells/models *in vitro* and *in vivo*, there are only a limited number of clinical trials in progress [36, 39]. The main reason for this was the classification of velogenic and mesogenic NDV strains as select agents by the US FDA in 2008 [39].

2.1.3.2. Vesicular stomatitis virus

Vesicular stomatitis virus (VSV) is an enveloped single-stranded, negative-sense RNA virus within the *Rhabdoviridae* family [57]. Its particles are characterized by a bullet-shaped morphology with a length of 180 nm and a diameter of 70 nm [58]. The non-segmented genome encodes five structural proteins: viral nucleocapsid protein (N), matrix protein (M), large protein (L), glycoprotein (G), and phosphoprotein (P). The N protein coats the viral genomic RNA and presents the bases to the L protein to initiate genome synthesis. The L protein and its cofactor (P protein) are part of the nucleocapsid and catalyze the transcription and replication of the mRNA in the cytoplasm [58]. The M protein serves as the primary structural element of VSV particles and plays a crucial role during the budding process. Here, it binds the viral nucleocapsid to the cytoplasmic surface of the host cell membrane and induces budding of virions [59]. The G protein mediates the binding to host cell receptors and promotes fusion of viral and cellular membranes during endocytosis [58]. As for NDV, detailed descriptions of the viral replication cycle of VSV are published in the literature and will not be discussed further in this thesis [58, 60, 61].

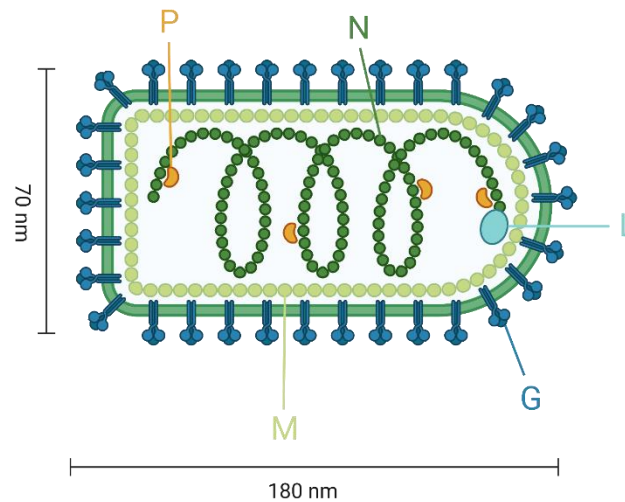


Figure 4 Schematic representation of vesicular stomatitis virus. The nucleocapsid protein (N), large protein (L), phosphoprotein (P), matrix protein (M), glycoprotein (G) are shown. Created with BioRender.com.

VSV primarily affects livestock as a veterinary pathogen but is also recognized as a zoonotic disease, capable of causing flu-like symptoms in humans. There is one reported case of encephalitis in humans following VSV infection, however, this seems to be a rare instance [57]. Extensive research into VSV's fundamental biology and its interactions with host immune responses has led to the development of various VSV vectors for vaccination [62], gene therapy, and OV therapy [63, 64]. Similar to NDV, VSV is characterized by a high sensitivity to IFN-mediated responses, facilitating tumor selectivity. Moreover, its high cytopathogenicity, fast replication cycle, negligible preexisting immunity in humans, and non-integration into the host genome, favor its application as an OV [63]. Lastly, VSV can be easily genetically manipulated, allowing for strong and adjustable levels of foreign gene expression to enhance oncolysis and specificity. While VSV is not considered as a significant human pathogen, it is associated with severe neurotoxicity and hepatotoxicity, modulated by its surface glycoprotein (VSV-G). These side effects after intranasal or intracranial application in mice, nonhuman primates, and humans limits its usability in clinical trials [63, 65]. Besides oncolytic applications, VSV is commonly used as a vaccine vector. In 2019, the first rVSV-based vector vaccine against Ebola (ERVEBO[®]) received approval in the US and EU [66, 67]. Several other rVSV-vectors have reported promising efficacy data in pre-clinical and clinical trials, including vectors expressing antigens from SARS-

CoV-2 [68], HIV [69], Zika virus [70], Marburg virus [71], Lassa virus [72], dengue fever virus [73], hepatitis C virus [74], respiratory syncytial virus [75], influenza A virus [76], and measles virus [77].

2.1.3.3. rVSV-NDV – “combining the benefits – removing the bad”

Balancing therapeutic efficacy with safety is paramount when considering OVs. Often, these two aspects are conflicting, with safer viruses typically offering less potent therapeutic effects, while highly effective viral vectors are frequently associated with toxicity. The objective in developing the recombinant hybrid of vesicular stomatitis virus and Newcastle disease virus (rVSV-NDV) was to combine the beneficial features, while eliminating the safety concerns of each. For this, a rVSV vector and an NDV vector containing a previously modified fusion protein (F3aa(L289A)) were used [4, 78]. Here, the surface G protein of VSV was pseudotyped with the envelope proteins of NDV (F3aa(L289A) and HN) (Figure 3). Deletion and replacement of the endogenous G protein improved the constructs neuro- and hepatic tropism, offering several beneficial features, including rapid and efficient tumor cell oncolysis generated by the induction of cell-cell fusion reactions (mediated by F and HN), while maintaining an exceptional safety profile [4].

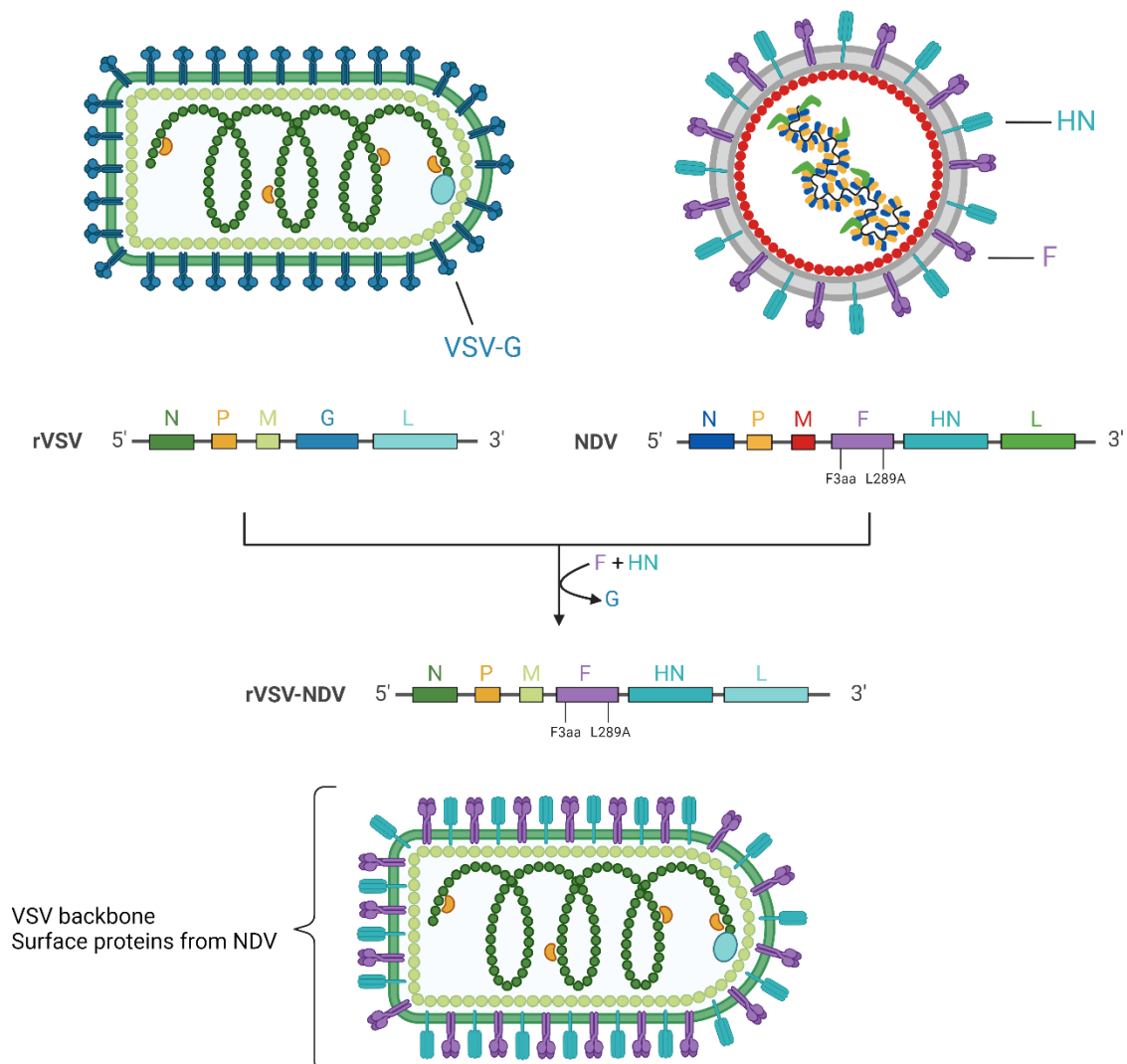


Figure 5 Construction of the hybrid rVSV-NDV virus. A full-length genome of recombinant vesicular stomatitis virus (rVSV) and a full-length previously modified Newcastle disease virus (rNDV/F3aa(L289A)) are being combined to engineer the chimeric rVSV-NDV virus. The G-protein of rVSV was pseudotyped by the modified F-protein (NDV-F3aa(L289A)) and HN-protein of NDV (HN) [4]. Created with BioRender.com.

2.2. Cell culture-based virus production

Compared to historical virus production (e.g. egg-based production for vaccines or isolation of virus inoculant out of infectious body fluids or tissue samples from infected patients for OV treatment), cell culture-based production allows the tight control of various process parameters within their optimal design space throughout the process in a closed system. Thus, cell culture is progressively being used for manufacturing of virus-based biopharmaceuticals (VBB) to pave the way for innovative treatments in various medical fields including cancer and gene therapy. However, optimal production systems are often neglected in the early stages of basic research, which primarily focus on the rescue of new constructs, investigation of the therapeutic potential, and evaluation of safety profiles. As development progresses and moves towards pre-clinical use, the demand for efficient and scalable production strategies gains importance to fulfill dose requirements, to ensure practicality and to achieve cost effectiveness.

Regardless of the intended use and type of the VBB, selection of a suitable host (Section 2.3) is critical for the development of a cell culture-based virus production process. Additionally, a cell line-specific growth medium allowing optimal growth and virus replication is required. While serum-containing media and adherent cell cultures have been traditional choices, they have several disadvantages (Section 2.3). Modern alternatives such as serum-free or chemically-defined media and transition to suspension cell cultures overcome most of these disadvantages, but achieving comparable results with respect to virus titers requires careful optimization and supplementation with growth factors (Section 2.3). Previously, our group compiled a comprehensive overview of factors that should be taken into account when determining the optimal process parameters (Figure 6) and intensification strategies (Section 2.4) for virus production in mammalian and avian cell culture [18, 79]. Generally, temperature is maintained at 37°C during the growth phase and lowered to 32-34°C during the infection phase. As viruses are sensitive to low or high pH values, for most applications pH value is tightly controlled between 7.0-7.6. Lastly, dissolved oxygen concentration is typically maintained above 30% and low agitation rates of 50-300 rpm are used. Following infection, peak titers are typically reached between 1-5 days p.i., depending on the used MOI, host cell, and virus [79]. The peak titer usually marks the

optimal time of harvest (Section 2.4.3.2), and can be either determined from empirical knowledge for established processes, estimated via a loss in cell viability, or integration of bio-capacitance probes. MOI has a direct effect on the progress of viral replication and occurrence of defective interfering particles (DIPs) [79]. The range of MOIs used is highly dependent on the type of virus, the application, and virus seed preparation. For vaccine manufacturing, low MOIs ranging from 10^{-1} to 10^{-5} are used to prevent formation of DIPs (as they can decrease infectious virus titers), cut costs (seed virus can account for up to 13-27% of total process cost [80]), and maximize the fold-increase of the produced virus. In contrast, most adenovirus productions for gene therapy or viral-vector based vaccines use single-hit infections with higher MOIs of 1 to speed up production times and harvest after a single viral lifecycle [81, 82]. However, modern productions developed during the COVID-19 pandemic, switched to lower MOIs to reduce the amount of required virus seed [83].

2.3. Production of OVs

OVs used in initial clinical trials in the beginning of the twentieth century were directly transplanted from infected tissue or body fluids of infected patients [1]. For today's ethical standards, this was very alarming and does not qualify for a scalable, safe or reproducible production for the general public. As the interest in OVs grew during the 1960-70s, OV production was shifted towards serial passaging in live animals, embryonated eggs, or cell culture using isolated human cancer cell tissues [84]. While serial passaging in rats, mice, or embryonated eggs reduced the virus's inherent pathogenicity and increased its oncolytic efficacy, this process was technical cumbersome and characterized by very low yields [84]. OVs passaged in isolated human cancer cell lines (e.g. HEp-2 or HEp-3 cells) were not harvested in the cell culture supernatant but transplanted into the patients' tumor within the host cell. As a result, the passaged virus was often only effective against the host cell line, which was used for propagation [84].

Nowadays, all OVs are produced in cell culture-based production systems and thoroughly purified before clinical use. The choice of the production cell line strongly depends on the type of OV. While oncolytic applications might allow inclusion of production cell lines known to be tumorigenic due to differences in risk-benefit analysis

compared to prophylactic applications (i.e. vaccines), it introduces an additional unknown variable to the process [85]. This will require additional costly and time-consuming steps including performing purity, safety and consistency studies to demonstrate a satisfactory safety profile to address regulatory concerns. For these reasons, most manufacturers use host cell lines that simultaneously de-risk the regulatory pipeline. Moreover, the need to produce high titers of OV for clinical application, calls for high producing cell lines. Taken together, the cell line should be well-characterized, genetically stable, high producing, and not contaminated with oncogenic viruses or other retroviruses, in order to facilitate subsequent clinical development [86]. Examples for continuous cell lines used for clinical-grade OV manufacturing include Vero cells (Herpes simplex virus, measles virus, and vaccinia virus), HEK293 cells (adenovirus, reovirus), A549 cells (adenovirus), HeLa cells (vaccinia virus), and some proprietary cell lines (e.g., EB66, PER.C6, and CAP) [5]. Three of the four approved OV treatments and most OVs in pre-clinical development use adherent cell lines in their manufacturing process (Table 1). Manufacturing of T-Vec and Delytact relies on adherent Vero cells cultivated in roller bottles [3, 87], RigVir is manufactured using an unknown adherent cell line.

Table 1 Overview of the production of several clinical grade OVs.

	Vaccinia virus	Adenovirus	Measles virus	Parovirus: H-1	VSV	NDV
Adherent producer cell(s)	HeLa cells, Vero cells	HEK293 cells, Per.C6 cells, A549-derived pTG6559 cells	Vero cells	human newborn kidney cells	BHK-21 cells [88, 89]	embryonated chicken eggs, Vero cells [90], ELL-0 chicken cells [89]
Culture vessels	cell factories, RC-40 roller bottle	spinner, roller bottle	cell factory	cell factory	T-flasks	chicken eggs, STR with cytodex-1 microcarriers,
Culture medium	DMEM + 10% FCS	SF CD293	VP-SFM	MEM + 5% FCS	DMEM + 10% FCS	DMEM + 10% FCS

STR: stirred tank bioreactor; DMEM: Dulbeccos modified eagle medium; FCS: fetal calf serum; SF: serum-free. Table modified from [5] (Free use under CC BY-NC-SA 4.0 Deed).

The scale-up of adherent cells is primarily constrained by surface area, in contrast to suspension cells that are limited by volume. Moreover, working with adherent cells requires more labor-intensive tasks such as washing and trypsinization. Traditionally, cells are cultured in serum-containing medium. Serum provides essential growth factors and nutrients required for cell attachment, proliferation and maintenance [91]. Yet, the use of serum can introduce inconsistencies due to batch variations and risk of microbial contaminations including viruses, bacteria, and prions [91]. As a result, animal-component free processes using serum-free or chemically-defined media are preferred nowadays, offering consistent and safe performance. However, achieving equivalent growth and virus yields in serum-free or chemically-defined media demands meticulous medium formulation optimization and the addition of growth factors. Transition to serum-free medium for production of oncolytic adenoviruses and NDV led to significant reductions in virus titers [5, 88]. Particularly for fusogenic OV, usage of adherent cells pose additional challenges in their production. As infected cells rapidly fuse with surrounding cells, large multinucleated syncytia are formed, which quickly die before high titers of the virus can be produced or released [4]. While this feature is generally considered to be beneficial in contributing to the enhanced safety of the fusogenic OV, production of e.g. rVSV-NDV in adherent production cell lines resulted in titers 3-4 logs lower than those achieved for the parental VSV [4]. Here, production in suspension cells seems favorable over adherent cells due to better process control, scalability, and the potential for intensified virus production in perfusion mode (Section 2.4). Currently there are only two clinical-grade OVs, which are produced in suspension cells. H101 (adenovirus) is produced in a HEK293 suspension cell line, achieving comparable yields of 3×10^{15} virus particles(vp)/batch in a 14 L NBS bioreactors [29] compared to adherent HEK293 cells cultivated with 10% FCS in an iCELLis 500 bioreactor (65 L working volume) with a yield of 6.1×10^{15} vp/batch [92]. Reolysin, an oncolytic reovirus investigated in phase III clinical trials for the treatment of metastatic breast cancer, is produced in HEK293 suspension cells using 100 L stirred tank bioreactors (STR) yielding 3.6×10^9 TCID₅₀/mL. Similar titers are achieved using adherent Vero cells grown on Cytodex-1 microcarriers in the presence of 5% FCS with 8.5×10^9 PFU/mL (corresponds to $\sim 4.7 \times 10^9$ TCID₅₀/mL when applying a conversion factor of 0.56) [93].

2.4. Process intensification strategies

VBBs comprise an expanding market of oncolytic vectors, viral vaccines, and gene transfer vectors. Since the introduction of viral vectors in 1972, their production and demand has expanded significantly. As a result, increasing efforts to reduce costs, overcome limitations of conventional production systems, and boost process yields are made. This requires improving productivity at every stage of the production process – beginning in the biphasic upstream stage from increasing e.g. infectious virus-particle yields, to debottlenecking purification strategies and optimizing modular solutions for manufacturing [18, 94]. One of the major challenges in the upstream stage is maintaining consistent product quality while ensuring safety and efficacy. To address this challenge, microscale and macroscale strategies can be pursued. Microscale strategies involve genetic manipulations at the cellular and sub-cellular level, including metabolic and genetic engineering techniques [94]. Macroscale strategies are used when genetic modifications are not feasible and focus on factors at the process scale. In upstream processing, these factors include optimizing the culture cultivation mode, such as switching from batch or fed-batch to perfusion production, cultivating cells at high cell concentrations for virus production, process parameter optimization, and improving media through the use of additives and supplements [94]. All efforts aim to maximize infectious virus titers, CSVY, and VVP. The CSVY gives the average number of infectious virus particles produced per cell after infection. STY described the amount of infectious virus particles produced considering the reactor volume and the total process time, whereas the VVP is the amount of infectious virus particles produced considering the total volume of spent medium during growth and virus replication phase and the total process time [18]. Both parameters allow for a comparison of the performance of different cell lines at different cultivation conditions, operation modes, and culture systems [18].

2.4.1. From batch cultures to intensified processes

All approved commercial OV manufacturing processes as well as most cell culture-based vaccine productions are operated in batch mode. If suspension cells are used, cells are grown in STRs to relatively low cell concentrations ($1.0\text{-}4.0 \times 10^6$ cells/mL) and subsequently infected [18]. Batch processes have gained widespread adoption in industry due to their ease of implementation, process robustness, and minimal sensor requirements. Moreover, batch processes enable high VVPs and efficient nutrient utilization, which minimizes the amount of medium required. Simple batch processes already offer multiple starting points for optimization including temperature p.i., MOI, infection mode, medium, aeration, and pH value (Figure 6) [8, 95, 96]. However, achieved virus yields are often low even after identification of optimal production conditions.

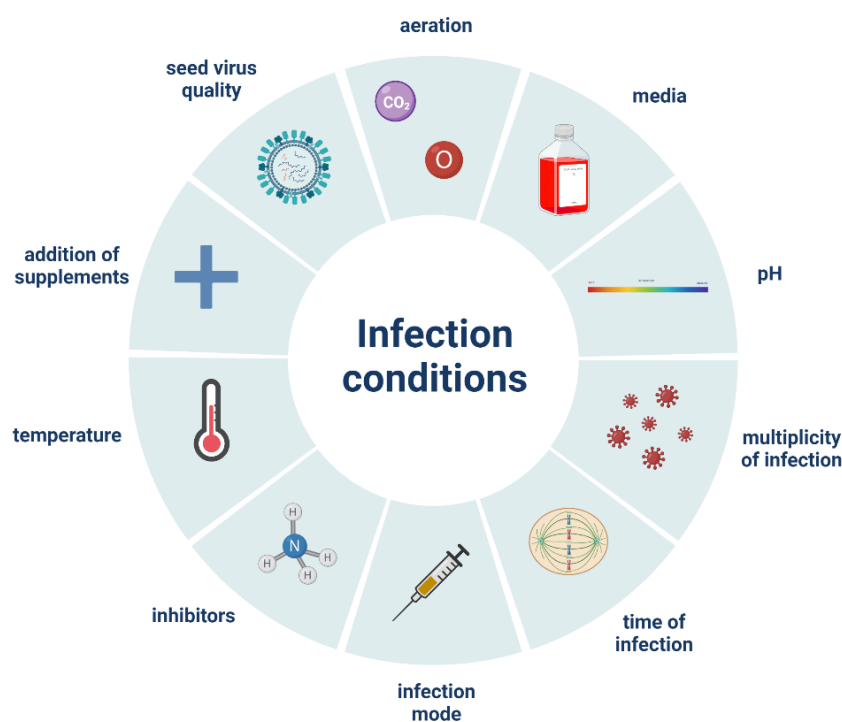


Figure 6 Overview of critical process parameters that can influence the efficiency of a virus production process.

Additionally, the planning, construction, validation, and commissioning of facilities for conventional large-scale stainless steel bioreactor operation in batch mode are both expensive and time-consuming [18, 97]. Extended downtime required for cleaning, setup for the next run, and sterilization, make these processes less economically viable. While some of these challenges can be overcome by transition to single-use production and scale-out operation of multiple bioreactors in parallel, there is a growing interest in intensifying the processes by implementation of fed-batch or perfusion modes.

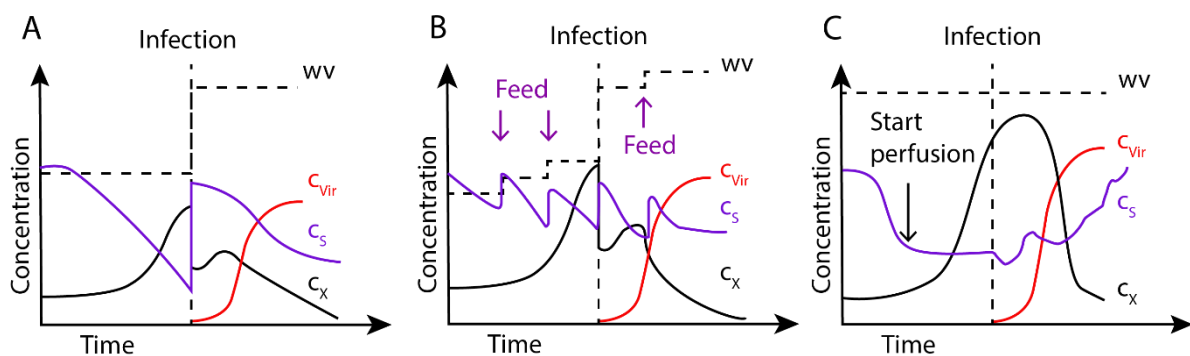


Figure 7 Schematic representation of virus production processes in modified batch (a), fed-batch (b), and perfusion (c) mode. Concentration profiles of various process parameters: wv , working volume; c_{vir} , virus particle concentration; c_s , substrate concentration (e.g. glucose), c_x , cell concentration. The dashed vertical line shows time of infection. For modified batch and fed-batch at time of infection a medium exchange/ dilution step by addition of medium results in a decrease of cell concentration and an increase in substrate level and working volume. Figure and caption taken from [18] (license acquired).

As a first step towards process intensification, a modified batch process can be applied. Particularly for vaccine manufacturing this modified batch was the standard for the last 40 years. Here a variation of a medium exchange (dilution step or complete exchange of medium at time of infection) is carried out to reduce levels of potential inhibitor concentrations interfering with virus production while providing additional substrates (Figure 4 a). Both variations have been reported to lead to increased titers for various viruses, however, performing a complete exchange of the medium at industrial scale is adding complexity and unit operations to the process [10, 13, 16, 98]. In order to increase cell concentrations before infection, a fed-batch strategy can be utilized.

Following an initial growth phase, fresh medium, concentrated feed, or selected substrates are added in a stepwise manner. This leads to an increase in the working volume and extends the exponential growth phase by providing additional nutrients to the cells (Figure 4 b). Compared to traditional batch production, this approach offers several advantages, such as achieving higher cell concentrations before infection, potentially resulting in increased virus titers and improved VVP [17, 18]. By applying a fed-batch strategy, Elahni et al. were able to increase HEK293SF cell concentration before infection by approx. 5-fold compared to batch processes, thereby increasing VSV titers by 5-fold [98]. However, maintaining an optimal balance between maximum cell concentration and the accumulation of secondary metabolites (e.g. lactate and ammonium) is essential to avoid inhibition of growth and virus production. Additionally, applicable feed volumes are limited due to volume constraints of the reaction vessel, aeration, mixing, or osmolality issues [17, 18].

Perfusion strategies became a key advancement in various areas of cell culture-based manufacturing and are also relevant to intensify processes for the production of lytic viruses. Through a constant supply of fresh medium while simultaneously removing an equivalent volume of spent medium, cells are provided with an optimal metabolic environment. Precisely, valuable nutrients for growth are supplied, while undesired metabolic by-products, protease inhibitors, carbon dioxide produced by the cells, and bicarbonate used for pH control are removed [17]. By that, cell densities, virus yields, and VVP can be enhanced. Compared to batch or fed-batch processes, significantly smaller bioreactors can be used for perfusion productions, reducing the required footprint and initial capital costs [17, 80]. Despite the advantages of perfusion processes, there are several drawbacks that need to be considered. Both perfusion rate as well as cell retention require a precise control adding complexity to the process. Surface aeration alone is not sufficient to provide oxygen in HCD cultures, so efficient aeration systems must be used. While usage of microspargers provide a high mass transfer, resulting in high volumetric mass transfer coefficient (kLa) values, the generated small bubbles can be associated with severe foaming issues and increased cell damage [99]. On the other hand, macrospargers produce larger bubbles, reducing foaming and cell death issues, but require higher gas flow rates to maintain similar oxygen transfer rates [18, 100]. Often two spargers are used at HCD: one for sparging

air and the other to sparge pure oxygen. Addition of pure oxygen can decrease the required gas flow rate and further mitigate foaming. Further challenges related to mixing, aeration and pH control are amplified by HCD and their elevated metabolic demands. Changes in the extracellular pH caused by by-products of cellular metabolism are actively buffered by a CO₂/bicarbonate system. Depending on the perfusion rate, addition of base (NaOH or NaHCO₃) is required to prevent sharp declines of pH caused by increased lactate concentration and accumulation of CO₂ at HCD. On the other hand, outgassing of accumulated CO₂ due to an increased gas flow to compensate the high oxygen requirements can reduce the amount of required base. However, the stripping of CO₂ is directly dependent on the sparger type used, with microspargers demonstrating a poor performance [100]. Mixing efficiencies decrease as the viscosity increases with HCD, resulting in slower mixing times. Moreover, ongoing base addition can lead to increased local pH levels, when homogenization within the bioreactor is impaired. This can result in cell lysis, leading to the release of cellular DNA, inactivation of infectious virus particles, and the formation of viscous regions with high pH [100]. Ultimately this can lead to local heterogeneities which require specific process control strategies to uphold ideal conditions for consistent virus production [18, 100]. Lastly, medium optimization is crucial for perfusion operation to maximize nutrient consumption and allow operation of lower rates, while minimizing the harvest volume for subsequent downstream purification trains. Alternatively, adaption of specific feeding schemes such as “hybrid fed-batch perfusion” can further reduce medium volume, thereby increasing VVP compared to perfusion-only strategies [14, 18, 80, 96, 101]. In the last 30 years, a variety of academic publications clearly demonstrated the applicability and effectiveness of perfusion systems for high titer virus production with cell concentrations ranging from 10-160x10⁶ cells/mL [10, 11, 13-15, 96, 101-115]. While perfusion systems are commonly applied for industrial production of recombinant proteins, generation of HCD cell banks [116], or N-1 seed train steps [117], adaption for in vaccine manufacturing is slow [118].

2.4.2. Cell retention devices

Initial set-up of a perfusion process can be a challenging task that requires thoughtful considerations and balancing of engineering as well as biological aspects. Choosing a suitable cell retention device (CRD) that efficiently retains the cells within the bioreactor without impacting the culture viability is an especially critical factor. Various CRDs with distinct characteristics are available that are mainly based on membrane filtration, gravitational settling or acoustic wave separation (Figure 8). The choice of cell retention device will determine whether virus particles accumulate with cells in the bioreactor or can be continuously harvested in the clarified permeate. This is pivotal as the accumulation of virus particles inside the bioreactor could lead to degradation of virus particles, thus loss of infectivity and reduction of yield. Literature by Chotteau et al. and Göbel et al. provide a comprehensive overview of all available technologies [17, 18].

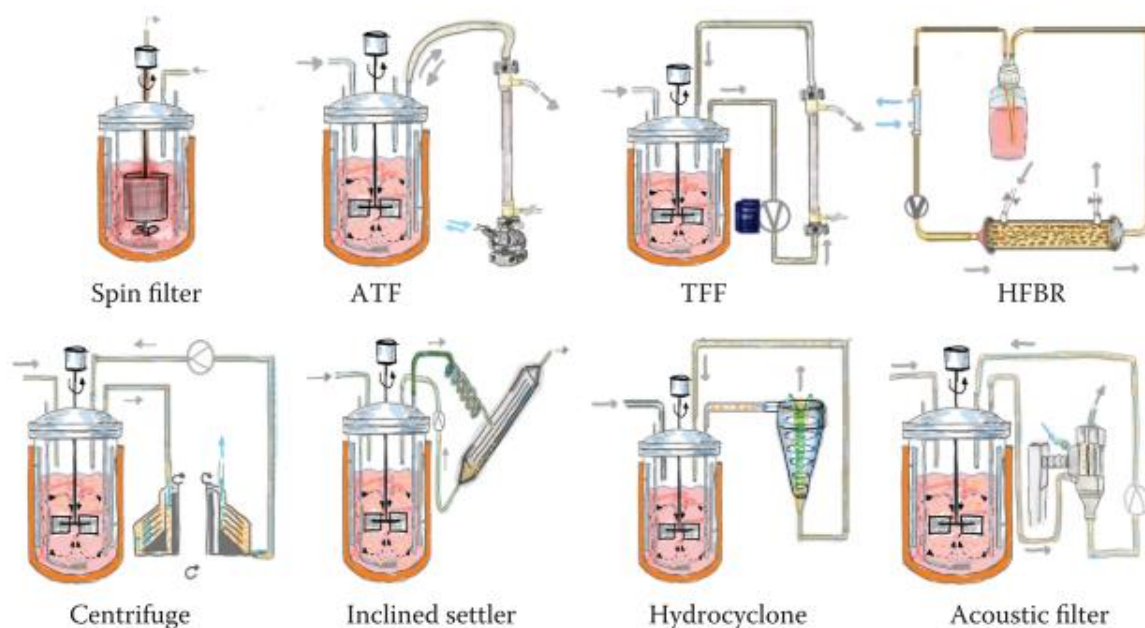


Figure 8 Cell retention devices and their connections to a bioreactor vessel. Gray arrows indicate the direction of flow, blue arrows indicate cooling systems or other flows (e.g., air for ATF diaphragm pump) with respective flow directions. The symbol (V) enclosed by a circle represents a pump. Orange dots represent cells. Abbreviations: ATF: alternating tangential flow filtration; TFF: tangential flow filtration; HFBR: hollow fiber bioreactor, here the bioreactor itself is responsible for the cell retention, therefore not explicitly further discussed as cell retention device. From [18] (license acquired).

2.4.2.1. Alternating tangential flow filtration

Among membrane-based technologies, alternating tangential flow filtration (ATF) was first introduced by Shevitz in 2000 and has become an indispensable tool in various bioprocessing applications since [119]. As for any perfusion process, a feed stream with fresh medium is added to the bioreactor, while spent medium is continuously removed at the same flow rate. In contrast to tangential flow filtration (TFF) operations, which employ an unidirectional flow, ATF is characterized by an alternating tangential movement of the cell culture broth across a semi-permeable hollow-fiber (HF) membrane. This generates a retentate stream retaining cells and large particles within the bioreactor, while the cell-free permeate stream carries solutes and small molecules. Depending on the membrane cut-off, cell debris or virus particles can be in either of those streams.

The HF unit is positioned between the bioreactor for growth and a diaphragm pump connected to a pressure-based ATF controller (Figure 9). The diaphragm pump pulls and pushes the cell suspension in the HF unit in an alternating way, creating an exhaust and pressure cycle [17]. During the pressure cycle, the convex diaphragm is pulled downwards by negative pressure increasing the liquid chamber volume and drawing the cell suspension into the filter unit. Within the filter unit, the HF serves as a physical barrier and tangential filtration of the cell broth occurs. In the subsequent exhaust cycle, pressurized air pushes the diaphragm back into the liquid chamber, creating a backflush that transfers the retentate stream into the bioreactor.

The ATF system is widely adopted and commercially accessible, with HF units available from multiple suppliers. In animal cell culture, exceptional separation efficacy has been demonstrated in HCD cultivations up to 2×10^8 cells/mL, making ATF systems currently being the preferred choice for most perfusion-based processes in recombinant protein production [107, 118, 120]. Vázquez-Ramírez et al. established an ATF-based perfusion process for MVA production using suspension AGE1.CR.pIX cells, reaching cell concentrations of up to 50×10^6 cells/mL with high infectious MVA titers around 1×10^{10} TCID₅₀/mL, thus demonstrating the potential of ATF systems also in virus production [14].

The periodic alternating flow pattern at rates ranging from 0.5-1.5 L/min minimizes shear stress on the cells by eliminating the need for an additional peristaltic pump. Thus, ATF systems are especially suitable for shear stress-sensitive cell lines such as suspension HEK293 cells, as they induce a lower total shear by a factor of 0.64 compared to TFF systems [121]. Moreover, the simplicity of connecting only one tube instead of two ports for a TFF system is often considered an advantage. Yet, this can limit scalability in comparison to TFF systems and also induce pressure issues at HCDs. A key benefit of ATF systems, is the reduced risk of membrane pore blockage and cake formation, commonly encountered in crossflow filtration, as the entire filter length is backflushed (also called Starling flow phenomenon) [122-124]. Nevertheless, with increasing cell concentrations, the viscosity of the cell suspension rises, while the pull or compression capacity of the diaphragm pump diminishes [125]. Thus, filter clogging can be encountered at HCDs and with prolonged growth cycles. But also the larger sizes (100-400 nm) and the lytic nature of some viruses or syncytia formation of fusogenic viruses [109] can contribute to filter clogging over time. Theoretically, increased pore sizes in the membrane (currently ranging from 45 kDa to 650 nm) could facilitate continuous virus particle harvesting, enhancing CSVY and virus stability by reducing the residence time in the bioreactor. For the production of recombinant proteins, continuous harvesting while retaining the cells is successfully carried out using ATF technology up to 500 L. For virus production, continuous harvesting using filtration is still a challenge and was, for instance, explored by Genzel et al. through the evaluation of three different ATF membrane cut-offs (45 kDa to 0.65 μm) for IAV production at 25×10^6 cells/mL. Pore sizes of 0.65 μm still proved inadequate for harvesting IAV virus particles of approximately 0.2 μm in size, underscoring the necessity for larger cut-offs or alternative membrane materials [10]. A recent study by Hein et al. introduced a novel tubular membrane (Artemis Biosystems), enabling the passage of all virus particles (IAV) [15]. However, this system is not yet available for larger scales.

Furthermore, prolonged cultivation durations may elevate the risk of potential adsorption of media components to the membranes, leading to alterations in the medium composition. However, the cell densities employed in virus production processes are not excessively high as of yet. Since most virus production studies have

been conducted in small-scale systems, the performance of both ATF and TFF systems at larger scales remains to be observed.

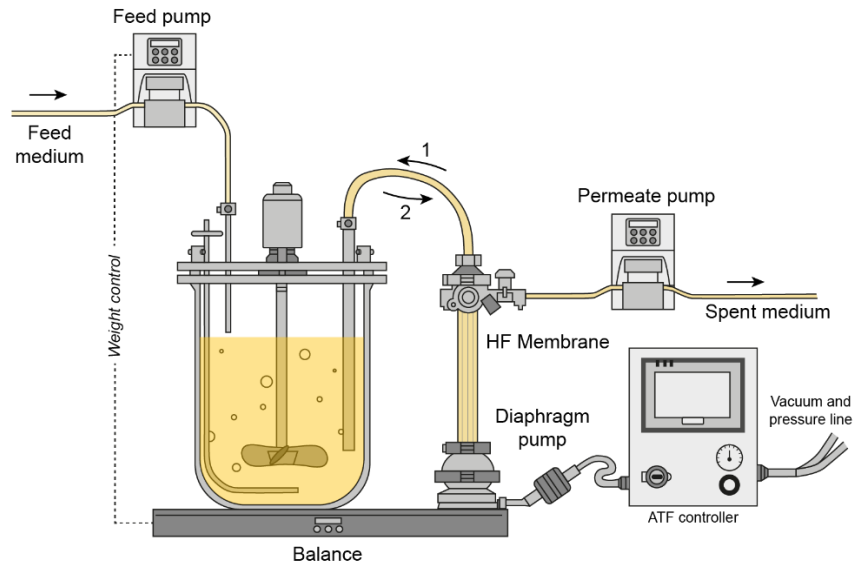


Figure 9: Schematic illustration of an ATF setup with a hollow-fiber unit. The diaphragm pump pushes the liquid in a bidirectional flow direction: 1) Exhaust cycle: Pressurized air is pressing the diaphragm into the liquid chamber, resulting in a backflush of the cells and medium into the bioreactor. 2) Pressure cycle: Negative pressure pulls the diaphragm into the liquid chamber, resulting in an inflow of the cell broth into the filter unit. The cell-free supernatant is removed through membrane pores during the pressure cycle, allowing fresh medium to be added to the bioreactor. From [18] (license acquired).

2.4.2.2. Acoustic settler

Acoustic settlers (AS) offer an alternative solution to address the challenges encountered in membrane-based perfusion processes. Since the early 1990s, their potential as a CRD has been explored and successful implementation could be shown in various perfusion cultivations involving both bacteria and mammalian cells [126-130]. In principle, AS leverage the fundamentals of acoustic wave technology to mimic natural sedimentation processes, facilitating the separation of cells and particles suspended in a culture broth. By exposing the cell culture broth to a controlled acoustic field, AS induce the formation of distinct layers based on the particle density, thereby enabling efficient sedimentation and pre-clarification.

In general, an AS is operated in cycles including filling the chamber with cell culture broth, applying a standing wave and interrupting the wave to allow cell sedimentation and backflush. When the chamber is filled with cell culture broth, a piezoelectric transducer generates acoustic waves. These waves are then directed through the liquid and reflected, causing them to travel back in the opposite direction of their initial propagation [127, 131]. As the acoustic waves transit through the liquid, they create a standing 3D wave. Within this wave, nodal pressure planes emerge, where the pressure oscillations caused by the wave cancel each other out, resulting in almost constant pressure fluctuations. At these areas, cells or other suspended particles, are more likely to become trapped due to the stable pressure conditions. As acoustic waves propagate through the liquid medium, particles are drawn towards these nodal pressure planes and gradually merge to form aggregates [127]. The resulting cell aggregates have a considerable mass, and are therefore subject to a high sinking velocity. Even after the acoustic field is turned off, the cell aggregates have enhanced settling properties [127]. Once settled at the bottom of the AS chamber, the aggregates are transferred into the bioreactor via the return flow [131]. Simultaneously, the cell-free permeate is removed from the top of the chamber using a peristaltic harvest pump and the next cycle begins. To reduce the residence time of the cells in the acoustic field, operation in duty cycles is implemented. Therefore, the acoustic field generated by the piezoelectric transducer and the permeate flow controlled by the harvest pump are periodically turned off [127]. Moreover, air-cooling of the acoustic chamber is applied to further protect the cells from damages caused by media over-heating [106].

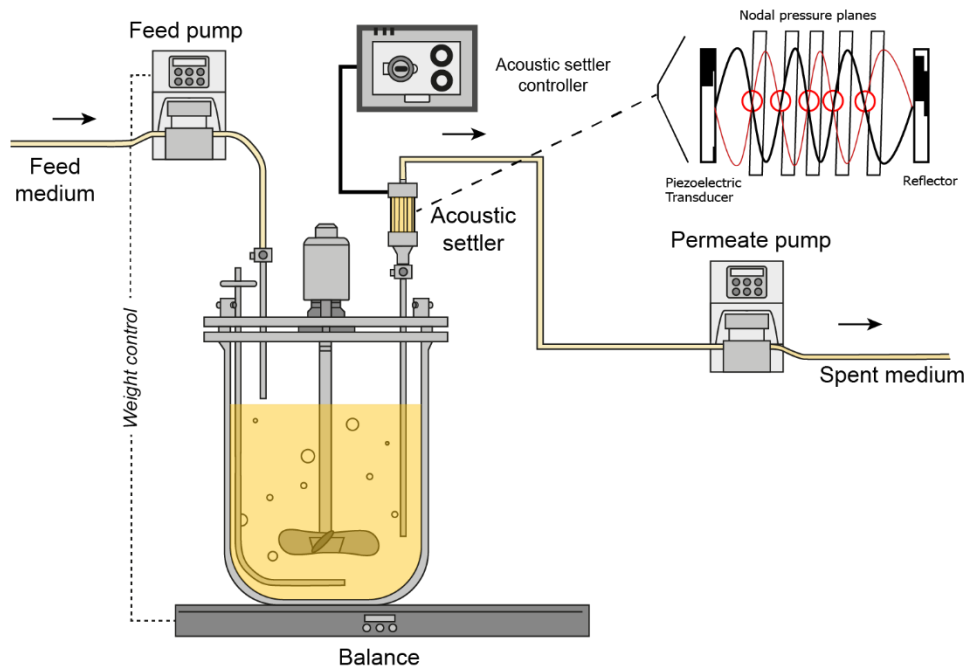


Figure 10: Schematic illustration of an acoustic settler setup and acoustic filter chamber for perfusion processes. The acoustic waves are generated by a piezoelectric transducer and reflected in the direction opposite to the propagation of the wave. As a result, cells are trapped at the nodal pressure planes of the standing 3D wave where they merge to form aggregates. The cell-free supernatant is removed in an intermittent way, allowing fresh medium to be added to the bioreactor. From [18] (license acquired).

HCDs can be achieved easily using an AS and very promising separation results were shown at for perfusion rates of up to 50 L/day [127, 132]. In recombinant protein production, CHO cell densities of 60×10^6 cells/mL, and for Sf9 cells, 30×10^6 cells/mL and 40×10^6 cells/mL have been reported [132-134]. Moreover, the applicability of an AS for virus production has been shown with a fully integrated MVA production process. Here, infected AGE1.CR.pIX cells reached HCDs of 50×10^6 cells/mL and the virus-containing harvest was pre-clarified for subsequent in-line purification steps [80]. Compared to membrane-based retention, AS hold practical benefits and offer potential cost savings. A physical barrier and moving parts are not required for cell retention, and the system is therefore less susceptible to mechanical failure and fouling [127]. Moreover, they are easily cleaned and sterilized-in-place. This results in reduced energy consumption, minimal equipment wear, and lower maintenance requirements. Additionally, the elimination of consumables such as filter membranes or centrifuge

tubes contributes to overall cost-effectiveness. The non-intrusive nature of acoustic waves, which can be applied uniformly across large volumes without compromising performance, allows theoretically for great scalability of the system, making AS an attractive investment for industrial-scale bioprocessing. However, only a limited amount of information is available about pilot/large-scale application of AS. So far, proof-of-principle studies show cultivations with perfusion rates of 200 and 400 L/day. Here, CHO cell densities of 10×10^6 cells/mL were reported at 100 L scale and hybridoma cultivations with about 5×10^6 cells/mL at 80 L scale [132, 135]. Although showing slightly lower separation efficiencies compared to membrane-based retention, AS appear to provide an efficient bypass and therefore, represent a relevant option for the production of recombinant proteins or viruses/viral vectors. Ryll et al. reported separation efficiencies of 95% or higher for CHO cell-based perfusion process and, similarly, Dalm et al. maintained 94-96% [133, 135]. For the production of IAV using AGE1.CR.pIX cells, up to 70×10^6 cells/mL were reached and retention efficiency of seven cultivations with distinct settings ranged between 87 and 99% over the entire production [106]. In general, the retention depends mostly on the cell radius, density, and compressibility. Thus, the retention of viable cells may exceed that of dead cells, consequently enhancing the overall viability in the reactor as dead cells are removed from the culture [18]. Moreover, Ryll et al. observed an inverse relationship with both, cell concentration and perfusion rate, implying that higher cell concentrations and higher perfusion rates decreased the separation efficiency [133]. With higher perfusion rates (>1 reactor volume (RV)/d), more viable cells will be washed out, resulting in a lower separation efficiency. However, high perfusion rates are usually required to avoid nutrient depletion at HCDs during the growth phase and virus production phase. Further external parameters that can affect the separation efficiency are the duty cycle, backflush frequency, and recirculation rate [127]. Although duty cycles have little influence on the AS performance, it was interestingly shown to be crucial to increase IAV yields [106]. To increase the retention efficiency, the backflush frequency, which describes the number of times the acoustic chamber is cleared of sedimented cells per hour, could be increased. The last external parameter, the recirculation rate, describes the flow rate with which sedimented cells in the acoustic chamber are recycled back into the bioreactor [18, 127]. Thus, the acoustic power is the only internal parameter

that can influence the retention efficiency, which could be improved by increasing the acoustic power input. However, most AS operate at a fixed frequency (between 2-3 MHz), as frequencies below this range can lead to cell damage caused by cavitation and heating of the medium and subsequently of cells in the acoustic chamber [18]. In general, AS offer gentle cell handling, as only gentle forces are exerted on the cells, minimizing shear stress and preserving cell viability and functionality. This is particularly beneficial for sensitive cell lines or products.

Moreover, AS can be used in a flexible and versatile manner, as they can be adapted to various bioprocessing scenarios, accommodating a wide range of cell and product types as well as process conditions. In a recent proof-of-concept study, it was suggested to integrate an AS for cell bleeding in a continuous perfusion process for recombinant protein production. This strategy aims to maintain a consistent cell concentration within the bioreactor by discarding only cells while recycling the product-containing suspension back into the bioreactor. Using this approach, Bielser et al. could significantly improve yields by 2.25-fold [136]. In Göbel et al. associated drawbacks and related issues for the AS were described in more detail [18].

2.4.2.3. Tangential flow depth filtration

More recently, tangential flow depth filtration (TFDF) (Repligen) became available as an alternative option to long-established membrane-based CRDs. This technology combines tangential flow and depth filtration (DF) in a single-use system that is commercially available from pilot to 2,000 L scale. Similar to other membrane-based perfusion operations, a filter module is positioned externally adjacent to a bioreactor, with a pump delivering the cell culture broth from the bioreactor to the filter module. Here, the broth is cleared and cell-free supernatant can be collected, while the retentate stream is pumped back into the bioreactor. Compared to most HF membranes, the whole system can be operated in a plug-and-play manner, as filter units are already pre-sterilized and the perfusion process can be controlled by an external TFDF control unit.

Although resembling a conventional HF setup, the TFDF filter exhibits distinct characteristics. Traditional HF membranes are made of polyethersulfone with a wall

thickness of 0.075 mm to 0.2 mm and a lumen diameter of 0.5 mm to 1 mm with an anisotropic structure. In contrast, TFDF filters are constructed from polypropylene/polyethylene terephthalate with an isotropic structure. They have a wall thickness of 5.0 mm and a large lumen size (4.6 mm in diameter). This filter composition results in an effective average pore range of 2–5 μm , and thus particles of 20–200 nm in diameter can pass through the TFDF filter into the permeate stream while retaining larger cells and debris.

Thus, viral particles have a shorter residence time within the reactor that can influence the quality, but also offers the possibility to immediately cool continuously harvested material. As described previously, continuous harvest can essentially enhance virus stability and, thus, overall efficiency. Owing to the included DF step, an initial purification is already performed and a more simplified downstream process can follow. All in all, this could allow for a direct integration of upstream (virus production) and downstream processing (virus purification), further reducing costs while increasing flexibility and productivity [80, 137].

Applicability of the system was shown for several production processes using HEK293 cell lines including a lentiviral vector [138, 139], adeno-associated virus [102], VSV [109], and IAV [101]. Together, the TFDF module offers a membrane-based perfusion set-up, that can combine continuous virus harvest and clarification in a single step, reducing the number of unit operations and therefore save time and money [102].

sampling can introduce contamination risks to the cultivation system, with limitations on both sampling frequency and volume. Among the traditional techniques for obtaining online VCC in bioreactors is the use of a mass spectrometer to analyze the rates of carbon dioxide [142] and oxygen uptake [141, 143]. However, this approach yields signals that are noisy and not reliable. To address this issue, optical density-based probes and various other optical methods such as laser light [144], Raman [145], in situ microscopy [146], and fluorescence spectroscopy [147] have been employed to estimate the total cell concentration. Nevertheless, these optical probes were unable to accurately measure VCC as they detect both cells and debris. Moreover, they often exhibit non-linear behavior at high cell concentrations (above 20×10^6 cells/mL) and are prone to fouling during extended bioreactor runs [141]. As a result, bio-capacitance (also referred to dielectric spectroscopy or permittivity) was introduced in the 1990s as a tool to monitor VCC in real-time [148]. There are many reviews and publications outlining the exact theories and mathematical equations of bio-capacitance, therefore this will not be introduced in detail here [141, 148-157]. Briefly, the technology relies on the capability of cells to act as capacitors under the influence of an electric field [141]. The resulting polarization of the cells with an intact insulating bilipid membrane can be measured as a change in capacity, allowing specific detection of viable cells while non-polarizable particles (e.g. gas bubbles, microcarriers, cell debris) are neglected. Although the technology was established more than 30 years ago, its adoption in the bio-pharmaceutical industry has been slow.

Early concerns emerged from discrepancies between capacitance measurements and offline Trypan blue dye exclusion measurements, particularly during the final stage of growth, when cells enter the death phase. Understanding the connection between capacitance, biovolume/biomass, and VCC is crucial for its application. Capacitance data directly correlate with viable biomass, especially during exponential growth. However, changes in cell properties due to stress or nutrient limitations can impact capacitance measurements. The size and shape of cells e.g. following infection or osmotic shifts can also affect the relationship between VCC and capacitance signals, as total biovolume is measured [141].

2.4.3.1. Capacitance for closed-loop perfusion control

HCD perfusion bioreactors require a precise and stringent control to allow for optimizations to increase the productivity. Traditional daily manual sampling for VCC is insufficient for precise process control, particularly for processes with high VCC and fluctuating nutrient concentrations. Using capacitance probes, a linear correlation between the online measurements and the offline reference method can be established. Single-frequency capacity measurements can either be correlated to offline VCC readings or used to estimate the viable cell volume (VCV). While good correlations between offline VCC and capacitance can be established in the exponential growth phase [109, 158], this correlation can be lost when cell size and electrical properties change drastically (cell death and/or virus infection) [141, 157, 159]. By taking the cell size and number into consideration, a more precise correlation between VCV and capacitance can be obtained. Using established correlation and online-measurements, the perfusion rate can be controlled in real-time based on the VCC or VCV in the bioreactor. Here, a pre-defined amount of medium per cell or cell volume is added in a fixed timeframe, resulting in a constant cell-specific perfusion rate (CSPR) or cell-volume-specific perfusion rate (CVSPR) [160]. This allows to maintain an adequate supply of nutrients and stable substrate levels, independent of VCC and biological variation between runs.

Unlike the production of recombinant proteins, virus production typically requires a biphasic process. Following an exponential growth phase, a (lytic) virus replication phase is initiated with addition of a seed virus. Infected cells can undergo significant morphological changes (e.g. syncytia formation for fusogenic OVAs) causing a loss of linearity between VCC and capacitance signal, as discussed before. While control of the perfusion rate based on CVSPR can prevent this to a certain degree, sharp increases in biovolume (e.g. cell swelling) can lead to severe overfeeding [161, 162]. As a result, capacitance-based automated perfusion control is usually only used during the initial growth phase and switched to a fixed RV exchange regime following infection. This phase-specific perfusion control has also been used in the publications included in this PhD thesis.

2.4.3.2. Use of capacitance probes for viral monitoring

With the increasing number of approved viral products for vaccination or therapeutic approaches, the need for continuous in-process analytical and monitoring technologies (PAT tools) arises. Rather than assuring compliance and quality through end-point controls, regulatory agencies emphasize the need to measure the accumulation of bioactive viral particles in cell culture in-line and to assure continuous real time quality by enabling quality-by-design of the process. To date, commercially available options for specific on-line and in-line monitoring of the accumulation of viral particles in cell culture have not been developed. Besides growth control, there have been several attempts to use capacitance probes as a tool to monitor and control virus production [80, 161, 163, 164]. As of now there is no publication describing that capacitance-derived measurements can be correlated with total or infectious virus concentration. However, several studies outline the value of measuring parameters derived from capacitance measurements during virus infection [141]. In particular through measurements of morphological and physiological alterations of cell populations occurring during the cycles of viral replication, biomass and physiological characteristics of the cultivated cells can serve as primary indicators of the progress of viral infection, progress and time of virus release [161, 163, 165-168].

2.4.3.3. Other applications of capacitance probes

Capacitance probes are commonly integrated to regulate bleeding rates during continuous production runs, ensuring that a specific VCC is maintained over an extended period [136, 141, 169]. Many commercial manufacturers (e.g. Biogen, Bristol Myers Squibb, Lonza) utilize capacitance probes in fed-batch processes to replace fixed-time bolus feeding, preventing over- or under-feeding [155, 170]. It can also be used to control the inoculation of seed train vessels, commonly used in large-scale breweries [171]. Lastly, capacitance probes could also be used for quality control to detect perturbations in the process in real-time. Established capacitance trajectories with defined standard deviations can be directly linked to an alarm, allowing identification of failed control systems (e.g. pumps, oxygen, etc.) or changes in media composition [141].

3. Manuscripts

For this cumulative dissertation, the following papers concerning the process optimization for production of the oncolytic fusogenic rVSV-NDV virus are included. Overall, the studies have resulted in four published manuscripts and two papers in preparation/submission (Not part of this thesis; 1. “Developing a purification process for a clinical-grade oncolytic virus”, Shared first author, submitted to Separation and Purification Technology; 2. “Production of Oncolytic rVSV-NDV in CCX.E10 Quail Cells by HCD Perfusion Culture”, Co-Author, in preparation). The published manuscripts address the objectives stated in the introduction and abstract and present the primary outcomes of the project. The project connected six industrial (ProBioGen, Nuvonis, Repligen, Fusix Biotech, CEVA animal health, Kühner AG) and three academic partners (TU Munich, iBET, McGill University). An overview is given below (Figure 12).

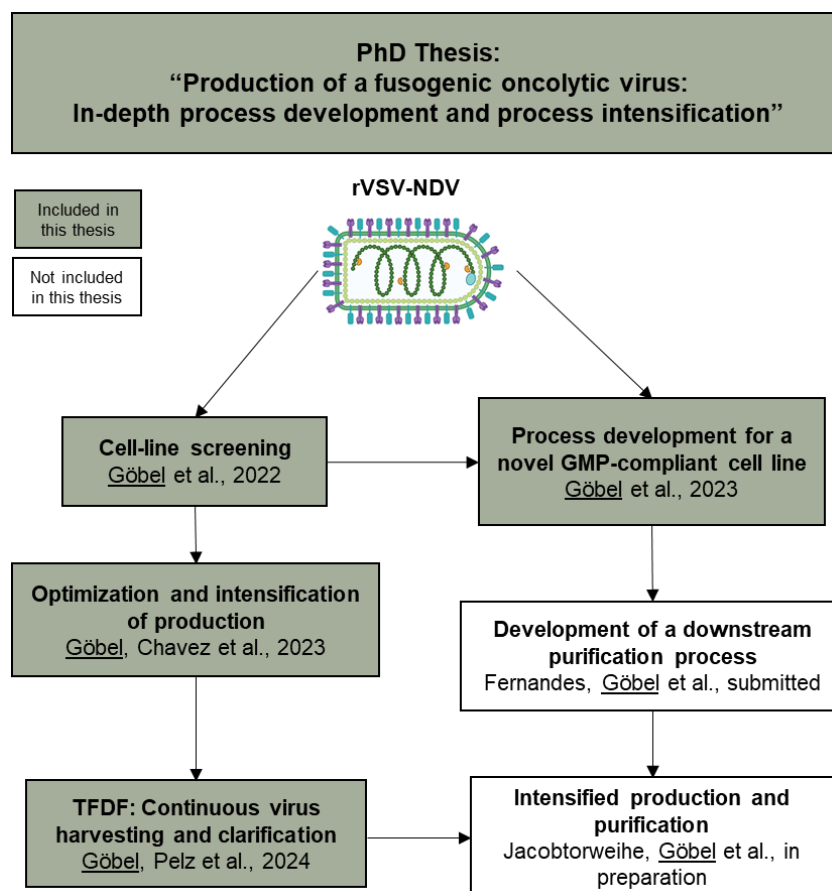


Figure 12 Overview of the publications included or associated with this doctoral thesis.

3.4. First Manuscript

In this study, the production of oncolytic rVSV-NDV-GFP was evaluated in four different suspension host cell lines under typical batch production conditions. The effect of cell-clumping and VCC on syncytia formation as well as cell-specific rVSV-NDV release dynamics were investigated. Furthermore, virus adaptation and MOI screenings were performed to maximize virus titers. The findings were then applied to select cell lines and transferred to 1 L STRs. This study described, for the first time, the production of a fusogenic OV in suspension cells using chemically-defined media. Compared to adherent cells, efforts resulted in 100-fold higher infectious virus titers.

Göbel, Sven; Kortum, Fabian; Chavez, Karim Jean; Jordan, Ingo; Sandig, Volker;
Reichl, Udo; Altomonte, Jennifer; Genzel, Yvonne

First author

Cell-line screening and process development for a fusogenic oncolytic virus in small-scale suspension cultures

Applied Microbiology and Biotechnology, 2022

[8]

Contribution Sven Göbel:

Conceptualization, formal analysis, investigation, methodology, project administration, writing – original draft, writing – review & editing.



Cell-line screening and process development for a fusogenic oncolytic virus in small-scale suspension cultures

Sven Göbel¹ · Fabian Kortum² · Karim Jaén Chavez² · Ingo Jordan³ · Volker Sandig³ · Udo Reichl^{1,4} · Jennifer Altomonte² · Yvonne Genzel¹

Received: 23 February 2022 / Revised: 9 May 2022 / Accepted: 10 June 2022 / Published online: 29 June 2022
© The Author(s) 2022

Abstract

Oncolytic viruses (OVs) represent a novel class of immunotherapeutics under development for the treatment of cancers. OVs that express a cognate or transgenic fusion protein is particularly promising as their enhanced intratumoral spread via syncytia formation can be a potent mechanism for tumor lysis and induction of antitumor immune responses. Rapid and efficient fusion of infected cells results in cell death before high titers are reached. Although this is an attractive safety feature, it also presents unique challenges for large-scale clinical-grade manufacture of OVs. Here we evaluate the use of four different suspension cell lines for the production of a novel fusogenic hybrid of vesicular stomatitis virus and Newcastle disease virus (rVSV-NDV). The candidate cell lines were screened for growth, metabolism, and virus productivity. Permissivity was evaluated based on extracellular infectious virus titers and cell-specific virus yields (CSVYs). For additional process optimizations, virus adaptation and multiplicity of infection (MOI) screenings were performed and confirmed in a 1 L bioreactor. BHK-21 and HEK293SF cells infected at concentrations of 2×10^6 cells/mL were identified as promising candidates for rVSV-NDV production, leading to infectious titers of 3.0×10^8 TCID₅₀/mL and 7.5×10^7 TCID₅₀/mL, and CSVYs of 153 and 9, respectively. Compared to the AGE1.CR.pIX reference produced in adherent cultures, oncolytic potency was not affected by production in suspension cultures and possibly even increased in cultures of HEK293SF and AGE1.CR.pIX. Our study describes promising suspension cell-based processes for efficient large-scale manufacturing of rVSV-NDV.

Key points

- Cell contact-dependent oncolytic virus (OV) replicates in suspension cells.
- Oncolytic potency is not encompassed during suspension cultivation.
- Media composition, cell line, and MOI are critical process parameters for OV production.
- The designed process is scalable and shows great promise for manufacturing clinical-grade material.

Keywords Cell line screening · Fusogenic oncolytic virus · Upstream processing · Cell culture-based production

Introduction

OVs have emerged as a promising anti-cancer therapeutics due to their intrinsic ability to selectively infect and lyse tumor cells while inducing potent secondary immune responses (Krabbe and Altomonte 2018; Cook and Chauhan 2020). OVs expressing fusogenic glycoproteins are of particular interest as they lead to the formation of multinucleated giant cells (syncytia), facilitating intratumoral viral spread and tumor cell killing via multimodal responses that include the induction of adaptive immune responses directed against the tumor (Krabbe and Altomonte 2018). One promising OV in this immunotherapeutic class is rVSV-NDV, a recombinant hybrid virus constructed of a vesicular stomatitis virus

✉ Yvonne Genzel
genzel@mpi-magdeburg.mpg.de

¹ Max Planck Institute for Dynamics of Complex Technical Systems, Bioprocess Engineering, Sandtorstr. 1, 39106 Magdeburg, Germany

² Department of Internal Medicine II, Klinikum Rechts Der Isar, Technische Universität München, Munich, Germany

³ ProBioGen AG, Herbert-Bayer-Str. 8, 13086 Berlin, Germany

⁴ Chair for Bioprocess Engineering, Otto-Von-Guericke-University Magdeburg, Universitätsplatz 2, 39106 Magdeburg, Germany

(VSV) backbone and the surface glycoproteins of Newcastle disease virus (NDV) (Abdullahi et al. 2018). rVSV-NDV is a rapidly replicating and hyperfusogenic vector, providing the clinical benefits of each parental virus while eliminating the safety concerns associated with each. Proof-of-concept investigations indicate that rVSV-NDV is an effective and safe therapeutic for the treatment of hepatocellular carcinoma (Abdullahi et al. 2018) and murine melanoma, especially when administered in combination with adoptive T-cell transfer (Krabbe et al. 2021).

However, the low virus yields obtained from adherent cell cultures strongly limit the testable dose range in preclinical models. Despite screening of multiple adherent cell lines for rVSV-NDV production, the highest achievable titers remained relatively low ($\sim 10^6$ TCID₅₀/mL in the culture harvest (Abdullahi et al. 2018) and a maximum of $\sim 2\text{--}5 \times 10^8$ TCID₅₀/mL after purification and concentration). Because dose-limiting effects have not been observed using the virus concentrations, currently available processes with higher yields for attaining $\geq 10^8$ virions/injection are desirable. Furthermore, translation to the clinical application would be facilitated if efficient large-scale manufacturing processes free of animal-derived components can be developed.

Despite a favorable regulatory environment, current approaches to using adherent AGE1.CR.pIX cells for rVSV-NDV production pose major challenges for large-scale production (Abdullahi et al. 2018). This includes limited monitoring of pH value and dissolved oxygen partial pressure. In addition, restricted cell harvesting options and limited control of cultivation parameters such as feeding rates can complicate the scale-up of anchorage-dependent cells. In contrast, the use of suspension cells allows for an easier transfer from laboratory-bench systems to large-scale industrial bioreactors (Gallo-Ramírez et al. 2015). For the clinical-grade manufacturing of OV, the absence of animal-derived components in the cultivation media is highly desirable. In particular, the use of fetal calf serum can not only raise production and purification costs and cause higher batch-to-batch variations but also involves the risk of contamination with adventitious agents (Caron et al. 2018).

Even though wild-type VSV possesses a very broad tropism for various cell lines (Hastie et al. 2013), only a few publications reported the yield of VSV-based vectors from suspension cell culture (Elahi et al. 2019; Shen et al. 2019), and rVSV-NDV production in suspension cells has never been addressed before. The unique structure and fusogenic capacity of this hybrid virus likely cause altered tropism and replication kinetics and, consequently, demands the identification of suitable production cell lines. This may even include cell lines known to be tumorigenic or possessing abnormal karyology that are considered a risk in traditional vaccine manufacturing, due to differences in risk–benefit analysis (ICH 1998; Jordan and Sandig 2014). In addition,

the high dose requirements of rVSV-NDV for further pre-clinical and first-in-human studies call for cell lines that achieve high cell-specific virus yields (CSVY). Furthermore, cell lines should be well-characterized, genetically stable, and demonstrated to be free of oncogenic viruses to facilitate subsequent clinical development (FDA 2010). Examples of safe and productive cell lines for vaccine and viral vector production include HEK293, AGE1.CR.pIX, EB66, Vero, and PER.C6 (Genzel 2015).

In the current study, we have evaluated the production of oncolytic rVSV-NDV-GFP (further referred to as VSV-NDV) in different suspension host cells under typical production conditions. Furthermore, virus adaptation and multiplicity of infection (MOI) screenings were performed to maximize virus titers. The findings were then applied to select cell lines that sustain high VSV-NDV titers and can be transferred to 1 L bioreactors for the establishment of a robust suspension cell-based process for oncolytic virus vector production. The latter was considered a critical requirement as oncolytic viruses are expected to enter mainstream clinical use. The screening and optimization steps outlined here can be easily adapted to other OV production platforms, particularly those involving fusogenic vectors, which present additional manufacturing challenges.

Materials and methods

Cell lines, media, and viral seed stock

A variety of different suspension cell lines (Supplement Table S1) were cultured and screened to identify a suitable cell substrate for the production of rVSV-NDV stocks. All cell lines had been adapted previously to anchorage-independent proliferation in suspension media. BHK-21 cells were maintained in Protein Expression Medium (Gibco, USA), supplemented with 8 mM L-glutamine (Sigma-Aldrich, USA) and 4 mM pyruvate (Sigma-Aldrich, USA) in the following PEM_s. AGE1.CR and AGE1.CR.pIX cells were maintained in chemically defined CD-U7 medium (Xell, Germany) supplemented with 2 mM L-glutamine, 2 mM alanine (Sigma-Aldrich, USA), and 10 ng/mL recombinant insulin-growth factor (LONG-R³, Sigma-Aldrich, USA). MDCK cells were cultured in chemically defined Smif8 medium (protein- and peptide-free, Gibco, USA/K. Scharfenberg, FH Emden/Leer, Germany) supplemented with 4 mM L-glutamine and 4 mM pyruvate, or in chemically defined Xeno medium (Driving-M) (Shanghai BioEngine Sci-Tech, China) supplemented with 8 mM L-glutamine. HEK293SF cells were maintained in PEM_s medium, Dynamis medium, or FreeStyle™ 293 Expression Medium (Gibco, USA). Cell suspensions, except HEK293SF cells, were cultivated in baffled 125 mL flasks (50 mL V_w,

Corning, USA) at 185 rpm, 37 °C, and 5% CO₂ in a Multi-tron Incubator Shaker (Infors AG, Switzerland) with a 5 cm orbit. HEK293SF cultures were agitated at 115 rpm, 37 °C, and 8% CO₂.

The engineering, rescue, amplification, and purification of rVSV-NDV-GFP have been described previously (Abdullahi et al. 2018). The viral seed stock (6.58×10^7 TCID₅₀/mL) used in this study was produced in adherent AGE1.CR.pIX cells (ProBioGen AG, Germany) and stored at –80 °C until use. For each subsequent experiment, a new aliquot of this stock was used to avoid potential loss of infectivity due to repeated freeze–thaw cycles.

Oncolytic viral potency assay

As a measure for the oncolytic virus potency, adherent human hepatocellular carcinoma cells (Huh7) were infected with escalating serially diluted MOIs. Cell viability was measured using the CellTiter-Glo® Luminescent Cell Viability Assay (Promega Corp., Madison, USA). From the resulting dose–response curves, IC₅₀ values were derived and interpreted as a readout for oncolytic potency. In brief, VSV-NDV-susceptible Huh7 cells were seeded in flat-bottom white-walled 96-well plates (# 655,088, Greiner Bio-One; Germany) at a density of 1×10^4 cells/well using DMEM GlutaMAX media containing 10% fetal bovine serum and incubated overnight at 37 °C and 5% CO₂. On the following day, serial half-log₁₀ dilutions of the virus sample were prepared in medium to a minimum of one virion per well (MOI 10^{–4}). For infection, the supernatant was removed and cells were infected with 100 µL of the prepared dilutions in quadruplicates, or left uninfected in fresh medium. A total of 48 h post-infection (hpi) the medium was replaced with 50 µL of fresh culture medium and 50 µL of the lytic assay substrate. Following the instructions in the kit manual, luminescence was recorded using a GloMax® Discover luminescence plate reader (Promega Corp., Madison, USA). After background subtraction of the medium, the reduction of cell viability was expressed relative to uninfected control cells and plotted against the log-MOI. Uninfected control cells were defined as 100% viable (top constraint = 1), whereas the bottom constraint was set to 0, representing 100% oncolysis.

Small-scale infection screening

For experiments at conventional cell concentrations (conventional cell density, CCDs), shake flasks were inoculated at $6.0\text{--}8.0 \times 10^5$ cells/mL and cultivated for 72 h to reach about $4.0\text{--}6.0 \times 10^6$ cells/mL before infection. For experiments using higher cell concentrations, shake flasks were inoculated at 1.0×10^6 cells/mL and cultivated for 72–96 h to reach about 1.0×10^7 cells/mL. At the time of infection (TOI), the viable cell concentration was adjusted to CCD

(2.0×10^6 cells/mL) or higher cell concentrations (5.0 or 10.0×10^6 cells/mL) by centrifuging the appropriate volume of cell suspension at $300 \times g$ for 5 min and re-suspending in fresh medium containing virus. Host cells were infected at an MOI of 0.01. Additional shake flasks were supplemented with CaCl₂ (0.3, 0.5, and 0.9 mM; Merck, Germany) to induce cell aggregation. Samples taken from the supernatant of infected cells were centrifuged for 5 min at $1100 \times g$ to remove cellular debris, then aliquoted and stored at –80 °C until further analysis.

For the screening of different MOIs, the same inoculation procedure was performed as described above for CCD experiments. MOIs ranging from 10^{–1} to 10^{–5} were tested. Samples taken from the supernatant of infected cells were centrifuged for 5 min at $1100 \times g$ to remove cellular debris, then aliquoted and stored at –80 °C until further analysis.

Virus adaptation

VSV-NDV was adapted sequentially to the cell substrates following the inoculation procedure at CCD described previously. After the first infection, specified volumes of supernatant from each cell substrate were transferred to subsequent shake flasks with cells growing in the exponential growth phase at cell line-specific time points (Supplement Table S2). Subsequent passages were carried out at the same time point or earlier to select for fast-propagating viruses. Samples taken from cell culture supernatant were centrifuged for 5 min at $1100 \times g$ to remove cellular debris, then aliquoted and stored at –80 °C until further analysis.

Infection in a small-scale bioreactor

Bioreactor cultures were performed in a DASGIP 1 L stirred tank bioreactor (STR) (Eppendorf AG, Germany) equipped with an InPro3100 pH sensor (Mettler Toledo, Switzerland), an InPro6800 polarographic dissolved oxygen sensor (Mettler Toledo, Switzerland), and a marine impeller. Additionally, an online capacitance probe connected to a controller (ArcView Controller 265, Hamilton, Switzerland) operating at a frequency range of 1 to 10 MHz was used to capture cell growth dynamics for future experiments. For aeration, a 3 sL/min air stream (21% O₂) was supplied to the culture through a drilled hole L-sparger. DO was controlled at 50% air saturation by increasing the volumetric flow rate of the O₂ content. The temperature was maintained at 37 °C using a heating blanket. For BHK-21 cells, the bioreactor was inoculated at a concentration of 0.5×10^6 cells/mL, with pre-cultures expanded in 250 mL shake flasks and operated at a working volume (V_w) of 350 mL, pH 7.2, and a stirring speed of 350 rpm. For HEK293SF cells, the bioreactor was inoculated at a concentration of 0.6×10^6 cells/mL with pre-cultures expanded in 250 mL shake flasks and operated at

V_w of 350 mL, pH 7.0, and stirring speed of 250 rpm. The pH was controlled at the respective set-point using 7.5% NaHCO_3 or carbon dioxide. The same supplemented PEM_S medium was used for BHK-21 and HEK293SF batch cultures (Sect. 0). After the cells reached a concentration of 4.0×10^6 cells/mL, 350 mL of fresh supplemented PEM_S medium containing virus was added, increasing the V_w to 700 mL. BHK-21 and HEK293SF cells were infected at an MOI of 10^{-4} and 10^{-2} , respectively. Samples for metabolite analysis and virus titration were centrifuged at $1100 \times g$ for 5 min to remove cell debris, aliquoted, and stored at -80°C until further analysis.

Analytcs

Percentage of viability and viable cell concentration were determined using an automatized ViCell™ XR cell viability analyzer (Coulter Beckman, USA). MDCK cells cultivated in Smith-8 medium were additionally incubated with $1 \times$ trypsin for 10 min at 37°C prior to measurement to break up aggregates. The metabolites, lactate, ammonium, glutamine, glutamate, and glucose were determined in single measurements with the BioProfile® 100 Plus (Nova Biomedical, USA). Virus-containing samples were inactivated at 80°C for 3 min before metabolite measurements to allow easier handling. For titration of VSV-NDV, a modified version of the previously described TCID_{50} assay (Nikolay et al. 2020) was performed using adherent AGE1.CR.pIX cells (standard deviation of $\pm 0.3 \log_{10}$ ($\text{TCID}_{50}/\text{mL}$)). The CSVY was calculated as previously described by Gränicher et al. (2021), taking into account only the error of the TCID_{50} assay ($-50\%/+100\%$ on a linear scale).

Flow cytometry

Flow cytometry was used to determine the percentage of VSV-NDV-infected cells at different time points post-infection. A total amount of 2.0×10^6 cells was fixed using 4% paraformaldehyde for 30 min at 4°C . Fixed cells were washed twice with FACS buffer [PBS, 2% (*w/v*) Glycin, 0.1% (*w/v*) BSA] ($300 \times g$, 10 min, 4°C) and re-suspended in 15 μL buffer. Analysis was performed using the ImageStream X Mark II (Amnis, EMD Millipore) by measurement of 10,000 single cells (debris and aggregates were excluded) at an excitation wavelength of 488 nm for detecting GFP + infected cells. Data analysis was carried out using the IDEAS software.

Statistical analysis

Using a nonlinear regression model in GraphPad Prism (Version 8), IC_{50} values were calculated and compared between the data sets using the extra-sum of squares *F*-test.

Results

Screening for host cell selection

In order to identify cell lines that have the capacity to produce high titers of VSV-NDV, we first performed a screening of five suspension cell lines using conventional cell concentrations of 2×10^6 cells/mL infected at an MOI of 0.01. For some of the cell lines, multiple media formulations were compared. As shown in Fig. 1, all cell lines tested could be infected with VSV-NDV but displayed different cell growth characteristics post-infection in shake flasks. MDCK cells growing in Smith-8 medium (MDCK-S8) and HEK293SF cells growing in PEM_S medium (HEK293SF-P) achieved the highest concentrations after infection ($9.1 \pm 1.2 \times 10^6$ cells/mL and $7.4 \pm 1.1 \times 10^6$ cells/mL, respectively). They also displayed high viabilities (above 90%) until 84 hpi (Fig. 1A,B). BHK-21, AGE1.CR, and AGE1.CR.pIX cell concentrations stagnated at $2.4 \pm 0.1 \times 10^6$ cells/mL until 12 hpi and subsequently began to decrease, whereas HEK293SF cells in Freestyle medium (HEK293SF-F) and Dynamis medium (HEK293SF-D), as well as MDCK cells in Driving-M medium (MDCK-DM), slowly increased their cell concentration until the end of the cultivation period, reaching $3.0\text{--}3.9 \pm 0.9 \times 10^6$ cells/mL (Fig. 1A). The pH decreased during the infection period for all cell lines, ranging from 6.9 to 7.6 depending on the cell type and medium (Fig. 1C). Sharp declines in viability (up to 30%) starting at about 24 hpi were observed for AGE1.CR.pIX, AGE1.CR, and BHK-21 cells. Generally, a continuous growth phase after infection resulted in higher cell viability at the later stages of infection (Fig. 1B). The formation of syncytia, monitored by brightfield and fluorescence (GFP) microscopy, was not observed in any suspension cell line (data not shown). Next, we measured the number of infectious virus particles in the supernatant by TCID_{50} assay. All cell lines showed evidence of virus replication and release starting from 12 hpi. For HEK293SF-DM, HEK293SF-F, HEK293SF-P, MDCK-S8, and MDCK-DM cells, the VSV-NDV titer increased during the entire infection period to a maximum ranging from 10^5 to 10^8 $\text{TCID}_{50}/\text{mL}$. Virus titers above 10^7 $\text{TCID}_{50}/\text{mL}$ were only achieved using BHK-21 and HEK293-SF-P cells, but the virus replication dynamics differed. A strong correlation between maximum viable cell concentration and maximum $\text{TCID}_{50}/\text{mL}$ was observed for all cell lines (Fig. 1A,D).

Interestingly, the VSV-NDV titer produced by HEK293SF cells progressively increased over the entire cultivation period and could be enhanced over 2 logs by using different growth media. This was also true for MDCK cells, where cultivation in the Smith-8 medium

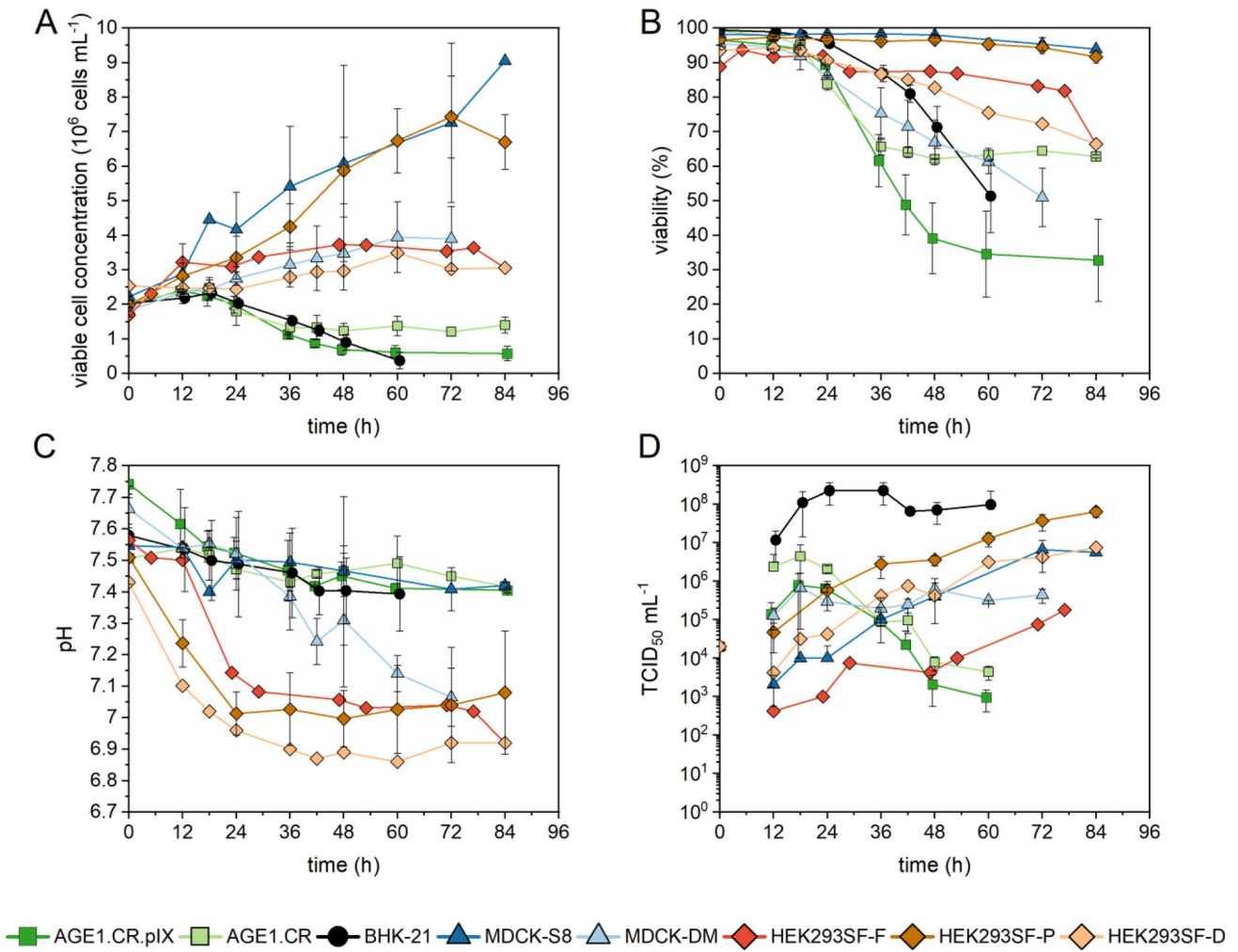


Fig. 1 Growth characteristics of different cell lines after infection with VSV-NDV. Cell growth (A), viability (B), pH (C), and TCID₅₀/mL (D) were compared between five cell lines. The medium was exchanged completely before infection. Cells were grown in baffled 125 mL shake flasks and infected at a viable cell concentration of 2×10^6 cells/mL with VSV-NDV at an MOI of $1E-2$. The TCID₅₀/mL

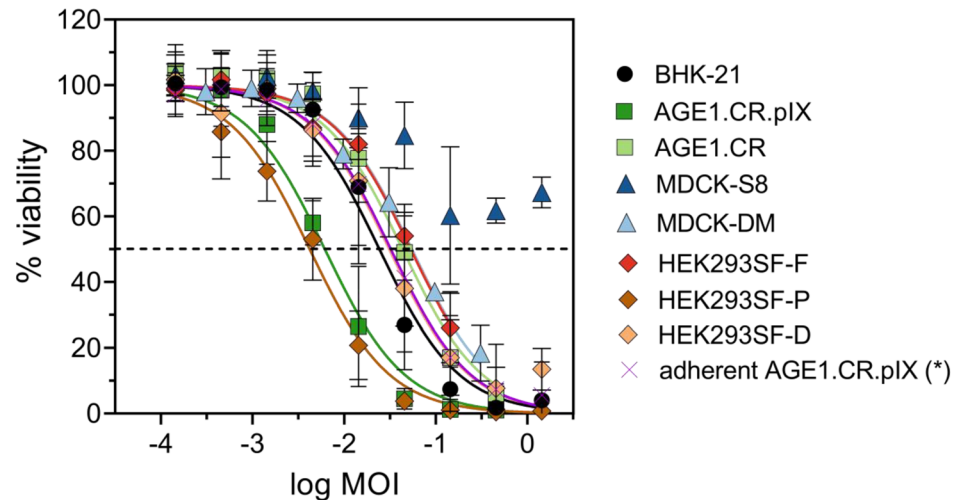
at 0 hpi was calculated empirically, corresponding to an MOI of $1E-2$ (only yellow symbol is visible, as the same MOI was used for all infections). Values (except HEK293SF-F and HEK293SF-D cells) are reported as the mean of a biological duplicate with two independent shake flasks. Error bars represent the standard deviation of duplicates

resulted in 1 log higher titers compared to the Driving-M medium. After reaching the maximum titer, AGE1.CR.pIX and AGE1.CR cells showed a sharp decline in TCID₅₀/mL with reductions up to 3 logs over 3 days (Fig. 1D). BHK-21 cells achieved the highest VSV-NDV titer (up to $2 \pm 1 \times 10^8$ TCID₅₀/mL), with only a 0.5 log₁₀ titer reduction over 3 days in this initial screening experiment. Although both AGE1.CR and AGE1.CR.pIX cells as well as BHK-21 cells exhibited a strong decline in cell concentration starting at 18 hpi, and the viral titer in BHK-21 cell cultures remained relatively stable. This may indicate the presence of a component in the PEM_s medium that could prevent virus degradation.

In order to rule out that the OV produced in suspension cultures did not alter its ability to efficiently kill cancer cells

in vitro, an oncolytic viral potency assay was designed, similar to a previously described method (Almstätter et al. 2015). Peak titers from the individual suspension cultivations infected at MOI 0.01 were compared to the viral supernatant from adherent AGE1.CR.pIX cells infected at MOI 0.01 (peak titers, 24 hpi, Figure S1). Susceptible human hepatocellular carcinoma cells were infected at defined, serial MOI dilutions, and at 48 hpi, cell viability was determined and plotted as dose–response curves normalized to uninfected cells. IC₅₀ values were derived and interpreted as a quantitative measure of VSV-NDV oncolytic potency (Fig. 2). For most cultivation conditions (BHK-21, HEK293SF-F, HEK293SF-D, MDCK-DM, and AGE1CR.pIX cells), oncolysis in Huh7 cells was only marginally affected and resulted in similar logIC₅₀ values compared

Fig. 2 Oncolytic viral potency assay for VSV-NDV produced in suspension cells. Huh7 cancer cell viability was determined at 48 hpi with VSV-NDV-GFP generated in the respective suspension cell line and compared to virus generated in adherent AGE1.CR.pIX cells (*). The graph shows dose–response curves after non-linear regression analysis to calculate the individual IC_{50} and $\log IC_{50}$ values. Values are reported as the mean \pm standard deviation of technical replicates, with $n=3$ for suspension samples and $n=8$ for adherent AGE1.CR.pIX



	BHK-21	AGE1.CR.pIX	AGE1.CR	MDCK-S8	MDCK-DM	HEK293SF-F	HEK293SF-P	HEK293SF-D	*
Log IC_{50}	-1.62	-2.21	-1.36	no value	-1.26	-1.27	-2.38	-1.51	-1.49
IC_{50}	0.0243	0.00615	0.0434	no value	0.0549	0.0532	0.00421	0.0310	0.0323

to virus generated in adherent AGE1.CR.pIX cells. Only virus sampled from MDCK cells infected in Smif8 medium was not able to induce more than 50% oncolysis, and hence, no IC_{50} value is reported. Of note, VSV-NDV generated in suspension AGE1.CR.pIX cells or HEK293SF-P cells cultivated in PEM₅ medium showed a clearly superior oncolytic potency, defined by almost 1 log lower IC_{50} values.

Effect of cell concentration and CaCl₂ supplementation on VSV-NDV production

Since rVSV-NDV is a fusogenic oncolytic virus, which spreads through the formation of syncytia (Abdullahi et al. 2018), close cell-to-cell contacts could improve virus propagation in suspension cell culture. Therefore, all five cell lines at CCD (2.0×10^6 cells/mL) were supplemented with CaCl₂ concentrations ranging from 0.3–1 mM to facilitate cell aggregation (Peshwa et al. 1993) and monitored regarding a

positive effect on the viral spread. The calcium concentration range was based on a previously conducted CaCl₂ sensitivity analysis identifying 0–1 mM to be the optimal range for all tested cell lines (data not shown). Furthermore, while virus propagation at higher cell concentrations often results in a reduction of CSVY (“cell density effect”) (Maranga et al. 2003; Kamen and Henry 2004), the use of appropriate medium exchange strategies before infection can overcome this limitation and further increase virus yields (Vázquez-Ramírez et al. 2018). Therefore, the impact of higher cell concentrations (5.0 and 10.0×10^6 cells/mL) at the time of infection on the maximum infectious virus titer was also evaluated. Each condition was assessed by comparing the respective maximum titers with the maximum titer reached in a control infection (Fig. 1) at 2.0×10^6 cells/mL (Table 1). A greater than 1 log increase/decrease in TCID₅₀/mL was considered a strong response, greater than 0.3 log increase/decrease a slight response, and smaller than 0.3 log increase/

Table 1 Impact of the cell concentration and various CaCl₂ concentrations at time of infection on the TCID₅₀/mL titer

Cell line	5 Mio	10 Mio	0.3 mM CaCl ₂	0.5 mM CaCl ₂	0.9 mM CaCl ₂	1 mM CaCl ₂
AGE1.CR.pIX	+	+	~	~	~	~
AGE1.CR	+	~	~	~	~	~
BHK-21	+	+	~	~	~	~
HEK293 Freestyle	--	--	~	~	~	-
MDCK Smith-8	+	~	n.d	~	n.d	~
MDCK Driving M	~	+	n.d	~	n.d	~

Each condition was rated based on the achieved effect on the TCID₅₀/mL titer compared to control infection at 2×10^6 cells/mL: ++: strong increase above 1 log, +: slight increase above 0.3 log, -: slight decrease below 0.3 log, —: strong decrease above 1 log, ~: no change (within the 0.3 log dilution error of the TCID₅₀ assay). n.d. = not determined

decrease no response, as it was within the dilution error of the TCID₅₀ assay. Although calcium supplementation led to increased cell aggregation (data not shown), viral productivity was not increased, as demonstrated by similar viral titers obtained in the presence of 0.3–1.0 mM CaCl₂ compared to the control. A concentration of 1 mM CaCl₂ led to a slight decrease in virus yield for HEK293SF-F cells. Although higher cell concentrations led to slight increases (between 0.3 and 1 log) or similar TCID₅₀/mL titers for AGE1.CR.pIX, AGE1.CR, BHK-21, MDCK-S8, and MDCK-DM cells compared to the control, increases were all close to the dilution error of the TCID₅₀ assay. Increasing the HEK293SF-F cell concentration before infection to 5.0 or 10.0 × 10⁶ cells/mL had a clear negative impact on the maximum TCID₅₀/mL.

VSV-NDV release dynamics for different cell lines

In the preceding experiments, we were able to identify the most promising cell lines for further optimization. Based on the maximum TCID₅₀/mL, regulatory aspects concerning the cell line as well as production medium (chemically-defined, GMP availability), AGE1.CR.pIX, AGE1.CR, BHK-21, and HEK293SF cells were chosen for further process evaluation. Besides the selection of a suitable host cell, insights into VSV-NDV release dynamics in suspension culture are essential for process optimization. Therefore, MOI studies as well as monitoring of viral spreading and infection ratios via flow cytometry were performed.

To determine the optimum MOI for each cell line and medium, cells were infected at MOIs ranging from 10⁻¹ to 10⁻⁵. As shown in Fig. 3, higher amounts of virus input did not result in higher TCID₅₀/mL for AGE1.CR.pIX, AGE1.CR, and BHK-21 cells. However, maximum values were reached earlier (between 18 and 48 hpi). Interestingly, for HEK293SF cells, lower MOIs resulted in a decrease of about one log in TCID₅₀/mL compared to other cells infected at an MOI of 10⁻². Furthermore, peak titers were reached at 96 hpi, independent of the initial virus load. For all other cell lines, the highest overall titers observed were 1.3 × 10⁹ TCID₅₀/mL at an MOI of 10⁻⁴ for BHK-21 cells at 42 hpi, 5.6 × 10⁷ TCID₅₀/mL for AGE1.CR cells at an MOI of 10⁻⁵ at 42 hpi, and 7.5 × 10⁶ TCID₅₀/mL for AGE1.CR.pIX cells at an MOI of 10⁻⁴ at 48 hpi. The infectious units declined after reaching the maximum titer at all conditions, although at different rates. As already observed in Fig. 1, AGE1.CR and AGE1.CR.pIX cells had the steepest reduction of TCID₅₀/mL by approximately 1.5–2.0 log within 12 h after reaching the peak, whereas HEK293SF and BHK-21 cells showed slower declines of 0.5–1.0 log within 24 h.

In addition to the maximum infectious virus titers achieved, the fold increase of infectious virions is one of the most important criteria in vaccine production. When

comparing the TCID₅₀/mL used at TOI with the peak TCID₅₀/mL achieved, the fold increase was around 37,000 fold, 2,800,000 fold, 3700 fold, and 6,700,000 fold at the optimal infection MOI for AGE1.CR.pIX, AGE1.CR, HEK293SF, and BHK-21 cells, respectively. Considering the CSVY reached an MOI of 10⁻², a twofold increase in CSVY for BHK-21, and a fivefold increase for AGE1.CR and a fourfold increase for AGE1.CR.pIX cells were achieved by lowering the MOI to 10⁻⁴–10⁻⁵. Only HEK293SF cells displayed a fivefold lower CSVY when decreasing the MOI to 10⁻⁴.

To identify the most suitable candidate cell line, optimal MOIs of the respective cell lines were repeated in three independent shake flasks (Table 2). VSV-NDV-mediated GFP expression in infected cells enabled flow cytometry analysis of the proportion of infected cells from shake flask cultivations of the most promising cell lines BHK-21, HEK293SF, and AGE1.CR (Fig. 4). For all cell lines, the first GFP-positive cells were detected at 12 hpi, although only a small fraction of the cells (1–3%) was GFP positive. For BHK-21 cells, the proportion of GFP-positive cells quickly increased to 89 ± 5% at 24 hpi and reached its maximum of 98.9 ± 0.2% at 36 hpi, indicating a complete infection of all cells. In contrast, the GFP-positive cell fraction only gradually increased for HEK293SF cells with 12 ± 3% infected at 24 hpi and 92 ± 1% at 96 hpi. A strong correlation between the time point of reaching the maximum fraction of infected cells and maximum infectious virus titer was observed for both BHK-21 and HEK293SF cells. Interestingly, a maximum of 80 ± 3% of AGE1.CR cells were infected at 36 hpi, while the VSV-NDV titer peaked earlier (at 24 hpi) but subsequently decreased by 2 log units within one day. Consistent with previous results (Sect. 0), VSV-NDV titers were more or less stable for BHK-21 and HEK293SF cell cultures using a PEM_s medium. While a continuous proliferation of HEK293SF cells until 84 hpi could explain the higher virus stability, this was not the case for BHK-21 or AGE1.CR cells.

Adaptation of VSV-NDV to different suspension cell lines

While the seed material, derived from adherent AGE1.CR.pIX cells, propagated well in BHK-21 cells (CSVY reaching 140 TCID₅₀/cell), extracellular titers obtained in AGE1.CR.pIX, AGE1.CR, and HEK293SF cells were relatively low (CSVY < 11 TCID₅₀/cell for AGE1.CR, < 2 TCID₅₀/cell for AGE1.CR.pIX, and < 11 TCID₅₀/cell for HEK293SF cells). Therefore, sequential virus passaging over five passages was conducted to evaluate whether adaptation of the virus to the corresponding host cell line could enhance production. It was hypothesized that sequential adaptation would lead to either: (i) an increase in maximum virus titers due to beneficial alterations

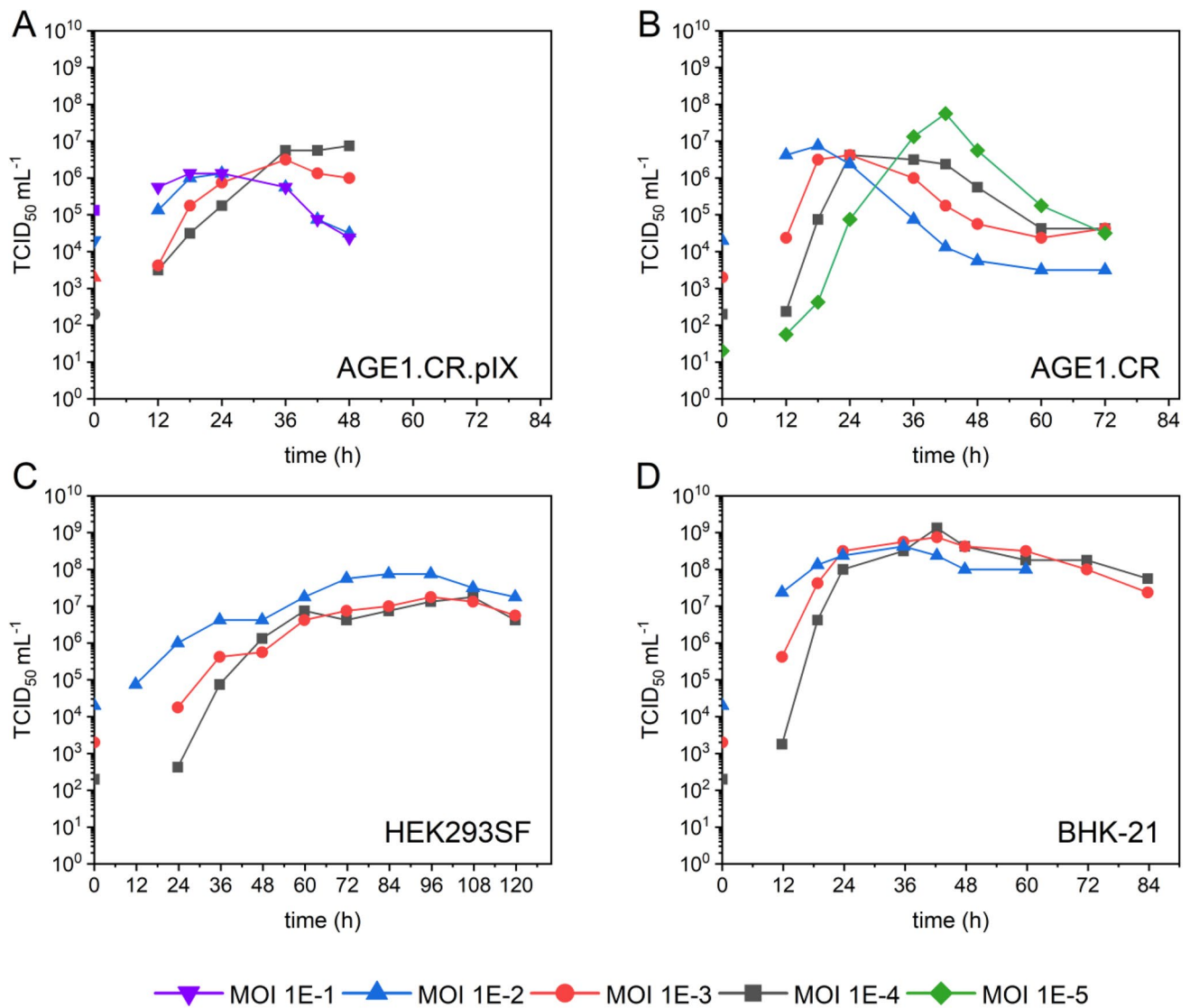


Fig. 3 VSV-NDV infection of four suspension cell lines at different MOIs ranging from 1E-5 to 1E-1 in 125-mL shake flasks. Infectious virus titers were calculated by TCID₅₀ assay and plotted against the time post-infection. The TCID₅₀/mL at 0 hpi was calculated empirically corresponding to the respective MOI. **A** AGE1.CR.pIX in

CD-U7 medium, **B** AGE1.CR pIX in CD-U7 medium, **C** HEK293SF in PEM medium, and **D** BHK-21 in PEM medium. This screening experiment was carried out once. For AGE1.CR and AGE1.CR.pIX, additional MOI were tested to verify the possible beneficial impact

Table 2 VSV-NDV-GFP production in suspension cell cultures. Yields and growth parameters of host cells after infection are shown. Cell concentration, virus decay time, and maximum infectious virus titers were measured in three independent shake flask cultivations

Cell line	Media	Optimum MOI	Max. viable cell concentration ($\times 10^6$ cells mL ⁻¹)	TCID ₅₀ mL ⁻¹	CSVY* (virions cell ⁻¹)	Time of max. titer (h)	1 log decay time (h)
BHK-21 _{sus}	PEM _s	1×10^{-4}	5.0 ± 1.0	$8.8 \times 10^8 \pm 5.6 \times 10^8$	140 ± 84	36–42	<24
HEK293SF	PEM _s	1×10^{-2}	7.7 ± 1.0	$8.3 \times 10^7 \pm 1.4 \times 10^7$	11 ± 3	96	<24
AGE1.CR	CD-U7	1×10^{-5}	4.3 ± 0.6	$4.3 \times 10^7 \pm 2.2 \times 10^7$	11 ± 4	42–48	<12
AGE1.CR.pIX	CD-U7	1×10^{-4}	3.3 ± 0.2	$5.4 \times 10^6 \pm 2.2 \times 10^6$	2 ± 1	48	<12

*CSVY, cell-specific virus yield

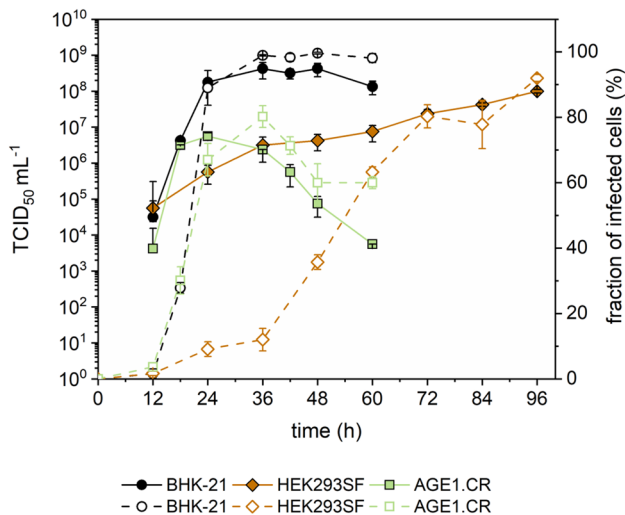


Fig. 4 Infection dynamics of VSV-NDV in BHK-21, AGE1.CR, and HEK293SF cells. BHK-21 and AGE1.CR cells were infected at an MOI of 10^{-4} , while HEK293SF cells were infected at an MOI of 10^{-2} . $\text{TCID}_{50}/\text{mL}$ (full symbols), as determined by TCID_{50} assay, and the fraction of GFP-positive cells determined by FACS analysis (empty symbols) are plotted against the time of infection. Cells were maintained in standard shake flasks and infected at 2×10^6 cells/mL after a complete medium exchange. The fraction of infected cells was determined with the ImageStream X Mark II. Values are reported as the mean \pm standard deviation of two shake flasks

of the viral fitness or virus stability, and/or (ii) a reduction of the timespan to reach the maximum titers due to a selection of fast-replicating viruses, or alternatively (iii) a decrease of infectious virus titers due to the potential enrichment of defective interfering particles (DIPs) or a selective pressure for virus variants that favor longer persistence in the host cell.

Despite blind passaging using non-optimized MOI conditions after the first infection, TCID_{50} titers virus remained high in any cell line. For BHK-21 cells, maximum titers of 2.4×10^8 $\text{TCID}_{50}/\text{mL}$ were obtained in the first passage with a CSVY of 80–100 $\text{TCID}_{50}/\text{cell}$. All subsequent passages achieved maximum titers of around 10^8 $\text{TCID}_{50}/\text{mL}$ at 24 hpi, although it was observed that later passages showed a faster degradation of infectious virus particles later on (Fig. 5D). Also, AGE1.CR and HEK293SF cells produced similar maximum virus titers over five passages (3.2×10^7 $\text{TCID}_{50}/\text{mL}$ and 3.2×10^5 $\text{TCID}_{50}/\text{mL}$, respectively) (Fig. 5B,C). In contrast, virus titers in AGE1.CR.pIX cell cultures increased over the first four passages by about 0.5 log, reaching 1×10^7 $\text{TCID}_{50}/\text{mL}$ (Fig. 5A). In addition, the timespan to reach maximum titers was reduced starting from passage three by one day for AGE1.CR and AGE1.CR.pIX cells and by two and a half days for HEK293SF cells. Although maximum titers could not be significantly increased, CSVYs slightly increased for all cell lines over the sequential passaging (data not shown).

Production of VSV-NDV in BHK-21 and HEK293SF cells in a bioreactor

Due to high yields and stable titers of VSV-NDV in BHK-21 and HEK293SF cell cultures, in the next step, VSV-NDV production was transferred to a 1 L STR ($V_W = 700$ mL) to allow for better control of process parameters and to evaluate the potential for further scale-up. Following the cell growth phase of 3.7 days for BHK-21 and 3.6 days for HEK293SF cells in half of the V_W of PEM_s medium, BHK-21 and HEK293SF cells were infected by addition of 350 mL fresh medium at an MOI of 10^{-4} and 10^{-2} , respectively. Before infection, cell-specific growth rates (μ_{mean}) of 0.027 1/h for both BHK-21 and HEK293SF cells were observed. After infection, BHK-21 cell concentration continued to increase for 12 hpi with a μ_{mean} of 0.023 1/h, followed by a decrease 12 h later due to the cytopathic effect caused by viral replication. Cell viability remained higher than 90% for 36 hpi and rapidly declined afterward (Fig. 6A). The pH remained stable and was efficiently controlled at 7.2 ± 0.1 (data not shown). In contrast, HEK293SF cell concentration continued to increase until 96 hpi with a μ_{mean} of 0.018 1/h, reaching a maximum cell concentration of 5.7×10^6 cells/mL. Cell viability was higher than 90% for the entire cultivation (Fig. 6B). The pH was efficiently controlled at 7.2 ± 0.2 , slightly increasing at the end of the cultivation (data not shown).

For BHK-21 cells, virus production peaked at 30 hpi with 2.4×10^8 $\text{TCID}_{50}/\text{mL}$ (CSVY of 84 $\text{TCID}_{50}/\text{cell}$). As before, the $\text{TCID}_{50}/\text{mL}$ slowly declined thereafter by 0.5 log within 24 h. Overall, maximum virus titer, CSVY, and virus stability were similar to the reference infections in shake flasks (Table 2), where no complete medium exchange was performed before infection. Although HEK293SF cells reached high virus titers in shake flasks (Table 2), this was not observed for the 1 L STR culture. At 58 hpi, a maximum infectious titer of only 2.4×10^5 $\text{TCID}_{50}/\text{mL}$ was reached, which corresponds to a 2.5 log reduction compared to previous shake flask runs. Due to the low virus titer and prolonged cell proliferation after infection, only a low CSVY of 0.04 $\text{TCID}_{50}/\text{cell}$ was obtained.

As an indication of the cell's metabolic activity, the concentration of the main carbon and energy sources, glucose and glutamine, as well as their metabolic by-products, lactate, and ammonium, were monitored before and after infection with VSV-NDV (Fig. 7). As expected, no limitation of glucose was observed for either cell line during the entire cultivation run. Despite high glutamine concentrations in the PEM_s medium, depletion occurred at 24 hpi for BHK-21 cells. Moreover, the addition of a new medium after infection could not prevent the accumulation of ammonium (2–3 mM) and lactate (20 mM) to high (and typical toxic) concentrations. Interestingly,

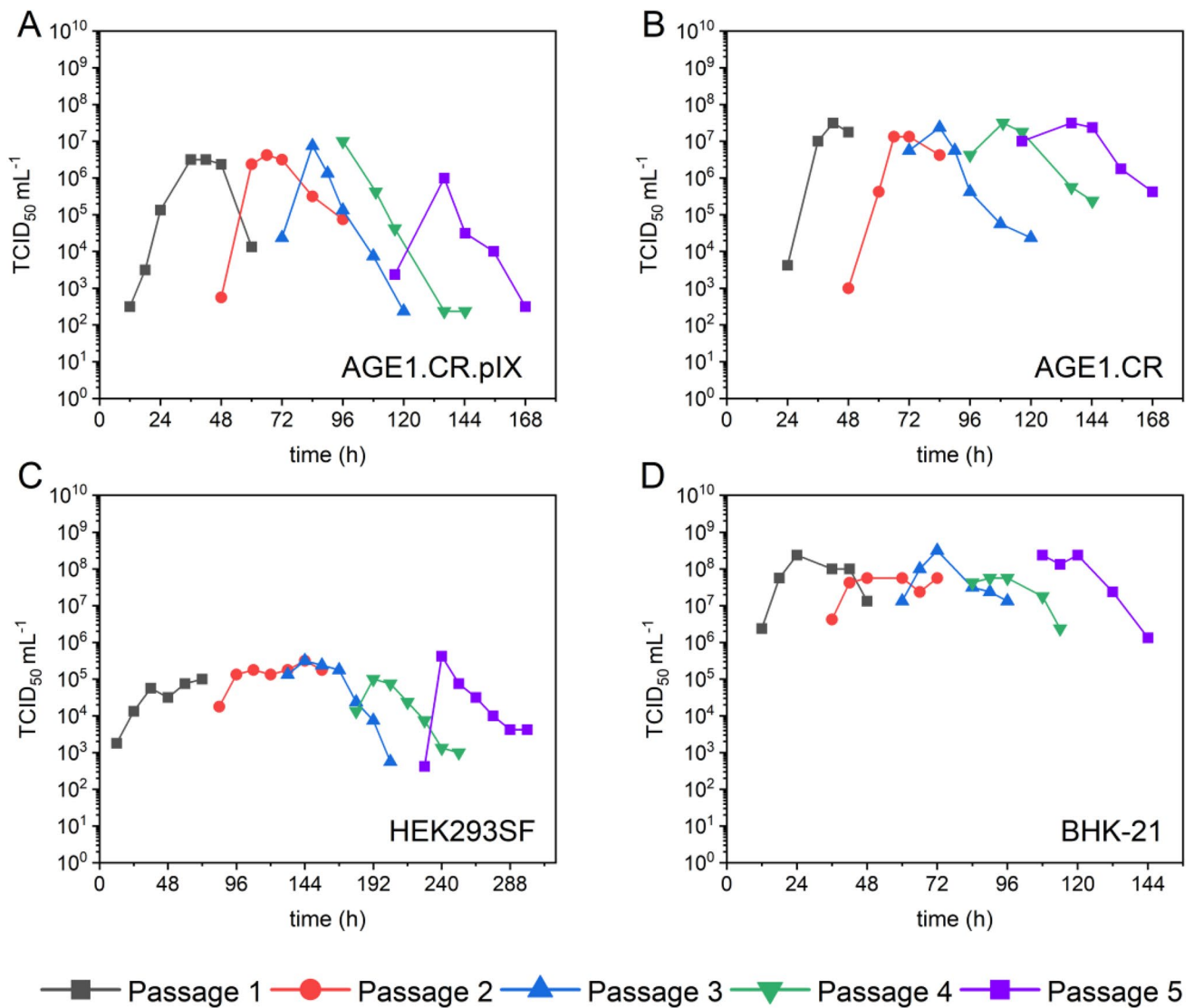


Fig. 5 Infectious virus titers during sequential adaptation of VSV-NDV in different suspension cell lines. AGE1.CR.pIX, AGE1.CR, HEK293SF, and BHK-21 cells were cultivated in shake flasks in CD-U7, Dynamis, and PEM medium, respectively. Initial infection occurred during the mid-exponential growth phase at the previously

determined optimal MOI. Subsequent virus passaging was performed blindly using a fixed volume. TCID₅₀/mL are plotted against the time post-infection. Each color indicates a different virus passage. Shake flask runs were carried out as individual experiments for time, workload, and cost reasons

for HEK293 cells, glutamine was sufficiently maintained during the entire cultivation, and ammonium, as well as lactate, remained below critical values during the virus production phase.

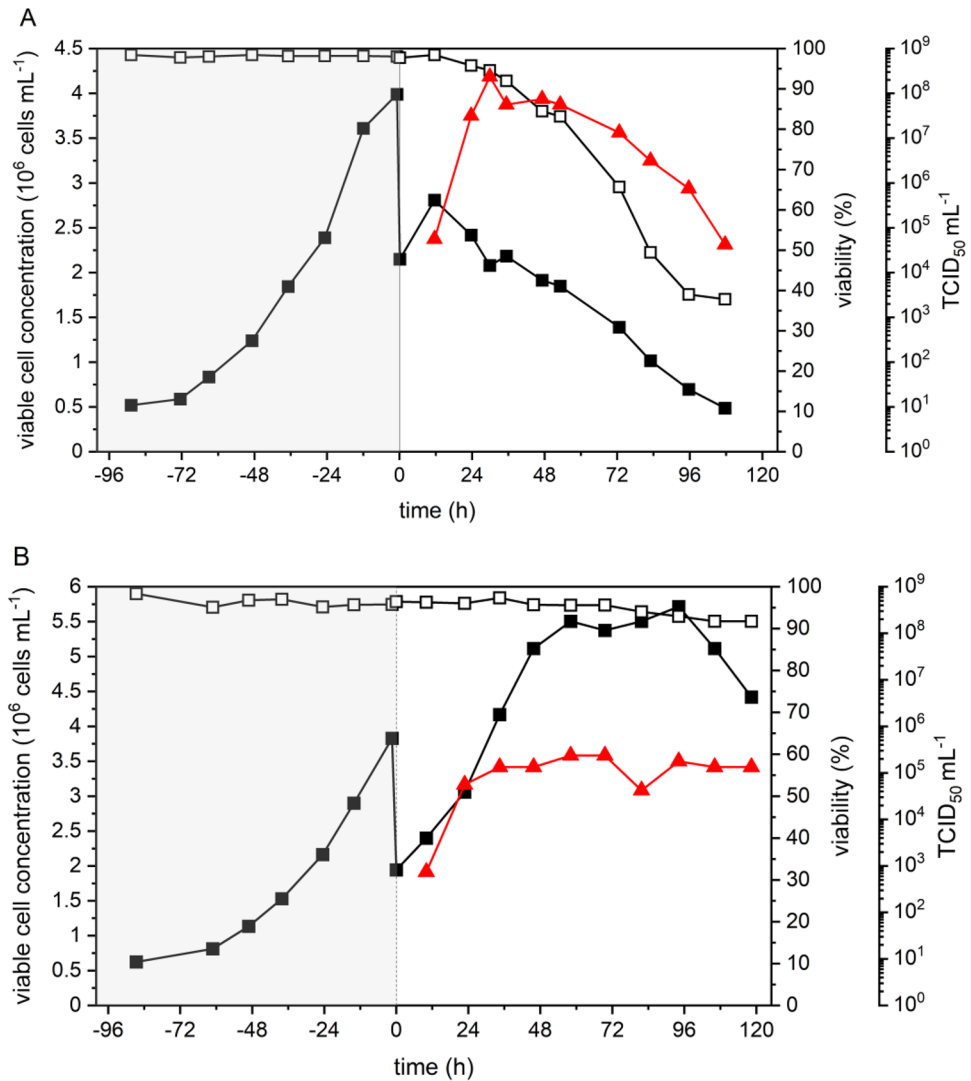
Next, we analyzed whether the process conditions in a STR affected the ability of the virus to induce oncolytic killing in susceptible Huh7 cells using the IC₅₀ potency assay. Samples from the bioreactor were compared to a seed virus stock generated in adherent AGE1.CR.pIX cells. As indicated in Fig. 8, VSV-NDV harvested from the 1 L STR of HEK293SF or BHK-21 cell cultures had a similar oncolytic potential in Huh7 cells compared to the control. Remarkably, the dose required to induce 50% cancer cell cytotoxicity was

more than 1 log lower for VSV-NDV produced in suspension bioreactor cultures.

Discussion

Currently, 80 clinical trials with oncolytic viruses are registered at ClinicalTrials.gov, and one such agent, an oncolytic herpes virus against melanoma (IMLYGIC®, Amgen Inc.) has obtained market approval in the US and Europe in 2015. As such novel therapies gain traction, the need for robust, efficient, and scalable manufacturing processes for oncolytic viruses becomes evident. The aim of this study was to

Fig. 6 Growth and rVSV-NDV production for BHK-21 and HEK293SF cells in a 1 L bioreactor. BHK-21 (A) and HEK293SF cells (B) were cultured in a 350 mL supplemented PEM medium. After a cell growth phase of 96 h, cells were infected with VSV-NDV at an MOI of 0.0001 and 0.01, respectively, by adding 350 mL of fresh PEM_s medium. Cell concentration (black square), VSV-NDV titer (red triangle), and viability (empty black square) are shown. The dotted vertical line indicates the time of infection; the gray area indicates the cell growth phase. Bioreactor runs were carried out as individual scouting experiments



explore the applicability of different suspension cell lines for the production of rVSV-NDV. As a fusogenic oncolytic virus, it poses unique challenges for manufacture because it kills host cells rapidly via syncytia formation and replicates to relatively poor yields in cell cultures. Previous results with anchorage-dependent AGE1.CR.pIX cells (Abdullahi et al. 2018) are not easily translated to large-scale manufacturing and process intensification (Genzel and Reichl 2009; Gallo-Ramírez et al. 2015). Therefore, cell lines already adapted to growth in suspension (Supplement Table S1) and have been used to produce other viruses in bioreactors (Jordan et al. 2009; Lohr et al. 2009, 2010; Chu et al. 2009; Grieger et al. 2016; Nikolay et al. 2018), were tested in this study against oncolytic VSV-NDV.

Screening for host cell selection

All tested cell lines (of avian, rodent, canine, and human origin) were permissive to VSV-NDV but differed in cell

line-specific virus growth characteristics, with maximum virus yields spread over 3 orders of magnitude (Fig. 1). The envelope of VSV-NDV contains two associated glycoproteins from NDV that mediate viral entry and cell-to-cell fusion: the hemagglutinin-neuraminidase (HN) and a modified fusion (F) protein for an enhanced cell–cell fusion potential (Sánchez-Felipe et al. 2014; Abdullahi et al. 2018). HN recognizes and binds to sialoglycoconjugates (Sia) on the cell surface, specifically α2,6-linked Sia, which appears to be present at comparably low levels in all tested cell lines (Genzel and Reichl 2009; Lohr et al. 2012; Chu et al. 2019). The observed differences in virus replication indicate that receptor abundance alone may not be a decisive factor in determining yields also of this replication-competent virus in a given host cell. However, it should be noted that VSV-NDV may utilize additional or alternative cell surface receptors for infection, as the modes of binding, entry, and fusion of this novel hybrid vector are not yet fully understood.

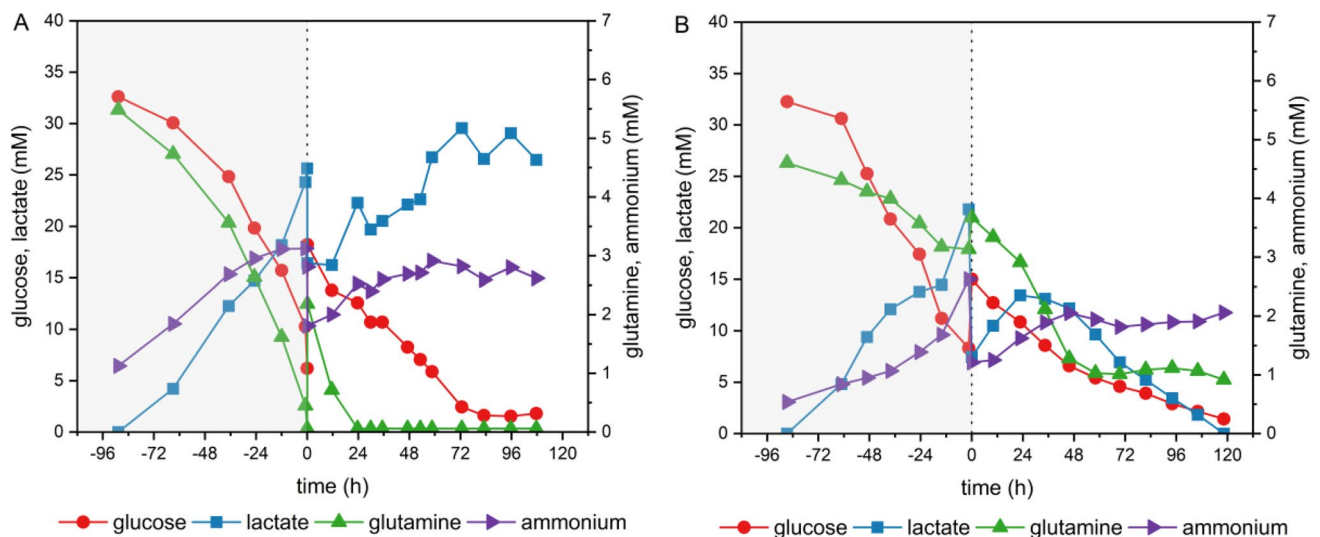
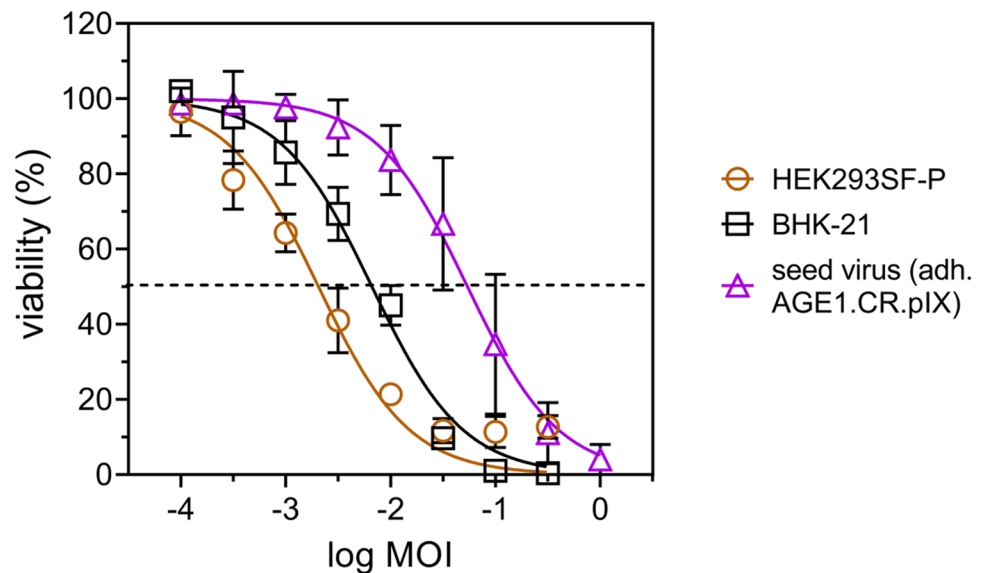


Fig. 7 Time course of metabolites for BHK-21 and HEK293SF cells in a 1 L bioreactor. BHK-21 (A) and HEK293SF cells (B) were cultured in 350 mL supplemented PEM medium. After a cell growth phase of 96 h, cells were infected with VSV-NDV at an MOI of 0.0001 and 0.01, respectively, by adding a 350 mL of fresh PEM_s

medium. Glucose, lactate, ammonium, and glutamine concentrations were measured with the BioProfile® 100 Plus (Nova Biomedical, USA). The dotted vertical line indicates the time of infection; the gray area indicates the cell growth phase. Bioreactor runs were carried out as a single scouting experiment

Fig. 8 Oncolytic potency of VSV-NDV produced in a 1 L STR. The cancer cell killing potential of VSV-NDV harvested from the individual bioreactor cultivations was assessed by IC₅₀ assay in human HCC cells (Huh7) and compared to the initial seed stock used for infection. Cell viability was monitored by CellTiter-Glo Assay (Promega). The graph shows dose–response curves after non-linear regression analysis to calculate the individual IC₅₀ and logIC₅₀ values shown in the table below. Values are reported as the mean ± standard deviation of technical replicates, with $n = 3$ for seed stock and bioreactor samples, respectively



	BHK-21	HEK293SF-P	seed virus (adh. AGE1.CR.pIX)
Log IC ₅₀	-2.18	-2.69	-1.27
IC ₅₀	0.00664	0.00205	0.05409

VSV-NDV has an inherent cancer cell specificity but was also shown to replicate in adherent, immortalized cell lines, e.g., AGE1.CR.pIX and BHK-21 cells, with modest titers of 10^6 TCID₅₀/mL (Abdullahi et al. 2018). In comparison, infections in suspension AGE1.CR, MDCK, HEK293SF, and BHK-21 cells (Fig. 1) yielded 10- to 100-fold increases in TCID₅₀/mL.

The heterogenous curves in Fig. 1 illustrate some of the counteracting processes during productive viral infections. Virus replication usually is strong in host cells in the log phase of proliferation when the supply of nutrients is not limiting. Here for VSV-NDV, maximum titers were achieved in all cell lines ± 12 h after peak cell concentration. As the productivity of infected cells declines, the stability of virions

becomes increasingly important. Productivity inversely correlates with viability decreased at different rates for the various cell lines. A pronounced decline was observed in AGE1.CR, AGE1.CR.pIX, and MDCK-DM cultures start about 18 hpi. CPE was strong also in BHK-21, and to a lesser degree in HEK293SF-D cultures.

The stability of virions can be affected by the absorption of cellular debris and the release of cellular proteases after virus-induced cell lysis. Depending on the culture environment (especially the capacity of the medium to buffer pH changes and content of hydrolysates, protein, and divalent cations), such effects can be more or less detrimental to the infectious units. In contrast to the avian cells, although the viability of BHK-21 and MDCK-DM cells clearly declined by 36 hpi, the TCID₅₀/mL remained relatively stable.

Previous studies showed that VSV-NDV primarily spreads through cell-to-cell contacts supported by the formation of syncytia in adherent cell cultures (Abdullahi et al. 2018). This suggests that aggregate formation in suspension cell cultures could also promote viral spread and productivity. Indeed, for MDCK cells growing as aggregates (MDCK-S8), we observed a 1 log higher TCID₅₀/mL compared to single-cell suspensions (MDCK-DM). Nevertheless, no syncytia formation was observed in suspension cultures for any cell line regardless of the used medium, and cell aggregation, in general, did not seem to be the most important factor for high VSV-NDV yields.

While efficient oncolytic virus manufacture in suspension cultures was our primary aim, the quality of the VSV-NDV product was an obvious concern. We confirmed that VSV-NDV stocks produced in the suspension cell lines investigated are not compromised in their oncolytic potency compared to virus stocks produced in adherent cultures. Only virus harvested from MDCK cells in Smif8 media caused poor oncolysis in susceptible Huh7 cells, although the titers were superior compared to the Driving medium. This observation underlines the importance of cultivation media and might point to a change in viral integrity or virus aggregation negatively influencing oncolysis. In contrast, the improved potency values for rVSV-NDV produced in AGE1.CR.pIX and HEK293SF-P cells might be explained by superior viral integrity or possibly by beneficial changes in the ratio of infectious virions to DIPs. As further discussed below, the impact of DIPs on tumor cell lysis and the CPE is being investigated in ongoing studies.

Effect of cell concentration and CaCl₂ supplementation on VSV-NDV production

Our data suggest that cell-to-cell contact is not critical for the production of VSV-NDV in suspension cultures. This was further confirmed as induction of cell clumping via supplementation of CaCl₂ did not lead to a measurable increase

in infectious virus titers (Table 1), taking into account the dilution error of the TCID₅₀ assay. Although cell-to-cell proximity should allow for a more efficient viral spread, virus production was not increased. This is in line with observations made for cancer cells, which demonstrated that tumor cell killing with VSV-NDV was similar to that of the parental VSV vector, despite virus replication of the hybrid virus being substantially attenuated compared to the parental VSV (Abdullahi et al. 2018). Although this is one of the safety benefits of VSV-NDV and other fusogenic OV_s (Krabbe and Altomonte 2018), it also causes manufacturing challenges. In fact, as mentioned before, this was one of the rationales for the establishment of a suspension culture-based VSV-NDV production process. The exact mechanisms of and dependencies on syncytial cell death and cell-to-cell spread are not yet fully understood for VSV-NDV, but they could be a potent parameter to further optimize viral replication during production. Moreover, closer cell-to-cell contacts induced by higher cell densities at the time of infection also did not result in a significant increase in titers for AGE1.CR, AGE1.CR.pIX, MDCK, and BHK-21 cells. Indeed, a substantial decrease in yields was observed for HEK293SF cells at higher cell densities. The latter is most likely due to nutrient limitations and/or inhibitor accumulation, the so-called “cell density effect,” commonly observed for adenovirus production in HEK293 cells (Kamen and Henry 2004).

VSV-NDV release dynamics for different cell lines

We next tried to improve viral titers by determining the optimal MOI. All cell lines, except HEK293SF, demonstrated a clear benefit of using lower MOIs (10^{-4} – 10^{-5}) (Fig. 3). Interestingly, for a lentogenic NDV dependent on an exogenous protease for replication in AGE1.CR.pIX cultures, high yields were obtained with an MOI as low as 10^{-7} (Jordan et al. 2016). Accordingly, options for further reductions in MOI should be tested in subsequent optimization studies to investigate whether the maximum infectious titers can be increased even more.

However, in addition to viral yield and titer, the ratio of the viral genome and subgenomic copies to the actual infectious units is an important parameter (Fernandes et al. 2016). A recent study with wild-type VSV reported increased accumulation of noninfectious viral genomes at lower MOIs of 10^{-3} – 10^{-4} , mainly caused by loss of infectious activity due to longer production times (Kiesslich et al. 2020). In follow-up studies, this aspect should be critically assessed to evaluate the potential effect of a reduction of MOI on the final product quality.

Variations in the abundance of DIPs as a consequence of the manufacturing process should also be monitored and carefully discussed in terms of downstream therapeutic implications. DIPs, by definition, interfere with the

replication of infectious viral progeny. However, because DIPs may stimulate type I IFN-mediated innate immune responses (Yang et al. 2019; Rand et al. 2021), they can contribute to an important therapeutic mechanism. Recent studies have highlighted antitumor effects of defective viruses, for example, via induction of cell-selective apoptosis in cancer cells through RIG-I-dependent signaling as well as activation of antitumor immunity induced by dendritic cells and T cells (Yang et al. 2019). As the accumulation of DIPs is more likely to occur upon infection at high MOIs, infection at low MOIs could lead to a reduction in DIP concentration (Heldt et al. 2013; Hein et al. 2021), thereby reducing the possible indirect antitumor effect, but potentially enhancing the direct oncolytic effect. As the competing mechanisms regarding the effects of contaminating DIPs in OV drug products are quite complex, this is beyond the scope of the current investigation. Further studies quantifying infectious virion to DIP ratios as well as characterizing their relevance during oncolysis and their therapeutic efficacy should be performed for optimization of virus-based cancer therapeutics.

In the next step, virus infection dynamics were studied in AGE1.CR, HEK293SF, and BHK-21 cell populations using flow cytometry (Fig. 4). The low percentage of infected cells during the first 12 hpi was mainly due to the low virus input (MOI 10^{-2} or 10^{-4}). Despite a 100-fold higher initial virus input for HEK293SF cells, the fraction of infected cells increased only slowly over the entire cultivation period, reaching a maximum of 96 hpi. This suggests a delay in the onset of intracellular replication. Especially with respect to increased shear forces due to stirring of suspension cultures, it was also speculated that VSV-NDV may spread primarily through single-cell infection rather than fusion, resulting in a slower gradual infection of the cell population. This could be the reason why lower MOIs led to lower TCID₅₀/mL in HEK293SF, as only a fraction of the cells could be infected.

The cell-specific differences in optimal MOI may also be explained by varying levels of efficiency in interferon (IFN) signaling in the respective cell lines. As an RNA virus, VSV-NDV is extremely sensitive to the antiviral actions of type I IFNs (Abdullahi et al. 2018). Upon infection with very low MOIs, IFN-functional cells would quickly sense the infection, trigger IFN signaling cascades, and alert neighboring, still uninfected cells to shift into an antiviral state. Thereby, virus replication in cells that become infected at later stages in the manufacturing process would be attenuated. Consistent with such a mechanism, complete infection of the AGE1.CR cells population was not achieved, and a maximum titer was encountered when only 70% of the population was infected. This indicates an efficient de novo generation of infectious virus, but induction of cell death before the whole population could be infected. Such a course is typically observed in highly susceptible adherent cancer cells, such as Huh7 and HepG2 cells (Abdullahi et al. 2018). From a

virus production perspective, it appears favorable to achieve a continuously increasing population of OV-infected cells rather than losing the cell-substrate due to fast oncolysis before high titers are reached. Accordingly, the influence of the MOI on the percentage of infected cells and virus yields should be further investigated. Alternatively, yields may also be higher in processes where interferons may be removed by perfusion cultivation.

Adaptation of VSV-NDV to different suspension cell lines

Adaptation of a virus to a host cell by serial passaging is likely to improve its replication dynamics. For example, an earlier onset of influenza virus release during virus adaptation has been described in Vero and HEK293 cells (Le Ru et al. 2010; Genzel et al. 2010) and for lentogenic NDV in CR.pIX cells (Jordan et al. 2016). In our study with VSV-NDV, serial passaging for five cycles also yielded an adapted oncolytic virus population with an earlier onset of virus accumulation in the supernatant. With the adapted virus seed, maximum titers were obtained one day faster for AGE1.CR and AGE1.CR.pIX cells and 2.5 days earlier for HEK293SF cells (Fig. 5). While TCID₅₀/mL was not increased significantly for any cell line, virus stability was drastically reduced. This is likely due to the enhanced CPE of the adapted virus, which reduced cell proliferation and led to increased cell lysis after infection compared to the non-adapted virus (Supplement Figure S2). We speculate that the shortened time span to reach maximum titers is a result of more efficient intracellular virus replication and shows that adaptations can be a crucial parameter to improving OV process performance.

A previous study described improved replication for a recombinant VSV virus expressing a chimeric Sindbis glycoprotein after low-MOI infection and adaptation over 15 passages (Gao et al. 2006). This was mainly credited to an increased expression of the glycoprotein on the viral surface, which resulted in higher infectivity and greater stability (Gao et al. 2006). Theoretically, an elevated expression of the HN and F-proteins on the rVSV-NDV surface could also lead to higher infectivity, but quantitative data on VSV-NDV glycoprotein expression levels are not yet available. Furthermore, as titers did not increase substantially and virus stability appeared to be reduced after repetitive passaging (Fig. 5), other mechanisms may apply under the conditions investigated here.

Furthermore, for VSV, it is known that lower passage numbers (1–8) can maintain viral fitness but are suboptimal for sustaining gains of function, and the passaging MOI is likewise critical for efficient adaptation (Gao et al. 2006; Thompson and Yin 2010). Moreover, as the passaging time span was reduced, lower (only retrospectively defined) MOIs

were used in subsequent passages due to lower virus titers at the respective time point. The observed unfavorable adaptation curves in Fig. 5 can be interpreted by generation and fast accumulation of DIPs that negatively affect infectious titers and counteract adaptation. They may also be caused if passaging with a low virus load leads to a phenomenon called Muller's ratchet, the progressive reduction of viral fitness when detrimental mutations become fixed in a viral population, thereby decreasing overall fitness (Chao 1990; Gao et al. 2006; Sanjuán and Domingo-Calap 2019). Generation of DIPs is favored by higher MOIs, whereas effects by Muller's ratchet are facilitated by low MOIs. Retrospective calculation of MOI over the five passages revealed broad cell line-dependent ranges: (i) BHK-21 cells 10^{-2} – 10^{-3} , (ii) AGE1.CR cells 10^{-4} – 10^{-7} , (iii) AGE1.CR.pIX cells 10^{-4} – 10^{-5} , and (iv) HEK293SF cells 10^{-2} – 10^{-6} . This variation in MOI could be resolved by switching from a fixed-volume-based passaging to a fixed-MOI passaging. In support of such an approach, Thompson et al. reported that changes in virus yield over the first six passages in fixed-MOI (0.1) passaging of wild-type VSV on adherent BHK-21 cells were prevented (Thompson and Yin 2010). Nevertheless, from the adaptation experiment performed with VSV-NDV, we are optimistic that, with a careful choice of MOI and timespan as soon as a final production process is defined, we can maximize viral fitness and adapt the oncolytic virus to the most favorable producer cell line. Next-generation sequencing of virus populations obtained by passaging could also be instructive in identifying virus adaptation at a genomic level and may allow targeted improvements.

Production of VSV-NDV in BHK-21 and HEK293SF cells in a bioreactor

Based on promising oncolytic virus titers obtained in small-scale shake flasks and the potential for process intensification, we used BHK-21 and HEK293SF cells as a model to scale the process to 1 L STR. The use of benchtop bioreactors resulted in slightly lower $\text{TCID}_{50}/\text{mL}$ titers (between 0.3 and 1 log) for BHK-21 cells and drastically reduced titers for HEK293SF cells compared to shake flask cultivations with similar virus dynamics. The addition of a fresh supplemented PEM medium at TOI could not prevent glutamine depletion and substantial accumulation of lactate and ammonium for BHK-21 cells. High concentrations of lactate (above 20 mM) and ammonium levels of 2–3 mM have been shown to negatively impact virus vaccine production (Schneider et al. 1996). However, these limits were not exceeded for the HEK293SF cell culture. Interestingly, a decrease in lactate concentration was observed starting at 24 hpi once the glucose level dropped below 10 mM, demonstrating the ability of HEK293SF cells to use lactate as a carbon source after glucose depletion (Liste-Calleja et al. 2015).

We suspect that the medium addition at TOI did not allow to provide sufficient nutrients and dilute spent metabolites for HEK293SF cells. This so-called cell density effect is well known, even at low cell densities (above 1×10^6 cells/mL) for adenovirus production in HEK293 cells (Kamen and Henry 2004). Despite an unfavorable metabolic state of BHK-21 cells in the STR, a relatively high CSVY of 84 was reached. In light of future preclinical and clinical studies using VSV-NDV and assuming a dose requirement of at least 1×10^8 $\text{TCID}_{50}/\text{patient}$, this CSVY would allow the production of approximately 1800 dose equivalents per 1 L run (disregarding losses during downstream processing at this time of the development).

The small number of replicates for most of the experiments and the large reported error of the TCID_{50} assay are limitations of this study. Because the scope of this study was to determine whether single-cell suspension cultures can be used at all to produce fusogenic oncolytic viruses at high titers in a potentially scalable production process, the focus was on the screening process. For this reason, no statistical analysis was carried out, and with exception of the evaluation of the optimum MOI, reproducibility was not further investigated. Results obtained here identify cell line-dependent challenges for upstream processing and should help to guide scale-up developments. To overcome metabolic limitations and augment the production of the fusogenic oncolytic virus, higher cell concentrations in a fed-batch or perfusion mode cultivation should be considered. Perfusion systems utilizing a variety of cell retention devices to achieve higher cell concentrations and higher virus titers have been used successfully for virus production (Gränicher et al. 2020; Coronel et al. 2020). For the production of cell contact-dependent fusogenic oncolytic viruses, high cell density suspension cultures have not been described so far. However, we believe that such approaches hold much promise for further productivity improvements.

Here, we defined cell substrate, media, and MOI as critical process parameters for VSV-NDV production. Beyond achieving high infectious virus titers, a comprehensive screening and testing of the produced material are required before a final decision regarding process conditions, including cell line and media selection, can be made for clinical-grade manufacturing. This concerns, for example, studies in mouse and rat tumor models and serum stability investigations. Moreover, further investigations involving multiple replicates to determine reproducibility for selected conditions are critical.

In summary, this work represents an important step forward in the establishment and optimization of efficient and scalable manufacturing processes for virotherapeutic drug development, particularly as OV's make their way into broader clinical applications. In addition to optimization of

infectious yields, the influence of process parameters on the oncolytic activity of virus preparations (possibly containing contaminating DIPs) needs to be confirmed by studies in preclinical tumor models.

Supplementary Information The online version contains supplementary material available at <https://doi.org/10.1007/s00253-022-12027-5>.

Acknowledgements The authors would like to thank Ilona Behrendt for the excellent technical support, Teresa Krabbe for her participation in fruitful discussions, and Shanghai BioEngine Sci-Tech and Prof. Tan from the East China University of Science and Technology for providing the Xeno™ medium. The help of M. Prömmel and B.Hundt (Ceva Innovation Center GmbH) on the BHK21 cells, I. Jordan and V. Sandig on the AGE1.CR and AGE1.CR.pIX cells, and Francesc Gòdia (Autonomous University of Barcelona), as well as C.F. Sheng (National Research Council of Canada), are equally acknowledged.

Author contributions Conceptualization: S.G., F.K., Y.G., U.R., and J.A. Methodology: S.G., F.K., and Y.G. Investigation: S.G., K.J.C., and F.K. Writing—original draft: S.G. and F.K. Writing—review and editing: S.G., F.K., K.J.C., I.J., V.S., Y.G., U.R., and J.A. Supervision: Y.G., U.R., and J.A. Project Administration: S.G. and Y.G.

Funding Open Access funding enabled and organized by Projekt DEAL. Part of the funding for this work was provided by the EXIST-Forschungstransfer program (financed by the Federal Ministry for Economic Affairs and Energy) under grant agreement #03EFOBY215 awarded to J. Altomonte.

Data availability Data is available in the article's Supplementary material. Additional data is available on request from the authors. The data that support the findings of this study are available from the corresponding author, Yvonne Genzel, upon reasonable request.

Declarations

Ethics approval This article does not contain any studies with human participants or animals performed by any of the authors.

Consent to participate Not applicable.

Consent for publication Not applicable.

Conflict of interest J. Altomonte (WO 2017/198779) holds a patent for the development and use of rVSV-NDV as an oncolytic therapy for cancer. I. Jordan and V. Sandig are employees of ProBioGen AG where AGE1.CR, AGE1.CR.pIX, and CD-U7 have been developed.

Open Access This article is licensed under a Creative Commons Attribution 4.0 International License, which permits use, sharing, adaptation, distribution and reproduction in any medium or format, as long as you give appropriate credit to the original author(s) and the source, provide a link to the Creative Commons licence, and indicate if changes were made. The images or other third party material in this article are included in the article's Creative Commons licence, unless indicated otherwise in a credit line to the material. If material is not included in the article's Creative Commons licence and your intended use is not permitted by statutory regulation or exceeds the permitted use, you will need to obtain permission directly from the copyright holder. To view a copy of this licence, visit <http://creativecommons.org/licenses/by/4.0/>.

References

- Abdullahi S, Jäkel M, Behrend SJ, Steiger K, Topping G, Krabbe T, Colombo A, Sandig V, Schiergens TS, Thasler WE, Werner J, Lichtenthaler SF, Schmid RM, Ebert O, Altomonte J (2018) A novel chimeric oncolytic virus vector for improved safety and efficacy as a platform for the treatment of hepatocellular carcinoma. *J Virol* 92:1–18. <https://doi.org/10.1128/jvi.01386-18>
- Almstätter I, Mykhaylyk O, Settles M, Altomonte J, Aichler M, Walch A, Rummey EJ, Ebert O, Plank C, Braren R (2015) Characterization of magnetic viral complexes for targeted delivery in oncology. *Theranostics* 5:667–685. <https://doi.org/10.7150/thno.10438>
- Caron AL, Biaggio RT, Swiech K (2018) Strategies to suspension serum-free adaptation of mammalian cell lines for recombinant glycoprotein production. In: *Methods in molecular biology*. Humana Press Inc., pp 75–85
- Chao L (1990) Fitness of RNA virus decreased by Muller's ratchet. *Nature* 348:454–455. <https://doi.org/10.1038/348454a0>
- Chu C, Lugovtsev V, Golding H, Betenbaugh M, Shiloach J (2009) Conversion of MDCK cell line to suspension culture by transfecting with human *siat7e* gene and its application for influenza virus production. *Proc Natl Acad Sci U S A* 106:14802–14807. <https://doi.org/10.1073/pnas.0905912106>
- Chu Z, Gao X, Liu H, Ma J, Wang C, Lu K, Han Q, Wang Y, Wang C, Adam FEA, Wang X, Xiao S, Yang Z (2019) Newcastle disease virus selectively infects dividing cells and promotes viral proliferation. *Vet Res* 50:27. <https://doi.org/10.1186/s13567-019-0644-0>
- Cook M, Chauhan A (2020) Clinical application of oncolytic viruses: a systematic review. *Int J Mol Sci* 21:1–36. <https://doi.org/10.3390/ijms21207505>
- Coronel J, Gränicher G, Sandig V, Noll T, Genzel Y, Reichl U (2020) Application of an inclined settler for cell culture-based influenza A virus production in perfusion mode. *Front Bioeng Biotechnol* 8:672. <https://doi.org/10.3389/fbioe.2020.00672>
- Elahi SM, Shen CF, Gilbert R (2019) Optimization of production of vesicular stomatitis virus (VSV) in suspension serum-free culture medium at high cell density. *J Biotechnol* 289:144–149. <https://doi.org/10.1016/j.jbiotec.2018.11.023>
- FDA (2010) Characterization and qualification of cell substrates and other biological materials used in the production of viral vaccines for infectious disease indications | FDA. <https://www.fda.gov/regulatory-information/search-fda-guidance-documents/characterization-and-qualification-cell-substrates-and-other-biological-materials-used-production>. Accessed 12 Mar 2021
- Fernandes P, Silva AC, Coroadinha AS, Alves PM (2016) Upstream bioprocess for adenovirus vectors. In: *Adenoviral vectors for gene therapy: second edition*. Elsevier Inc., pp 139–161
- Gallo-Ramírez LE, Nikolay A, Genzel Y, Reichl U (2015) Bioreactor concepts for cell culture-based viral vaccine production. *Expert Rev Vaccines* 14:1181–1195
- Gao Y, Whitaker-Dowling P, Watkins SC, Griffin JA, Bergman I (2006) Rapid adaptation of a recombinant vesicular stomatitis virus to a targeted cell line. *J Virol* 80:8603–8612. <https://doi.org/10.1128/jvi.00142-06>
- Genzel Y (2015) Designing cell lines for viral vaccine production: where do we stand? *Biotechnol J* 10:728–740
- Genzel Y, Reichl U (2009) Continuous cell lines as a production system for influenza vaccines. *Expert Rev Vaccines* 8:1681–1692
- Genzel Y, Dietzsch C, Rapp E, Schwarzer J, Reichl U (2010) MDCK and Vero cells for influenza virus vaccine production: A one-to-one comparison up to lab-scale bioreactor cultivation. *Appl Microbiol Biotechnol* 88:461–475. <https://doi.org/10.1007/s00253-010-2742-9>

- Gränicher G, Coronel J, Trampler F, Jordan I, Genzel Y, Reichl U (2020) Performance of an acoustic settler versus a hollow fiber-based ATF technology for influenza virus production in perfusion. *Appl Microbiol Biotechnol* 104:4877–4888. <https://doi.org/10.1007/s00253-020-10596-x>
- Yang Y, Lyu T, Zhou R, He X, Ye K, Xie Q, Zhu L, Chen T, Shen C, Wu Q, Zhang B, Zhao W (2019) The antiviral and antitumor effects of defective interfering particles/genomes and their mechanisms. *Front Microbiol* 10. <https://doi.org/10.3389/fmicb.2019.01852>
- Gränicher G, Tapia F, Behrendt I, Jordan I, Genzel Y, Reichl U (2021) Production of modified Vaccinia Ankara virus by intensified cell cultures: a comparison of platform technologies for viral vector production. *Biotechnol J* 16:2000024. <https://doi.org/10.1002/biot.202000024>
- Grieger JC, Soltys SM, Samulski RJ (2016) Production of recombinant adeno-associated virus vectors using suspension HEK293 cells and continuous harvest of vector from the culture media for GMP FIX and FLT1 clinical vector. *Mol Ther* 24:287–297. <https://doi.org/10.1038/mt.2015.187>
- Hastie E, Cataldi M, Marriott I, Grzelishvili VZ (2013) Understanding and altering cell tropism of vesicular stomatitis virus. *Virus Res* 176:16–32
- Hein MD, Kollmus H, Marichal-Gallardo P, Püttker S, Benndorf D, Genzel Y, Schughart K, Kupke SY, Reichl U (2021) OP7, a novel influenza A virus defective interfering particle: production, purification, and animal experiments demonstrating antiviral potential. *Appl Microbiol Biotechnol* 105:129–146. <https://doi.org/10.1007/s00253-020-11029-5>
- Heldt FS, Frensing T, Pflugmacher A, Gröpler R, Peschel B, Reichl U (2013) Multiscale modeling of influenza A virus infection supports the development of direct-acting antivirals. *PLoS Comput Biol* 9:1003372. <https://doi.org/10.1371/journal.pcbi.1003372>
- Hencarriey O, Dormond E, Perrier M, Kamen A (2004) Insights into adenoviral vector production kinetics in acoustic filter-based perfusion cultures. *Biotechnol Bioeng* 86:765–774. <https://doi.org/10.1002/bit.20074>
- ICH (1998) ICH Topic Q 5 D Quality of biotechnological products: derivation and characterisation of cell substrates used for production of biotechnological/biological products step 5 note for guidance on quality of biotechnological products: derivation and character
- Jordan I, Sandig V (2014) Matrix and backstage: cellular substrates for viral vaccines. *Viruses* 6:1672–1700
- Jordan I, Vos A, Beilfuss S, Neubert A, Breul S, Sandig V (2009) An avian cell line designed for production of highly attenuated viruses. *Vaccine* 27:748–756. <https://doi.org/10.1016/j.vaccine.2008.11.066>
- Jordan I, John K, Höwing K, Lohr V, Penzes Z, Gubucz-Sombor E, Fu Y, Gao P, Harder T, Zádori Z, Sandig V (2016) Continuous cell lines from the Muscovy duck as potential replacement for primary cells in the production of avian vaccines. *Avian Pathol* 45:137–155. <https://doi.org/10.1080/03079457.2016.1138280>
- Kamen A, Henry O (2004) Development and optimization of an adenovirus production process. *J Gene Med* 6:S184–S192. <https://doi.org/10.1002/jgm.503>
- Kiesslich S, Vila-Chã Losa JP, Gélinas JF, Kamen AA (2020) Serum-free production of rVSV-ZEBOV in Vero cells: microcarrier bioreactor versus scale-X™ hydro fixed-bed. *J Biotechnol* 310:32–39. <https://doi.org/10.1016/j.jbiotec.2020.01.015>
- Krabbe T, Marek J, Groll T, Steiger K, Schmid RM, Krackhardt AM, Altomonte J (2021) Adoptive T cell therapy is complemented by oncolytic virotherapy with fusogenic VSV-NDV in combination treatment of murine melanoma. *Cancers (basel)* 13:1044. <https://doi.org/10.3390/cancers13051044>
- Krabbe T, Altomonte J (2018) Fusogenic viruses in oncolytic immunotherapy. *Cancers (Basel)* 10. <https://doi.org/10.3390/cancers10070216>
- Le Ru A, Jacob D, Transfiguracion J, Ansorge S, Henry O, Kamen AA (2010) Scalable production of influenza virus in HEK-293 cells for efficient vaccine manufacturing. *Vaccine* 28:3661–3671. <https://doi.org/10.1016/j.vaccine.2010.03.029>
- Liste-Calleja L, Lecina M, Lopez-Repullo J, Albiol J, Solà C, Cairó JJ (2015) Lactate and glucose concomitant consumption as a self-regulated pH detoxification mechanism in HEK293 cell cultures. *Appl Microbiol Biotechnol* 99:9951–9960. <https://doi.org/10.1007/s00253-015-6855-z>
- Lohr V, Rath A, Genzel Y, Jordan I, Sandig V, Reichl U (2009) New avian suspension cell lines provide production of influenza virus and MVA in serum-free media: studies on growth, metabolism and virus propagation. *Vaccine* 27:4975–4982. <https://doi.org/10.1016/j.vaccine.2009.05.083>
- Lohr V, Genzel Y, Behrendt I, Scharfenberg K, Reichl U (2010) A new MDCK suspension line cultivated in a fully defined medium in stirred-tank and wave bioreactor. *Vaccine* 28:6256–6264. <https://doi.org/10.1016/j.vaccine.2010.07.004>
- Lohr V, Genzel Y, Jordan I, Katinger D, Mahr S, Sandig V, Reichl U (2012) Live attenuated influenza viruses produced in a suspension process with avian AGE1.CR.pIX cells. *BMC Biotechnol* 12:79. <https://doi.org/10.1186/1472-6750-12-79>
- Maranga L, Brazão TF, Carrondo MJT (2003) Virus-like particle production at low multiplicities of infection with the baculovirus insect cell system. *Biotechnol Bioeng* 84:245–253. <https://doi.org/10.1002/bit.10773>
- Nikolay A, Castilho LR, Reichl U, Genzel Y (2018) Propagation of Brazilian Zika virus strains in static and suspension cultures using Vero and BHK cells. *Vaccine* 36:3140–3145. <https://doi.org/10.1016/j.vaccine.2017.03.018>
- Nikolay A, Bissinger T, Gränicher G, Wu Y, Genzel Y, Reichl U (2020) Perfusion control for high cell density cultivation and viral vaccine production. In: Pörtner R (ed) *Animal cell biotechnology. Methods in Molecular Biology*, vol 2095. Humana, New York. https://doi.org/10.1007/978-1-0716-0191-4_9
- Peshwa MV, Kyung Y-S, McClure DB, Hu W-S (1993) Cultivation of mammalian cells as aggregates in bioreactors: effect of calcium concentration of spatial distribution of viability. *Biotechnol Bioeng* 41:179–187. <https://doi.org/10.1002/bit.260410203>
- Rand U, Kupke SY, Shkarlet H, Hein MD, Hirsch T, Marichal-Gallardo P, Cicin-Sain L, Reichl U, Bruder D (2021) Antiviral activity of influenza A virus defective interfering particles against SARS-CoV-2 replication in vitro through stimulation of innate immunity. *bioRxiv* Sánchez-Felipe L, Villar E, Muñoz-Barroso I (2014) Entry of Newcastle disease virus into the host cell: role of acidic pH and endocytosis. *Biochim Biophys Acta - Biomembr* 1838:300–309. <https://doi.org/10.1016/j.bbamem.2013.08.008>
- Sanjuán R, Domingo-Calap P (2019) Genetic diversity and evolution of viral populations. In: *Reference Module in Life Sciences*. Elsevier, p 53
- Schneider M, Marison IW, Von Stockar U (1996) The importance of ammonia in mammalian cell culture. *J Biotechnol* 46:161–185
- Shen CF, Guilbault C, Li X, Elahi SM, Ansorge S, Kamen A, Gilbert R (2019) Development of suspension adapted Vero cell culture process technology for production of viral vaccines. *Vaccine* 37:6996–7002. <https://doi.org/10.1016/j.vaccine.2019.07.003>
- Thompson KAS, Yin J (2010) Population dynamics of an RNA virus and its defective interfering particles in passage cultures. *Virology* 7:257. <https://doi.org/10.1186/1743-422X-7-257>
- Vázquez-Ramírez D, Genzel Y, Jordan I, Sandig V, Reichl U (2018) High-cell-density cultivations to increase MVA virus production. *Vaccine* 36:3124–3133. <https://doi.org/10.1016/j.vaccine.2017.10.112>

Publisher's note Springer Nature remains neutral with regard to jurisdictional claims in published maps and institutional affiliations.

3.5. Second Manuscript

As a follow-up to the previously mentioned work, process intensification methods were established. This involved the production of rVSV-NDV in three candidate suspension cell lines in shake flasks as a small-scale screening model in semi-perfusion mode. Optimized culture conditions were subsequently transferred to full perfusion cultivations in STRs employing an AS for cell retention and a closed-loop process control strategy. This study described, for the first time, a fully scalable process for the manufacture of a fusogenic OV using HCD culture. Maximum VCCs ranging from $15\text{-}30 \times 10^6$ cells/mL and infectious virus titers up to 2.4×10^9 TCID₅₀/mL were reached, corresponding to 4-100 fold-improvements compared to optimized batch processes.

Göbel, Sven*; Chavez, Karim Jean*; Dorn, Marie; Neumeyer, Victoria; Jordan, Ingo; Sandig, Volker; Reichl, Udo; Altomonte, Jennifer; Genzel, Yvonne

*Shared first author

Process intensification strategies toward cell culture-based high-yield production of a fusogenic oncolytic virus




Biotechnology and Bioengineering, 2023

[96]

Contribution Sven Göbel:

Conceptualization, formal analysis, investigation, methodology, project administration, writing – original draft, writing – review & editing.

Process intensification strategies toward cell culture-based high-yield production of a fusogenic oncolytic virus

Sven Göbel¹ | Karim E. Jaén^{1,2} | Marie Dorn^{1,3}  | Victoria Neumeyer² | Ingo Jordan⁴  | Volker Sandig⁴ | Udo Reichl^{1,5} | Jennifer Altomonte² | Yvonne Genzel¹ 

¹Bioprocess Engineering, Max Planck Institute for Dynamics of Complex Technical Systems, Magdeburg, Germany

²Department of Internal Medicine II, Klinikum Rechts der Isar, Technische Universität München, München, Germany

³Faculty of Process and Systems Engineering, Otto-von-Guericke-University Magdeburg, Magdeburg, Germany

⁴ProBioGen AG, Berlin, Germany

⁵Chair for Bioprocess Engineering, Otto-von-Guericke-University Magdeburg, Magdeburg, Germany

Correspondence

Yvonne Genzel, Bioprocess Engineering, Max Planck Institute for Dynamics of Complex Technical Systems, Sandtorstr. 1, 39106 Magdeburg, Germany.
Email: genzel@mpi-magdeburg.mpg.de

Funding information

Max-Planck-Gesellschaft; EXIST

Abstract

We present a proof-of-concept study for production of a recombinant vesicular stomatitis virus (rVSV)-based fusogenic oncolytic virus (OV), rVSV-Newcastle disease virus (NDV), at high cell densities (HCD). Based on comprehensive experiments in 1 L stirred tank reactors (STRs) in batch mode, first optimization studies at HCD were carried out in semi-perfusion in small-scale cultivations using shake flasks. Further, a perfusion process was established using an acoustic settler for cell retention. Growth, production yields, and process-related impurities were evaluated for three candidate cell lines (AGE1.CR, BHK-21, HEK293SF) infected at densities ranging from 15 to 30×10^6 cells/mL. The acoustic settler allowed continuous harvesting of rVSV-NDV with high cell retention efficiencies (above 97%) and infectious virus titers (up to 2.4×10^9 TCID₅₀/mL), more than 4–100 times higher than for optimized batch processes. No decrease in cell-specific virus yield (CSVY) was observed at HCD, regardless of the cell substrate. Taking into account the accumulated number of virions both from the harvest and bioreactor, a 15–30 fold increased volumetric virus productivity for AGE1.CR and HEK293SF was obtained compared to batch processes performed at the same scale. In contrast to all previous findings, formation of syncytia was observed at HCD for the suspension cells BHK 21 and HEK293SF. Oncolytic potency was not affected compared to production in batch mode. Overall, our study describes promising options for the establishment of perfusion processes for efficient large-scale manufacturing of fusogenic rVSV-NDV at HCD for all three candidate cell lines.

KEYWORDS

cell culture-based production, fusogenic oncolytic virus, high cell density culture, perfusion, process intensification, upstream processing

Abbreviations: μ , cell-specific growth rate; CRE, cell retention efficiency; CSPR, cell-specific perfusion rate; CSVY, cell-specific virus yield; CVSPR, cell volume-specific perfusion rate; F, fusion protein; GFP, green fluorescent protein; HCD, high cell density; hpi, hours post infection; IAV, influenza A virus; IC₅₀, half maximal inhibitory concentration; IFN, interferon; MOI, multiplicity of infection; NDV, Newcastle disease virus; NS, nutrient supplementation; OV, oncolytic virus; PEM, protein expression medium; rVSV-NDV, recombinant hybrid virus: VSV backbone and surface glycoproteins of NDV used in this study; rVSV-NDV-GFP, recombinant hybrid virus expressing GFP; STR, stirred tank bioreactor; TCID₅₀, 50% tissue culture infective dose; TOI, time of infection; VCC, viable cell concentration; VSV, vesicular stomatitis virus; V_w, working volume; VVP, volumetric virus productivity.

Sven Göbel and Karim E. Jaén contributed equally to this study.

This is an open access article under the terms of the Creative Commons Attribution-NonCommercial-NoDerivs License, which permits use and distribution in any medium, provided the original work is properly cited, the use is non-commercial and no modifications or adaptations are made.

© 2023 The Authors. *Biotechnology and Bioengineering* published by Wiley Periodicals LLC.

1 | INTRODUCTION

Cancer poses a high burden on worldwide societal and health care systems, both epidemiologically and financially. Due to a globally aging and still growing human population, cancer is projected to have a significant impact in the coming decades. Cancer immunotherapy is revolutionizing clinical oncology as an exciting paradigm shift by recruiting the patients' immune system against tumors. Originally developed as direct cytotoxic agents, oncolytic viruses (OVs), as therapeutic vaccines, offer an elegant approach to cancer therapy. On the one side, they have the ability to cause direct tumor cell lysis, while on the other side, they can stimulate immune responses directed against the tumor (Cook & Chauhan, 2020; Krabbe & Altomonte, 2018). By expressing endogenous or heterologous fusion glycoproteins, an enhanced intratumoral spread of OVs via syncytia formation can be achieved. The novel engineered recombinant vesicular stomatitis virus-Newcastle disease virus (rVSV-NDV), a recombinant vesicular stomatitis virus (VSV) backbone with fusogenic mutant glycoproteins of NDV, demonstrated preclinical efficacy in various cancer models (Abdullahi et al., 2018; Krabbe et al., 2021).

Manufacturing methods for several oncolytic viruses (herpes simplex virus, vaccinia virus, reovirus, and adenovirus) for clinical trials, but also for rVSV-NDV, are mainly performed in anchorage-dependent cell lines (Abdullahi et al., 2018; Ungerechts et al., 2016). The use of adherent cells can be beneficial due to established and automated production facilities, years of experience with regulatory approval, and high cell-specific virus yields (CSVY) (Pelz et al., 2022). However, for fusogenic OVs that cause formation of large multinucleated syncytia that die rapidly after induction only relatively low virus yields were achieved in several tested adherent cell lines (Abdullahi et al., 2018). This property presents unique challenges for large-scale clinical-grade manufacturing, further compounded as scaling-up of processes for adherent cells is mainly achieved by scaling-out (e.g., increasing the surface area by multiplying the number of culture vessels) or the use of microcarrier systems. In static culture systems, there are also only limited options for monitoring and control of cultivation parameters such as pH values, dissolved oxygen concentration, feeding rates (Gallo-Ramírez et al., 2015; Pelz et al., 2022). Moreover, media for most adherent cells are supplemented with animal-derived components such as fetal calf serum, which can lead to batch-to-batch variations, increased production and purification costs, and elevated contamination risks.

To overcome such limitations, manufacturing can be shifted toward suspension cells using chemically defined media. Suspension cells allow for easy scale-up and passaging while maintaining rapid cell growth. Cultivation in stirred tank bioreactors (STR) can achieve high cell concentration in a small footprint, decreasing labor expenditures (Pelz et al., 2022). Moreover, suspension cultures allow the use of advanced process monitoring methods, enable process automation, and tight control of culture conditions.

As a first step, suitable suspension cell substrates were identified for the development of an efficient and scalable OV production process using a green fluorescent protein (GFP)-expressing variant of rVSV-NDV (rVSV-NDV-GFP). Infection at cell concentrations of about 2×10^6 cells/mL yielded titers in the order of 10^8 TCID₅₀/mL in BHK-21, HEK293SF, and AGE1.CR suspension cells (Göbel, Kortum et al., 2022). However, clinical treatment with OVs will require manufacturing processes that consistently achieve even higher virus titers. Because dose-limiting effects of rVSV-NDV have not been observed in preclinical investigations, processes enabling the production of $\geq 10^9$ – 10^{10} virions/injection are desired. To further increase virus titers in bioreactor harvests, intensification strategies commonly applied in manufacturing of viral vaccines and viral vectors can be adopted. In particular, a switch from batch to perfusion mode and the implementation of high cell density (HCD) processes have been shown as a successful strategy for various virus-host cell systems (Genzel et al., 2014; Gränicher et al., 2021; Lavado-García et al., 2020; Nikolay et al., 2018; Pihl et al., 2018; Vázquez-Ramírez et al., 2018; Wu et al., 2021). Moreover, by adapting feeding schemes after infection (e.g., “hybrid fed-batch/perfusion” [Vázquez-Ramírez et al., 2019]) both CSVY and volumetric virus productivity (VVP) can be further increased compared to perfusion-only strategies. Cell retention devices used to keep cells inside the bioreactor can also influence the performance of production processes (Gränicher et al., 2020). While membrane clogging and accumulation of viruses inside bioreactors are well known drawbacks of membrane-based cell retention (Genzel et al., 2014; Hadpe et al., 2017; Hein, Chawla et al., 2021; Nikolay, Grooth, et al., 2020), both tangential flow filtration (Coronel et al., 2019; Nikolay et al., 2018) and alternating tangential flow filtration (ATF) (Genzel et al., 2014; Gränicher et al., 2020; Gränicher et al., 2021; Hein, Chawla et al., 2021; Vázquez-Ramírez et al., 2019) have been applied successfully in academic research. Effective continuous harvesting of lytic viruses has been demonstrated with devices such as acoustic settlers (Coronel et al., 2020; Gränicher et al., 2020; Gränicher et al., 2021; Henry et al., 2004; Manceur et al., 2017; Petiot & Kamen, 2013). Using an acoustic settler, Gränicher et al. demonstrated an increase of CSVY of at least 1.5-fold through continuous removal of an influenza A virus (IAV) compared to an ATF system (Gränicher et al., 2020). Moreover, by preclarifying the virus-containing harvest for subsequent in-line purification steps, fully integrated virus production processes can be established (Gränicher et al., 2021).

In this study, we investigated process intensification strategies for further improvement of the production of rVSV-NDV in three candidate suspension cell lines. Shake flasks were used as a small-scale screening model in semi-perfusion mode and optimized culture conditions were subsequently transferred to STRs. Acoustic settler perfusion processes in bioreactors using manual and automated perfusion control were established to increase virus titers. Results demonstrate the applicability of perfusion HCD processes for the production of fusogenic oncolytic viruses in suspension cell culture to achieve higher virus titers as well as improved VVP compared to conventional batch production for all candidate cell lines.

2 | MATERIALS AND METHODS

2.1 | Cell lines, media, and viral seed stock

Three different suspension cell lines (Supporting Information: Table S1) were cultured and screened to identify a suitable cell substrate for the HCD production of rVSV-NDV. AGE1.CR cells were cultivated in chemically defined medium CD-U7 (Xell), supplemented with 2 mM alanine, 2 mM glutamine (Sigma Aldrich), and 10 ng/mL recombinant insulin-growth factor (LONG-R³, Sigma-Aldrich). BHK-21 and HEK293SF cells were cultivated in Protein Expression Medium (PEM) (Gibco) supplemented with 8 mM L-glutamine and 4 mM pyruvate (Sigma-Aldrich). All three cell lines were cultivated in baffled 125 mL shake flasks with vent caps (Corning) with a working volume (V_w) of 50 mL, and incubated in a Multitron orbitally shaken incubator (Infors AG) with 50 mm shaking diameter. BHK-21 and AGE1.CR cells were incubated at 185 rpm, 37°C, and 5% CO₂. HEK293SF cells were incubated at 130 rpm, 37°C, and 8% CO₂. Adherent Huh7 cells were cultivated in T75 flasks (Greiner Bio-one) in high glucose DMEM (Gibco) supplemented with 10% fetal calf serum, 1x nonessential amino acids (Gibco) and 1 mM sodium pyruvate (Gibco) and incubated at 37°C and 5% CO₂.

For infections, the non-GFP-expressing construct (VSV-NDV) of the previously described rVSV-NDV-GFP (Abdullahi et al., 2018; Göbel, Kortum et al., 2022) was used. Virus stocks were generated from the first passage of rVSV-NDV produced in adherent AGE1.CR-pIX cells (ProBioGen AG) with a titer of 2.47×10^7 TCID₅₀/mL (rVSV-NDV(pIX)). After subsequent expansion in either AGE1.CR (rVSV-NDV (CR)) or BHK-21 (rVSV-NDV(BHK)) suspension cells, titers of 5.92×10^5 TCID₅₀/mL and 1.33×10^9 TCID₅₀/mL, respectively, were achieved. Aliquots of the stocks were stored at -80°C and were used once for each experiment to prevent loss of infectivity due to repeated freeze-thaw cycles. Both preparations were used in experiments. Although enveloped viruses may adapt to a cellular substrate also by incorporation of host cell proteins in their viral envelope we do not expect an impact on production of VSV-NDV: We have not observed significant changes in infectious titers for any cell line and passaging cycle in earlier experiments (Göbel, Kortum et al., 2022), and infection of AGE1.CR, HEK293SF or BHK-21 cells with virus material produced in the respective other cell lines did not significantly affect maximum infectious virus titers (data not shown).

2.2 | Small-scale infection studies

For a multiplicity of infection (MOI) screening, HEK293SF cells were inoculated at 2×10^6 cells/mL (centrifugation of the appropriate volume at 300g for 5 min; resuspension in 75 mL fresh PEM medium supplemented with 4 mM pyruvate and 8 mM glutamine) in single use 125 mL baffled shake flasks with vent caps (Thermo Fisher Scientific) at 37°C, 8% CO₂ and 130 rpm orbital shaking. Cells were subsequently infected at MOIs of 1E-2–1E-4 at time of infection with rVSV-NDV(CR).

Semi-perfusion was performed by manually exchanging the medium to maintain sufficient metabolite concentrations. For cell growth, a cell-specific perfusion rate (CSPR)-based strategy was used and switched to a strategy based on fixed-reactor volume (RV) after infection as the lytic nature of rVSV-NDV complicated cell count-based feeding strategies. The required exchange volume was calculated according to Vázquez-Ramírez et al. (2018). Cultures were started with a viable cell concentration (VCC) of 2×10^6 cells/mL in 50 mL supplemented CD-U7 or PEM medium in single-use 250 mL baffled shake flasks with vented cap (Thermo Fisher Scientific) at the respective cultivation conditions. To avoid potential nutrient limitations, the medium was partially exchanged every 24 h at a CSPR of 50 pL/cell/d for AGE1.CR cells and 83 pL/cell/d for HEK293SF cells targeting for a minimum glucose concentration of 10 mM, respectively, starting at 24 h post inoculation. The calculated cell culture volume was transferred from the shake flasks to 50 mL centrifuge tubes (Greiner Bio One) and centrifuged at 300g for 5 min at room temperature. After removing the supernatant, cells were recovered in an equal volume of fresh medium and transferred back to the shake flasks.

AGE1.CR cells were infected with rVSV-NDV(pIX) in 125 mL baffled shake flasks at a VCC of 20.0×10^6 cells/mL following a complete medium exchange. After infection, the manual exchange was paused, and the V_w was increased from 25 to 50 mL at 12 h post infection (hpi) similar to the process described by Vazquez-Ramírez et al. (2019) and Gränicher et al. (2021) ("Hybrid fed-batch perfusion"). Starting from 24 hpi, a constant perfusion rate of 1.6 RV/d was maintained. A total of six different conditions were investigated as outlined in Table 1.

HEK293SF cells were infected at VCCs of 10.0×10^6 and 20.0×10^6 cells/mL at a MOI of 1E-3 with rVSV-NDV(CR). Upon infection, medium was exchanged at a fixed perfusion rate of 1.8 RV/d. Medium was further supplemented to yield 35 mM glucose after 96 h, and 35 mM glucose and 12 mM glutamine 144 h post inoculation with the aim to maintain glutamine and glucose concentrations above 4 and 10 mM, respectively.

2.3 | Batch cultivations in STR

Bioreactor cultivations were carried out in a 1 L STR (DASGIP, Eppendorf AG). The bioreactors were instrumented with pH (Hamilton) and polarographic pO₂ (Hamilton) probes. Additionally, permittivity probes were used for on-line monitoring of VCC. Cultures were stirred using a pitched blade impeller at 180 rpm (AGE1.CR), 250 rpm (HEK293SF), and 350 rpm (BHK-21). Aeration was carried out through a submerged L-drilled holes sparger at a rate of 3 sL/h. pH value was controlled at 7.2 (AGE1.CR and BHK-21) or 7.0 (HEK293SF) by either sparging CO₂ up to 10% volume or by the addition of 7.5% NaHCO₃ solution. pO₂ was kept equal or above 50% air saturation for the growth phase by sparging O₂ and either 5% air saturation in hypoxic cultivations or equal or above 50% air saturation for the infection phase. Temperature was set at 37°C for

TABLE 1 Conditions for the hybrid fed-batch perfusion strategy with AGE1.CR cells infected with rVSV-NDV.

Condition	1	2	3	4	5	6
MOI	1E-3	1E-4	1E-5	1E-4	1E-4	1E-4
Temperature pi	37	37	37	34	37	37
Medium	CD-U7	CD-U7	CD-U7	CD-U7	CD-U7/PEM (75:25)	CD-U7 + 1/6 F12

Note: Cells were grown until they reached a density of 20.0×10^6 cells/mL (VW = 50 mL). At time of infection (TOI) a complete medium exchange was performed, and the VW was set to 25 mL. Twenty-five milliliter of fresh medium was added once at 12 hpi. Starting at 24 hpi, a constant perfusion rate of 1.6 RV/d was maintained. F12: Ham's Nutrient Mixture F12 (Sigma Aldrich). Temperature in °C.

Abbreviations: MOI, multiplicity of infection; NDV, Newcastle disease virus; pi, post infection; rVSV, recombinant vesicular stomatitis virus.

the growth phase and either 34 or 37°C for the infection phase, and was controlled by means of an electrical heating blanket.

Bioreactors were inoculated at a VCC of 0.8×10^6 cells/mL for AGE1.CR and 0.5×10^6 cells/mL for BHK-21 and HEK293SF cells, from pre-cultures expanded in 250 mL baffled shake flasks with vented cap (Corning). For the infection phase, an equal V_w of prewarmed fresh media containing the rVSV-NDV(CR) was transferred to the bioreactor. For the nutrient supplementation (NS) experiments, the infection medium for BHK-21 and HEK293SF cells consisted of PEM supplemented with 60 mM glucose, 17.4 mM glutamine and 8 mM pyruvate. For AGE1.CR cells, CD-U7 medium supplemented as described above was used for infection.

2.4 | Perfusion cultivations in STR

Bioreactor perfusion cultivations were carried out in a 1 L STR (DASGIP, Eppendorf AG) (AGE1.CR and BHK-21) and in a 1 L STR Biostat B Plus (Sartorius) (HEK293SF). Cells grew initially in batch mode at 37°C. Cultures were stirred using a pitched blade impeller at 180 rpm. Once they reached a threshold concentration of glucose (5–15 mM), perfusion was started at a rate of 1 RV/d. Subsequently, medium was exchanged on a CSPR basis of 55 pL/cell/d for AGE1.CR, 197 pL/cell/d for HEK293SF, and 110 pL/cell/d for BHK-21 cells. At the STR outlet, cells were retained in a Sono Sep APS-10 acoustic settler (SonoSep Technologies) operated in pump-mode at 3 W and 2.1 Mhz, with backflush every 3 min for 30 s. The feed pump was integrated to the bioreactor weight control system, which comprised a ICS425 scale (Mettler-Toledo) (AGE1.CR and BHK-21) or Midrics 1 (Sartorius) (HEK293SF) to keep a constant weight in the bioreactor during the continuous harvesting performed by a peristaltic pump. For AGE1.CR cells, the permeate flow rate was controlled automatically through a multi-frequency capacitance probe and pre-amplifier (Incyte Hamilton), both connected with a M12 cable to the ArcView controller 265 (Hamilton). The controller was connected to a peristaltic pump (120U, Watson Marlow) by a 4–20 mA output box (Hamilton), with an open-end AUX M12 to the output port of the ArcView and an open-end cable with a 15-pin D-SUB male connector to the pump (Gränicher et al., 2021; Hein, Kollmus et al., 2021; Nikolay, 2020). The cell culture in the bioreactor was monitored in real-time by measuring the permittivity

every 12 min in the range of 0.1–10 MHz. Linear regression between the permittivity signal and the VCC was used to determine a “cell factor” of 0.67 which was stored in the ArcView controller to set the cell volume-specific perfusion rate (CVSPR) of $0.04 \text{ pL}/\mu\text{m}^3/\text{d}$ for AGE1.CR cells. For BHK-21 and HEK293SF cells, the CSPR was adjusted manually by increasing the pump once a day based on off-line VCC and metabolite measurements.

Cells were recirculated by a peristaltic pump (Watson Marlow 120U, UK) through a 5 mm inner diameter silicon tubing, operated at 3–5 RV/d. For the infection phase, a volume of medium of 50 mL containing the rVSV-NDV was transferred to the bioreactor. HEK293SF cells were infected with rVSV-NDV(BHK) with a MOI of 1E-3, BHK-21 cells with rVSV-NDV(BHK) with a MOI of 1E-4, and AGE1.CR cells with rVSV-NDV(BHK) with a MOI of 1E-5. After infection, the temperature was shifted to 34°C, the recirculation rate was increased to 5 RV/d for all cell lines, and the perfusion rate was set at 3 RV/d for HEK293SF cells. For AGE1.CR and BHK-21 cells, the previously described “hybrid fed-batch” strategy was pursued, which consisted of a 1:1.8 dilution by addition of fresh medium at 12 hpi and subsequent exchange with 2 RV/d starting 24 hpi. All the cultures were performed in a V_w of 400–600 mL at pH 7.2 and at pO_2 equal or above 50% air saturation during the entire cultivation time. The overall setup including devices for control of perfusion is shown in Figure 1.

2.5 | Oncolytic viral potency assay

The half maximal inhibitory concentration (IC₅₀) potency assay determines the MOI of VSV-NDV, which results in 50% cell killing at a defined time point, as a quantitative parameter to compare the relative potency of VSV-NDV-mediated cytotoxicity derived from the different production cell lines. Huh7 cells were seeded one day before infection at a density of 1.0×10^4 cells/well in an opaque-walled flat-bottom 96-well plate in DMEM. After overnight incubation, cells were infected in half-log steps from MOI 1E1 to MOI 1E-4 with VSV-NDV produced in perfusion cultures from BHK-21, AGE1.CR or HEK293SF cells. At 48 hpi, cell viability was measured using the CellTiter-Glo Assay (Promega) according to the manufacturer's instructions, and luminescence was measured using the Promega GloMax Plate Reader (Promega). For the analysis of IC₅₀ values, GraphPad PRISM software (GraphPad Software Inc) was used. Briefly, viability data was

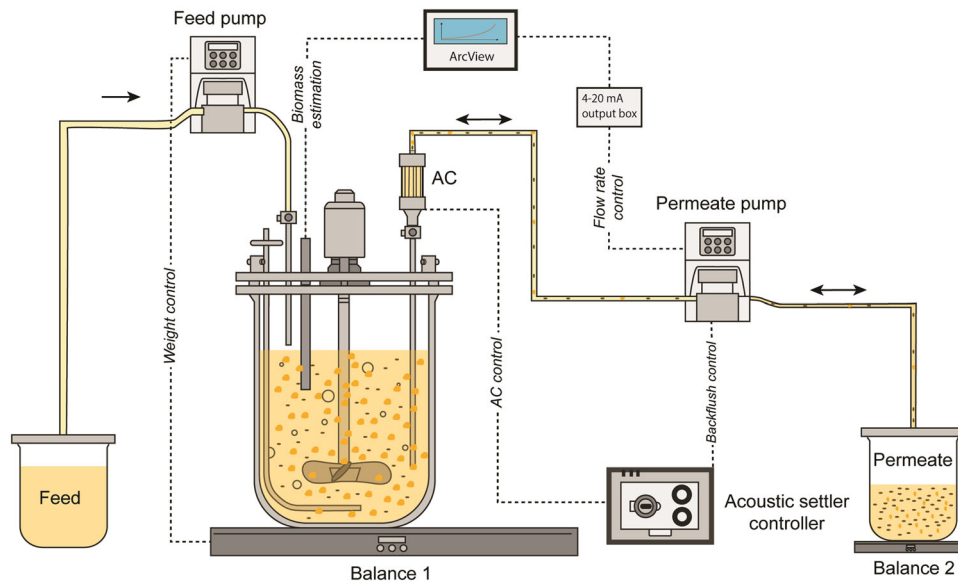


FIGURE 1 Scheme of the acoustic settler setup for perfusion cultivations (adapted from [Göbel, Pelz et al., 2022]). Cell retention was achieved by generation of a standing wave field in the APS-10 acoustic settler (AC) chamber. For AGE1.CR cell cultivations, viable cell volume was monitored on-line using a capacitance probe and used to maintain the cell volume-specific perfusion rate at a steady state during the cell growth phase. Permeate flow rates were confirmed by using balance 2. As separation depended strongly on the cell diameter, viable cells were retained while dead cells were washed out into the permeate. Virus particles, not effected by the generated wave field, were collected in the permeate vessel. Orange circles indicate cells, orange dots indicate cell debris, black ellipses indicate virus particles, and dashed lines indicate different types of signal transmissions.

normalized to untreated controls and data was transformed. Then, IC50 values were calculated by nonlinear regression curve fitting using a log (agonist) versus normalized response (variable slope) curve fit.

2.6 | Other analytics

Samples from cultures were collected every 24 h during growth phase and every 12 h during the infection phase. Samples of 1 mL were used for pH and osmolality measurements, and cell counting to determine the VCC, cell viability and cell diameter in a ViCell-XR (Beckman Coulter). Off-line pH was measured in a pH7110 potentiometer (Inolab). Osmolality was measured in a vapor pressure osmometer VAPRO 5600 (Wescor, Inc). Samples of 1 mL for virus titration, metabolite and impurity measurements were centrifuged at 1100g for 5 min. The supernatant was recovered and distributed in 500 μ L aliquots in 2 mL cryovials stored at -80°C until further analysis. Metabolite concentrations (glucose, lactate, glutamine, glutamate, and ammonium) were determined using a Bioprofile 100 (Nova Biomedical). For titration of VSV-NDV, the previously described TCID₅₀ assay (Göbel, Kortum et al., 2022) was performed using adherent AGE1.CR. pIX cells. The CSVY was calculated as previously described by Gränicher et al. (2020) taking into account only the error of the TCID₅₀ assay ($-50\%/+100\%$ on a linear scale).

To determine the amount of impurities (protein and DNA), the methodology of Marichal-Gallardo et al. (2017) was used. Supernatant samples were dialyzed in PBS buffer at $2-8^{\circ}\text{C}$ for at least 16 h, using 14 kDa MWCO cellulose acetate membranes (Spectrum). Protein

concentrations were quantified using the colorimetric BCA assay according to the manufacturer's instructions (Thermo Fischer Scientific). After incubation at 37°C for 30 min, the absorbance was measured in an Infinite M200 plate reader (Tecan) at 562 nm. Protein concentrations were obtained after relating absorbance measurements from the standard calibration curve. A pico-green fluorescence-based assay was used to quantify the concentration of double stranded host cell DNA (dsDNA). Briefly, 200 μ L of the blank (PBS), lambda DNA standards and dialyzed samples were loaded in duplicate in a 96-flat bottom black multi-well plate. After addition of 50 μ L of 1:60 pico-green solution, the plate was incubated and shaken at room temperature and 1000 rpm for 5 min in a Thermomixer Comfort (Eppendorf). The fluorescence was read in a Tecan M200 Pro (Tecan) at 480 nm (excitation)/520 nm (emission). DNA concentrations were obtained after relating fluorescence measurements from a standard calibration curve.

Purification of virus was performed using ultracentrifugation and a sucrose gradient. Briefly, medium containing viral particles was obtained and virus was pelleted by ultracentrifugation at 65,000 rcf for 1 h at 4°C . Viral particles were purified via ultracentrifugation over a sucrose gradient and the pellet was resuspended in phosphate-buffered saline (PBS) after an additional ultracentrifugation step.

Computation of the TCID₅₀ was carried out according to the Reed and Muench method (Rammanikhrisan 2016). The stoichiometric lactate to glucose yield ($Y_{\text{Lac}/\text{Glc}}$), the total number of accumulated virus particles (vir_{tot}), the CSVY, the VVP and the accumulated mass of dsDNA and protein (Prot) were calculated as described by Gränicher et al. (2020); as follows:

$$Y_{Lac/Glc} = \frac{(C_{Lac,n} - C_{Lac,n-1}) + 0.5 \times (C_{Lac} + C_{Lac,n-1}) \times \frac{V_p}{V_w}}{(C_{Glc,n-1} - C_{Glc,n}) + (C_{Glc,0} - 0.5 \times (C_{Glc} + C_{Glc,n-1})) \times \frac{V_p}{V_w}} \quad (1)$$

$$vir_{tot} = C_{vir,STR} \cdot V_w + \sum 0.5 \times (C_{vir,H,n} + C_{vir,H,n-1}) \times V_H \quad (2)$$

$$CSVY = \frac{vir_{tot}}{X_{v,STR,max} \times V_w} \quad (3)$$

$$VVP = \frac{vir_{tot}}{V_{tot} \times t_{tot}} \quad (4)$$

$$dsDNA = C_{dsDNA,Br} \times V_w + \sum 0.5 \times (C_{dsDNA,H,n} + C_{dsDNA,H,n-1}) \times V_H \quad (5)$$

$$Prot = C_{Prot,tot,Br} \times V_w + \sum 0.5 \times (C_{Prot,tot,H,n} + C_{Prot,tot,H,n-1}) \times V_H \quad (6)$$

where $C_{Lac,n}$ is the lactate concentration at time n (t_n) (mM), V_p is the perfused volume between t_n and t_{n-1} , and $C_{Glc,0}$ and $C_{Glc,n}$ is the glucose concentration at time 0 and n , respectively. vir_{total} is the total number of accumulated infectious viral particles (TCID₅₀), $C_{vir,STR}$, $C_{vir,H,n}$, and $C_{vir,H,n-1}$ (TCID₅₀/mL) are the infectious virus concentrations in the bioreactor and the harvests at t_n and t_{n-1} , respectively. V_H is the volume harvested between t_n and t_{n-1} (mL). $X_{v,STR,max}$ (cells/mL) is the maximum viable cell concentration upon infection in the bioreactor, V_{tot} is the total medium spent including cell growth phase, t_{tot} is the total process time from inoculation until the time point of maximum vir_{tot} . $C_{dsDNA,STR}$, $C_{dsDNA,H,n}$, and $C_{dsDNA,H,n-1}$ (μg/mL) are the concentrations of double stranded DNA in the bioreactor and the harvests at t_n and t_{n-1} , respectively. Finally, $C_{Prot,STR}$, $C_{Prot,H,n}$, and $C_{Prot,H,n-1}$ (μg/mL) are the concentrations of protein in the bioreactor and the harvests at t_n and t_{n-1} , respectively.

The cell retention efficiency of the acoustic settler (CRE) (%) was calculated as follows:

$$CRE = \left(1 - \frac{X_{v,H}}{X_{v,Br}}\right) \times 100, \quad (7)$$

Where $X_{v,H}$ and $X_{v,STR}$ are the viable cell concentrations in the harvest and in the bioreactor, respectively.

3 | RESULTS

We previously identified three promising suspension cell lines (AGE1.CR, HEK293SF, BHK-21) for the batch production of rVSV-NDV-GFP in shake flasks and STRs (Göbel, Kortum et al., 2022). To confirm that the reported process parameters would still be applicable for the production of rVSV-NDV (same construct but without the GFP reporter gene for use in clinical studies) shake flask experiments were performed. This included infections using the optimal MOIs identified. Here, no significant differences were found (data not shown).

3.1 | rVSV-NDV production in STR in batch mode

Previously, the use of a STR resulted in slightly lower TCID₅₀/mL titers for BHK-21 cells and drastically reduced titers for HEK293SF cells (Göbel, Kortum et al., 2022). Therefore, the impact of nutrient supplementation (NS) on the rVSV-NDV production was now additionally evaluated for BHK-21 and HEK293SF cells, respectively. Moreover, the effect of a temperature shift (34°C) (BHK-21), hypoxia (pO₂ 5%) and trypsin addition (5 U/mL) (HEK293SF) on the infection phase were investigated (Figure 2).

During the growth phase, AGE1.CR cells grew exponentially at a specific rate of 0.018 1/h with a viability above 90%. Once a VCC of about 4.0×10^6 cells/mL was reached, a V_w of freshly supplemented CD-U7 medium containing the rVSV-NDV(pIX) virus was added to the bioreactor to infect the cells at a MOI of 1E-5. At 36 hpi, cell viability was below 90% and a maximum infectious virus titer of 7.50×10^5 TCID₅₀/mL (Figure 2d) and CSVY of 0.3 TCID₅₀/cell were reached. Addition of nutrient-enriched medium at time of infection (TOI) for BHK-21 cells maintained glucose and glutamine concentrations above 15 and 2 mM, respectively (Supporting Information: Figure S1). This did not influence the cell growth (Figure 2b), but resulted in a two-fold increase in the maximum infectious virus titer (Figure 2e) and the CSVY. Shifting the temperature to 34°C after infection, neither affected cell growth nor the maximum infectious virus titer (Figure 2b,e) and CSVY compared to the cultivation performed at 37°C. For HEK293SF cells, increasing the glucose (60 mM) and glutamine (17 mM) concentrations in the infection medium restored the concentration of both substrates at the levels observed upon inoculation (Supporting Information: Figure S1). In all conditions, cells first grew exponentially from 2.0×10^6 to 5.4×10^6 cells/mL within 48 hpi but cell concentrations stagnated for the rest of the cultivation (Figure 2c). Cell viability slightly declined from 48 hpi onwards, but remained above 90% until 120 hpi (Figure 2c). rVSV-NDV production was barely increased by nutrient supplementation (Figure 2f). In comparison to the rVSV-NDV-GFP infection at MOI 1E-2 (Figure 2c,f reference) with a maximum titer of 1.0×10^6 TCID₅₀/mL, infections with rVSV-NDV(CR) at MOI 1E-3 resulted in titers lower than 1×10^6 TCID₅₀/mL but an up to four-fold increase in CSVY. However, these subtle improvements were suppressed under hypoxia, where the infectious virus titer was similar to the reference (Figure 2c,f) but with a 50% lower CSVY. Trypsin addition led to a 30% increase in maximum infectious virus titer (Figure 2f) and CSVY. Overall, it seems that overcoming substrate limitations was pivotal to improve rVSV-NDV production in 1 L STR cultures (Table 2).

3.2 | Medium switch and transition to semi-perfusion mode for AGE1.CR cells

As for HEK293SF cells, the maximum infectious virus titer for AGE1.CR cells was decreased by more than one order of magnitude after transfer from shake flask cultivations (Figure 2) to STR operated in batch mode. Two strategies were followed to increase the maximum virus titers:

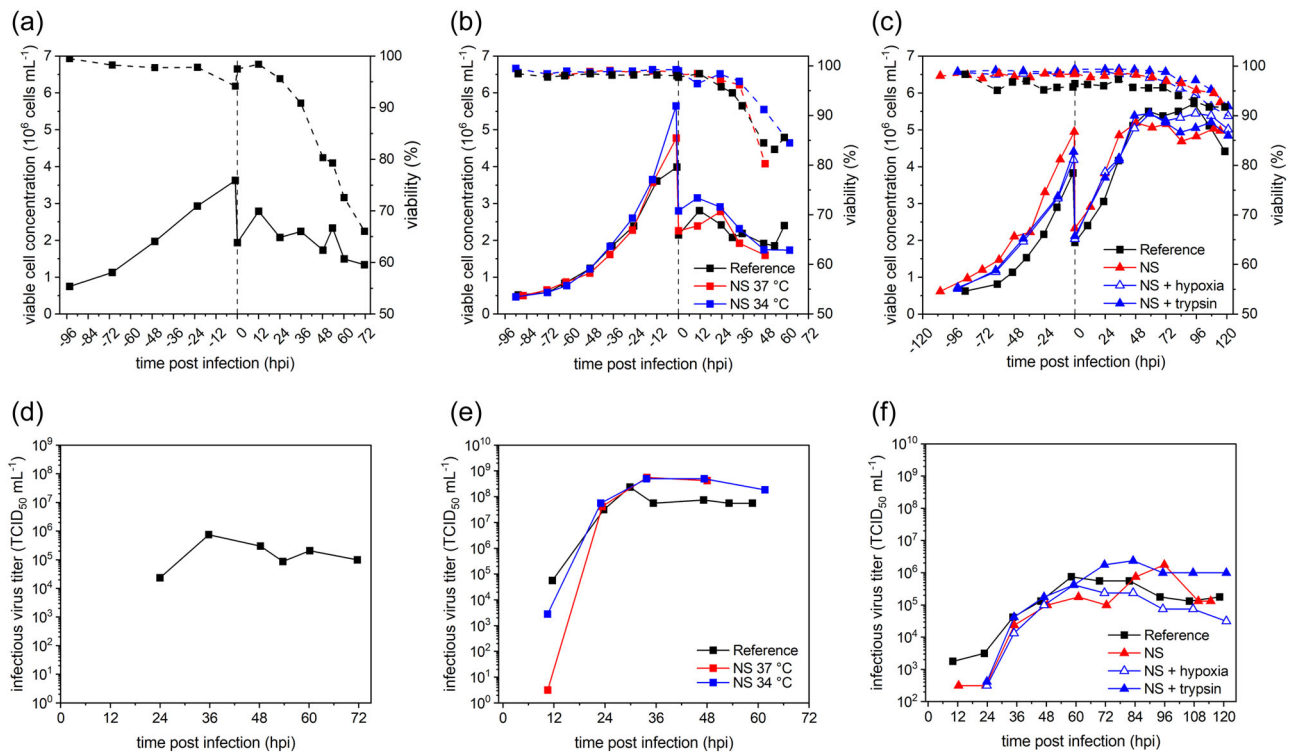


FIGURE 2 rVSV-NDV production in candidate cell lines in 1 L STR in batch mode. rVSV-NDV production in AGE1.CR cells (a, d); Influence of nutrient supplementation (NS) and temperature shift to 34°C on rVSV-NDV production in BHK-21 cells (b, e), and hypoxia (pO₂ 5%) and trypsin addition (5 U/mL) on rVSV-NDV production in HEK293SF cells (c, f), in 1 L STR cultures in batch mode. All cultures were infected at 2 × 10⁶ cells/mL following a 1:2 dilution step with fresh medium. (a–c) Viable cell concentration (solid lines) and viability (dashed lines), (d–f) infectious virus titer. Reference refers to the data obtained from Göbel, Kortum et al. (2022) with the rVSV-NDV-GFP construct (37°C without NS). NDV, Newcastle disease virus; rVSV, recombinant vesicular stomatitis virus; STR, stirred tank bioreactors.

TABLE 2 Growth and rVSV-NDV production in 1 L STR cultures in batch mode with three candidate cell lines.

Cell line	Condition	MOI (virus)	pO ₂ (%)	μ (h ⁻¹)	Max. VCC p.i (×10 ⁶ cell mL ⁻¹)	Max. infec. virus titer (TCID ₅₀ mL ⁻¹)	Time of max. titer (hpi)	CSVY (TCID ₅₀ /cell)	VVP (×10 ⁸ TCID ₅₀ /L/d)
AGE1.CR	37°C	1E-5 (pIX)	≥50	0.018	2.79	7.50 × 10 ⁵	36.0	0.3	1.2
BHK-21	Reference	1E-4 (pIX)	≥50	0.027	2.81	2.37 × 10 ⁸	29.8	84.0	480
BHK-21	NS 37°C	1E-4 (CR)	≥50	0.028	2.79	5.62 × 10 ⁸	33.8	202.0	1126
BHK-21	NS 34°C	1E-4 (CR)	≥50	0.033	3.16 ± 0.25	5.01 × 10 ⁸ ± 8.70 × 10 ⁷	33.8 ± 0.1	161.0 ± 40	937 ± 266
HEK293SF	Reference	1E-2 (pIX)	≥50	0.027	5.72	7.50 × 10 ⁵	45.8	0.1	1.4
HEK293SF	NS	1E-3 (CR)	≥50	0.020	5.20	1.78 × 10 ⁶	95.8	0.3	2.1
HEK293SF	NS + hypoxia	1E-3 (CR)	5	0.019	5.45	4.22 × 10 ⁵	59.1	0.1	0.6
HEK293SF	NS + trypsin	1E-4 (CR)	≥50	0.020	5.45	2.37 × 10 ⁶	83.2	0.4	3.2

Note: Reference refers to the data obtained from Göbel, Kortum et al. (2022) with the rVSV-NDV-GFP construct (37°C, without NS). CR and pIX refer to the previously described cell source used for production of the stock virus. BHK-21 NS 34°C cultures are reported as the mean and standard deviation of two independent STR cultivations.

Abbreviations: CSVY, cell-specific virus yield; NS, nutrient supplementation; p.i., post infection; VVP, volumetric virus productivity; ≥, equal or greater than.

1. Exchange to PEM medium at TOI, as high virus titers for both HEK293SF and BHK-21 cells were achieved in PEM medium in shake flasks, respectively.
2. Transfer to semi-perfusion to mimic lab-scale perfusion processes and achieve HCD.

We previously reported a rapid decrease of infectious virus titer in AGE1.CR cells in CD-U7 medium in shake flasks for the rVSV-NDV-GFP construct (Göbel, Kortum et al., 2022). Although the infectious virus titer of rVSV-NDV was stable in STR batch cultivations for AGE1.CR cells (see Section 4.1), a similar degradation kinetic was observed in shake flask

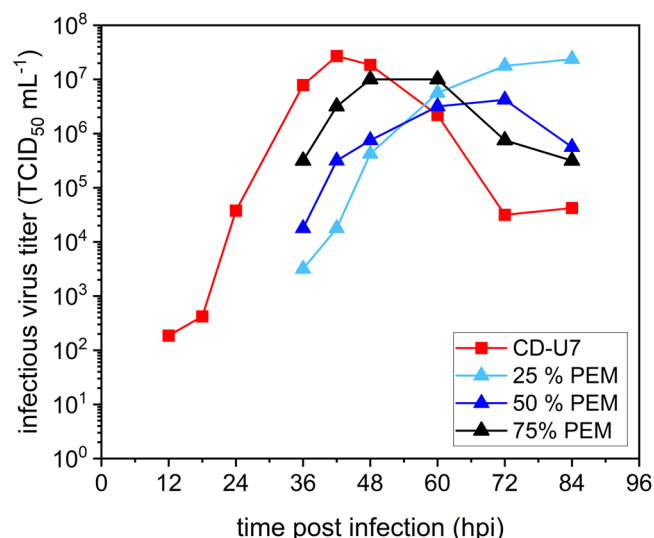


FIGURE 3 Effect of medium replacement at time of infection on virus stability at time of infection for rVSV-NDV production in AGE1.CR cells. AGE1.CR cells were grown in baffled 125 mL shake flasks ($V_w = 50$ mL, 185 rpm) and infected at a viable cell concentration of 2.0×10^6 cells/mL with rVSV-NDV(pIX) at a MOI of $1E-5$. At time of infection, the growth medium was removed completely and exchanged to the respective CD-U7/PEM mixtures. NDV, Newcastle disease virus; rVSV, recombinant vesicular stomatitis virus.

cultivations (Figure 3). On the other hand, infectious virus titers remained stable in PEM medium used for cultivation of BHK-21 and HEK293SF cells, although strong declines in viability were observed. Our initial hypothesis was that CD-U7 medium, as opposed to PEM medium, was lacking a compound that could prevent virus degradation. To evaluate the potential of a medium exchange at TOI for AGE1.CR cells, various media with CD-U7/PEM ratios ranging from 25% to 75% were tested in shake flask cultivations (Figure 3).

Addition of PEM medium at time of infection did not result in an increase of the maximum infectious virus titer compared to the infection carried out with CD-U7 medium, regardless of the ratio. However, as shown in Figure 3, ratio-dependent changes in virus dynamics could be observed: While the maximum infectious virus titer in CD-U7 media was reached 42 hpi, a slower replication kinetic was observed for all PEM contents. Here, the maximum infectious virus titer was reached faster with increasing PEM contents, 84i, 72, and 48 hpi for 25%, 50%, and 75%, respectively. Interestingly, a strong reductions of infectious virus titers could be prevented for a PEM content of 25% within 84 hpi. However, viability of all PEM spiked cultures stayed above 90% over the entire infection period, while it decreased to 50% at 60 hpi for CD-U7 (data not shown).

A commonly applied strategy to overcome nutrient limitations and the accumulation of inhibitors is the transition from batch mode to perfusion. Here, fresh media is added constantly, while spent medium is simultaneously removed. As higher cell concentrations can be reached in perfusion mode, overall higher virus titers and VVPs can be attained if the CSVY is kept constant. As for now, rVSV-NDV was not investigated in high cell density cultivations above 10.0×10^6 cells/mL. Therefore, a

semi-perfusion strategy was evaluated in shake flasks to achieve higher cell concentrations ($>20.0 \times 10^6$ cells/mL) to optimize process conditions for subsequent bioreactor processes in perfusion mode. Several parameters that can influence the virus production were varied: temperature at time of infection, media composition and MOI (Table 1). For six different conditions (C1-C6), a MOI screening with MOIs $1E-3$ – $1E-5$, a temperature shift to 34°C , and two different media compositions, were investigated.

During cell propagation, CD-U7 medium was used for C1–C5, whereas for C6 a mixture of CD-U7 and F12 medium (6:1) was used. For all conditions, cells grew without a noticeable lag-phase with an average μ of 0.024 1/h (Figure 4d). With the initiation of the semi-perfusion mode 48 h after inoculation, the metabolite concentrations started to stabilize at levels between 15 and 25 mM for glucose, 10–20 mM for lactate, 1.5 mM for glutamine, and 0.5 mM for ammonium (data not shown). After a complete medium exchange at TOI, the cells continued to grow until 18–36 hpi (Figure 4). Shortly thereafter, the cell viability started to decline and dropped below 80% at 48 hpi for C1–C3. After the complete medium exchange, the metabolite concentrations reached a stable level at 12 hpi, which was maintained with feeding and the re-start of the semi-perfusion mode until the end of the cultivations (data not shown).

For all conditions, except for C3, the start of infectious virus production was observable at 12–18 hpi. As shown in Figure 4a, higher MOIs did not result in higher infectious virus titers although maximum values were reached earlier. For C1 and C2, virus production peaked at 36 hpi with maximum titers of 1.0×10^6 TCID₅₀/mL and 1.3×10^6 TCID₅₀/mL before decreasing until the end of the cultivation. In comparison, the maximum infectious virus titers reached with a MOI of $1E-5$ (C3) were increased by more than one order of magnitude compared to the higher MOI. However, the infectious virus titer declined faster (by 1 log within 12 h) after reaching the maximum value (Figure 4a). Shifting the temperature to 34°C after infection (C4) resulted in a 3-fold increase of maximum infectious virus titer at a MOI of $1E-4$. Titters of C3 continued to increase until 42 hpi peaking at a maximum of 4.2×10^6 TCID₅₀/mL before slowly declining until the end of the process. Interestingly, the decrease in temperature was not able to slow down the degradation of infectious virus particles (Figure 4b). Lastly, two different media compositions with supplementation of CDU7 with PEM medium (C5) and F12 medium (C6) were tested (Figure 4c). For both conditions, the infectious virus titers increased exponentially and maximum values of 5.6×10^6 TCID₅₀/mL at 42 hpi (C6) and 3.2×10^7 TCID₅₀/mL at 48 hpi (C5) were achieved, respectively (Figure 4c). This corresponded to a 20-fold (PEM) and 4-fold (F12) increase in maximum infectious virus titers compared to the cultivation with CD-U7 base medium (C2) (Table 3). Nevertheless, neither supplementation with PEM nor addition of F12 medium were able to prevent virus degradation after the maximum titer was reached (Figure 4c). When comparing the maximum accumulated infectious virus titers of the best conditions (C3 and C5), an increase was achieved by supplementing PEM medium compared to C3. Regardless of the strategy used, the CSVY was significantly

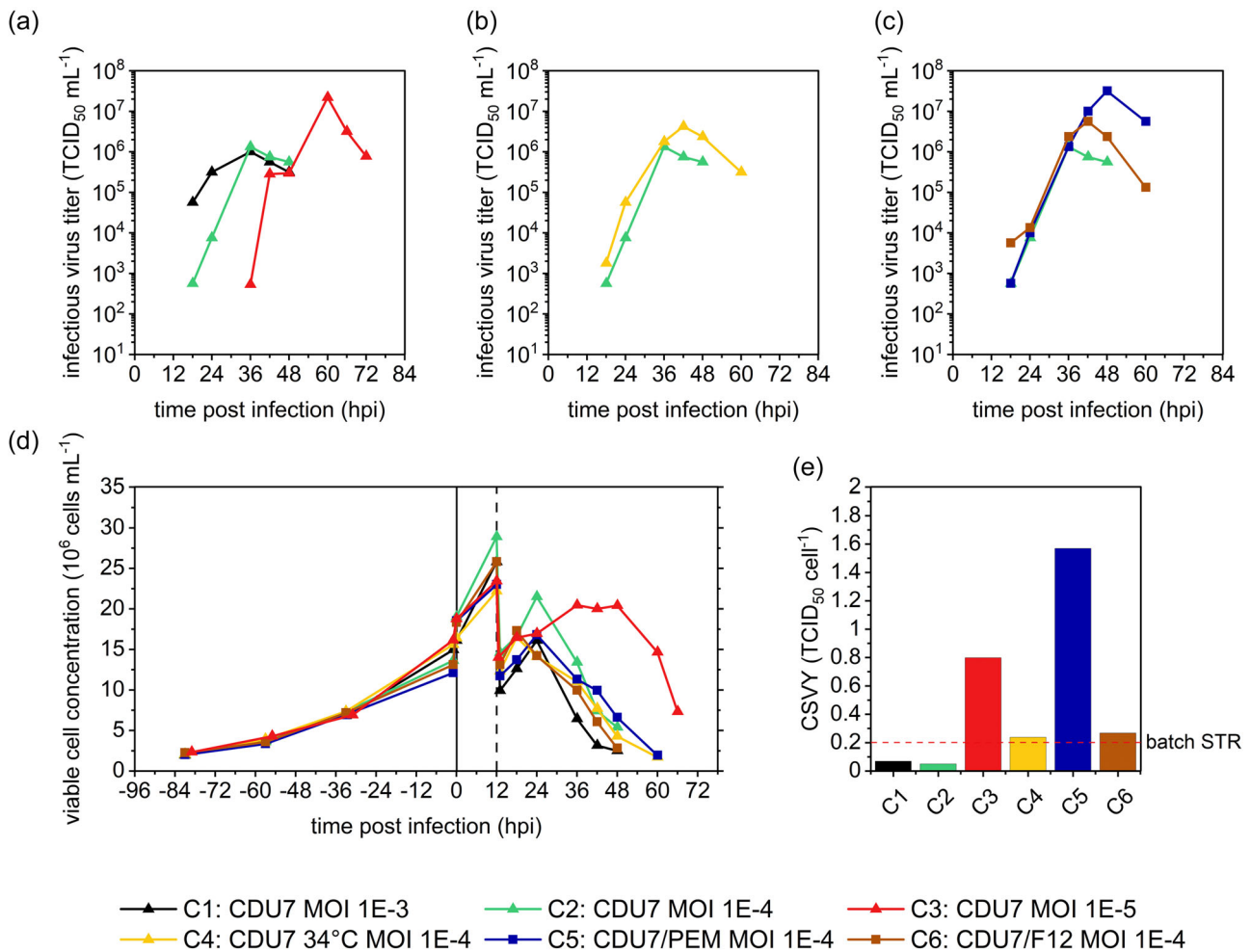


FIGURE 4 Infectious virus titers, cell growth and CSVY for AGE1.CR cells infected with rVSV-NDV(pIX) in semi-perfusion mode in shake flasks. AGE1.CR cells were grown to high cell concentrations (HCD) in 125 mL shake flasks ($V_w = 50$ mL) in semi-perfusion mode and infected at 20×10^6 cells/mL after a complete medium exchange. Fresh medium was added at 12 hpi (two-fold dilution; dashed line). C1–C3 were infected with MOIs ranging from $1E-3$ to $1E-5$ and continuously maintained in CD-U7 medium at 37°C . Similarly, C4–C6 were infected with a MOI of $1E-4$, but parameters were modified. For C4, the temperature was decreased to 34°C after infection, while for C5 the medium was changed to a mixture of 75% CDU7% and 25% PEM. Cells of C6 were continuously maintained in CDU7/F12 (6:1) at 37°C . Semi-perfusion with 1.6 RV/d was restarted 24 hpi, where 80% of the culture supernatant was exchanged 36, 48, and 60 hpi. (a–c) infectious VSV-NDV titer for (a) MOI screening at HCD, (b) temperature shift 37°C to 34°C at HCD, (c) medium composition at HCD, (d) cell growth, (e) CSVY. CSVY, cell-specific virus yield; NDV, Newcastle disease virus; rVSV, recombinant vesicular stomatitis virus.

decreased compared to shake flask cultivations in batch mode. Nevertheless, compared to the batch cultivation in the STR (Table 2), a more than five-fold increase in CSVY was achieved for C5. Moreover, the VVP was 200-fold higher for C5 compared to the batch cultivation in the STR, suggesting a benefit of HCD cultivations not only for increasing virus titers but also for reducing medium consumption (Table 3).

3.3 | High cell density production of rVSV-NDV in HEK293SF cells in semi-perfusion mode

In the preceding experiments, we were able to confirm the potential of semi-perfusion culture for the production of rVSV-

NDV. Therefore, infection cell concentrations of 10.0×10^6 and 20.0×10^6 cells/mL were evaluated for HEK293SF cells in a next step. Upon infection, VCC increased to 25.2×10^6 and 26.8×10^6 cells/mL with viabilities above 90%, respectively (Figure 5a). From 72 hpi onwards, cell viability rapidly declined. Interestingly, growth of cells infected at higher cell concentrations was significantly slower although optimal metabolite levels were maintained throughout the infection phase (Supporting Information: Figure S2). Nevertheless, maximum titers up to 8.0×10^7 TCID₅₀/mL were achieved in both cultures around 84–96 hpi (Figure 5b). Semi-perfusion cultures either infected at 10.0×10^6 or 20.0×10^6 cells/mL displayed no differences in either maximum titers (4.2×10^7 – 1.0×10^8 TCID₅₀/mL) (Figure 5b) or CSVY (Table 3), also if compared against shake

TABLE 3 Cell growth and rVSV-NDV production in the shake flask cultures of AGE1.CR and HEK293SF cells in semi-perfusion mode.

Cell line	Condition	MOI (virus)	μ (h^{-1})	Max. VCC p.i ($\times 10^6$ cell mL^{-1})	Max. infec. virus titer (TCID_{50} mL^{-1})	Time of max. titer (hpi)	CSVY ($\text{TCID}_{50}/\text{cell}$)	VVP ($\times 10^8$ $\text{TCID}_{50}/\text{L}/\text{d}$)
AGE1.CR	C1	1E-3 (pIX)	0.026	16.1	1.0×10^6	36	0.01	1.6
AGE1.CR	C2	1E-4 (pIX)	0.024	21.5	1.3×10^6	36	0.01	1.3
AGE1.CR	C3	1E-5 (pIX)	0.025	21.3	2.3×10^7	60	0.10	10.8
AGE1.CR	C4	1E-4 (pIX)	0.026	14.1	4.2×10^6	42	0.05	3.5
AGE1.CR	C5	1E-4 (pIX)	0.023	16.8	3.2×10^7	48	1.60	22.0
AGE1.CR	C6	1E-4 (pIX)	0.022	14.2	5.6×10^6	42	0.06	4.0
HEK293SF	10×10^6 cells/mL	1E-3 (CR)	0.023	25.2 ± 1.4	1.0×10^8	78 ± 9	11 ± 1	20.5 ± 2.4
HEK293SF	20×10^6 cells/mL	1E-3 (CR)	0.027 ± 0.001	26.8 ± 3.3	$7.1 \times 10^7 \pm 4.1 \times 10^7$	84 ± 17	7 ± 2	11.0 ± 4.6

Note: All maximum cell concentrations are normalized to the highest dilution applied after infection at 12 hpi. CR and pIX refer to the previously described cell source used for production of the stock virus. Results for HEK293SF cells are reported as the mean and standard deviation of two independent shake flask cultivations. CSVY: cell-specific virus yield, p.i: post infection, VVP: volumetric virus productivity.

Abbreviations: CSVY, cell-specific virus yield; NDV, Newcastle disease virus; pi, post infection; rVSV, recombinant vesicular stomatitis virus; VVP, volumetric virus productivity.

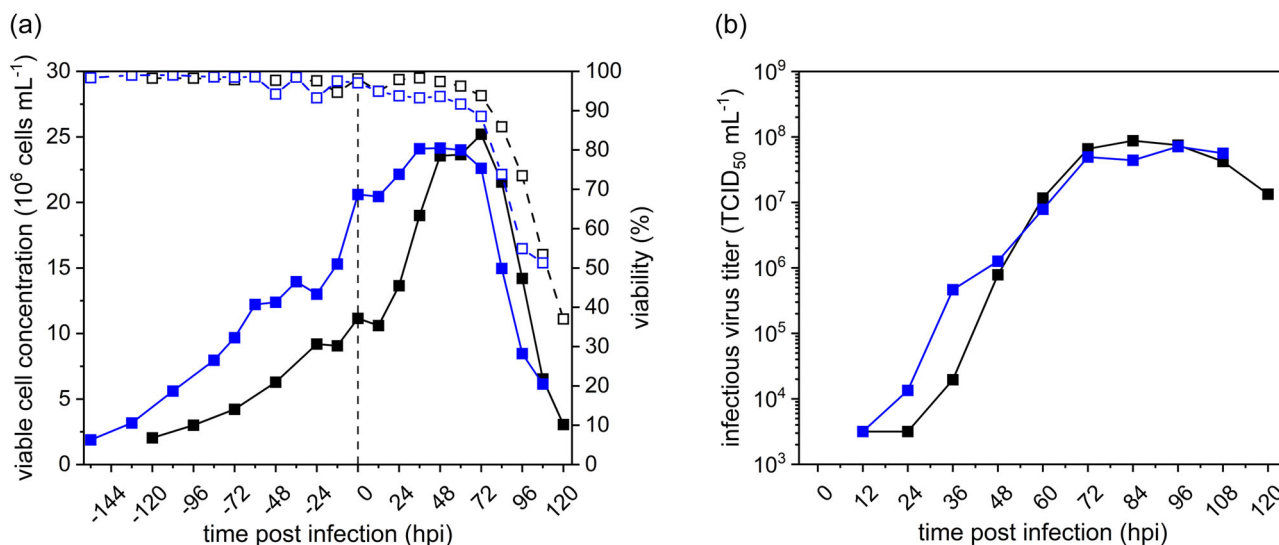


FIGURE 5 Effect of cell density at time of infection on rVSV-NDV production in HEK293SF cells in semi-perfusion cultures in shake flasks. (a) Viable cell concentration (solid lines) and viability (dash lines and open symbols) during growth and virus production of HEK293SF cells infected at viable cell concentrations of 10.0×10^6 cells/mL (black) and 20.0×10^6 cells/mL (blue), respectively; (b) infectious virus titer of cells infected at viable cell concentrations of (black) 10.0×10^6 cells/mL and (blue) 20.0×10^6 cells/mL, respectively. Values are reported as the mean of a biological duplicate of two independent shake flasks. NDV, Newcastle disease virus; rVSV, recombinant vesicular stomatitis virus.

flask batch cultures infected at 2.0×10^6 cells/mL (data not shown).

Nevertheless, there were benefits in terms of virus production by doubling the infection cell concentration. Compared to the batch STR run (Table 2), a 36-fold increase in CSVY was achieved for cells infected at 10.0×10^6 cells/mL, indicating a possible advantage of a semi-perfusion strategy for rVSV-NDV production. Additionally, the VVP was up to 6-fold higher in comparison to the highest VVP achieved in the 1 L STR, which exemplifies that higher productivities could be achieved at lower V_w .

3.4 | Process intensification in STRs using perfusion mode

Finally, cultivations of AGE1.CR, BHK-21 and HEK293SF cells were carried out in perfusion mode using a 1 L STR and an acoustic settler as cell retention device. A cell concentration of 30.0×10^6 cells/mL was targeted for AGE1.CR and BHK-21 cells at TOI using the DASGIP STR system. In contrast, based on results obtained in semi-perfusion mode in shake flasks, HEK293SF cells were infected at lower cell concentrations of 15.0×10^6 cells/mL in the Biostat B STR system. All cell lines displayed viabilities exceeding 95% and consistent growth during the exponential

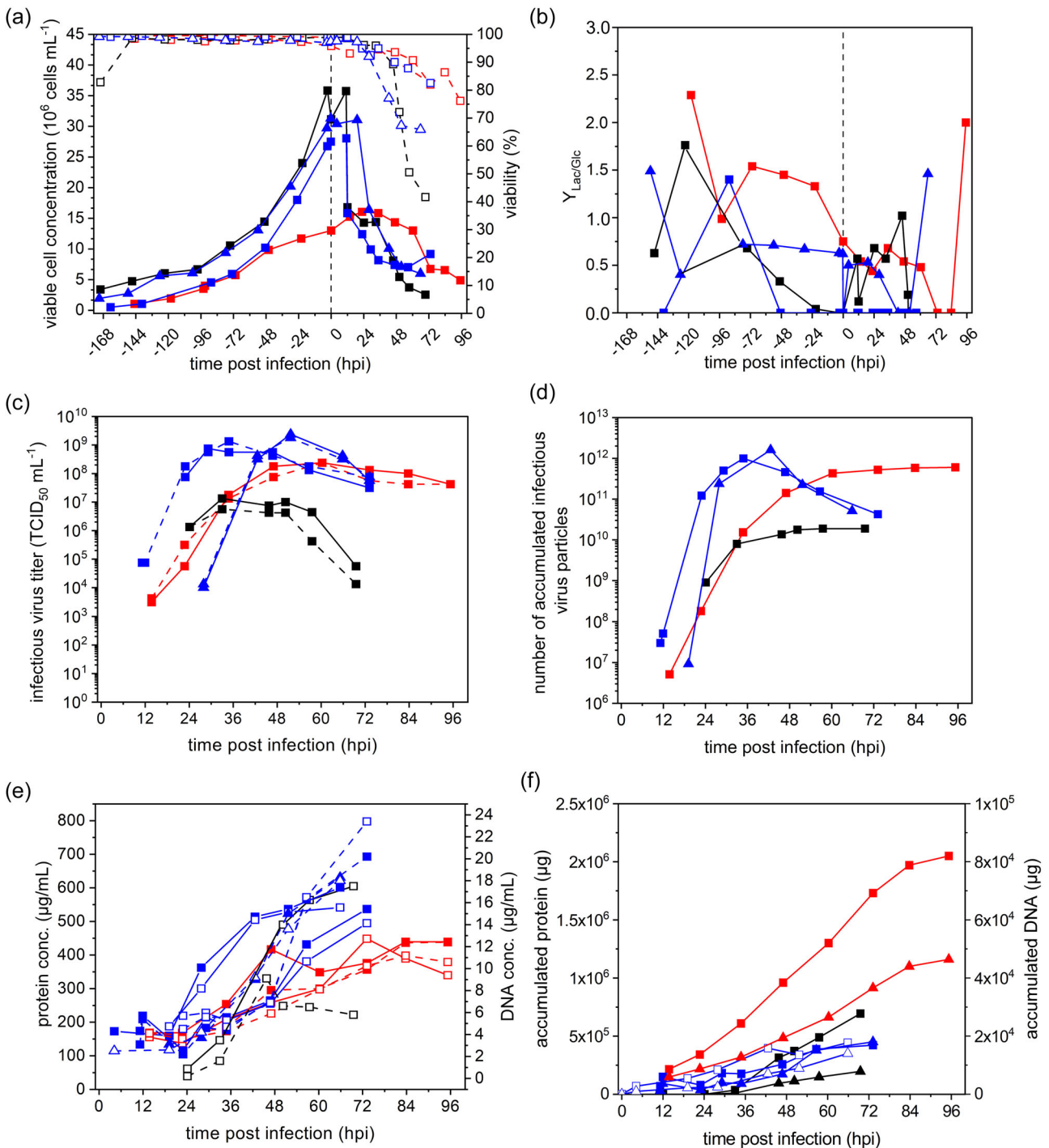


FIGURE 6 rVSV-NDV production in AGE1.CR (black), BHK-21 (blue), and HEK293SF (red) cells in 1 L STR cultures in perfusion mode using an acoustic settler for cell retention. (a) Viable cell concentration (solid lines) and viability (dashed lines and open squares), (b) $Y_{Lac/Glc}$ yield, (c) infectious virus titer in the bioreactor (dashed lines) and in the harvest (solid lines) fractions, (d) accumulated number of infectious virus particles, (e) concentration of protein (solid line) and DNA (dashed line) in the bioreactor (filled squares) and in the harvests (empty squares), and (f) accumulated total protein (squares) and host cell DNA (triangles). AGE1.CR and BHK-21 cells were cultivated in a DASGIP system, HEK293SF cells were cultivated in a Biostat system. BHK-21 cultivation II data is shown in triangles in (a–e), and as empty symbols in (f). NDV, Newcastle disease virus; rVSV, recombinant vesicular stomatitis virus.

growth phase. HEK293SF cells grew exponentially in batch mode with $\mu = 0.024$ 1/h during 48 h, reaching 3.2×10^6 viable cells/mL. Cells continued growing under perfusion with $\mu = 0.018$ 1/h, and within 96 h reached 12.0×10^6 viable cells/mL with a viability above 95%. Upon

infection, cells had a brief growth period of 24 h reaching a maximum VCC of 16.0×10^6 cells/mL (Figure 6a). During batch mode, AGE1.CR cells grew slowly with $\mu = 0.012$ 1/h reaching 6.7×10^6 cells/mL. After initiation of perfusion, cells expanded exponentially with $\mu = 0.018$ 1/h

TABLE 4 Cell growth and rVSV-NDV production in 1 L STR cultures in perfusion mode.

Cell line	Condition	MOI (virus)	μ (h ⁻¹)	Max. VCC p.i ($\times 10^6$ cell mL ⁻¹)	Max. infec. virus titer (TCID ₅₀ mL ⁻¹)	Time of max. titer (hpi)	CSVY (TCID ₅₀ /cell)	VVP ($\times 10^8$ TCID ₅₀ /L/d)
AGE1.CR	Hybrid FB	1E-5(BHK)	0.016	[31.15] 16.80	1.3×10^7	33.0	1.5	3.8
BHK-21Cultivation I	Hybrid FB	1E-4(BHK)	0.022	[28.05] 15.85	7.5×10^8	29.2	110	428.0
BHK-21Cultivation II	Hybrid FB	1E-4(BHK)	0.017	[31.40] 16.40	2.4×10^9	42.6	126	343.0
HEK293SF	Perfusion	1E-3(BHK)	0.018	[13.00] 16.05	2.4×10^8	60.2	75	49.3

Note: Maximum viable cell concentrations are given at time of infection [] and during infection. (BHK) refers to the previously described cell source used for production of the stock virus.

Abbreviations: CSVY, cell-specific virus yield; FB, fed-batch; NDV, Newcastle disease virus; pi, post infection; rVSV, recombinant vesicular stomatitis virus; VVP, volumetric virus productivity.

reaching 35.0×10^6 cells/mL within 96 h (Figure 6a). The fact that specific growth rates were similar to batch cultivations in bioreactors for HEK293SF and AGE1.CR cells (Table 2) suggests that cell growth was not impaired by high cell concentrations and use of the acoustic settler. For BHK-21 cells, μ was in the range 0.025–0.030 1/h during batch mode. After initiation of perfusion, μ dropped to 0.020 and 0.014 h⁻¹ but cell concentration continued to increase to 28.5–31.0 $\times 10^6$ cells/mL, respectively for both replicates (Figure 6a). For all cultivations, a cell retention efficiency above 97% was achieved during cell growth phase using the acoustic settler (Supporting Information: Figure S4).

Glucose and glutamine concentrations were above 10 and 3 mM, respectively, over the entire cultivation period for all cell lines. Lactate accumulated to maximum concentrations of 28 mM for HEK293SF, 18 mM for BHK-21 and 12 mM for AGE1.CR cells during batch mode, and decreased to about 20 mM for HEK293SF, 13 mM for BHK-21, and 2 mM for AGE1.CR cells during perfusion. Ammonium and glutamate concentrations were below 1.5 and 3 mM, respectively, over the entire cultivation period for all cell lines (Supporting Information: Figure S3). pH value and osmolality were 7.0–7.6 and 250–340 mOsmol/Kg for all cultures, respectively (Supporting Information: Figure S4).

To assess the metabolic performance of the cells, the lactate to glucose yield ($Y_{Lac/Glc}$), was calculated. Maximum values of the $Y_{Lac/Glc}$ were reached predominantly during the growth phase in batch mode. The $Y_{Lac/Glc}$ was stabilized during the growth phase in perfusion mode at values around 1.5 mmol lactate/mmol glucose for HEK293SF cells, 0.25 mmol lactate/mmol glucose for BHK-21 cells, and 0 mmol lactate/mmol glucose for AGE1.CR cells. Upon infection, the $Y_{Lac/Glc}$ exhibited an abrupt increase for all cell lines, particularly toward the end of the cultivations, to levels close to that observed during growth in batch mode.

As mentioned before, higher cell concentrations can lead to increased amounts of nonquantified substrates and virus production inhibitors, which can decrease the CSVY and virus titers. Mammalian cell growth requires at least 13 amino acids (Eagle, 1959). Therefore, to avoid limitations of nonquantified metabolites, cell culture medium was additionally exchanged with a high flow-rate (5 RV/d) 2 h before infection. This high exchange rate resulted in a 14% loss of cells for the AGE1.CR cultivation through the acoustic chamber (Figure 6a).

By reducing the maximum flow rate to 4 RV/d, a retention efficiency of 99% was achieved for BHK-21 and HEK293SF cells, respectively (Supporting Information: Figure S4).

Overall, a maximum infectious virus titer of 2.4×10^8 TCID₅₀/mL for HEK293SF, 1.3×10^7 TCID₅₀/mL for AGE1.CR and 7.5×10^8 – 2.4×10^9 TCID₅₀/mL for BHK-21 cell cultivations was achieved 36–60 hpi in bioreactors (Table 4). As expected, infectious virus titers from bioreactor and harvest vessel samples were practically the same for all cultivations. AGE1.CR and BHK-21 cells continued to grow until 12 hpi in batch mode before being subsequently diluted with fresh medium. HEK293SF cells continued to grow until 24 hpi, after which VCC and viability steadily decreased until the end of the experiment to about 33% of the maximum VCC and 75% viability, respectively (Figure 6a). CSVYs of 75 TCID₅₀/cell for HEK293SF, 1.5 TCID₅₀/cell for AGE1.CR and 110–126 TCID₅₀/cell for BHK-21 cells were obtained in perfusion mode (Table 4). This corresponded to a 250-fold and 1.5-fold increase for HEK293SF and AGE1.CR cells, respectively. For BHK-21 cells no difference was found compared to the best results obtained in batch mode (Table 2). An exchange rate of 2–3 RV/d was sufficient to prevent any limitations in glucose concentrations, and—most likely—the accumulation of inhibitors (Supporting Information: Figure S3). The VVP in perfusion mode was equal to 3.8×10^8 TCID₅₀/L/d for AGE1.CR, 4.9×10^9 TCID₅₀/L/d for HEK293SF, and 3.4 – 4.3×10^{10} TCID₅₀/L/d for BHK-21 cells, which was around 15–30-fold higher for AGE1.CR and HEK293SF cells compared to batch processes performed at the same scale (Table 4). For BHK-21 cells, the VVP was 3-fold lower in perfusion mode compared to the batch process (Table 2). Interestingly, the VVP was reduced by 6-fold for AGE1.CR cells when comparing semi-perfusion in shake flasks to perfusion cultivations in STR, although the permeate flow was controlled tightly in the latter. This was not the case for HEK293SF cell cultivations, for which the switch from semi-perfusion to perfusion mode yielded a 2-fold increase in VVP.

To assess the potential burden of high cell concentrations on performance of subsequent downstream purification trains, DNA and total protein levels in the bioreactor and the harvest vessel were determined. During the first 24 hpi, the protein concentration was about 150–200 μ g/mL and then began rising in both the bioreactor and harvest vessel for all cell lines (Figure 6e). Samples from the bioreactor displayed slightly higher protein concentrations than

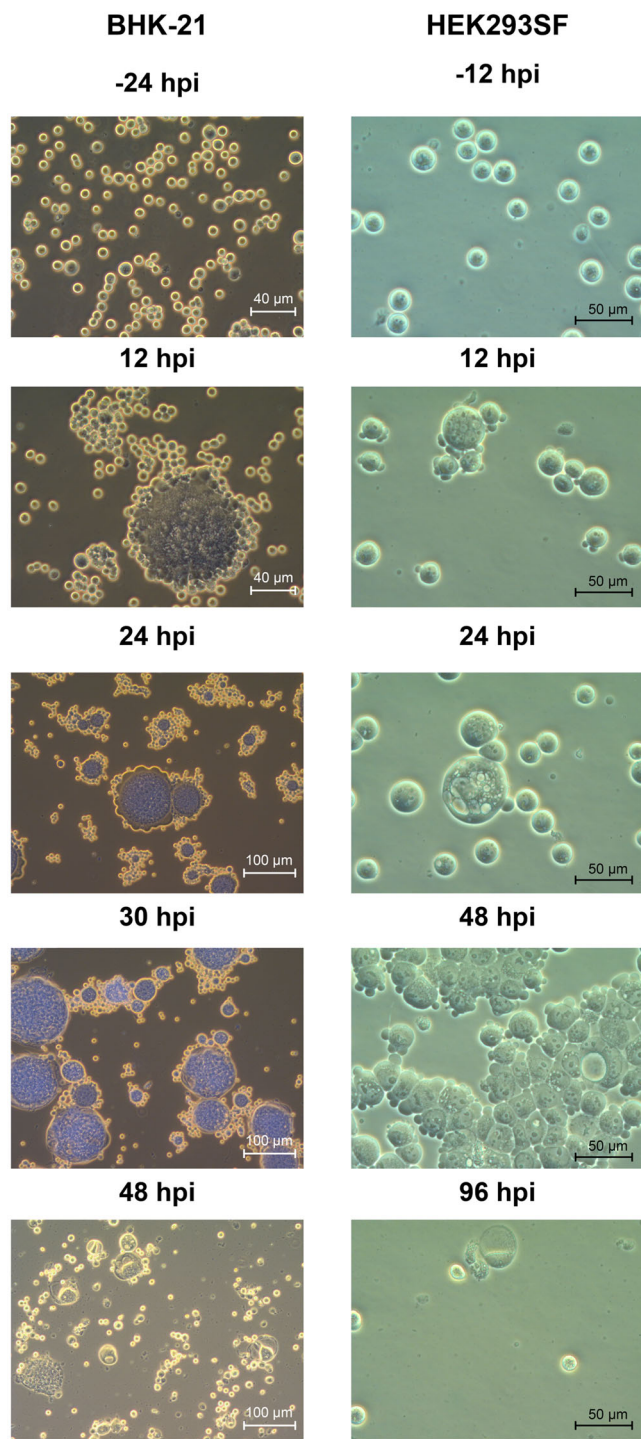
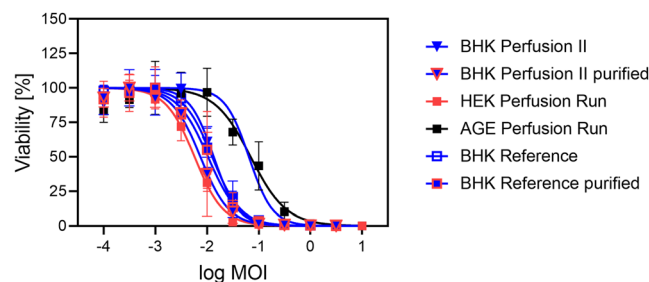


FIGURE 7 Syncytia formation during rVSV-NDV production in 1 L STR perfusion cultures of BHK-21 and HEK293SF cells. Starting 12 hpi, clusters of fused and enlarged cells appeared in the STR and they lysed after 48 hpi for BHK-21 and 96 hpi for HEK293SF. AGE1.CR did not form syncytia in perfusion culture (not shown). NDV, Newcastle disease virus; rVSV, recombinant vesicular stomatitis virus.

samples from the harvest vessel until about 60 hpi, and reached about 450 $\mu\text{g}/\text{mL}$ at the end of the experiment for HEK293SF cells. Maximum protein concentrations of 600 $\mu\text{g}/\text{mL}$ were reached for BHK-21 and AGE1.CR cells, respectively. The level of DNA began



	BHK-21 reference	BHK-21 reference purified	BHK-21 Cultivation II	BHK-21 Cultivation II purified	HEK293SF	AGE1.CR
Log IC ₅₀	-1.90	-1.98	-1.87	-2.13	-2.24	-1.16
IC ₅₀	0.0126	0.0104	0.0135	0.0074	0.0057	0.0699

FIGURE 8 Oncolytic viral potency values for rVSV-NDV produced in perfusion mode. Viability of Huh7 cancer cells was determined 48 hpi with rVSV-NDV generated in the respective suspension cell line grown in perfusion mode and compared to virus generated in BHK-21 cells cultivated in STR in batch mode. Sucrose-gradient purified material of the reference STR batch culture as well as BHK II perfusion culture was additionally included. IC₅₀ and log IC₅₀ values determined from the dose-response curves after nonlinear regression analysis. Values are reported as the mean of technical triplicates, with $n = 3$ for all samples. NDV, Newcastle disease virus; rVSV, recombinant vesicular stomatitis virus.

accumulating from 36 hpi from 4 up to 12 $\mu\text{g}/\text{mL}$ for HEK293SF and AGE1.CR cells, and 18–23 $\mu\text{g}/\text{mL}$ for BHK-21 cells, respectively (Figure 6e). Taking into account the total volume harvested after infection, virus material produced in the HEK293SF cell cultivation had the highest levels of DNA and protein (Figure 6f), approximately four to six-fold higher than for the other cell lines.

In our previous study we found no evidence of syncytia formation in various suspension cell sources, even when inducing cell clumping via supplementation of CaCl_2 (Göbel, Kortum et al., 2022). Monitoring bioreactor samples by bright-field microscopy confirmed this finding for AGE1.CR cells. No syncytia formation was observed for any time point post infection. Surprisingly, syncytia formation was found for BHK-21 and HEK293 perfusion cultures. Here, clusters of fused and enlarged cells appeared within the first 12 hpi (Figure 7). These clusters reached sizes from 70 to 80 μm in HEK293 to 100–120 μm in BHK-21 cells.

Finally, we investigated whether the production rVSV-NDV at HCD or syncytia formation in perfusion mode has an impact on its oncolytic properties in susceptible Huh7 cells using the IC₅₀ potency assay. Samples from all STR perfusion cultures were compared to material previously produced in BHK-21 suspension cells in STR culture (Table 2 NS 34°C). Additionally, sucrose-gradient purified material of the reference culture as well as BHK perfusion culture II was tested, to investigate the potential effect of contaminants at HCD on oncolytic potency.

As indicated in Figure 8, rVSV-NDV harvested from the perfusion cultures of HEK293SF cells and BHK-21 run II cell cultures had a similar oncolytic potential in Huh7 cells as the BHK-21 cell reference. Interestingly, the dose required to induce 50% cancer cell

cytotoxicity was 0.7 log higher for rVSV-NDV produced in AGE1.CR cells. Overall, regardless of the cell line, perfusion mode and HCD cultivations did not alter the ability of the produced virus to induce oncolysis. Purification via sucrose-gradient reduced the dose required to induce 50% cancer cell cytotoxicity regardless of the cultivation mode. However, a greater increase in potency was achieved for material produced in perfusion mode.

4 | DISCUSSION

Due to the significant advances in oncolytic virotherapy, more and more production modalities are required for clinical studies and applications. To our knowledge, advanced HCD cell culture technologies have not yet been reported for production of clinical grade oncolytic herpes simplex virus, vaccinia virus, and reovirus, (Ungerechts et al., 2016). Among the few descriptions for manufacture at HCD, Grein et al. studied production of oncolytic measles virus in Vero cells attached to microcarriers (Grein et al., 2019). An oncolytic adenovirus was produced in tumor suspension-adapted cells in perfusion cultures in ATF mode (Yuk et al., 2004). Both studies had the goal to achieve a high number of doses containing the up to 10^{11} infectious virus particles per dose that are required for clinical efficacy. Compared to traditional OV, OV vector platforms that induce syncytia formation in infected cells pose additional challenges to the manufacturing process. In our previous study, we identified several suspension cell substrates that are able to support the replication of the fusogenic rVSV-NDV to high titers in batch mode (Göbel, Kortum, et al., 2022). This study aimed to establish an improved rVSV-NDV manufacturing process for generating high titer stocks from HCD suspension cultures optimizing cell culture medium formulation and infection conditions.

4.1 | rVSV-NDV production in STR in batch mode

HEK293 is a well-known host cell line for the production of viral vectors and recombinant proteins (Abaandou et al., 2021; Dumont et al., 2016; Venereo-Sanchez et al., 2016), and has also been explored for the manufacturing of vaccines (Le Ru et al., 2010). HEK-293 cultures are also fully permissive for rVSV-NDV (Göbel, Kortum et al., 2022). However, only low virus titers were obtained in a scale-up from shake flask to 1 L STR in batch mode. To overcome this limitation, several strategies were applied. The first one consisted in a medium supplementation with glucose and glutamine. Providing an optimal metabolic state with a sufficient supply of extracellular substrates is critical to achieve high virus yields (Aunins, 2003). The increase in concentration of these major sources of carbon and energy metabolism doubled rVSV-NDV titers. In addition, a reduction in oxygen partial pressure to 5% pO₂ during virus replication (hypoxia) was considered. Exposing adherent Vero cells to low oxygen levels increased production yields for VSV (Lim et al., 1999). rVSV-NDV is an RNA virus that is highly sensitive to antiviral actions of type I interferons (IFN) (Abdullahi et al., 2018). We previously reported a slow, gradual, and incomplete infection of HEK293SF cells even at higher

MOIs (Göbel, Kortum et al., 2022). Continuously increasing the population of infected cells without losing the cell source due to oncolysis appears favorable if a shift to an antiviral state by IFN signaling cascades can be prevented. Therefore, virus replication was expected to be enhanced if cellular defenses against viral infections mediated by IFN can be inactivated by oxygen limitation (Miar et al., 2020). Trypsin addition was tested along nutrient supplementation to promote virus entry into the cell by hemagglutinin cleavage as required for the production of influenza A virus (Klenk et al., 1975). Trypsin addition has also enhanced influenza A virus replication by proteolytic degradation of IFN (Seitz et al., 2012). While both measures allowed only a modest increase in rVSV-NDV titers (0.5 log), cell growth was not compromised. With the current data a potential accumulation of nonquantified compounds inhibiting viral vector replication cannot be excluded. Such an effect was suggested by the results obtained for BHK-21 cells, where adjustments in medium formulation yielded a doubling of the rVSV-NDV titers and CSVY. A reduction of temperature at time of infection was often found to increase virion stability and/or maximum virus titers (Elahi et al., 2019; Genzel & Reichl, 2009; Kaptein et al., 1997; Nikolay et al., 2018; Petiot et al., 2011; Wechuck et al., 2002). However, in our case, a reduction of temperature to 34°C after infection had neither an effect on cell growth nor on virus stability, maximum infectious virus titer or CSVY. Similar results were obtained for AGE1.CR cells. Overall, we suspect a limitation of nonquantified metabolites or an accumulation of inhibiting molecules to be the reason for this drastic reduction in viral vector titers in comparison to the titers achieved in shake flasks with complete medium exchange at TOI. In a subsequent study, the impact of pH-drifts, as observed in shake flask cultivations, and of differences in shear forces between STR and shake flasks on maximum infectious virus titers could be further investigated.

4.2 | Medium switch and transition to semi-perfusion mode for AGE1.CR cells

A rapid decline of infectious activity was observed for both rVSV-NDV (Figure 3) and, previously, for rVSV-NDV-GFP (Göbel, Kortum et al., 2022) in studies with AGE1.CR cultures. To improve titers and virion stability, we investigated an alteration of medium properties at the time of infection (Jordan et al., 2011, 2016). Supplementation of PEM to CD-U7 medium improved viability of AGE1.CR cells for the entire infection period. Although maximum titers did not increase, the level of infectious units were best maintained in cultures with CD-U7 medium containing 25% PEM. We suspect that recombinant insulin, trace elements, or polyamines in PEM could be responsible for improved infectious stability. Hydrolysates are an important component of many serum-free media that can increase buffering capacity and delay cell death so that production intervals are prolonged (Ho et al., 2021). However, CD-U7 does not and (to our knowledge) PEM may also not contain hydrolysates. Polyamines are contained in different ratios and configurations in various advanced and basal media (such as putrescine in F12). They have pleiotropic effects that can support or interfere with viral replication (Mounce et al., 2017). Insulin and insulin-like growth factors have been

demonstrated to inhibit apoptosis in CHO cells (Adamson & Walum, 2007; Ghafari-Esfahani et al., 2020; Sunstrom et al., 2000). Prolonged cell survival may not only increase production of recombinant protein (Ghafari-Esfahani et al., 2020) but may also help in infected cultures to replenish virions lost to degradation. Insulin was furthermore identified as a strong activator of the PI3K/Akt pathway supporting early entry uptake, viral RNA expression, and inhibition of premature apoptosis after IAV infection (Planz, 2013). However, there are also reports discussing contrary results such as a delayed viral replication of IAV or fowl plague virus at low MOIs following insulin supplementation (Scholtissek et al., 1986). For hepatitis B virus in a human hepatoma cell line (Gripon et al., 1989), and for hepatitis A virus in PLC/PRF/5 cells (Gauss-Müller & Deinhardt, 1984) reduced titers reported in media with low insulin concentrations compared to cultivations with media containing other supplements or no supplementation. In summary, as observed here, mixtures of media with different levels of supplementation with factors such as polyamines, insulin and insulin-like growth factor may exhibit complex effects on the kinetic of virus replication and maintenance of infectious units.

In a second step, a semi-perfusion strategy was evaluated in shake flasks to achieve higher cell concentrations ($>20.0 \times 10^6$ cells/mL) and optimize process conditions for subsequent bioreactor processes performed in perfusion mode. Multiple studies demonstrated increased MVA and IAV virus titers and VVP by applying hybrid perfusion strategies (hybrid fed-batch) after infection (Gränicher et al., 2021; Vázquez-Ramírez et al., 2019). Compared to shake flask cultivations in batch mode, HCD cultivations often resulted in a drastically reduced CSVY. This so-called cell density effect has been shown for a variety of virus production processes (Bock et al., 2011; Ferreira et al., 2007; Kamen & Henry, 2004; Nadeau & Kamen, 2003; Perrin et al., 1995; Tapia et al., 2016; Wood et al., 1982). In this study, no nutrient limitation was observed for any of the investigated cultivations. Also, cultivation at HCD did not require an adaptation of the MOI (Figure 4a). However, by decreasing the temperature after infection to 34°C (C4) and additional supplementation with F12 medium (C6), higher infectious virus titers and CSVYs were obtained for AGE1.CR cells compared to 37°C. Furthermore, addition of PEM to CD-U7 medium (C5) after infection of AGE1.CR cells resulted in yet higher infectious virus titers and CSVYs above 1.5 TCID₅₀/cell, although a nonoptimal MOI of 1E-4 was used. Compared to the batch STR cultivation (Table 2), both CSVY and VVP were drastically increased by transition to semi-perfusion at HCD (Table 3).

4.3 | High cell density production of rVSV-NDV in HEK293SF cells in semi-perfusion mode

Although HEK293 cells are being used for production of viral vaccines and viral vectors for over 30 years, production at HCD remains impacted by reductions of CSVYs with increasing cell concentrations. This cell density effect is thoroughly described in the literature for a variety of viruses, particularly for adenovirus (Gálvez et al., 2012; Kamen & Henry, 2004; Nadeau & Kamen, 2003),

but also IAV (Petiot & Kamen, 2013), retroviruses (Rodrigues et al., 2013), and virus-like particles (Fontana et al., 2014). Here, infections at concentrations of 10.0×10^6 and 20.0×10^6 cells/mL did not result in a reduction of CSVY compared to batch cultivations (2.0×10^6 cells/mL), neither in shake flasks nor in STRs. However, there was no benefit in terms of VVP, virus titer or CSVY by increasing the infection cell concentration to 20.0×10^6 cells/mL. Although the CSVY in the 20.0×10^6 cells/mL infected cultivation at TOI was slightly lower compared to the 10.0×10^6 cells/mL infected cultivation at TOI, the difference is negligible and can therefore not be classified as a cell density effect. For these reasons, a concentration below 20.0×10^6 cells/mL at TOI was considered as optimal to further investigate rVSV-NDV production in perfusion applications.

For HEK293SF cells, periodically exchanging the medium with a fixed rate of 1.8 RV/d seemed to be sufficient to avoid the aforementioned accumulation or depletion of nonquantified compounds causing a drastic loss of viral vector productivity in STRs. This was also described by Henry et al., who observed increasing CSVYs with increasing perfusion rates for HEK293 for the production of adenoviral vectors using an acoustic settler for perfusion (Henry et al., 2004). Here, compared to cultivation in batch mode in STRs, CSVY was increased by 36-fold, and VVP was up to six-fold, proving this approach to be valuable both for increasing virus titers but also reducing media consumption.

4.4 | Process intensification in STRs with perfusion mode

Based on the positive results obtained for rVSV-NDV production in semi-perfusion mode, cultivation of all three candidate cell lines in a STR operated in perfusion mode was evaluated. In the systems tested, a HCD above 10×10^6 cells/mL was achieved for all three cell lines. For AGE1.CR cells, cultivation up to 50.0×10^6 cells/mL (Genzel et al., 2014) in perfusion mode employing an ATF system was described previously. HEK293SF cells have been grown up to 15.0×10^6 cells/mL in perfusion mode using an acoustic settler (Petiot et al., 2011). For a process involving other HEK293 cells, up to 80.0×10^6 cells/mL were reached (Schwarz et al., 2020). For BHK-21 cultures, up to 6.0×10^6 cells/mL in perfusion mode using a spin filter for the production of rabies virus (Perrin et al., 1995) was obtained; in semi-perfusion mode even up to 60.0×10^6 cells/mL were reached (Nikolay, 2020).

Uptake rates for glucose and glutamine for HEK293SF and BHK-21 cells during the cell growth phase were higher than for AGE1.CR cells and consequently a higher CSPR of 197 and 110 pL/cell/d for HEK293SF and BHK-21 cells was needed to maintain sufficient metabolite levels. For comparison, AGE1.CR cells were able to utilize a lower CSPR of 55 pL/cell/d, which was in the same range as shown in previous studies (Gränicher et al., 2021; Vázquez-Ramírez et al., 2018, 2019). Control of the perfusion rate using a capacitance probe allowed a robust process control with stable CSPR values over the entire growth phase (Supporting Information: Figure S4d). Similar

findings were reported for a variety of other cell lines, further underlining the versatility of this method (Gränicher et al., 2021; Hein, Kollmus et al., 2021; Nikolay et al., 2018; Wu et al., 2021).

The $Y_{\text{Lac/Glc}}$ provides an insight on the glucose usage. Remarkably, HEK293SF cells exhibited higher $Y_{\text{Lac/Glc}}$ values compared to the other cell lines, beyond 2 mmol lactate/mmol glucose, consistent with previous findings (Petiot et al., 2015). Upon infection, an additional decrease in $Y_{\text{Lac/Glc}}$ was also observed mainly for HEK293SF cells. The observed shifts may be due to a combination of an increased perfusion rate and from a metabolic redirection caused by the infection process, in which more carbon is channeled to the tricarboxylic acid cycle instead of being converted to lactate with the concomitant NADH oxidation (Petiot et al., 2011, 2015). As observed by Gränicher et al. (2020), the $Y_{\text{Lac/Glc}}$ of AGE1.CR.pIX cells in perfusion cultures using ATF and acoustic settlers also increased toward the end of the cultivation and coincided with the loss of cell viability. Due to the fusogenic potential of the rVSV-NDV, the acoustic filter was chosen as retention device to avoid possible clogging of membranes in ATF or TFF applications. To address low virus stability, direct harvesting during cultivation was implemented. The acoustic settler in this work was operated in pump recirculation mode that previously was demonstrated to deliver higher virus productivities than valve recirculation mode (Gränicher et al., 2020). As expected, infectious virus titers of the bioreactor and the harvest vessel were similar and allowed accumulation of infectious virus particles above 10^{11} TCID₅₀ in HEK293SF and BHK-21 cultures. Virus production was considerably improved in comparison to the batch cultures. Although for BHK-21 cells the difference was minimal, they showed in all cultivations the highest CSVY and VVP making BHK-21 the best producer host from the productivity point of view. Possibly, direct cooling of the harvested material could further improve virus stability and thereby increase virus yield. This however, was not tested in the current study.

Regarding the accumulation of impurities, levels of total protein and dsDNA were within the same order of magnitude as reported by Gränicher et al. (2020) for a HCD MVA production process in AGE1.CR.pIX cells. While concentrations of total protein and dsDNA were low for HEK293SF in comparison to BHK-21 cells, accumulated levels of impurities of HEK293SF cells were highest. This is especially surprising as the maximum concentration of HEK293SF cells was much lower than for the other cell lines.

Whether syncytia formation of BHK-21 and HEK293 cells but not of AGE1.CR cells had an effect on the production of the rVSV-NDV remains open. High VCC after infection in AGE1.CR cells would support this phenomenon, but there was no evidence of syncytia formation at low cell concentrations even after induction of aggregation with CaCl₂ (Göbel, Kortum et al., 2022). Particle sizes of the syncytia were in the range of 70–120 μm. Their formation might cause fluid dynamic stress and cell losses due to syncytia-sycytia and syncytia-impeller impacts (Nienow, 2021). While cell retention without a physical barrier (acoustic or inclined settlers and centrifuges) was demonstrated to be efficient, such a requirement introduces new challenges compared to the currently preferred

membrane-based systems (ATF and TFF). Small lumen sizes of hollow-fiber membranes are likely to prevent passage of syncytia, potentially leading to a faster blocking of fibers. On the other side, the use of membrane-based systems could potentially prevent syncytia formation and, therefore, facilitate scale-up of manufacturing processes. In this context, the use of novel membrane systems such as the TDFD from Repligen with large lumen sizes could be an interesting approach for future investigations.

Finally, selective replication, OV spreading and lysis of cancer cells are attributes that need to be considered for production of OVs. This was assessed through a potency assay (EMA, 2009). The scope of the potency measurement was to determine whether cultivation at HCD affected the ability of the virus to induce oncolysis. As crude harvests produced at HCD contain more contaminants (proteins, DNA etc.) than crude material produced in batch culture which are likely to interfere with infectivity and thus potency, increased potency values after purification can be expected. Therefore, a comparison between crude harvest and purified material harvested from the second perfusion cultivation in BHK-21 was carried out and included in the measurement. For a fair comparison, purified material should be used for all perfusion samples, however this was outside of the scope of this study. As demonstrated, for all cell lines, the rVSV-NDV material produced in perfusion mode and at HCD (with and without syncytia formation) was able to induce adequate oncolysis. Compared to material produced in batch mode, the oncolytic potency of material produced in AGE1.CR cells was slightly reduced. Purification via sucrose-gradient led to a greater increase in potency for material produced in perfusion mode compared to batch mode.

In conclusion, evaluation of a series of process conditions in semi-perfusion shake flask and STR batch cultures led to successful implementation of a scalable perfusion HCD process for all three candidate cell lines. This enabled production of rVSV-NDV above 10^{11} infectious virus particles. Using an acoustic settler, the direct harvesting of rVSV-NDV will allow for a seamless integration into downstream processing trains. The influence of HCD conditions, perfusion mode, and syncytia formation during production on the oncolytic potency of rVSV-NDV must still be confirmed in preclinical tumor models. Nevertheless, results clearly represent an important step toward a high-yield manufacturing process for rVSV-NDV and other potential OVs.

AUTHOR CONTRIBUTIONS

Sven Göbel: Conceptualization; methodology; investigation; writing—original draft; writing—review and editing; project administration. **Karim E. Jaén:** Conceptualization; methodology; investigation; writing—original draft; writing—review and editing; project administration. **Yvonne Genzel:** Conceptualization; methodology; writing—review and editing; supervision; project administration. **Udo Reichl:** Conceptualization; writing—review and editing; supervision. **Jennifer Altomonte:** Conceptualization; writing—review and editing; supervision. **Marie Dorn:** Investigation; writing—review and editing. **Victoria Neumeyer:** Investigation; writing—review and editing. **Ingo Jordan:** Writing—review and editing. **Volker Sandig:** Writing—review and editing.

ACKNOWLEDGMENTS

The authors would like to thank Ilona Behrendt for the excellent technical support, Pavel Marichal Gallardo for his support in the quantification of DNA and protein, and Fabian Kortum and Teresa Krabbe for their participation in fruitful discussions. The help of M. Prömmel and B. Hundt (Ceva Innovation Center GmbH) on the BHK-21 cells is equally acknowledged. Part of the funding for this work was provided by the EXIST-Forschungstransfer program (financed by the Federal Ministry for Economic Affairs and Energy) under the grant agreement #03EFOBY215 awarded to Jennifer Altomonte. Open Access funding enabled and organized by Projekt DEAL.

CONFLICTS OF INTEREST STATEMENT

Jennifer Altomonte (WO 2017/198779) holds a patent for the development and use of rVSV-NDV as an oncolytic therapy of cancer and is co-founder of Fusix Biotech GmbH, which is developing the rVSV-NDV technology for clinical use. Ingo Jordan and Volker Sandig are employees of ProBioGen AG where AGE1.CR.pIX, and CD-U7 have been developed.

DATA AVAILABILITY STATEMENT

Data available in article supplementary material. Additional data is available on request from the authors. The data that support the findings of this study are available from the corresponding author, Yvonne Genzel, upon reasonable request.

ETHICS STATEMENT

This article does not contain any studies with human participants or animals performed by any of the authors.

ORCID

Marie Dorn  <http://orcid.org/0000-0002-5188-258X>

Ingo Jordan  <http://orcid.org/0000-0003-2711-7252>

Yvonne Genzel  <http://orcid.org/0000-0002-2264-5569>

REFERENCES

- Abaandou, L., Quan, D., & Shiloach, J. (2021). Affecting HEK293 cell growth and production performance by modifying the expression of specific genes. *Cells*, 10(7), 1667. <https://doi.org/10.3390/cells10071667>
- Abdullahi, S., Jäkel, M., Behrend, S. J., Steiger, K., Topping, G., Krabbe, T., Colombo, A., Sandig, V., Schiergens, T. S., Thasler, W. E., Werner, J., Lichtenhaler, S. F., Schmid, R. M., Ebert, O., & Altomonte, J. (2018). A novel chimeric oncolytic virus vector for improved safety and efficacy as a platform for the treatment of hepatocellular carcinoma. *Journal of Virology*, 92(23);e01386-18. <https://doi.org/10.1128/jvi.01386-18>
- Adamson, L., & Walum, E. (2007). Insulin and IGF-1 mediated inhibition of apoptosis in CHO cells grown in suspension in a protein-free medium. *Alternatives to Laboratory Animals*, 35(3), 349–352.
- Aunins, J. G. (2003). Viral Vaccine Production in Cell Culture. In R. E. Spier (Ed.), *Encyclopedia of Cell Technology* (p. 12). <https://doi.org/10.1002/0471250570.spi105>
- Bock, A., Schulze-Horsel, J., Schwarzer, J., Rapp, E., Genzel, Y., & Reichl, U. (2011). High-density microcarrier cell cultures for influenza virus production. *Biotechnology Progress*, 27(1), 241–250. <https://doi.org/10.1002/btpr.539>
- Cook, M., & Chauhan, A. (2020). Clinical application of oncolytic viruses: A systematic review. *International Journal of Molecular Sciences*, 21(20), 7505. <https://doi.org/10.3390/ijms21207505>
- Coronel, J., Behrendt, I., Bürgin, T., Anderlei, T., Sandig, V., Reichl, U., & Genzel, Y. (2019). Influenza A virus production in a single-use orbital shaken bioreactor with ATF or TFF perfusion systems. *Vaccine*, 37(47), 7011–7018. <https://doi.org/10.1016/j.vaccine.2019.06.005>
- Coronel, J., Gränicher, G., Sandig, V., Noll, T., Genzel, Y., & Reichl, U. (2020). Application of an inclined settler for cell culture-based influenza A virus production in perfusion mode. *Frontiers in Bioengineering and Biotechnology*, 8, 672. <https://doi.org/10.3389/fbioe.2020.00672>
- Dumont, J., Eewart, D., Mei, B., Estes, S., & Kshirsagar, R. (2016). Human cell lines for biopharmaceutical manufacturing: History, status, and future perspectives. *Critical Reviews in Biotechnology*, 36(6), 1110–1122. <https://doi.org/10.3109/07388551.2015.1084266>
- Eagle, H. (1959). Amino acid metabolism in mammalian cell cultures. *Science*, 130(3373), 432–437.
- Elahi, S. M., Shen, C. F., & Gilbert, R. (2019). Optimization of production of vesicular stomatitis virus (VSV) in suspension serum-free culture medium at high cell density. *Journal of Biotechnology*, 289, 144–149.
- EMA. (2009). *ICH considerations oncolytic viruses*. ((EMA/CHMP/ICH/607698/2008)). https://www.ema.europa.eu/en/documents/scientific-guideline/international-conference-harmonisation-technical-requirements-registration-pharmaceuticals-human-use_en-2.pdf
- Emma, P., & Kamen, A. (2013). Real-time monitoring of influenza virus production kinetics in HEK293 cell cultures. *Biotechnology Progress*, 29(1), 275–284.
- Ferreira, T. B., Carrondo, M. J. T., & Alves, P. M. (2007). Effect of ammonia production on intracellular pH: Consequent effect on adenovirus vector production. *Journal of Biotechnology*, 129(3), 433–438. <https://doi.org/10.1016/j.jbiotec.2007.01.010>
- Fontana, D., Kratje, R., Etcheverrigaray, M., & Prieto, C. (2014). Rabies virus-like particles expressed in HEK293 cells. *Vaccine*, 32(24), 2799–2804.
- Gallo-Ramírez, L. E., Nikolay, A., Genzel, Y., & Reichl, U. (2015). Bioreactor concepts for cell culture-based viral vaccine production. *Expert Review of Vaccines*, 14(9), 1181–1195. <https://doi.org/10.1586/14760584.2015.1067144>
- Gálvez, J., Lecina, M., Solà, C., Cairó, J. J., & Gòdia, F. (2012). Optimization of HEK-293S cell cultures for the production of adenoviral vectors in bioreactors using on-line OUR measurements. *Journal of Biotechnology*, 157(1), 214–222.
- Gauss-Muller, V., & Deinhardt, F. (1984). Effect of hepatitis A virus infection on cell metabolism in vitro. *Experimental Biology and Medicine*, 175(1), 10–15.
- Genzel, Y., & Reichl, U. (2009). Continuous cell lines as a production system for influenza vaccines. *Expert Review of Vaccines*, 8(12), 1681–1692. <https://doi.org/10.1586/erv.09.128>
- Genzel, Y., Vogel, T., Buck, J., Behrendt, I., Ramirez, D. V., Schiedner, G., Jordan, I., & Reichl, U. (2014). High cell density cultivations by alternating tangential flow (ATF) perfusion for influenza A virus production using suspension cells. *Vaccine*, 32(24), 2770–2781. <https://doi.org/10.1016/j.vaccine.2014.02.016>
- Ghafari-Esfahani, A., Shokri, R., Sharifi, A., Shafiee, L., Khosravi, R., Kaghazian, H., & Khalili, M. (2020). Optimization of parameters affecting on CHO cell culture producing recombinant erythropoietin. *Preparative Biochemistry & Biotechnology*, 50(8), 834–841.
- Göbel, S., Kortum, F., Chavez, K. J., Jordan, I., Sandig, V., Reichl, U., & Genzel, Y. (2022). Cell-line screening and process development for a fusogenic oncolytic virus in small-scale suspension cultures. *Applied Microbiology and Biotechnology*, 106(13–16), 4945–4961. <https://doi.org/10.1007/s00253-022-12027-5>

- Göbel, S., Pelz, L., Reichl, U., & Genzel, Y. (2022). Chapter 5 upstream processing for viral vaccines—Process intensification. In L. C. Amine Kamen (Ed.), *Bioprocessing of Viral Vaccines* (Vol. 1, pp. 79–137). Taylor & Francis Group.
- Gränicher, G., Babakhani, M., Göbel, S., Jordan, I., Marichal-Gallardo, P., Genzel, Y., & Reichl, U. (2021). A high cell density perfusion process for modified vaccinia virus Ankara production: Process integration with inline DNA digestion and cost analysis. *Biotechnology and Bioengineering*, 118, 4720–4734. <https://doi.org/10.1002/bit.27937>
- Gränicher, G., Coronel, J., Trampler, F., Jordan, I., Genzel, Y., & Reichl, U. (2020). Performance of an acoustic settler versus a hollow fiber-based ATF technology for influenza virus production in perfusion. *Applied Microbiology and Biotechnology*, 104(11), 4877–4888. <https://doi.org/10.1007/s00253-020-10596-x>
- Grein, T. A., Loewe, D., Dieken, H., Weidner, T., Salzig, D., & Czermak, P. (2019). Aeration and shear stress are critical process parameters for the production of oncolytic measles virus [original research]. *Frontiers in Bioengineering and Biotechnology*, 17(7):78. <https://doi.org/10.3389/fbioe.2019.00078>
- Gripon, P., Diot, C., Corlu, A., & Guguen-Guillouzo, C. (1989). Regulation by dimethylsulfoxide, insulin, and corticosteroids of hepatitis B virus replication in a transfected human hepatoma cell line. *Journal of Medical Virology*, 28(3), 193–199. <https://doi.org/10.1002/jmv.1890280316>
- Hadpe, S. R., Sharma, A. K., Mohite, V. V., & Rathore, A. S. (2017). ATF for cell culture harvest clarification: Mechanistic modelling and comparison with TFF. *Journal of Chemical Technology & Biotechnology*, 92(4), 732–740. <https://doi.org/10.1002/jctb.5165>
- Hein, M. D., Chawla, A., Cattaneo, M., Kupke, S. Y., Genzel, Y., & Reichl, U. (2021). Cell culture-based production of defective interfering influenza A virus particles in perfusion mode using an alternating tangential flow filtration system. *Applied Microbiology and Biotechnology*, 105(19), 7251–7264. <https://doi.org/10.1007/s00253-021-11561-y>
- Hein, M. D., Kollmus, H., Marichal-Gallardo, P., Püttker, S., Benndorf, D., Genzel, Y., & Reichl, U. (2021). OP7, a novel influenza A virus defective interfering particle: Production, purification, and animal experiments demonstrating antiviral potential. *Applied Microbiology and Biotechnology*, 105(1), 129–146. <https://doi.org/10.1007/s00253-020-11029-5>
- Henry, O., Dormond, E., Perrier, M., & Kamen, A. (2004). Insights into adenoviral vector production kinetics in acoustic filter-based perfusion cultures. *Biotechnology and Bioengineering*, 86(7), 765–774. <https://doi.org/10.1002/bit.20074>
- Ho, Y. Y., Lu, H. K., Lim, Z. F. S., Lim, H. W., Ho, Y. S., & Ng, S. K. (2021). Applications and analysis of hydrolysates in animal cell culture. *Bioresources and Bioprocessing*, 8(1), 93. <https://doi.org/10.1186/s40643-021-00443-w>
- Jordan, I., John, K., Höwing, K., Lohr, V., Penzes, Z., Gubucz-Sombor, E., Fu, Y., Gao, P., Harder, T., Zádori, Z., & Sandig, V. (2016). Continuous cell lines from the Muscovy duck as potential replacement for primary cells in the production of avian vaccines. *Avian Pathology*, 45(2), 137–155. <https://doi.org/10.1080/03079457.2016.1138280>
- Jordan, I., Northoff, S., Thiele, M., Hartmann, S., Horn, D., Höwing, K., Bernhard, H., Oehmke, S., von Horsten, H., Rebeski, D., Hinrichsen, L., Zelnik, V., Mueller, W., & Sandig, V. (2011). A chemically defined production process for highly attenuated poxviruses. *Biologicals*, 39(1), 50–58. <https://doi.org/10.1016/j.biologicals.2010.11.005>
- Kamen, A., & Henry, O. (2004). Development and optimization of an adenovirus production process. *The Journal of Gene Medicine*, 6(S1), S184–S192.
- Kaptein, L., Greijer, A., Valerio, D., & van Beusechem, V. (1997). Optimized conditions for the production of recombinant amphotropic retroviral vector preparations. *Gene Therapy*, 4(2), 172–176. <https://doi.org/10.1038/sj.gt.3300373>
- Klenk, H. D., Rott, R., Orlich, M., & Blödorn, J. (1975). Activation of influenza A viruses by trypsin treatment. *Virology*, 68, 426–439.
- Krabbe, T., & Altomonte, J. (2018). Fusogenic viruses in oncolytic immunotherapy. *Cancers*, 10(7), 216. <https://www.mdpi.com/2072-6694/10/7/216>
- Krabbe, T., Marek, J., Groll, T., Steiger, K., Schmid, R. M., Krackhardt, A. M., & Altomonte, J. (2021). Adoptive T cell therapy is complemented by oncolytic virotherapy with fusogenic VSV-NDV in combination treatment of murine melanoma. *Cancers*, 13(5), 1044. <https://www.mdpi.com/2072-6694/13/5/1044>
- Lavado-García, J., Cervera, L., & Gòdia, F. (2020). An alternative perfusion approach for the intensification of virus-like particle production in HEK293 cultures. *Frontiers in Bioengineering and Biotechnology*, 8, 617. <https://doi.org/10.3389/fbioe.2020.00617>
- Le Ru, A., Jacob, D., Transfiguración, J., Ansonge, S., Henry, O., & Kamen, A. A. (2010). Scalable production of influenza virus in HEK-293 cells for efficient vaccine manufacturing. *Vaccine*, 28(21), 3661–3671. <https://doi.org/10.1016/j.vaccine.2010.03.029>
- Lim, H. S., Chang, K. H., & Kim, J. H. (1999). Effect of oxygen partial pressure on production of animal virus (VSV). *Cytotechnology*, 31(3), 265–270. <https://doi.org/10.1023/A:1008060502532>
- Manceur, A. P., Kim, H., Misić, V., Andreev, N., Dorion-Thibaudeau, J., Lanthier, S., Bernier, A., Tremblay, S., Gélinas, A. M., Broussau, S., Gilbert, R., & Ansonge, S. (2017). Scalable lentiviral vector production using stable HEK293SF producer cell lines. *Human Gene Therapy Methods*, 28(6), 330–339. <https://doi.org/10.1089/hgtb.2017.086>
- Marichal-Gallardo, P., Pieler, M. M., Wolff, M. W., & Reichl, U. (2017). Steric exclusion chromatography for purification of cell culture-derived influenza A virus using regenerated cellulose membranes and polyethylene glycol. *Journal of Chromatography A*, 1483, 110–119. <https://doi.org/10.1016/j.chroma.2016.12.076>
- Miar, A., Arnaiz, E., Bridges, E., Beedie, S., Cribbs, A. P., Downes, D. J., Beagrie, R. A., Rehwinkel, J., & Harris, A. L. (2020). Hypoxia induces transcriptional and translational downregulation of the type I IFN pathway in multiple cancer cell types. *Cancer Research*, 80(23), 5245–5256. <https://doi.org/10.1158/0008-5472.CAN-19-2306>
- Mounce, B. C., Olsen, M. E., Vignuzzi, M., & Connor, J. H. (2017). Polyamines and their role in virus infection. *Microbiology and Molecular Biology Reviews*, 81(4), e00029–17. <https://doi.org/10.1128/mmr.00029-17>
- Nadeau, I., & Kamen, A. (2003). Production of adenovirus vector for gene therapy. *Biotechnology Advances*, 20(7-8), 475–489.
- Nienow, A. W. (2021). The impact of fluid dynamic stress in stirred bioreactors—the scale of the biological entity: A personal view. *Chemie Ingenieur Technik*, 93(1-2), 17–30.
- Nikolay, A. (2020). *Intensified yellow fever and Zika virus production in animal cell culture*, PhD Thesis, Otto-von-Guericke-Universität, Magdeburg. <https://doi.org/10.25673/33512>
- Nikolay, A., Grooth, J., Genzel, Y., Wood, J. A., & Reichl, U. (2020). Virus harvesting in perfusion culture: Choosing the right type of hollow fiber membrane. *Biotechnology and Bioengineering*, 117(10), 3040–3052. <https://doi.org/10.1002/bit.27470>
- Nikolay, A., Léon, A., Schwamborn, K., Genzel, Y., & Reichl, U. (2018). Process intensification of EB66® cell cultivations leads to high-yield yellow fever and Zika virus production. *Applied Microbiology and Biotechnology*, 102(20), 8725–8737. <https://doi.org/10.1007/s00253-018-9275-z>
- Pelz, L., Göbel, S., Chavez, K., Reichl, U., & Genzel, Y. (2022). Chapter 5 Upstream processing for viral vaccines—General aspects. In L. C. Amine Kamen (Ed.), *Bioprocessing of Viral Vaccines* (Vol. 1, pp. 79–137). Taylor & Francis Group.
- Perrin, P., Madhusudana, S., Gontier-Jallet, C., Petres, S., Tordo, N., & Merten, O.-W. (1995). An experimental rabies vaccine produced with a new BHK-21 suspension cell culture process: Use of

- serum-free medium and perfusion-reactor system. *Vaccine*, 13(13), 1244–1250. [https://doi.org/10.1016/0264-410X\(94\)00022-F](https://doi.org/10.1016/0264-410X(94)00022-F)
- Petiot, E., Cuperlovic-Culf, M., Shen, C. F., & Kamen, A. (2015). Influence of HEK293 metabolism on the production of viral vectors and vaccine. *Vaccine*, 33(44), 5974–5981.
- Petiot, E., Jacob, D., Lanthier, S., Lohr, V., Ansoerge, S., & Kamen, A. A. (2011). Metabolic and kinetic analyses of influenza production in perfusion HEK293 cell culture. *BMC Biotechnology*, 11, 84. <https://doi.org/10.1186/1472-6750-11-84>
- Pihl, A. F., Offersgaard, A. F., Mathiesen, C. K., Prentoe, J., Fahnøe, U., Krarup, H., Bukh, J., & Gottwein, J. M. (2018). High density Huh7.5 cell hollow fiber bioreactor culture for high-yield production of hepatitis C virus and studies of antivirals. *Scientific Reports*, 8(1), 17505. <https://doi.org/10.1038/s41598-018-35010-5>
- Planz, O. (2013). Development of cellular signaling pathway inhibitors as new antivirals against influenza. *Antiviral Research*, 98(3), 457–468.
- Rodrigues, A. F., Formas-Oliveira, A. S., Bandeira, V. S., Alves, P. M., Hu, W. S., & Coroadinha, A. S. (2013). Metabolic pathways recruited in the production of a recombinant enveloped virus: Mining targets for process and cell engineering. *Metabolic Engineering*, 20, 131–145. <https://doi.org/10.1016/j.ymben.2013.10.001>
- Scholtissek, C., Müller, K., & Herzog, S. (1986). Influence of insulin and 12-O-tetradecanoylphorbol-13-acetate (TPA) on influenza virus multiplication. *Virus Research*, 6(3), 287–294.
- Schwarz, H., Zhang, Y., Zhan, C., Malm, M., Field, R., Turner, R., Sellick, C., Varley, P., Rockberg, J., & Chotteau, V. (2020). Small-scale bioreactor supports high density HEK293 cell perfusion culture for the production of recombinant erythropoietin. *Journal of Biotechnology*, 309, 44–52. <https://doi.org/10.1016/j.jbiotec.2019.12.017>
- Seitz, C., Isken, B., Heynisch, B., Rettkowski, M., Frensing, T., & Reichl, U. (2012). Trypsin promotes efficient influenza vaccine production in MDCK cells by interfering with the antiviral host response. *Applied Microbiology and Biotechnology*, 93(2), 601–611. <https://doi.org/10.1007/s00253-011-3569-8>
- Sunstrom, N. A. S., Gay, R. D., Wong, D. C., Kitchen, N. A., DeBoer, L., & Gray, P. P. (2000). Insulin-like growth factor-I and transferrin mediate growth and survival of Chinese hamster ovary cells. *Biotechnology Progress*, 16(5), 698–702.
- Tapia, F., Vázquez-Ramírez, D., Genzel, Y., & Reichl, U. (2016). Bioreactors for high cell density and continuous multi-stage cultivations: Options for process intensification in cell culture-based viral vaccine production. *Applied Microbiology and Biotechnology*, 100(5), 2121–2132.
- Ungerechts, G., Bossow, S., Leuchs, B., Holm, P. S., Rommelaere, J., Coffey, M., Coffin, R., Bell, J., & Nettelbeck, D. M. (2016). Moving oncolytic viruses into the clinic: Clinical-grade production, purification, and characterization of diverse oncolytic viruses. *Molecular Therapy. Methods & Clinical Development*, 3, 16018. <https://doi.org/10.1038/mtm.2016.18>
- Vázquez-Ramírez, D., Genzel, Y., Jordan, I., Sandig, V., & Reichl, U. (2018). High-cell-density cultivations to increase MVA virus production. *Vaccine*, 36(22), 3124–3133.
- Vázquez-Ramírez, D., Jordan, I., Sandig, V., Genzel, Y., & Reichl, U. (2019). High titer MVA and influenza A virus production using a hybrid fed-batch/perfusion strategy with an ATF system. *Applied Microbiology and Biotechnology*, 103(7), 3025–3035.
- Venereo-Sanchez, A., Gilbert, R., Simoneau, M., Caron, A., Chahal, P., Chen, W., Ansoerge, S., Li, X., Henry, O., & Kamen, A. (2016). Hemagglutinin and neuraminidase containing virus-like particles produced in HEK-293 suspension culture: An effective influenza vaccine candidate. *Vaccine*, 34(29), 3371–3380.
- Wechuck, J. B., Ozuer, A., Goins, W. F., Wolfe, D., Oligino, T., Glorioso, J. C., & Atai, M. M. (2002). Effect of temperature, medium composition, and cell passage on production of herpes-based viral vectors. *Biotechnology and Bioengineering*, 79(1), 112–119. <https://doi.org/10.1002/bit.10310>
- Wood, H. A., Johnston, L. B., & Burand, J. P. (1982). Inhibition of *Autographa californica* nuclear polyhedrosis virus replication in high-density *Trichoplusia ni* cell cultures. *Virology*, 119(2), 245–254. [https://doi.org/10.1016/0042-6822\(82\)90085-x](https://doi.org/10.1016/0042-6822(82)90085-x)
- Wu, Y., Bissinger, T., Genzel, Y., Liu, X., Reichl, U., & Tan, W.-S. (2021). High cell density perfusion process for high yield of influenza A virus production using MDCK suspension cells. *Applied Microbiology and Biotechnology*, 105(4), 1421–1434. <https://doi.org/10.1007/s00253-020-11050-8>
- Yuk, I. H. Y., Olsen, M. M., Geyer, S., & Forestell, S. P. (2004). Perfusion cultures of human tumor cells: A scalable production platform for oncolytic adenoviral vectors. *Biotechnology and Bioengineering*, 86(6), 637–642. <https://doi.org/10.1002/bit.20158>

SUPPORTING INFORMATION

Additional supporting information can be found online in the Supporting Information section at the end of this article.

How to cite this article: Göbel, S., Jaén, K. E., Dorn, M., Neumeyer, V., Jordan, I., Sandig, V., Reichl, U., Altomonte, J., & Genzel, Y. (2023). Process intensification strategies toward cell culture-based high-yield production of a fusogenic oncolytic virus. *Biotechnology and Bioengineering*, 120, 2639–2657. <https://doi.org/10.1002/bit.28353>

3.6. Third Manuscript

In parallel to the before-mentioned study, a novel immortalized continuous suspension cell line derived from quail cells CCX.E10 was investigated as a valuable alternative for high-yield production of rVSV-NDV. This included a detailed characterization of parameters relevant in upstream processing while monitoring contaminant levels considered to be challenges in downstream processes for systems ranging from 15 mL to 10 L. For the first time, VCCs above 8×10^6 cells/mL were reached for this cell line. A transfer into 3 L benchtop STRs resulted in infectious virus titers up to 4.2×10^8 TCID₅₀/mL which were in a similar range compared to the previously described best producer BHK-21.

Göbel, Sven; Chavez, Karim Jean; Fernandes, Rita; Reiter, Manfred; Altomonte, Jennifer; Reichl, Udo; Genzel, Yvonne

First author

Characterization of a quail suspension cell line for production of a fusogenic oncolytic virus

Biotechnology and Bioengineering, 2023

[95]

Contribution Sven Göbel:

Conceptualization, formal analysis, investigation, methodology, project administration, writing – original draft, writing – review & editing.

Characterization of a quail suspension cell line for production of a fusogenic oncolytic virus

Sven Göbel¹  | Karim E. Jaén^{1,2} | Rita P. Fernandes³ | Manfred Reiter⁴ | Jennifer Altomonte² | Udo Reichl^{1,5} | Yvonne Genzel¹

¹Bioprocess Engineering, Max Planck Institute for Dynamics of Complex Technical Systems, Magdeburg, Germany

²Department of Internal Medicine II, Klinikum Rechts der Isar, Technische Universität München, Munich, Germany

³Instituto de Biologia Experimental e Tecnológica (iBET), Oeiras, Portugal

⁴Nuvonis Technologies GmbH, Vienna, Austria

⁵Chair for Bioprocess Engineering, Otto-von-Guericke-University Magdeburg, Magdeburg, Germany

Correspondence

Yvonne Genzel, Bioprocess Engineering, Max Planck Institute for Dynamics of Complex Technical Systems, Sandtorstr. 1, 39106 Magdeburg, Germany.
Email: genzel@mpi-magdeburg.mpg.de

Funding information

Federal Ministry for Economic Affairs and Energy, Grant/Award Number: #03EFOBY215

Abstract

The development of efficient processes for the production of oncolytic viruses (OV) plays a crucial role regarding the clinical success of virotherapy. Although many different OV platforms are currently under investigation, manufacturing of such viruses still mainly relies on static adherent cell cultures, which bear many challenges, particularly for fusogenic OVs. Availability of GMP-compliant continuous cell lines is limited, further complicating the development of commercially viable products. BHK21, AGE1. CR and HEK293 cells were previously identified as possible cell substrates for the recombinant vesicular stomatitis virus (rVSV)-based fusogenic OV, rVSV-NDV. Now, another promising cell substrate was identified, the CCX.E10 cell line, developed by Nuvonis Technologies. This suspension cell line is considered non-GMO as no foreign genes or viral sequences were used for its development. The CCX.E10 cells were thus thoroughly investigated as a potential candidate for OV production. Cell growth in the chemically defined medium in suspension resulted in concentrations up to 8.9×10^6 cells/mL with a doubling time of 26.6 h in batch mode. Cultivation and production of rVSV-NDV, was demonstrated successfully for various cultivation systems (ambr15, shake flask, stirred tank reactor, and orbitally shaken bioreactor) at vessel scales ranging from 15 mL to 10 L. High infectious virus titers of up to 4.2×10^8 TCID₅₀/mL were reached in orbitally shaken bioreactors and stirred tank reactors in batch mode, respectively. Our results suggest that CCX.E10 cells are a very promising option for industrial production of OVs, particularly for fusogenic VSV-based constructs.

KEYWORDS

ambr15, avian suspension cells, cell culture-based production, fusogenic oncolytic virus, upstream processing

Abbreviations: CCX.E10, QOR2/2E11 cells; CSVY, cell-specific virus yield; GMP, good manufacturing practice; hpi, hours postinfection; MOI, multiplicity of infection; NDV, Newcastle disease virus; OSB, orbitally shaken bioreactor; OTR, oxygen transfer rate; OV, oncolytic virus; q_{glc} , cell-specific glucose uptake rate; q_{lac} , cell-specific lactate production rate; q_{NH_4} , cell-specific ammonium production rate; rVSV-NDV, recombinant hybrid virus: VSV backbone and surface glycoproteins of NDV used in this study; SCGM, supplemented Freestyle293 expression medium; STR, stirred tank bioreactor; TCID₅₀, 50% tissue culture infectious dose; TOI, time of infection; VCC, viable cell concentration; VSV, vesicular stomatitis virus; VVP, volumetric virus productivity; v_w , working volume; μ , cell-specific growth rate.

This is an open access article under the terms of the Creative Commons Attribution-NonCommercial-NoDerivs License, which permits use and distribution in any medium, provided the original work is properly cited, the use is non-commercial and no modifications or adaptations are made.

© 2023 The Authors. *Biotechnology and Bioengineering* published by Wiley Periodicals LLC.

1 | INTRODUCTION

Oncolytic virotherapy describes the use of oncolytic viruses (OVs) to selectively infect and kill cancerous cells as a treatment against various types of cancer. By utilizing the natural propensity of OVs to exploit various defects in cellular antiviral pathways often present in cancer cells, a direct destruction through oncolysis without harming surrounding healthy cells can be achieved, with a secondary therapeutic initiation of systemic antitumor immune responses (Flint, 2020). Modification of OVs through genetic engineering, for example, expression of optimized endogenous or heterologous fusion glycoproteins can further improve their efficacy. rVSV-NDV, a recombinant vesicular stomatitis virus (VSV) backbone with fusogenic mutant glycoproteins of Newcastle disease virus (NDV) demonstrated promising preclinical data in both single and combination therapy in various cancer models (Abdullahi et al., 2018; Krabbe et al., 2021).

The majority of OVs currently under development and in clinical testing are being produced in static adherent cell cultures (Ungerechts et al., 2016). Talimogene laherparepvec, so far the only approved OV in the market, is manufactured in adherent Vero cells using roller bottles, where the collected harvest is pooled and purified in several steps comprising endonuclease digestion, clarification by filtration, ultrafiltration/diafiltration, two chromatography steps (ion exchange + size exclusion), and a final sterile filtration (EMA, 2015). Specific properties of fusogenic OVs, for example, the formation of large multinucleated syncytia that die rapidly after induction, present unique challenges for large-scale clinical-grade manufacturing. Despite screening of several adherent cell lines, relatively low virus yields were achieved for rVSV-NDV, so far (Göbel et al., 2022). Ideally, producer cell lines should: i) show sufficient susceptibility to the respective OV, ii) demonstrate robust growth in suspension culture with doubling times <30 h, iii) allow to generate high virus titers in chemically defined media, and iv) meet regulatory requirements, for example, documented origin, full characterization, stability, and absence of tumorigenicity. Using a suspension HEK293 producer cell line fulfilling most of these requirements, Pelareorep, a non-fusogenic oncolytic reovirus, is produced in stirred-tank bioreactors followed by a multistep purification train and is currently under investigation in clinical phase III trials for the treatment of metastatic breast cancer (Ungerechts et al., 2016).

So far, there are only a few continuous cell lines available for clinical-grade OV manufacturing. These include mainly Vero cells (herpesvirus, measles virus, and vaccinia virus), A549 cells (adenovirus), HeLa cells (vaccinia virus), HEK293 cells (adenovirus, reovirus), and some proprietary cell lines (e.g., EB66, PER.C6, and CAP) (Ungerechts et al., 2016). Other continuous suspension cell lines, such as BHK-21, AGE1.CR, MDCK, and HEK293SF cells, have been evaluated for efficient production of fusogenic rVSV-NDV (Göbel, 2022, 2023). The highest reported rVSV-NDV yields were obtained in BHK-21 suspension cells with titers up to 5×10^8 TCID₅₀/mL in optimized batch processes in stirred tanks and 2×10^9 TCID₅₀/mL in perfusion cultures infected at high cell density

(Göbel, 2023). First studies performed with the avian cell line AGE1.CR, which is fully characterized and GMP-compliant, resulted in relatively low virus yields. Although therapeutic indications of OVs may allow a different risk-benefits analysis compared with traditional viral vaccines, and fewer constraints regarding the use of cell lines known to be tumorigenic or possessing abnormal karyology (ICH, 1998; Jordan & Sandig, 2014), cell substrates demonstrating a good safety profile should be preferred.

In this study, we investigated an immortalized continuous suspension cell line derived from quail cells CCX.E10 (Nuvonis Technologies GmbH). CCX.E10 cells were extensively characterized by Nuvonis Technologies. They fulfill all critical regulatory requirements, are grown in chemically defined medium, and are qualified as source material for Good Manufacturing Practice (GMP)-compliant production (Kraus et al., 2011). Therefore, these cells represent a valuable alternative for high-yield production of VSV-NDV without the regulatory risks associated with BHK-21. For the first time, a fully scalable, production process in quail suspension cells for the fusogenic rVSV-NDV OV is described. Both upstream and downstream processing aspects were considered to assess the efficiency of the established production train. High rVSV-NDV yields were obtained in batch mode in various production systems at different vessel scales (15 mL–10 L) with maximum titers up to 4.2×10^8 TCID₅₀/mL.

2 | MATERIALS AND METHODS

2.1 | Cell culture, media, and viral seed stock

SCGM suspension cell growth medium was used for CCX.E10 cells. SCGM is based on the commercially available chemically defined Freestyle™293 Expression medium (Gibco), but is supplemented with growth factors.

Cells were cultivated in baffled 125 mL shake flasks with vent caps (Corning) with a working volume (vw) of 50 mL. A Multitron orbitally shaken incubator (Infors AG) with 50 mm shaking diameter was used to incubate cells at 185 rpm, 37°C, and 5% CO₂. Cells were inoculated at a cell concentration of 0.8×10^6 cells/mL and passaged twice per week.

For all infections, a CCX.E10 cell-derived virus seed (rVSV-NDV) concentrated by ultracentrifugation, followed by purification on sucrose gradients (1.05×10^8 TCID₅₀/mL), was used in this study.

2.2 | Batch cultivations in orbitally shaken bioreactors

For infection studies in shake flasks, CCX.E10 cells were inoculated at 0.4×10^6 cells/mL and cultivated for 96 h to reach about 4.0×10^6 cells/mL. At time of infection (TOI), the viable cell concentration (VCC) was adjusted to 2×10^6 cells/mL by either diluting the vw two-fold with fresh medium or by centrifugation of the appropriate volume at 300g for 5 min and re-suspending the cells in fresh

medium. Cells were subsequently infected at a multiplicity of infection (MOI) of $1E-4$ with rVSV-NDV.

Cultivation in the SB10-X orbital shaken bioreactor (OSB) (Adolf Kühner AG) was carried out with a 12 L single-use standard bag. CCX.E10 cells were inoculated at 0.8×10^6 cells/mL with 3 L initial vw at 37°C with a shaking frequency of 100 rpm (50 mm shaking diameter). Aeration was carried out through headspace gassing at a rate of 300 mL/min with air. Partial pressure of dissolved oxygen (DO) and pH values were controlled at 80% and 7.3, respectively, by automatic adjustment of the gas composition in the output flow. At TOI, the bioreactor vw was increased from 3 L to 6 L with fresh medium containing virus. CCX.E10 cells were infected with an MOI of $1E-4$ and temperature was decreased to 34°C .

2.3 | Batch cultivations in STR and ambr15

Bioreactor cultivations in 1 L DASGIP bioreactor systems (Eppendorf AG) were used with 350 mL initial vw. Bioreactors were inoculated from shake flask pre-cultures at a VCC of 0.8×10^6 cells/mL. Cells were agitated with a pitched blade impeller (50 mm diameter) at 80–180 rpm (upflow) with aeration by a submerged L-drilled hole sparger. pH value was controlled at 7.2 by sparging CO_2 . Oxygen and nitrogen flow rates were controlled between 3–9 L/h to maintain a DO level equal or above 50%. Temperature was set at 37°C for the growth phase and 34°C for the infection phase. At TOI, cells were infected at an MOI of $1E-4$ by addition of an equal vw of pre-warmed fresh medium containing rVSV-NDV (350 mL).

The bioreactor cultivation in a 3 L DASGIP bioreactor system (Eppendorf AG) was started with 1300 mL initial vw. For agitation, two pitched blade impellers (50 mm diameter) at 180 rpm (upflow) with aeration by a submerged L-drilled hole sparger were used. To maintain a DO level equal or above 50%, oxygen and nitrogen flow rates were controlled between 9 and 12 L/h. Inoculation and process parameters were identical to the previously described 1 L system.

Cultivations in the ambr15™ unit (kindly provided by Sartorius AG) were carried out with a vw of 15 mL. The reactor volume was kept above 10 mL throughout the cultivation for all vessels. DO was controlled at 50% by oxygen enrichment through a pipe sparger and pH was controlled by CO_2 enrichment or addition of 7.5% NaHCO_3 . Off-set adjustments of pH were carried out daily by off-line measurement with an additional pH7110 potentiometer (Inolab). The effects of pH adjustments to 7.0, 7.2, or 7.4 during cell growth and virus production were evaluated. Agitation speed of the integrated pitched blade impeller (diameter = 11.4 mm) was scaled down based on tip-speed of the 1 L STR experiment and set to 800 rpm. Individual ambr vessels were sampled daily to measure VCC, offline-pH, and virus titer.

2.4 | Analytics

An automated cell counter (ViCell; Coulter Beckman) was used to determine VCC and viability. Off-line pH was measured in a pH7110

potentiometer (Inolab), and lactate, ammonium, glutamine, glutamate, and glucose were determined with a Cedex Bio Analyzer (Roche). To allow easier handling, virus-containing samples were heat-inactivated at 80°C for 3 min before metabolite measurements. For titration of rVSV-NDV, the previously described TCID₅₀ assay (Göbel et al., 2022) was performed using adherent AGE1.CR.PIX cells (kindly provided by ProBioGen). The cell-specific virus yields (CSVY) was calculated as previously described by Gränicher et al. (2020), taking into account only the error of the TCID₅₀ assay ($-50\%/+100\%$ on a linear scale). Total protein was assessed with Pierce™ BCA assay kit (ThermoFisher) and total DNA was quantified with Quant-iT™ PicoGreen dsDNA assay kit (ThermoFisher) used according to the manufacturer's instructions. Cell-specific substrate consumption rates (q_s) were determined as described by Gränicher et al. (2020).

$$q_s = \frac{\mu}{Y_{x/s}} \quad (1)$$

$$Y_{x/s} = \frac{x(t_{n+1}) - x(t_n)}{c_s(t_n) - c_s(t_{n+1})}, \quad (2)$$

where x is the VCC, t is the cultivation time, n is the sampling time point, and c_s is the cell culture compound concentration.

3 | RESULTS AND DISCUSSION

Addressing key parameters in both the cell growth and virus production phase is critical for the evaluation of a cell substrate for the production of fusogenic oncolytic viruses. Therefore, in the first step, the transfer to orbitally shaken systems from stirred spinner flask systems was investigated. Here, baseline cell growth over multiple passages and metabolism of the CCX.E10 cell line was evaluated in the absence of virus infection. Subsequently, rVSV-NDV production was characterized and optimized in batch mode in various production systems at different scales (15 mL–6 L).

3.1 | Evaluation of cell growth after transfer to orbitally shaken systems

Until now, CCX.E10 cells were sub-cultured in spinner flasks, reaching only moderate viable cell concentrations (up to $2.0\text{--}3.0 \times 10^6$ cells/mL) after multiple days of growth (Reiter et al., 2014). A direct transfer to an orbitally shaken environment, by thawing the cells in unbaffled shake flasks and splitting to baffled shake flasks after passage 2, resulted in a lag phase of 7 days without a negative impact on cell viability (Figure 1a). As thawing is a harsh and stressful procedure for most animal cells, delays in cell growth are common (González Hernández, 2007). Although shear rates are lower in shake flasks compared to stirred tanks (Giese et al., 2014), the direct transfer to the new orbitally shaken environment was expected to cause a lag phase. However, after Day 10, robust cell growth up to $4.0\text{--}6.0 \times 10^6$ cells/mL, with doubling times of around

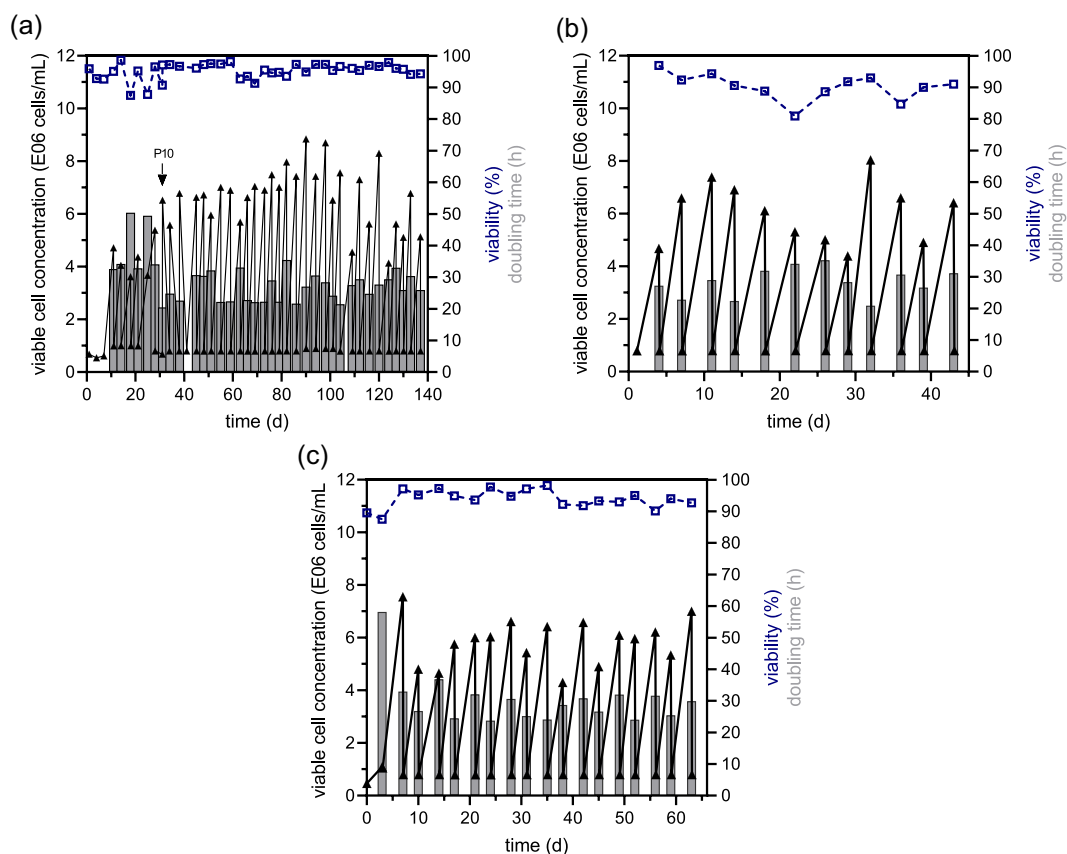


FIGURE 1 Serial passing of CCX.E10 cells and adaptation to growth in an orbitally shaken system. CCX.E10 cells were first thawed in 125 mL unbaffled shake flasks and subsequently transferred to 125 mL baffled shake flasks after passage 2 (all vv: 50 mL, 50 mm shaking diameter, 185 rpm, 37°C, 5% CO₂). Here, CCX.E10 cells were cultivated over 40 passages, and average doubling time (gray bars), viable cell concentration (black squares), and viability (blue empty squares) were recorded. (a) Cultivation in SCGM medium. (b) Cultivation starting from P10 in SCGM medium without putrescine dihydrochloride. (c) Cultivation of adapted cell bank generated at P10 in SCGM medium. CCX.E10, QOR2/2E11 cells; SCGM, supplemented Freestyle293 expression medium.

30–50 h was achieved. By Day 30, the average doubling time decreased to 25–30 h and was maintained until end of cultivation (140 d). At Day 30 (passage 10), cells were considered to be fully adapted to growth in the orbital shaker, and a cell bank was established for all further experiments. Interestingly, even higher maximum cell concentrations of up to 8.8×10^6 cells/mL with high viabilities (above 97%) were reached between Days 60 and 120 (Figure 1a). Over the entire cultivation period, CCX.E10 cells had an average doubling time of 29 h and an average cell diameter of 15.2 μm . Putrescine dihydrochloride is a common component in cell culture medium (e.g., Dulbecco's Modified Eagle Medium F12) and has an established role on regulation of division, differentiation and maturation of cells, DNA and RNA synthesis as well as apoptosis (Hesterberg et al., 2018; Zdrojewicz & Lachowski, 2014). However, due to the acute toxicity (category 3–4) for humans, subpassaging without this compound was carried out. Omission of putrescine dihydrochloride in a sub-culture of passage 10, had a negative impact on the average doubling time (29 h compared with 26.6 h) compared to the fully supplemented medium. Moreover, a decrease in maximum viable cell concentrations as well as a reduced viability (below 90%) was observed from passage 2–12 (Figure 1b). Although

maximum viable cell concentration recovered after passage 12, cell viability remained low around 90%. After thawing adapted cells (P10) in shake flasks, no lag phase was observed and cells grew up to 6.0×10^6 cells/mL with high viabilities in further passages (Figure 1c). As demonstrated for CHO cells, once cells have physiologically adapted to a new environment, here an orbitally shaken system, their growth performance remained stable as long as cultivation parameters were kept (Wurm & Wurm, 2021).

Fully adapted CCX.E10 cells were able to grow to cell concentrations above 8.5×10^6 cells/mL with low doubling times of 26.6 ± 2.6 h in batch mode (Figure 2a, Table 1). Viability remained above 96% over the cell growth phase and only decreased from 96 h onwards after the maximum cell concentration was reached and after glucose was depleted (Figure 2a,b). The depletion of critical nutrients (e.g., glucose) is well known to limit cell growth and to cause a decrease in cell viability (Tsao et al., 2005). Accumulation of secondary by-products of metabolism such as lactate (above 20 mM) and ammonium (2–3 mM) have also been shown to negatively impact cell growth and virus production (Schneider, 1996). However, these limits were not exceeded during the exponential growth phase (Figure 2b).

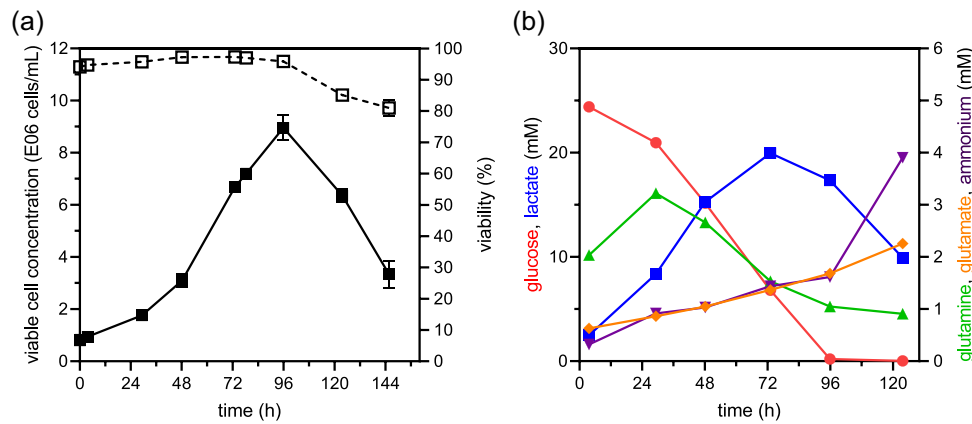


FIGURE 2 Growth and metabolism of CCX.E10 cells in SCGM medium in shake flasks. CCX.E10 cells were inoculated at 0.8×10^6 cells/mL and cultivated in baffled 125 mL shake flasks. (a) viable cell concentration (full squares) and viability (empty squares), (b) glucose (red circles), lactate (blue squares), glutamine (green triangles), glutamate (orange triangles), and ammonium (purple triangles) concentrations. Values are reported as the mean \pm SD of biological replicates ($n = 3$). CCX.E10, QOR2/2E11 cells; SCGM, supplemented Freestyle293 expression medium; SD, standard deviation.

TABLE 1 Calculated parameters for CCX.E10 cells cultivated in batch mode in shake flasks.

	Cultivation time range (h)	Shake flask ($n = 3$)
Cell-specific growth rate (1/h)	0–96	0.026 ± 0.003
Doubling time (h)	0–96	26.6 ± 2.6
Cell diameter	0–96	15.7 ± 0.12
q_{Glc} (10^{-11} *mmol/(cell*h))	0–96	-7.9 ± 0.6
q_{Lac} (10^{-11} *mmol/(cell*h))	0–72	8.6 ± 0.9
$q_{\text{NH}_4^+}$ (10^{-11} *mmol/(cell*h))	0–123	0.4 ± 0.04

Note: Values are reported as the mean \pm SD of biological replicates ($n = 3$). Abbreviations: CCX.E10, QOR2/2E11 cells; max., maximum (see Equation 1); q_{Glc} , cell-specific glucose consumption rate; q_{Lac} , cell-specific lactate release rate; $q_{\text{NH}_4^+}$, cell-specific ammonium release rate; SD, standard deviation.

Similar to mammalian cells, such as HEK293 cells (Petiot et al., 2015), MDCK cells (Bissinger et al., 2019) and PBG.PK2.1 cells (Gränicher et al., 2019), CCX.E10 cells shifted their metabolism from lactate production towards lactate consumption in the middle of the cultivation period once glucose level was less than 10 mM (Figure 2b). As Freestyle medium contains the supplement GlutaMAX™, the measured glutamine concentrations do not accurately represent the freely available glutamine in the culture medium. However, accumulation of glutamate over the cultivation time suggested an active glutamine metabolism (Figure 2b) (Newsholme et al., 2003). The cell-specific glucose uptake rate q_{glc} of $-7.9 \pm 0.6 \times 10^{-11}$ mmol/(cell*h) (Table 1) and the lactate yield based on glucose consumption $Y_{\text{lac/glc}}$ of 0.9 were in the range observed for other avian cell lines, such as AGE1.CR.pIX, with q_{glc} varying between 5 and 7.5×10^{-11} mmol/(cell*h) and $Y_{\text{lac/glc}}$ of 0.8–1 mmol/cell (Coronel et al., 2020).

The achieved doubling time and maximum cell concentration are not only comparable to other avian suspension cell lines, such as

AGE1.CR cells (25 h; 8.7×10^6 cells/mL (Coronel et al., 2019; Genzel et al., 2014a), AGE1.CR.pIX cells (27.5 h; 13.0×10^6 cells/mL (Coronel et al., 2019; Lohr, 2014; Lohr, Hädicke, et al., 2014), EB66 cells (19–23 h; 14.0×10^6 cells/mL; Nikolay et al., 2018), and DuckCelt®-T17 (29 h; 6.5×10^6 cells/mL; Petiot et al., 2018) but also to MDCK suspension cells (20 h; 10.0×10^6 cells/mL; Bissinger et al., 2019), BHK-21 cells (25 h; Göbel, 2023), and HEK293 suspension cells (33 h; 4.0 – 5.0×10^6 cells/mL; Abaandou et al., 2021) cultivated in batch mode.

3.2 | Virus propagation in orbitally shaken systems

MOI effects have been thoroughly investigated for a variety of virus-host cell systems. Particularly for rVSV-NDV, the optimal MOI seems to be highly cell-line dependent (Göbel et al., 2022). Consequently, evaluations of MOI ranging from $1\text{E}-2$ – $1\text{E}-5$ were performed with rVSV-NDV for the CCX.E10 cells. Although similar maximum infectious virus titers were reached for all MOIs, $1\text{E}-4$ was identified as optimal as the highest virus titers were reached (data not shown). Subsequently, the effect of a medium exchange at TOI was analyzed and compared with a two-fold dilution with fresh medium (at TOI). Growth parameters after infection, as well as virus replication dynamics were very similar for both conditions (Figure 3a,b). Maximum titers of $5.0 \times 10^8 \pm 2.2 \times 10^8$ TCID₅₀/mL and 3.2×10^8 TCID₅₀/mL and CSVYs of 110 ± 43 and 83 ± 9 TCID₅₀/cell were reached for the two-fold dilution and complete medium exchange, respectively. This was surprising as previous studies using avian AGE1.CR cultures for production of rVSV-NDV showed only moderate virus titers when switching from a complete medium exchange at TOI in shake flask cultures to a two-fold dilution in STRs (Göbel, 2023). Moreover, it has been reported that providing an optimal metabolic state with a sufficient supply of substrates plus removal of inhibiting molecules by a complete media exchange, led to

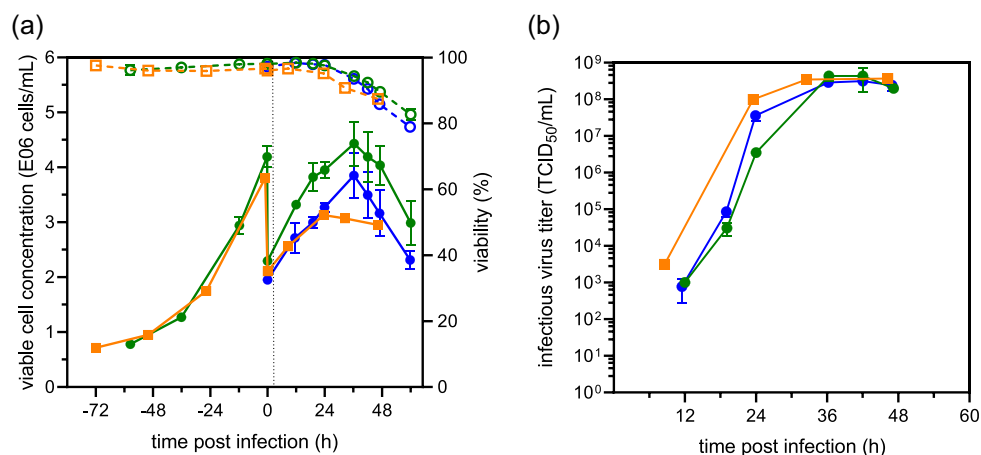


FIGURE 3 rVSV-NDV production in CCX.E10 cells in a shaker flask compared to an orbitally shaken system. Cells were grown in 125 mL baffled shake flasks (circles) or in the SB10-X bioreactor (squares) and infected at an MOI of $1E-4$ at 2×10^6 cells/mL. To determine the effect of a medium exchange at TOI, the medium was either exchanged completely (blue circles) or diluted two-fold with fresh SCGM medium (green circles). Scale-up to SB10-X bioreactor with two-fold dilution at TOI (orange square). (a) Cell growth (full symbols) and viability (empty symbols); (b) infectious virus titers determined by TCID₅₀ assay. Values for shake flasks are reported as the mean \pm SD of biological replicates ($n = 3$). CCX.E10, QOR2/2E11 cells; MOI, multiplicity of infection; SCGM, supplemented Freestyle293 expression medium; SD, standard deviation; TOI, time of infection.

increased titers for various viruses (Genzel et al., 2014a; Elahi et al., 2019; Vázquez-Ramírez et al., 2018). Most likely, a two-fold dilution with fresh supplemented SCGM medium provided enough essential nutrients necessary for optimal virus replication while also reducing the concentration of inhibiting or toxic by-products from metabolism. Therefore, no reductions of virus titers by metabolic limitations and accumulation of inhibiting molecules were expected for subsequent scale-up experiments in OSBs and STRs. As hypothesized, maximum infectious virus titers achieved following a complete medium exchange were in the same range compared to the previously identified optimal cell substrate, BHK-21, but 0.6–1.0 log higher than for HEK293 and AGE1.CR cells (Göbel et al., 2022).

In a second step, the virus production process was scaled-up from a 125 mL shake flask on an orbital platform to a single-use SB10-X OSB. Both cultures displayed cell viabilities exceeding 95% and a consistent growth with a μ of 0.024 1/h and a doubling time of 28.8 h during the exponential growth phase. VCC increased until 24–36 h postinfection (hpi), reaching maximum concentrations of $3\text{--}4.2 \times 10^6$ cells/mL, after which VCC and viability steadily decreased until the end of the cultivation (Figure 3a). Maximum cell concentrations postinfection were slightly higher in shake flask cultures compared to the SB10-X, most likely due to batch-to-batch variability. Overall maximum infectious virus titers of $3.7\text{--}4.2 \times 10^8$ TCID₅₀/mL (Figure 3b) and CSVY of 118–121 TCID₅₀/cell (Table 2) were achieved at 29–32 hpi, respectively. The k_{1a} for the shake flask for the described culture conditions (37°C, 185 rpm, 50 mL vw) was estimated based on correlations from Schiefelbein et al. (2013). For the SB10-X bioreactor, the k_{1a} was determined for a shaking frequency of 100 rpm and a vw of 6 L, as described by Kühner (AG, 2017). For the described conditions, a k_{1a} of 99 1/h for the baffled shake flask and 15 1/h for the SB10-X should be expected. In addition, oxygen transfer rates (OTRs) for the shake flask and SB10-X were calculated based on

correlations from Meier et al. (2016). and (AG, 2017), respectively. Here, OTRs of 11 mmol/(L*h) for the shake flask and 3 mmol/(L*h) for SB10-X were calculated. The k_{1a} and OTR were not maintained throughout the scale up, but kept above 10 1/h and 1 mmol/(L*h) to ensure a sufficient amount of oxygen. On the other hand, mixing times in the shake flask (~ 3 s (Tan et al., 2011)) and the SB10-X approximately 5 s (AG, 2017)) were kept constant across scales. This underlines the facilitated scale-up (over two orders of magnitude) in orbitally shaken systems with similar geometrical characteristics when mixing and aeration principles are maintained (Klößner et al., 2014).

3.3 | Virus production in STR

As an alternative production system, cells were cultivated in DASGIP bioreactors with 350 mL vw using the previously optimized MOI and medium dilution at TOI. To identify optimal cultivation conditions for both growth and virus production, different agitation speeds (80–180 rpm) were evaluated. Here, cells were cultivated until a VCC of 4.0×10^6 cells/mL was achieved and diluted two-fold with fresh medium before infection. During cell growth, the lowest $\mu = 0.017$ 1/h, corresponding to a doubling time of 40.8 h was achieved for 80 rpm (Table 2). Low agitation speeds can lead to insufficient mixing, causing localized areas of nutrient depletion and suboptimal conditions for cell growth. Moreover, lower oxygen transfer rates are achieved, potentially resulting in reduced cell growth rates and cell viabilities. However, viability remained constantly above 96% for all conditions (Figure 4a). Compared to shake flask cultivations (Figure 3), slightly higher doubling times but no major differences in cell viability or average cell diameter were detected. Different metabolite profiles were observed for the different stirring speeds: The prolonged growth phase of cells cultivated

TABLE 2 rVSV-NDV production in CCX.E10 cells considering key parameters for both upstream and downstream processing. Cell growth parameters were determined before infection.

	SF	SB10-X	STR 1 L 80 rpm	130 rpm	180 rpm	STR 3 L 180 rpm	ambr15
Cell-specific growth rate (1/h)	0.026	0.024	0.017	0.022	0.022	0.024	0.022
Doubling time (h)	26.6	28.9	40.7	31.5	31.5	28.9	31.5
q_{Glc} (10^{-11} *mmol/(cell*h))	-7.9	n.d.	-18.8	-15.8	-15.9	-13.5	n.d.
q_{Lac} (10^{-11} *mmol/(cell*h))	8.6	n.d.	15.3	16.4	15.3	12.3	n.d.
$q_{\text{NH}_4^+}$ (10^{-11} *mmol/(cell*h))	0.4	n.d.	0.3	0.6	0.6	0.8	n.d.
Total process time (h)	126	118	177	152	142	143	128
max. VCC p.i. (10^6 cells/mL)	4.4	3.1	3.7	4.2	3.4	4.2	3.6
max. infectious virus titer (10^8 TCID ₅₀ /mL)	5.0	3.7	0.1	1.8	3.2	4.2	1.0-2.0
CSVY (TCID ₅₀ /cell)	111	118	3	42	94	100	70
VVP (10^{10} virions/L/d)	10.2	7.5	0.1	2.8	5.2	7.0	2.0
dsDNA impurity level at optimal harvest time point ($\mu\text{g/mL}$)	n.d.	n.d.	6.8	16.5	9.7	14.1	n.d.
Protein impurity level at optimal harvest time point (mg/mL)	n.d.	n.d.	2.3	1.8	2.5	2.0	n.d.

Note: Optimal harvest time point was defined as time point when the maximum infectious virus titer with lowest impurity level was reached in the supernatant.

Abbreviations: Glc, cell-specific glucose consumption rate; n.d., not determined; p.i., postinfection; q_{Lac} , cell-specific lactate production rate; $q_{\text{NH}_4^+}$, cell-specific ammonium production rate; qmax., maximum; SF, shake flask; VCC, viable cell concentration.

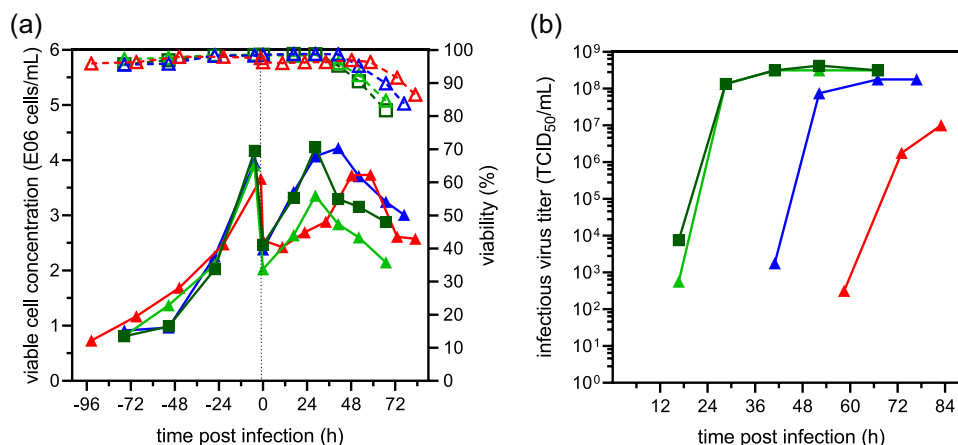


FIGURE 4 rVSV-NDV production in CCX.E10 cells in 1 L (triangles) and 3 L STRs (squares) in batch mode. All cultures were infected at an MOI of $1\text{E}-4$ at 2×10^6 cells/mL following a two-fold dilution step with fresh medium. (a) Viable cell concentration (solid lines, full symbols) and viability (dashed lines, empty symbols) for STRs operated with 80 rpm (red), 130 rpm (blue), 180 rpm (light (1 L STR) + dark green (3 L STR)). (b) Infectious virus titer. CCX.E10, QOR2/2E11 cells; MOI, multiplicity of infection; rVSV-NDV, recombinant hybrid virus: VSV backbone and surface glycoproteins of NDV used in this study; STRs, stirred tank bioreactors.

at 80 rpm resulted in complete consumption of glucose until the TOI (Figure S1A). Over the course of the virus production phase, no limitation in glucose was observed at 80 rpm as well as 180 rpm regardless of the scale (Figure S1C,D). Due to the prolonged growth phase at 130 rpm, glucose was depleted at 48 hpi (Figure S1B). Moreover, as a consequence of cell death and release of intracellular metabolites, ammonium concentrations increased but stayed below

1 mM for all conditions. The highest lactate concentrations were reached at 130 rpm, exceeding 30 mM at 36 hpi (Figure S1B). Variation of agitation speed had no effect on q_{glc} and cell-specific lactate (q_{lac}) or ammonium (q_{NH_4}) release rate (Table 2). However, q_{glc} and q_{lac} were about 2–3 times higher compared with cultivations in shake flasks, which may indicate a higher cell stress (from stirring or aeration) compared with orbitally shaken systems.

Surprisingly, the different stirrer speeds had only a major impact on virus replication. Maximum infectious virus titers of 3.2×10^8 TCID₅₀/mL, 1.8×10^8 TCID₅₀/mL, and 1×10^7 TCID₅₀/mL were reached 36 hpi, 72 hpi, and 84 hpi for 180 rpm, 130 rpm, and 80 rpm, respectively (Figure 4b). Overall, extended cell growth phases after infection were observed for lower agitation speeds. CSVY's of 3 TCID₅₀/cell for 80 rpm, 42 TCID₅₀/cell for 130 rpm, and 94 TCID₅₀/cell for 180 rpm (Table 2) were obtained. Compared with optimized batch runs with BHK-21 cells (the previously identified best producer cell line), slightly lower maximum virus titers (0.3 log) were obtained (Göbel, 2023). However, this is within the standard deviation of our TCID₅₀ assay (Genzel, 2014b). Moreover, the highest CSVY obtained in STRs was 20% lower compared to CSVY's obtained in orbitally shaken systems. While high stirring speeds, and consequently increased agitator-dependent shear stress, can result in drastically reduced virus titers for, for example, measles virus (Grein et al., 2019), this was clearly not an issue here. Cell-damaging effects of aeration and bubble bursting have also been identified as another factor influencing cell growth and virus production in STRs (Grein et al., 2019; Chisti, 2000). Michaels et al. (1996). found that low agitation speeds (below 200 rpm) can cause cell-to-bubble interactions leading to increased cell damage. However, due to the low reactor heights and volume flows (3 L/h) in small-scale laboratory processes, this should be negligible. We suspect the limitation of glucose or the accumulation of inhibiting molecules (e.g., lactate) to be the reason for the drastic reduction in viral titers for 80 and 130 rpm. While addition of fresh medium at TOI increased glucose concentrations to 10 mM for 80 rpm, the cells were likely not in an optimal metabolic state at the time of infection. Low glucose levels can lead to metabolic shifts prioritizing cell maintenance over growth and proliferation, as well as a reduction in the levels of phosphorylated precursors required for enzymatic syntheses and draining of intracellular pools of compounds required for protein or membrane synthesis. As a consequence, virus replication could also be impeded compared to cells infected at a late exponential growth phase with a surplus of substrate supply. Furthermore, OV's in particular, are dependent on the host cell glycolysis, and delayed reactivation of host cell glycolysis modulated by rVSV-NDV after infection could further negatively impact virus replication (Goyal & Rajala, 2023). For production at 130 rpm, glucose limitation and the high lactate concentration at 48 hpi, before maximum titers were reached, most likely had a negative impact on virus replication.

Performance of subsequent virus purification trains depends on several factors, that is, the accumulation of protein and host cell DNA in the medium. To assess the potential burden, the impact of process conditions on impurity levels were examined to determine the optimal harvest time point. Following host cell DNA and total protein levels over time, we determined the best time of harvest (maximum infectious virus titer, minimum impurity levels in the supernatant) to be 83 hpi for 80 rpm, 67 hpi for 130 rpm, and 35 hpi for 180 rpm. As cells grew to the highest VCC after infection for 130 rpm, higher host cell DNA concentrations were expected (Table 2). Interestingly, protein concentrations at the optimal harvest time point were around

2–2.5 mg/mL for all conditions. Similar DNA and protein contents in avian AGE1.CR.pIX cell and MDCK-derived STR batch harvests have been described before and efficiently tackled by subsequent purification trains (Gränicher, 2021; Marichal-Gallardo et al., 2017).

In the last step, the process was transferred to a 3 L bioreactor. As the scale-up was carried out within the same order of magnitude, agitation speed (180 rpm) was kept constant. To ensure homogeneous mixing, two pitched-blade impellers were used. Moreover, gas flow rates were scaled proportionally to the increased vw. A comparable cell growth with high viabilities (above 96%) and a μ of 0.024 1/h was achieved (Figure 4a). By addition of fresh medium at TOI, levels of nutrients were recovered to some extent, and accumulated by-products were diluted. Similar to the 1 L STR operated at 180 rpm, no limitation of glucose was found over the process time (Figure S1D). Even though lactate accumulated rapidly after infection, concentrations remained moderate, increasing, but not exceeding 25 mM in the late infection phase (Figure S1D). rVSV-NDV dynamics, as well as the determined metabolic rates, were very similar to those obtained at the 1 L scale (Figure 4b, Table 2), indicating a successful scale-up. The maximum infectious virus titer was 4.2×10^8 TCID₅₀/mL, corresponding to a CSVY of 100 TCID₅₀/cell. Host cell DNA (14.1 μ g/mL dsDNA) and total protein (2.0 mg/mL total) impurity levels in the supernatant were also in line with results obtained at the 1 L scale (Table 2). While a transfer to 3 L STR does not constitute a significant scale-up, the similar performance by implementation of two pitched-blade impellers sets the first benchmark for further increase in production volumes. The finding that similar virus titers and productivities were also achieved, indicates the usefulness of both bioreactor systems for efficient rVSV-NDV production. Currently, virus production under cGMP conditions of most manufacturers relies on stainless steel STRs but also on single-use vessels (Zhou et al., 2010). However, orbitally shaken bioreactors also fulfill these requirements without the need of stirrers, which introduce additional shear stress and raise costs in single-use applications. Further experiments are necessary to better understand how the choice of the bioreactor system will impact optimized virus production, e.g. at high cell density and potential formation of syncytia. Adjustments in medium formulation at TOI as demonstrated for BHK-21 and HEK293 cells, could further improve virus titers in batch mode (Göbel, 2023). Furthermore, higher yields could be potentially obtained in perfusion mode with retention devices that enable continuous virus harvesting and reduce virus degradation (Göbel, 2023; Gränicher, 2021).

3.4 | Cultivation in ambr15: Scale down and pH evaluation

In a final step, the production process was scaled down to an ambr15 system. Here, the traditional scale-up rule of “equal tip speed” was used for scale-down, rather than the “power per unit volume” approach (Amanullah et al., 2003; Nienow, 2021; Nienow et al., 2013; Tajssoleiman et al., 2019). To evaluate if cell growth and virus

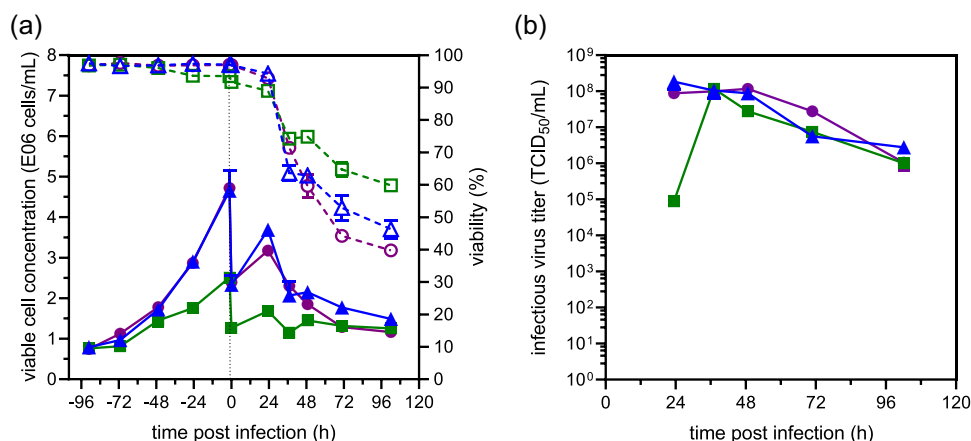


FIGURE 5 Effect of pH on cell growth (a) and rVSV-NDV production (b) in CCX.E10 cells in 15 mL ambr15 STR vessels in batch mode. Ambr15 vessels were inoculated at 0.8×10^6 cells/mL and operated in batch mode at the respective pH set point. At time of infection a two-fold dilution with fresh medium containing virus (MOI: $1E-4$) was carried out. (a) Viable cell concentration (solid lines, full symbols) and viability (dashed lines, empty symbols) for STRs operated at pH 7.0 (green squares), pH 7.2 (blue triangles), and pH 7.4 (purple circles). (b) Infectious virus titer. Values are reported as the mean \pm SD of a duplicate with two independent ambr15 vessels. CCX.E10, QOR2/2E11 cells; MOI, multiplicity of infection; rVSV-NDV, recombinant hybrid virus: VSV backbone and surface glycoproteins of NDV used in this study; SD, standard deviation; STRs, stirred tank bioreactors.

production could be further improved, different pH values ranging from 7.0 to 7.4 were tested. As expected, pH had a strong impact on cell growth (Figure 5a). While cell growth was already severely impeded at pH 7.0, there was no difference for pH 7.2 and 7.4. Maximum cell-specific growth rates of 0.020–0.022 1/h were achieved, comparable to growth rates achieved at the 1 and 3 L scale STR (Table 2). After infection, a steep decline in cell viability was noticeable starting from 24 hpi (Figure 5a). While a reduction of temperature to 34°C had no positive effect on virus production for rVSV-NDV, drastic declines in cell viability were prevented in STRs for both CCX.E10 and BHK-21 cells (Göbel, 2023; Figure 4a). Despite the impeded cell growth at pH 7.0, maximum infectious virus titers of $1.0\text{--}2.0 \times 10^8$ TCID₅₀/mL were achieved for all conditions respectively. This resulted in decreasing CSVYs (70, 59, and 36 TCID₅₀/cell) for increasing pH values (7.0, 7.2, and 7.4). While there was no measurable difference in terms of maximum titer, pH 7.0 resulted in a delayed virus replication, achieving maximum titers at 36 hpi compared with 24 hpi for pH 7.2 and 7.4 (Figure 5b). Stability of virions can be affected by absorption to cellular debris and release of cellular proteases after virus-induced apoptosis and cell lysis, therefore, lower stability was expected in the ambr15 system from 24 hpi compared with STRs or orbitally shaken systems. Moreover, low pH values (below 7.0) are generally found to negatively impact virus production and stability (Ferreira et al., 2007; Zimmer et al., 2013). For the tested pH range, however, stability was not impacted. Due to the impeded cell growth at pH 7.0, a biphasic process could be designed, controlling the pH between 7.2 and 7.4 for the cell growth phase and lowering the pH set-point to 7.0 after infection to minimize cell growth and thereby reduce the level of contaminants, to facilitate the design of subsequent clarification trains and further process intensification strategies. Nevertheless, the ambr15 system was identified as a suitable small scale system for

process optimization, reaching similar cell growth parameters and virus titers as compared with larger scale STRs.

4 | CONCLUSION

In this study, CCX.E10 cells were identified as a viable host cell substrate for the manufacturing of the fusogenic oncolytic virus, rVSV-NDV. CCX.E10 cells demonstrated robust growth to high concentrations in batch mode with low accumulation rates of metabolic by-products such as lactate and ammonium. Moreover, they could be cultivated in various systems, including shake flasks, OSB, STR and ambr15 with similar cell growth performance and high virus yields.

Maximum infectious virus titers above 10^8 TCID₅₀/mL with high CSVYs were reached regardless of the bioreactor system selected. Compared to other suspension cells infected in optimized batch STR processes, similar (BHK-21 cells) or drastically higher (HEK293 and AGE1.CR cells) volumetric virus productivities were achieved with CCX.E10 (Göbel, 2023). While oncolytic applications could possibly allow the use of production cell lines known to be tumorigenic (e.g., BHK-21 cells) due to the unique risk–benefit ratio compared with other (i.e., prophylactic) applications, regulatory authorities would likely require additional purity and safety studies to demonstrate a satisfactory quality profile, which introduces additional cost, time, and risk to the process. Therefore, the identification of a cell line that produces high yields of virus product, while also offering a de-risked regulatory pathway, represents a valuable step in process development.

With regard to downstream processing, harvesting at the time-point of maximum virus titer resulted in maximum dsDNA concentrations of 14.1 μ g/mL and protein contamination of 2.0 mg/mL at the 3 L STR (180 rpm), respectively. Chromatography-based purification methods including steric exclusion chromatography have been

reported to allow effective handling of such impurity levels (Marichal-Gallardo et al., 2017). Additional screening and testing of the produced OV regarding oncolytic potency, efficacy in preclinical models as well as whole blood and serum stability in human and animal systems should be carried out. Current OV platforms require a dose input of 10^9 – 10^{10} virions/injection to achieve a therapeutic effect and effective delivery to tumor sites. Therefore, development of OV production processes that allow to generate even higher virus yields is essential. Process intensification by transition from batch production to perfusion mode could further increase titers as much higher cell concentrations can be reached (Genzel et al., 2014a; Göbel, 2023; Gränicher, 2021; Nikolay et al., 2018; Lavado-García et al., 2020; Wu et al., 2021).

Taken together, the CCX.E10 cell line is a promising host for industrial production of OVs due to the high cell concentrations obtained in the chemically-defined medium in batch mode and options for scale-up. The ability to achieve similarly high rVSV-NDV yields, regardless of the production system used, as well as compliance of the cell line with regulatory guidelines, makes it an attractive host for large-scale production of this virus and potentially other similar fusogenic viruses that are under development as clinical oncolytic viral drug products.

AUTHOR CONTRIBUTIONS

Conceptualization: Sven Göbel, Karim E. Jaén, Rita P. Fernandes, Yvonne Genzel, Udo Reichl, and Jennifer Altomonte. **Methodology:** Sven Göbel, Karim E. Jaén, Rita P. Fernandes, and Yvonne Genzel. **Investigation:** Sven Göbel and Karim E. Jaén. **Writing—original draft:** Sven Göbel. **Writing—review and editing:** Sven Göbel, Karim E. Jaén, Rita P. Fernandes, Manfred Reiter, Udo Reichl, Jennifer Altomonte, and Yvonne Genzel. **Supervision:** Yvonne Genzel, Udo Reichl, and Jennifer Altomonte. **Project administration:** Sven Göbel, Karim E. Jaén, and Yvonne Genzel.

ACKNOWLEDGMENTS

The authors would like to thank Corina Siewert for the excellent technical support regarding general lab work and cell culture. The authors would like to thank Carole Langlois and Diogo Mattos from Sartorius for allowing us to use their ambr15 for these experiments. Furthermore, the kind support from Kühner (Tibor Anderlei) with discussions for the OSB10 run, ProBioGen for providing the adherent AGE1.CR.pIX cells, and Marc Hein for carrying out initial experiments are equally acknowledged. Part of the funding for this work was provided by the EXIST-Forschungstransfer Program (financed by the Federal Ministry for Economic Affairs and Energy) under the grant agreement #03EFOBY215 awarded to J. Altomonte.

CONFLICT OF INTEREST STATEMENT

J. Altomonte (WO 2017/198779) holds a patent for the development and use of rVSV-NDV for oncolytic therapy of cancer and is cofounder of Fusix Biotech GmbH, which is developing the rVSV-NDV technology for clinical use. M. Reiter is an employee of Nuvonis Technologies, which owns the CCX.E10 cells.

DATA AVAILABILITY STATEMENT

The data that support the findings of this study are available from the corresponding author upon reasonable request. Data is available in article's supplementary material. Additional data is available on request from the authors. The data that support the findings of this study are available from the corresponding author, Yvonne Genzel, upon reasonable request.

ETHICS STATEMENT

This article does not contain any studies with human participants or animals performed by any of the authors.

ORCID

Sven Göbel  <http://orcid.org/0000-0002-2264-5569>

REFERENCES

- Abaandou, L., Quan, D., & Shiloach, J. (2021). Affecting HEK293 cell growth and production performance by modifying the expression of specific genes. *Cells*, 10(7), 1667.
- Abdullahi, S., Jäkel, M., Behrend, S. J., Steiger, K., Topping, G., Krabbe, T., Colombo, A., Sandig, V., Schiergens, T. S., Thasler, W. E., Werner, J., Lichtenthaler, S. F., Schmid, R. M., Ebert, O., & Altomonte, J. (2018). A novel chimeric oncolytic virus vector for improved safety and efficacy as a platform for the treatment of hepatocellular carcinoma. *Journal of Virology*, 92(23), e01386-18.
- Adolf Kühner AG. (2017). User Manual OrbShake Bioreactor SB10-X (# 52409 version 2).
- Amanullah, A., Buckland, B. C., & Nienow, A. W. (2003). Mixing in the fermentation and cell culture industries, *Handbook of industrial mixing* (pp. 1071–1170). Wiley & Sons.
- Bissinger, T., Fritsch, J., Mihut, A., Wu, Y., Liu, X., Genzel, Y., Tan, W. S., & Reichl, U. (2019). Semi-perfusion cultures of suspension MDCK cells enable high cell concentrations and efficient influenza A virus production. *Vaccine*, 37(47), 7003–7010.
- Chisti, Y. (2000). Animal-cell damage in sparged bioreactors. *Trends in Biotechnology*, 18(10), 420–432.
- Coronel, J., Behrendt, I., Bürgin, T., Anderlei, T., Sandig, V., Reichl, U., & Genzel, Y. (2019). Influenza A virus production in a single-use orbital shaken bioreactor with ATF or TFF perfusion systems. *Vaccine*, 37(47), 7011–7018.
- Coronel, J., Gränicher, G., Sandig, V., Noll, T., Genzel, Y., & Reichl, U. (2020). Application of an inclined settler for cell culture-based influenza A virus production in perfusion mode. *Frontiers in Bioengineering and Biotechnology*, 8, 672–673.
- Elahi, S. M., Shen, C. F., & Gilbert, R. (2019). Optimization of production of vesicular stomatitis virus (VSV) in suspension serum-free culture medium at high cell density. *Journal of Biotechnology*, 289, 144–149.
- EMA. (2015). Assessment report Imlygic. Committee for Medicinal Products for Human Use (CHMP).
- Ferreira, T. B., Carrondo, M. J. T., & Alves, P. M. (2007). Effect of ammonia production on intracellular pH: Consequent effect on adenovirus vector production. *Journal of Biotechnology*, 129(3), 433–438.
- Flint, S. J., Racaniello, V. R., Rall, G. F., Hatzioannou, T., & Skalka, A. M. (2020). *Principles of virology: Pathogenesis and control* (Vol. 2). John Wiley & Sons.
- Genzel, Y., Rödig, J., Rapp, E., & Reichl, U. (2014). Vaccine production: Ustream processing with adherent or suspension cell Lines. *Animal Cell Biotechnology: Methods and Protocols*, 1104, 371–393.
- Genzel, Y., Vogel, T., Buck, J., Behrendt, I., Ramirez, D. V., Schiedner, G., Jordan, I., & Reichl, U. (2014a). High cell density cultivations by

- alternating tangential flow (ATF) perfusion for influenza A virus production using suspension cells. *Vaccine*, 32(24), 2770–2781.
- Giese, H., Klöckner, W., Peña, C., Galindo, E., Lotter, S., Wetzel, K., Meissner, L., Peter, C. P., & Büchs, J. (2014). Effective shear rates in shake flasks. *Chemical Engineering Science*, 118, 102–113.
- Göbel, S., Jaén, K. E., Dorn, M., Neumeyer, V., Jordan, I., Sandig, V., Reichl, U., Altomonte, J., & Genzel, Y. (2023). Process intensification strategies towards cell culture-based high-yield production of a fusogenic oncolytic virus. *Biotechnology and Bioengineering*. Advance online publication.
- Göbel, S., Kortum, F., Chavez, K. J., Jordan, I., Sandig, V., Reichl, U., Altomonte, J., & Genzel, Y. (2022). Cell-line screening and process development for a fusogenic oncolytic virus in small-scale suspension cultures. *Applied Microbiology and Biotechnology*, 106(13–16), 4945–4961.
- González Hernández, Y. (2007). Serum-free culturing of mammalian cells—adaptation to and cryopreservation in fully defined media. *ALTEX: Alternativen zu Tierexperimenten*, 24(2), 110–116.
- Goyal, P., & Rajala, M. S. (2023). Reprogramming of glucose metabolism in virus infected cells. *Molecular and Cellular Biochemistry*. Advance online publication.
- Gränicher, G., Babakhani, M., Göbel, S., Jordan, I., Marichal-Gallardo, P., Genzel, Y., & Reichl, U. (2021). A high cell density perfusion process for modified vaccinia virus Ankara production: process integration with inline DNA digestion and cost analysis. *Biotechnology and Bioengineering*, 118(12), 4720–4734.
- Gränicher, G., Coronel, J., Pralow, A., Marichal-Gallardo, P., Wolff, M., Rapp, E., Karlas, A., Sandig, V., Genzel, Y., & Reichl, U. (2019). Efficient influenza A virus production in high cell density using the novel porcine suspension cell line PBG.PK2.1. *Vaccine*, 37(47), 7019–7028.
- Gränicher, G., Coronel, J., Trampler, F., Jordan, I., Genzel, Y., & Reichl, U. (2020). Performance of an acoustic settler versus a hollow fiber-based ATF technology for influenza virus production in perfusion. *Applied Microbiology and Biotechnology*, 104(11), 4877–4888.
- Grein, T. A., Loewe, D., Dieken, H., Weidner, T., Salzig, D., & Czermak, P. (2019). Aeration and shear stress are critical process parameters for the production of oncolytic measles virus. *Frontiers in Bioengineering and Biotechnology*, 7(78), fbioe.2019.00078.
- Hesterberg, R., Cleveland, J., & Epling-Burnette, P. (2018). Role of polyamines in immune cell functions. *Medical Sciences*, 6(1), 22.
- ICH. (1998). Quality of biotechnological products: Derivation and characterisation of cell substrates used for production of biotechnological/biological products. ICH harmonised tripartite guideline. *Developments in Biological Standardization*, 93, 223–234.
- Jordan, I., & Sandig, V. (2014). Matrix and backstage: Cellular substrates for viral vaccines. *Viruses*, 6(4), 1672–1700.
- Klöckner, W., Diederichs, S., & Büchs, J. (2014). Orbitally shaken single-use bioreactors. *Advances in Biochemical Engineering/Biotechnology*, 138, 45–60.
- Krabbe, T., Marek, J., Groll, T., Steiger, K., Schmid, R. M., Krackhardt, A. M., & Altomonte, J. (2021). Adoptive T cell therapy is complemented by oncolytic virotherapy with fusogenic VSV-NDV in combination treatment of murine melanoma. *Cancers*, 13(5), 1044.
- Kraus, B., von Fircks, S., Feigl, S., Koch, S. M., Fleischanderl, D., Terler, K., Dersch-Pourmojib, M., Konetschny, C., Grillberger, L., & Reiter, M. (2011). Avian cell line - Technology for large scale vaccine production. *BMC Proceedings*, 5(Suppl. 8), P52.
- Lavado-García, J., Cervera, L., & Godia, F. (2020). An alternative perfusion approach for the intensification of virus-like particle production in HEK293 cultures. *Frontiers in Bioengineering and Biotechnology*, 8, 617.
- Lohr, V. (2014). Characterization of the avian designer cells AGE1.CR and AGE1.CR.pIX considering growth, metabolism and production of influenza virus and modified vaccinia virus Ankara (MVA) bioprocess engineering. *Max Planck Institute for Dynamics of Complex Technical Systems*, Otto-von-Guericke Universität, Magdeburg. <https://hdl.handle.net/11858/00-001M-0000-0024-3EDE-2>
- Lohr, V., Hädicke, O., Genzel, Y., Jordan, I., Büntemeyer, H., Klamt, S., & Reichl, U. (2014). The avian cell line AGE1.CR.pIX characterized by metabolic flux analysis. *BMC Biotechnology*, 14(1), 72.
- Marichal-Gallardo, P., Pieler, M. M., Wolff, M. W., & Reichl, U. (2017). Steric exclusion chromatography for purification of cell culture-derived influenza A virus using regenerated cellulose membranes and polyethylene glycol. *Journal of Chromatography A*, 1483, 110–119.
- Meier, K., Klöckner, W., Bonhage, B., Antonov, E., Regestein, L., & Büchs, J. (2016). Correlation for the maximum oxygen transfer capacity in shake flasks for a wide range of operating conditions and for different culture media. *Biochemical Engineering Journal*, 109, 228–235.
- Michaels, J. D., Mallik, A. K., & Papoutsakis, E. T. (1996). Sparging and agitation-induced injury of cultured animals cells: Do cell-to-bubble interactions in the bulk liquid injure cells? *Biotechnology and Bioengineering*, 51(4), 399–409.
- Newsholme, P., Procopio, J., Lima, M. M. R., Pithon-Curi, T. C., & Curi, R. (2003). Glutamine and glutamate—Their central role in cell metabolism and function. *Cell Biochemistry and Function*, 21(1), 1–9.
- Nienow, A. W. (2021). The impact of fluid dynamic stress in stirred bioreactors—the scale of the biological entity: A personal view. *Chemie Ingenieur Technik*, 93(1–2), 17–30.
- Nienow, A. W., Rielly, C. D., Brosnan, K., Bargh, N., Lee, K., Coopman, K., & Hewitt, C. J. (2013). The physical characterisation of a microscale parallel bioreactor platform with an industrial CHO cell line expressing an IgG4. *Biochemical Engineering Journal*, 76, 25–36.
- Nikolay, A., Léon, A., Schwamborn, K., Genzel, Y., & Reichl, U. (2018). Process intensification of EB66[®] cell cultivations leads to high-yield yellow fever and Zika virus production. *Applied Microbiology and Biotechnology*, 102(20), 8725–8737.
- Petiot, E., Cuperlovic-Culf, M., Shen, C. F., & Kamen, A. (2015). Influence of HEK293 metabolism on the production of viral vectors and vaccine. *Vaccine*, 33(44), 5974–5981.
- Petiot, E., Proust, A., Traversier, A., Durous, L., Dappozze, F., Gras, M., Guillard, C., Balloul, J. M., & Rosa-Calatrava, M. (2018). Influenza viruses production: Evaluation of a novel avian cell line DuckCelt[®]-T17. *Vaccine*, 36(22), 3101–3111.
- Reiter, M., Portsmouth, D., & Barrett, P. N. (2014). Avian suspension culture cell lines for production of vaccines and other biologicals. *Industrial scale suspension culture of living cells* (pp. 390–409). Wiley & Sons.
- Schiefelbein, S., Fröhlich, A., John, G. T., Beutler, F., Wittmann, C., & Becker, J. (2013). Oxygen supply in disposable shake-flasks: prediction of oxygen transfer rate, oxygen saturation and maximum cell concentration during aerobic growth. *Biotechnology Letters*, 35(8), 1223–1230.
- Schneider, M. (1996). The importance of ammonia in mammalian cell culture. *Journal of Biotechnology*, 46(3), 161–185.
- Tajsoleiman, T., Mears, L., Krühne, U., Germaey, K. V., & Cornelissen, S. (2019). An industrial perspective on scale-down challenges using miniaturized bioreactors. *Trends in Biotechnology*, 37(7), 697–706.
- Tan, R.-K., Eberhard, W., & Büchs, J. (2011). Measurement and characterization of mixing time in shake flasks. *Chemical Engineering Science*, 66(3), 440–447.
- Tsao, Y.-S., Cardoso, A. G., Condon, R. G. G., Voloch, M., Lio, P., Lagos, J. C., Kearns, B. G., & Liu, Z. (2005). Monitoring Chinese hamster ovary cell culture by the analysis of glucose and lactate metabolism. *Journal of Biotechnology*, 118(3), 316–327.
- Ungerechts, G., Bossow, S., Leuchs, B., Holm, P. S., Rommelaere, J., Coffey, M., Coffin, R., Bell, J., & Nettelbeck, D. M. (2016). Moving oncolytic viruses into the clinic: Clinical-grade production,

- purification, and characterization of diverse oncolytic viruses. *Molecular Therapy: Methods & Clinical Development*, 3, 16018.
- Vázquez-Ramírez, D., Genzel, Y., Jordan, I., Sandig, V., & Reichl, U. (2018). High-cell-density cultivations to increase MVA virus production. *Vaccine*, 36(22), 3124–3133.
- Wu, Y., Bissinger, T., Genzel, Y., Liu, X., Reichl, U., & Tan, W. S. (2021). High cell density perfusion process for high yield of influenza A virus production using MDCK suspension cells. *Applied Microbiology and Biotechnology*, 105(4), 1421–1434.
- Wurm, M. J., & Wurm, F. M. (2021). Naming CHO cells for biomanufacturing: Genome plasticity and variant phenotypes of cell populations in bioreactors question the relevance of old names. *Biotechnology Journal*, 16(7), 2100165.
- Zdrojewicz, Z., & Lachowski, M. (2014). The importance of putrescine in the human body. *Postępy Higieny i Medycyny Doświadczalnej*, 68, 393–403.
- Zhou, W., Seth, G., Guardia, M. J., & Hu, W.-S. (2010). Mammalian cell bioreactors. *Encyclopedia of Industrial Biotechnology*, 1, 1–10.

- Zimmer, B., Summermatter, K., & Zimmer, G. (2013). Stability and inactivation of vesicular stomatitis virus, a prototype rhabdovirus. *Veterinary Microbiology*, 162(1), 78–84.

SUPPORTING INFORMATION

Additional supporting information can be found online in the Supporting Information section at the end of this article.

How to cite this article: Göbel, S., Jaén, K. E., Fernandes, R. P., Reiter, M., Altomonte, J., Reichl, U., & Genzel, Y. (2023). Characterization of a quail suspension cell line for production of a fusogenic oncolytic virus. *Biotechnology and Bioengineering*, 120, 3335–3346.
<https://doi.org/10.1002/bit.28530>

3.7. Fourth Manuscript

As a follow-up of the second manuscript, the applicability of the TFDF module as a perfusion system for high-titer production of recombinant VSV vectors was evaluated. Moreover, benefits that TFDF might have over conventional ATF operations, namely continuous virus harvesting and clarification were investigated. Using suspension BHK-21 cells, the TFDF unit allowed to achieve high VCC ($16.4\text{-}20.6 \times 10^6$ cells/mL), continuous vector harvesting and clarification. Compared to the previously optimized batch process, 11-fold higher infectious virus titers were obtained in the permeate (maximum 7.5×10^9 TCID₅₀/mL). This is so far the highest reported infectious virus titer for this virus and corresponds to a 7500-fold increase compared to the initial production process in adherent pIX cells.

Göbel, Sven*; Pelz, Lars*; Silva, Cristina A. T.; Brühlmann, Béla; Hill, Charles; Altomonte, Jennifer; Kamen, Amine; Reichl, Udo; Genzel, Yvonne

*Shared first authorship

Production of recombinant vesicular stomatitis virus-based vectors by tangential flow depth filtration

Applied Microbiology and Biotechnology, 2024

[109]

Contribution Sven Göbel:

Conceptualization, formal analysis, investigation, methodology, project administration, writing – original draft, writing – review & editing.



Production of recombinant vesicular stomatitis virus-based vectors by tangential flow depth filtration

Sven Göbel¹ · Lars Pelz¹ · Cristina A. T. Silva² · Béla Brühlmann³ · Charles Hill³ · Jennifer Altomonte⁴ · Amine Kamen⁵ · Udo Reichl^{1,6} · Yvonne Genzel¹

Received: 17 October 2023 / Revised: 14 February 2024 / Accepted: 16 February 2024
© The Author(s) 2024

Abstract

Cell culture-based production of vector-based vaccines and virotherapeutics is of increasing interest. The vectors used not only retain their ability to infect cells but also induce robust immune responses. Using two recombinant vesicular stomatitis virus (rVSV)-based constructs, we performed a proof-of-concept study regarding an integrated closed single-use perfusion system that allows continuous virus harvesting and clarification.

Using suspension BHK-21 cells and a fusogenic oncolytic hybrid of vesicular stomatitis virus and Newcastle disease virus (rVSV-NDV), a modified alternating tangential flow device (mATF) or tangential flow depth filtration (TFDF) systems were used for cell retention. As the hollow fibers of the former are characterized by a large internal lumen (0.75 mm; pore size 0.65 μm), membrane blocking by the multi-nucleated syncytia formed during infection could be prevented. However, virus particles were completely retained. In contrast, the TFDF filter unit (lumen 3.15 mm, pore size 2–5 μm) allowed not only to achieve high viable cell concentrations (VCC, 16.4–20.6 $\times 10^6$ cells/mL) but also continuous vector harvesting and clarification. Compared to an optimized batch process, 11-fold higher infectious virus titers were obtained in the clarified permeate (maximum 7.5 $\times 10^9$ TCID₅₀/mL).

Using HEK293-SF cells and a rVSV vector expressing a green fluorescent protein, perfusion cultivations resulted in a maximum VCC of 11.3 $\times 10^6$ cells/mL and infectious virus titers up to 7.1 $\times 10^{10}$ TCID₅₀/mL in the permeate. Not only continuous harvesting but also clarification was possible. Although the cell-specific virus yield decreased relative to a batch process established as a control, an increased space-time yield was obtained.

Key points

- Viral vector production using a TFDF perfusion system resulted in a 460% increase in space-time yield
- Use of a TFDF system allowed continuous virus harvesting and clarification
- TFDF perfusion system has great potential towards the establishment of an intensified vector production

Keywords Tangential flow depth filtration · Alternating tangential flow filtration · Bioreactor · Perfusion · Recombinant VSV-based vectors · Oncolytics · Vaccines

Sven Göbel and Lars Pelz contributed equally to this work.

✉ Yvonne Genzel
genzel@mpi-magdeburg.mpg.de

¹ Bioprocess Engineering, Max Planck Institute for Dynamics of Complex Technical Systems, Sandtorstr. 1, 39106 Magdeburg, Germany

² Department of Chemical Engineering, Polytechnique Montréal, Montréal, Québec, Canada

³ Repligen, Waltham, MA, USA

⁴ Department of Internal Medicine II, Klinikum rechts der Isar, Technische Universität München, Munich, Germany

⁵ Department of Bioengineering, McGill University, Montréal, Québec, Canada

⁶ Chair for Bioprocess Engineering, Otto von Guericke University Magdeburg, Universitätsplatz 2, 39106 Magdeburg, Germany

Introduction

In the relentless pursuit to combat infectious diseases, recombinant vector-based vaccines produced in cell culture have gained popularity during the last decade. Compared to other vaccine platforms, viral vector-based vaccines retain their ability to infect cells, thereby inducing robust immune responses by increasing both humoral and cellular immunity (Ura et al. 2014). Successful large-scale applications of adenoviral-based vectors against SARS-CoV-2 (Mendonça et al. 2021) combined with their potential application against a wide array of infectious diseases, resulted in tremendous research efforts to develop new recombinant vector-based vaccines (accounting for 14% of global R&D vaccine landscape in 2023 (Yue et al. 2023)) and to improve current manufacturing processes. One such vector is based on the recombinant vesicular stomatitis virus (rVSV). Due to its broad tropism, fast replication kinetics to high titers, low viral pathogenicity, rare pre-existing anti-vector immunity in humans, and ease of genetic manipulation, rVSV has gained popularity for both vaccine and oncolytic applications (Ura et al. 2021). Replacing the native glycoprotein of rVSV to any glycoprotein of interest allows delivery of foreign antigens to elicit robust humoral and cellular immunity for vaccine applications, while simultaneously reducing the manufacturing-associated biosafety standards (e.g., for highly pathogenic viruses) (Zhang and Nagalo 2022). Various vaccine candidates manufactured using a rVSV production platform have shown prophylactic effects against Ebola (Suder et al. 2018), SARS-CoV-2 (Ura et al. 2021), Marburg virus (Jones et al. 2005), Lassa virus (Geisbert et al. 2005), Andes virus (Brown et al. 2011), hepatitis B virus (Cobleigh et al. 2010), *Yersinia pestis* (Palin et al. 2007), respiratory syncytial virus (Kahn et al. 2001), dengue virus (Laurettil et al. 2016), chikungunya virus (van den Pol et al. 2017), Nipah virus (DeBuysscher et al. 2016), Zika virus (Emanuel et al. 2018), human papillomavirus (Liao et al. 2008), and influenza virus (Roberts et al. 1998) in animal models; and some are being tested in clinical trials. Despite the well-demonstrated prophylactic efficacy, currently only one VSV-based vaccine against Zaire ebolavirus (rVSV-ZEBOV) gained FDA and EMA approval in 2019 (EMA 2019; FDA 2019). Usage of rVSV as oncolytic agents is particularly interesting, as its high cytopathogenicity, fast replication cycle, non-integration into the host genome, IFN-sensitivity, selective infection, and potent induction of apoptosis in cancer cells fulfill all critical features for virotherapy (Zhang and Nagalo 2022). Further genetic modification approaches such as pseudotyping innate glycoproteins with heterologous fusion glycoproteins, generating chimeric constructs that can convey fusogenic-based viral propagation, further enhance the

oncolytic abilities of rVSV-based constructs (Abdullahi et al. 2018). One such novel rVSV-based construct contains the fusogenic mutant proteins of Newcastle disease virus (NDV) and has shown promising pre-clinical efficacy in various cancer models (Abdullahi et al. 2018; Krabbe et al. 2021).

To address the unprecedented demand, as well as the high input doses required for many rVSV-based therapies, current batch-based manufacturing strategies need to be intensified. Usage of suspension cell lines in chemically defined media allows for the design of processes that are easier to scale-up, for higher cell concentrations and for smaller footprints compared to traditional adherent-based manufacturing (Pelz et al. 2022). By the establishment of perfusion cultures, where depleted medium is continuously exchanged with fresh medium, while the cells are retained in the bioreactor by the use of a cell retention device, even higher cell concentrations can be achieved. Process intensification in perfusion mode to increase virus titers, cell-specific virus yields (CSVYs), space-time yield (STY), and volumetric virus productivity (VVP) have already been elaborated for different viruses and vectors such as for Zika virus (Nikolay et al. 2018), influenza A virus (IAV) (Wu et al. 2021), lentiviral vectors (LV) (Tran and Kamen 2022; Tona et al. 2023), adeno-associated virus (AAV) (Mendes et al. 2022), rVSV-COV-2 (Yang et al. 2023), rVSV-NDV (Göbel et al. 2023a), and modified vaccinia virus Ankara (Gränicher et al. 2021a; Gränicher et al. 2021b). However, by targeting higher cell concentrations, the CSVY might be decreased (high-cell density effect) thus lowering the STY and VVP (Bock et al. 2011; Nadeau and Kamen 2003).

For high-cell concentration cultivations, membrane-based systems, i.e., alternating tangential flow (ATF) and tangential flow filtration (TFF) modules are widely employed. One major drawback of these systems is the risk of filter fouling (despite the self-cleaning backflush of the ATF) and retention of virus particles, which leads to unwanted accumulation of virus inside the bioreactor within the cell environment until full harvest of the bioreactor broth is possible (Genzel et al. 2014; Hadpe et al. 2017; Nikolay et al. 2020; Nikolay et al. 2018; Tona et al. 2023; Vázquez-Ramírez et al. 2019). As virus release typically leads to cell lysis, cell debris and DNA increase over time, equally increasing viscosity of the culture broth and further increasing the risk of membrane clogging. Prolonged retention inside the bioreactor can have a negative impact on virus infectivity due to a release of cellular proteases, adsorption of virions to cellular debris, and viral temperature sensitivity (Aunins 2003; Eccles 2021; Genzel et al. 2010; Göbel et al. 2023a; Gränicher et al. 2020; Wu et al. 2021). Additionally, fusogenic oncolytic constructs such as rVSV-NDV that lead to the formation of large multi-nucleated syncytia (>100 µm)

in perfusion cultures are likely to block the small lumen sizes of commonly used hollow-fiber membranes (Göbel et al. 2023a). One approach to overcome this issue is the use of non-membrane-based systems such as an acoustic filter (Göbel et al. 2023a; Gränicher et al. 2020; Manceur et al. 2017) or an inclined settler (Coronel et al. 2020); however, these systems are often complex or not compatible with industrial size bioreactors and have a lower cell retention efficiency. Alternatively, membranes that allow virus particles to pass through could be used. This has been recently demonstrated for the production of IAV defective interfering particles utilizing a tubular membrane (VHU, pore size ~10 µm) coupled to an ATF system (Hein et al. 2021). Using tangential flow depth filtration (TFDF) perfusion modules (pore size 2–5 µm), continuous harvest of LV as well as AAV has been already shown (Mendes et al. 2022; Tona et al. 2023; Tran and Kamen 2022). This allows for shorter residence times of infectious virus particles and the possibility to immediately store harvested material in cooled tanks to increase virus stability and, thus, virus yields and productivity. For instance, continuous virus harvest using an acoustic settler for IAV production enhanced CSVY and VVP by a factor of 1.5 relative to a perfusion run with a hollow fiber membrane with PES (0.2 µm cut-off) (Gränicher et al. 2020). Moreover, the TFDF module can combine continuous virus harvest and clarification in a single step, reducing the number of unit operations and therefore saving time and money (Mendes et al. 2022). All in all, this could allow for a direct integration of upstream (virus production) and downstream processing (virus purification), further reducing costs while increasing flexibility and productivity (Gränicher et al. 2021a; Moleirinho et al. 2020).

In this study, we evaluated the applicability of the TFDF perfusion system as a novel cell retention device and virus transmission away for the host cell environment for both perfusion cultivation and continuous harvest filtration with clarification (turbidity reduction) in a single operation. The process intensification of the production of two different rVSV-based vectors, one which induces classical cytopathic effects and one that mediates cell fusion reactions, was compared to optimized batch processes.

Materials and methods

Cell lines, media, and viral seed stock

Baby hamster kidney (BHK-21) cells (CEVA Animal Health) were cultivated in protein expression medium (PEM) (Gibco, USA) supplemented with 4-mM pyruvate and 8 mM L-glutamine (Sigma-Aldrich, USA). Cells were sub-cultured to 0.5×10^6 cells/mL twice a week using vented, baffled 125-mL shake flasks (50 mL working volume (WV)) at 37

°C and 5% CO₂ with controlled agitation (185 rpm, shaken diameter of 50 mm, Infors HT, Switzerland). Human embryonic kidney (HEK293-SF) cells were kindly provided by National Research Council of Canada (NRC, Montreal, Canada) and grown in vented, non-baffled 125-mL shake flasks (TriForest Enterprises, USA) in HyClone HyCell TransFx-H medium (Cytiva, USA) supplemented with 6 mM glutamine and 0.1% Koliphor P188 (Merck, USA). HEK293-SF cells were passaged three times a week at 0.2×10^6 or 0.5×10^6 cells/mL and grew in a humified Multitron orbital shaker (shaking diameter of 25 mm, Infors HT, Switzerland) at 135 rpm, 37 °C, and 5% CO₂. Adherent Huh7 cells were cultivated at 37 °C and 5% CO₂ in T75 flasks in high glucose Dulbecco's Modified Eagle Medium (DMEM, Gibco, USA), supplemented with 1 mM sodium pyruvate (Gibco, USA), 1× non-essential amino acids (Gibco, USA), and 10% FCS. Adherent HEK293 cells were maintained in T75 or T175 flasks in DMEM (Wisent Bioproducts, Canada) supplemented with 10% FCS (Wisent Bioproducts, Canada) at 37 °C and 5% CO₂ in a humidified incubator and sub-cultured twice a week by using TrypLE Express (Thermo Fisher Scientific, USA). Adherent AGE1.CR.pIX cells were maintained at 37 °C, 5% CO₂ in T75 flasks in DMEM-F12 medium (Gibco, USA).

For infections, the previously described BHK-21-derived virus seed (rVSV-NDV) with a titer of 1.33×10^9 50% tissue culture infectious dose (TCID₅₀)/mL was used (Göbel et al. 2023a). Moreover, we used rVSV-green fluorescent protein (GFP) virus seed with a titer of 2.12×10^9 TCID₅₀/mL, which was derived from suspension HEK293 cells and kindly provided by NRC. Aliquots of the stocks and clarified samples were stored at –80 °C and were used once for each experiment or assay to prevent loss of infectivity due to repeated freeze-thaw cycles.

Perfusion mode production of rVSV-NDV in an orbitally shaken bioreactor

To evaluate applicability of membrane-based cell retention for production of fusogenic oncolytic viruses, a perfusion run employing a modified alternating tangential flow filtration device (mATF) as a cell retention device was carried out. Here, a SB10-X orbital shaken bioreactor (OSB) (Adolf Kühner AG) was used with the novel 3 L modular adapter and standard 3-L single-use bags. BHK-21 cells were inoculated at 0.9×10^6 cells/mL with 2.4 L WV at 37 °C and shaken at 100 rpm (50-mm shaking diameter). Aeration was solely carried out through headspace gassing using 300 mL/min air/O₂. By automatic adjustments of the gas composition in the output flow, dissolved oxygen (DO) and pH were controlled at 80% and 7.20, respectively. Perfusion was initiated once viable cell concentration (VCC) reached 4– 10^6 cells/mL. The perfusion rate was manually increased over time

to maintain a cell-specific perfusion rate (CSPR) of 115 pL/cell/day. For virus production, temperature was decreased to 34 °C, and the perfusion rate was set to 1.8 RV/day. Coupling of the 3-L single-use bag to a hollow fiber membrane (0.65- μm modified polyethersulfone (mPES), 1075 cm², Repligen, USA) connected to the mATF (Repligen, USA) was carried out as described previously (Coronel et al. 2019). Exchange flow rates of the diaphragm pump were set to 1.5 L/min. As the ATF2 module was placed below the SB10-X, a height differential of 40 cm was set, while other parameters were kept as given by the supplier.

Perfusion mode production of rVSV-NDV in a STR

Bioreactor perfusion cultivations were performed using a 3-L stirred tank bioreactor (STR) (DASGIP, Eppendorf AG, Germany) equipped with two pitched blade impellers (50-mm diameter; 180 rpm) and a L-drilled hole sparger, as well as a microsparger for gas supply. The DO setpoint of 50% was maintained by varying the gas flow rates (3–9 L/h) and the percentage of O₂ in the gas mixture (21–100%). pH was controlled at 7.20 by sparging CO₂. Temperature was set to 37 °C for the growth phase and 34 °C for the infection phase. BHK-21 cells were inoculated at 0.8 \times 10⁶ cells/mL at 1.3 L WV, and the cells were grown in batch mode until a VCC of 4.0 \times 10⁶ cells/mL was reached. Then, perfusion was started, and medium was exchanged with a CSPR of 130 pL/cell/day for BHK-21 cells. For cell retention, a 30-cm² TFDF cartridge (polypropylene and polyethylene terephthalate, pore size 2–5 μm , Repligen) connected to a Krosflo TFDF system (Repligen) was used. Using the KrosFlo's integrated flow sensor and weight control system, the recirculation rate and WV were maintained at 0.9 L/min and 1.3 L, respectively. Permeate flow rates were either updated daily based on VCC and the CSPR or controlled automatically through a capacitance probe and pre-amplifier connected to the ArcView controller 265 (Incyte Hamilton, USA), as described previously (Göbel et al. 2023a). A “cell factor” of 0.25 was used to set the cell volume-specific perfusion rate (CVSPR) of 0.06 pL/ μm^3 /day. At time of infection (TOI), an RV was exchanged by temporarily increasing the permeate flow rate to 8–10 mL/min, and cells were subsequently infected with a multiplicity of infection (MOI) of 1E-4. After infection, permeate flow was paused for up to 2 h and then fixed to 1.8 RV/day (1.7 mL/min). The clarified permeate was collected continuously into sterile polyethylene terephthalate bottles, previously filled with sucrose equal to 5% final concentration, at room temperature. The final one-step bioreactor harvest was carried out using a modified concentration-diafiltration-concentration (C1/DF/C2) process (Table S1), where the permeate flow was paused during the diafiltration step. Furthermore, either sterile PBS (TFDF1) or supplemented medium (TFDF2) was used for

diafiltration. The overall setup including devices for control of perfusion is shown in Fig. 1.

Other analytics for rVSV-NDV experiments

VCC and viability were quantified using the automated cell counter ViCell (Coulter Beckman, USA). A pH7110 potentiometer (Inolab, USA) was used to measure off-line pH, and metabolite concentrations (glucose, lactate, glutamine, glutamate, ammonium) were determined by a Cedex Bio Analyzer (Roche, Switzerland). Titration of rVSV-NDV was carried out using adherent AGE1.CR.pIX cells and the previously described TCID₅₀ assay (Göbel et al. 2022a, 2022b). Oncolytic viral potency was confirmed using the previously described half maximal inhibitory concentration (IC₅₀) potency assay in Huh7 cells (Göbel et al. 2023a; Göbel et al. 2022a). Taking into account only the error of the TCID₅₀ assay (–50%/+100% on a linear scale), the CSVY was calculated as previously described by Gränicher et al. 2020. Total DNA and protein were quantified using the Quant-iT™ PicoGreen dsDNA assay kit (Thermo Fisher Scientific, USA) and with Pierce™ BCA assay kit (Thermo Fisher Scientific, USA), respectively, according to the manufacturer's instructions. The solution turbidity of bioreactor and permeate samples was measured using a turbidimeter (2100 Qis Portable, HACH).

Production of rVSV-GFP in shake flasks

For production of rVSV-GFP in batch mode using shake flasks, HEK293-SF cells growing in exponential growth phase were centrifuged (300 \times g, 5 min, room temperature (RT)), supernatant was discarded, and cells were resuspended in penicillin/streptomycin (Pen/Strep)-containing fresh medium. Subsequently, cells were seeded at 0.4 \times 10⁶ cells/mL into a shake flask and grown to 1.1 \times 10⁶ cells/mL. Cells were infected at an MOI of 1E-3, and temperature was reduced from 37 to 34 °C. Supernatant samples were centrifuged (1200 \times g, 5 min, 4 °C) and stored at –80 °C for analytics.

Batch mode production of rVSV-GFP in a STR

Production of rVSV-GFP in batch mode was conducted in a 3 L (2100 mL WV) or 1 L (700 mL WV) STR (Applikon Biotechnology, Netherlands), which was equipped with two (3 L STR) or one (1 L STR) marine impeller(s) (100 rpm). Continuous surface aeration (12.5 mL/min), with sparging of O₂ (microsparger) when necessary, was used to control dissolved oxygen above 40% DO. The pH set point of 7.15 was controlled by CO₂ injection into the headspace of the bioreactor or addition of 9% NaHCO₃. HEK293-SF cells cultured in shake flasks were centrifuged (300 \times g, 5 min, RT), resuspended in fresh Pen/Strep-containing medium

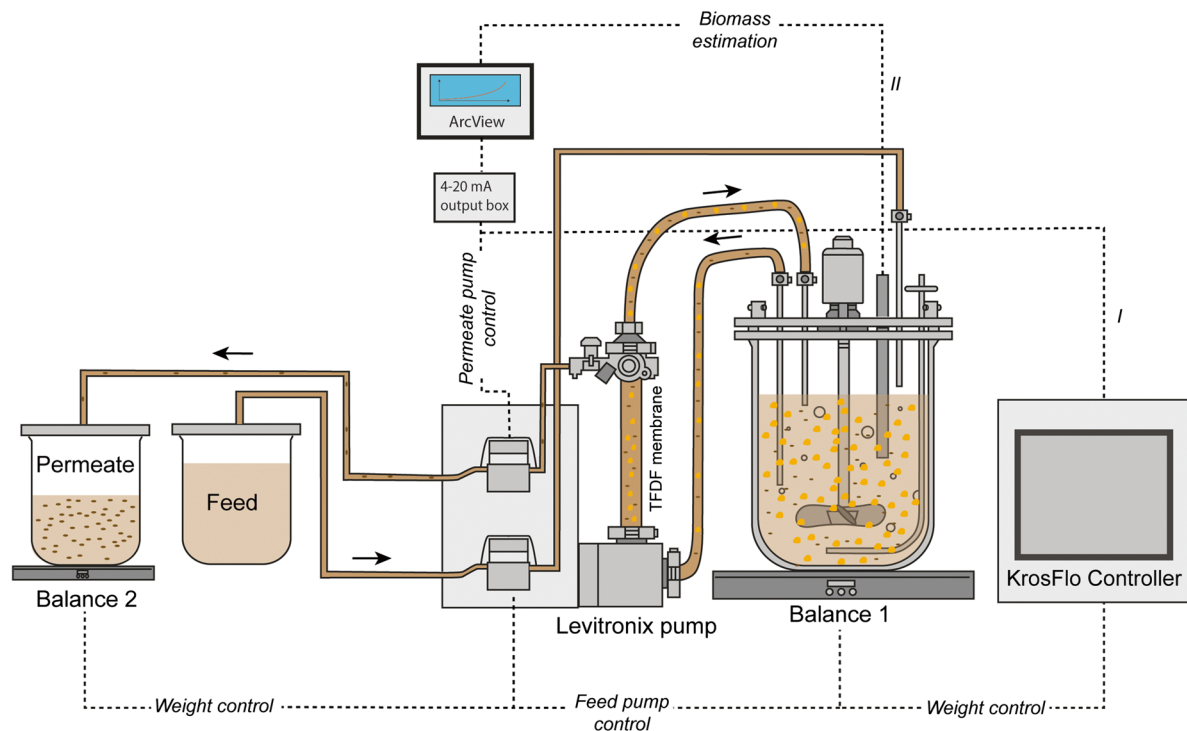


Fig. 1 Scheme of the TFDF setup for perfusion cultivations with manual adjustment (I) or automated (II) perfusion control (adapted from (Göbel et al. 2022b)). BHK-21 cells were continuously pumped through a 30-cm² TFDF cartridge (pore size 2–5.0 μm) by a levitronix impeller pump in unidirectional flow. Flow rates for feed and inlet were controlled using balances and KrosFlo’s integrated flow sensor,

respectively. For the cell growth phase, the permeate flow was either manually adjusted (I, using the KrosFlo controller) or controlled (II, using a capacitance probe). Larger orange circles indicate cells, black ellipses indicate virus particles, and dashed lines indicate different types of signal transmission

and inoculated at about 0.3×10^6 cells/mL into the STR. HEK293-SF cells were grown at 37 °C up to $1.2\text{--}1.3 \times 10^6$ cells/mL. Prior to infection, the temperature was reduced to 34 °C, and cells were infected at an MOI of 1E-3.

Perfusion mode production of rVSV-GFP in a STR

For perfusion mode production of rVSV-GFP, a 3 L STR was used at 2100 mL WV. Standard bioreactor setup and process parameters are similar to those described in the previous chapter. Before inoculation, recirculation was started with a recirculation rate of 1.0 L/min. HEK293-SF cells growing in shake flasks in the exponential growth phase were centrifuged ($300 \times g$, 5 min, RT), resuspended in fresh Pen/Strep-containing medium, and seeded at 0.8×10^6 cells/mL. After a cell growth phase in batch mode for 24 h, perfusion was initiated with a permeate flow rate of 0.9 mL/min (0.6 RV/d). In the following, the permeate flow rate was adjusted manually based on a CSPR of 115 pL/cell/day. The bioreactor weight was used to control the feed flow rate. Prior to infection, one RV with medium was exchanged by temporarily increasing the permeate flow rate to 20–33 mL/min. Temperature was reduced to 34 °C, and HEK293-SF cells (10×10^6 cells/mL) were infected

at an MOI of 1E-3. Following infection, the permeate flow was stopped for 1 h, and then set at a constant rate of 2.2 mL/min (1.5 RV/day). Supernatant samples were taken from the bioreactor and permeate line. After infection, the accumulated clarified permeate in the permeate bottle was stored on ice and transferred to a storage bottle (stored at 4 °C) at each sample taking. Lastly, a final “pool sample” was taken from the storage bottle containing the entire volume of collected permeate, without the final harvest step. For final one-step harvest at 31-h post infection (hpi), the recirculation rate was increased to 2.1 L/min to prevent filter fouling and promote self-cleaning. In more detail, a C1/DF/C2 process was conducted (Table S2). In the first step, 980 mL cell broth was pumped (31.3 mL/min) from the bioreactor through the TFDF filter into the harvest bottle. Next, 1049 mL medium was pumped (31.3 mL/min) into the bioreactor for washing, while harvest continued. In the last step, feeding of medium was stopped, while another 491 mL of suspension was pumped from the bioreactor through the TFDF filter into the harvest bottle. Supernatant samples were centrifuged ($1200 \times g$, 5 min, 4 °C) and stored at –80 °C until further analysis. For metabolite measurements, virus was removed using a Vivaspin 500 (Cytiva, USA, molecular weight cut-off of 100 kDa, 10,000×rpm, 5 min).

Other analytics for rVSV-GFP experiments

Quantification of VCC, viability, and cell diameter was performed using a cell counter (Vi-Cell™ XR, Beckman Coulter, USA). Metabolite concentrations were quantified by Bioprofile® FLEX 2 (Nova Biomedical, USA). A TCID₅₀ assay was used to quantify infectious virus titer of rVSV-GFP samples. In brief, adherent HEK293 cells were seeded at a concentration of 0.2×10^5 cells/well (100 μ L per well) in 96-well plates using DMEM (10% FCS, 1% Pen/Strep), followed by incubation for 24 h at 37 °C. Prior to infection, medium was gently removed from wells by a vacuum aspirator (8-channel adaptor). Cells were infected (infection medium: 2% FCS, 1% Pen/Strep) with eight replicates (100 μ L/well) per dilution (serial dilution of 1:10) and incubated for 7 days at 34 °C. Wells containing cytopathic effect under standard light microscope were considered as positive. Spearman/Kärber method was used to calculate TCID₅₀ titer. Each sample was quantified twice in independent TCID₅₀ assays.

Calculations

Metabolite consumption/production rates (q_s), CSVY (TCID₅₀/cell), volumetric virus productivity (VVP; TCID₅₀/L/day), space-time yield (STY, TCID₅₀/L/day), and cell retention efficiency (CRE) were calculated as follows:

$$q_s = \frac{\mu}{Y_{x/s}} \quad (1)$$

$$Y_{x/s} = \frac{x(t_n) - x(t_{n-1})}{c_s(t_{n-1}) - c_s(t_n)} \quad (2)$$

where μ is the cell-specific growth rate (1/h), $Y_{x/s}$ is the biomass yield, x is the VCC (cells/mL) at the cultivation time n (t_n), and c_s the metabolite concentration (mM).

vir_{acc} is the accumulated number of infectious virus particles (TCID₅₀) and was calculated for different production modes as follows:

$$\text{Batch : } vir_{acc} = C_{vir, BR} \times V_{BR} \quad (3)$$

$C_{vir, BR}$ is the infectious virus concentration (TCID₅₀/mL) in the bioreactor. V_{BR} (mL) is the working volume of the cultivation vessel.

$$\text{ATF, AS : } vir_{acc} = C_{vir, BR} \times V_{BR} + \sum \frac{(C_{vir, P, n} + C_{vir, P, n-1})}{2} \times V_H \quad (4)$$

$C_{vir, P, n}$ and $C_{vir, P, n-1}$ are the infectious virus concentrations in the permeate between t_n and t_{n-1} , respectively. V_H represents the harvest volume collected between t_n and t_{n-1} .

$$\text{TFDF : } vir_{acc} = C_{vir, FH} \times V_{FH} + \sum C_{vir, B, n} \times V_{B, n} \quad (5)$$

$C_{vir, FH}$ is the infectious virus concentrations of the final harvest step. V_{FH} represents the volume of the final harvest step. $C_{vir, B, n}$ and $C_{vir, B, n-1}$ are the infectious virus concentrations in the harvest bottles, which were exchanged every sample time point for rVSV-NDV. $V_{B, n}$ represents the volume in the harvest bottle. For the TFDF run with rVSV-GFP, the collected permeate (stored at 4 °C) was sampled combined, and final harvest step was sampled individually. For the TFDF run with rVSV-NDV, all harvest bottles were sampled individually and not combined.

$$\text{CSVY} = \frac{vir_{acc}}{x_{max} \times V_{BR}} \quad (6)$$

$$\text{VVP} = \frac{vir_{acc}}{V_{acc} \times t_{tot}} \quad (7)$$

$$\text{STY} = \frac{vir_{acc}}{V_{BR} \times t_{tot}} \quad (8)$$

x_{max} (cells/mL) is the maximum viable cell concentration reached post-infection in the cultivation vessel. V_{acc} (mL) is the accumulated medium spent during the entire process, and t_{tot} (h) is the total process time until maximum vir_{tot} is reached.

Percentage of infectious virus (P_{Perm}) passing through the membrane was calculated as follows:

$$P_{Perm} = \frac{1}{n} \sum \left(\frac{C_{vir, P, n}}{C_{vir, BR, n}} \right) \times 100\% \quad (9)$$

Cell retention efficiency (CRE), shear rate (γ), and permeate flux (J) were calculated as follows:

$$\text{CRE} = \left(1 - \frac{x_H}{x_{BR}} \right) \times 100 \quad (10)$$

$$\gamma = \frac{4 \times Q}{z \times \pi \times R^3} \quad (11)$$

$$J = \frac{\dot{V}_p}{A} \quad (12)$$

where x_H and x_{BR} are the measured VCC in the permeate line and in the bioreactor, respectively. Q represents the volumetric recirculation rate (m³/s, based on the exchange flow rate of the ATF system or recirculation rates of the TFDF system), R the internal radius of the fiber (m), and z the number of hollow-fibers of the ATF/TFDF membrane. The permeate flux is calculated as the ratio of the permeate flow rate \dot{V}_p (L/h) to the total filtration area of the hollow-fiber membrane A (m²).

Results

rVSV-NDV production using mATF

To evaluate the virus retention of commonly used hollow-fiber membranes and the applicability for fusogenic oncolytic viruses forming large multi-nucleated syncytia, an initial perfusion run using the novel 3-L modular adapter on a SBX-10 OSB with a 0.65- μm mPES membrane connected to a mATF was carried out. Previously, it has been shown that OSB and STR bioreactors perform similarly for cell growth and, therefore, to demonstrate all possible applications, an OSB was chosen (Coronel et al. 2019; Göbel et al. 2023b) for this study. To prevent potential syncytia from blocking the hollow fibers, a membrane with fiber lumen larger than previously observed syncytia (120–140 μm) was chosen (0.75-mm internal fiber lumen). Following inoculation at 0.8×10^6 cells/mL at 2.4 L WV, perfusion was initiated once

VCC reached 4×10^6 cells/mL. Manual adjustment of the perfusion rate allowed growth to 44.5×10^6 cells/mL with viabilities above 98% (Fig. 2A) without any limitations in glucose and glutamine (data not shown); however, the CSPR could not be controlled stably (Figure 2B). In order to conserve medium, no medium exchange prior to infection was carried out for this run. Cells were directly infected at an MOI of $1 \text{E-}4$ once cells reached a VCC of 44.5×10^6 cells/mL, temperature was reduced to 34 °C, and perfusion was paused for 4 h. Following re-initiation of perfusion, VCC stagnated until 36 hpi, after which viability and VCC slowly declined (Fig. 2A). Maximum infectious virus titers of 3.2×10^9 TCID₅₀/mL were reached at 42 hpi in the bioreactor, corresponding to a CSVY of 67 TCID₅₀/cell and a VVP of 4.0×10^{10} TCID₅₀/L/day (Table 1).

To assess the virus retention by the 0.65- μm hollow fiber membrane, samples were taken from the bioreactor and the permeate line, respectively. Already at 18 hpi, infectious

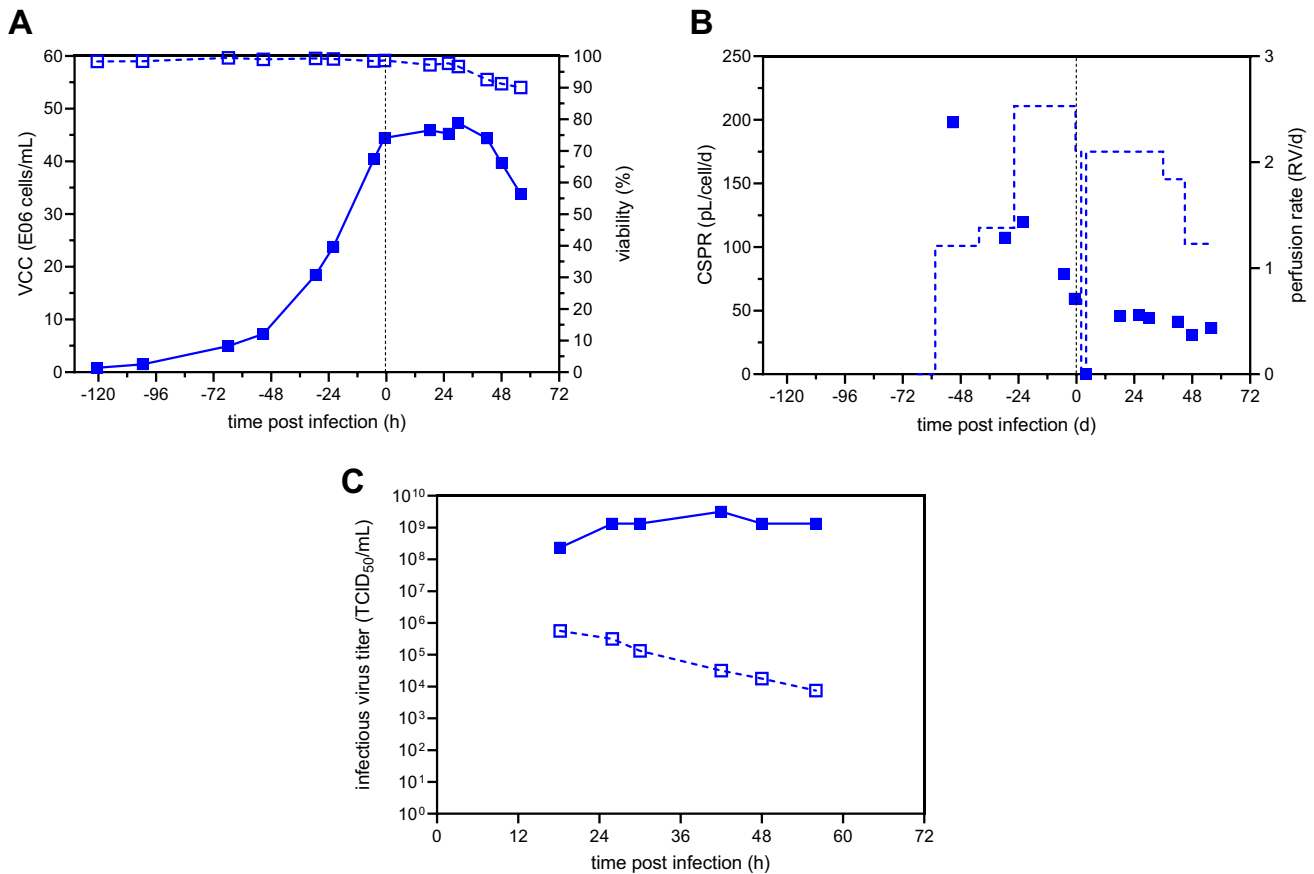


Fig. 2 rVSV-NDV production in BHK-21 cells in perfusion mode using a SB10-X equipped with a 3-L modular adapter and connected to a mATF. BHK-21 cells were inoculated at 0.9×10^6 cells/mL, and perfusion was started 56 h after batch growth phase. The perfusion rate was adjusted manually over time. For cell retention, a 0.65- μm mPES hollow fiber membrane was used. Infection was carried out once a VCC of 44.5×10^6 cells/mL was reached (MOI of $1 \text{E-}4$), tem-

perature was reduced to 34 °C, and perfusion was paused for 4 h. A VCC (full symbols) and viability (hollow symbols). **B** Cell-specific perfusion rate (full symbols) and perfusion rate (dashed lined, weight of collected permeate divided by WV). **C** Infectious virus titer measured inside the bioreactor (full symbols) and the permeate line (hollow symbols)

virus titers in the permeate were significantly reduced compared to the bioreactor (>2 log), corresponding to 97.0% retention. With increasing process time, virus retention further increased to up to 5 log or nearly 100% (Fig. 2C). Surprisingly, the high flow rate through the hollow fiber membrane of 1.5 L/min and the resulting high shear stress of 5490 1/s neither impacted cell growth (Fig. 2A) nor virus replication (Fig. 2C) and did not prevent the formation of large multi-nucleated syncytia (50–75 μm , Figure S4).

rVSV-NDV production using TFDF

In a next step, we carried out two rVSV-NDV production runs in a 3 L STR using TFDF as the cell retention device for perfusion as a proof of concept for continuous virus harvesting with clarification, targeting a VCC at TOI of 14×10^6 cells/mL. For both TFDF runs, BHK-21 cells were inoculated at 0.8×10^6 cells/mL in 1.3 L WV and grown in batch mode until a VCC of 4×10^6 cells/mL was reached. In a next step, after initiation of perfusion, cell broth was recirculated with a constant recirculation rate of 0.9 L/min, corresponding to a shear rate of 1650 1/s. The perfusion rate was either manually adjusted (TFDF1) or controlled based on capacitance (TFDF2), where the signal was correlated to the biovolume. Both control strategies, enabled cells to grow up to 14×10^6 cells/mL with viabilities above 97%, but with a slightly reduced cell-specific growth rate compared to the initial batch phase ($\mu=0.026$ 1/h to $\mu=0.035 \pm 0.005$

1/h). A linear correlation of the permittivity signal with the VCC was obtained during the growth phase for both runs, enabling the monitoring of cell growth throughout the cultivation and the accurate control of the perfusion rate at the pre-defined CSPR of 130 ± 5 pL/cell/day for TFDF2 (Figure S1, Fig. 3B). As the perfusion rate for TFDF1 was adjusted manually in a step-wise manner (Fig. 3B), the CSPR did not stay stable and varied around 168 ± 36 pL/cell/day during cell growth (Fig. 3B). This resulted in a 15% lower total medium consumption for the growth phase for the capacitance-based control compared to the manual adjustment (Table 1). Interestingly, the glucose uptake rate of TFDF2 was 1.9-fold higher compared to TFDF1 (Table 1) resulting in an increase in lactate concentration up to 20 mM compared to 10 mM for TFDF1 (Figure S2B). However, all measured metabolite concentrations were still in the expected range with no notable limitations (Figure S2), and substrate uptake rates of TFDF 1 were comparable to both acoustic settler and ATF cultivations (Table 1, Göbel et al. 2023a, 2023b). For both runs, high cell retention rates of $>99.9\%$ and turbidity reductions $>95\%$ were achieved over the entire cultivation period (Fig. 3C). Transmembrane pressure (TMP) remained low (<0.1 psi) throughout the entire run, only showing a slight increase to 0.3 psi at 60 hpi for TFDF1 (Fig. 3D).

Prior to infection of cells with rVSV-NDV at an MOI of $1E-4$, the medium was completely exchanged using a flow rate of 10 mL/min, and the temperature was reduced to 34 °C. Compared to the mATF perfusion, the permeate flow was

Table 1 Comparison of rVSV-NDV production in BHK-21 cells for different production modes. Cell growth parameters were determined before infection.

	Batch _a	Perfusion AS _a	ATF	Perfusion TFDF	
				TFDF1	TFDF2
Bioreactor vessel	STR (1 L)	STR (1 L)	OSB (3 L)	STR (3 L)	STR (3 L)
Cell-specific growth rate (1/h)	0.033	0.019 ± 0.003	0.031	0.027	0.030
Doubling time (h)	21.0	36.1 ± 6.5	22.1	25.9	23.0
qGlc (10^{-11} \times mmol/(cell/h))	5.1 ± 0.9	6.5 ± 2.1	8.25	8.06	15.2
qGln (10^{-11} \times mmol/(cell/h))	3.0 ± 0.7	3.1 ± 2.0	2.42	2.21	3.21
Max. VCC p.i. (10^6 cells/mL)	3.2 ± 0.3	29.7 ± 2.4	44.5	20.6	16.4
Max. infectious virus titer (10^8 TCID ₅₀ /mL)	5.0 ± 0.9	15.8 ± 11.7	31.6	75.0	56.2
CSVY (TCID ₅₀ /cell)	161 ± 40	118 ± 11	67	365	342
VVP (10^{10} TCID ₅₀ /L/d)	9.4 ± 2.6	3.9 ± 0.6	4.0	8.8	11.5
STY (10^{10} TCID ₅₀ /d)	13.4 ± 3.7	29.0 ± 5.2	43.0	75.5	95.4
Used medium (L)	0.7	6.9 ± 1.9	25.1	11.0	9.3
dsDNA level at optimal harvest time point ($\mu\text{g/mL}$)	n.d.	14.0 ± 0.5	n.d.	7.5	13.9
Protein level at optimal harvest time point (mg/ml)	n.d.	0.5	n.d.	2.0	2.5

qGlc, cell-specific glucose consumption rate; qGln, cell-specific glutamine consumption rate; max., maximum; VCC, viable cell concentration; p.i., post infection; n.d., not determined. Optimal harvest time point was defined as time point when the maximum infectious virus titer was reached in the supernatant. a: Values taken from Göbel et al. 2023a, 2023b carried out as biological replicates with $n=2$

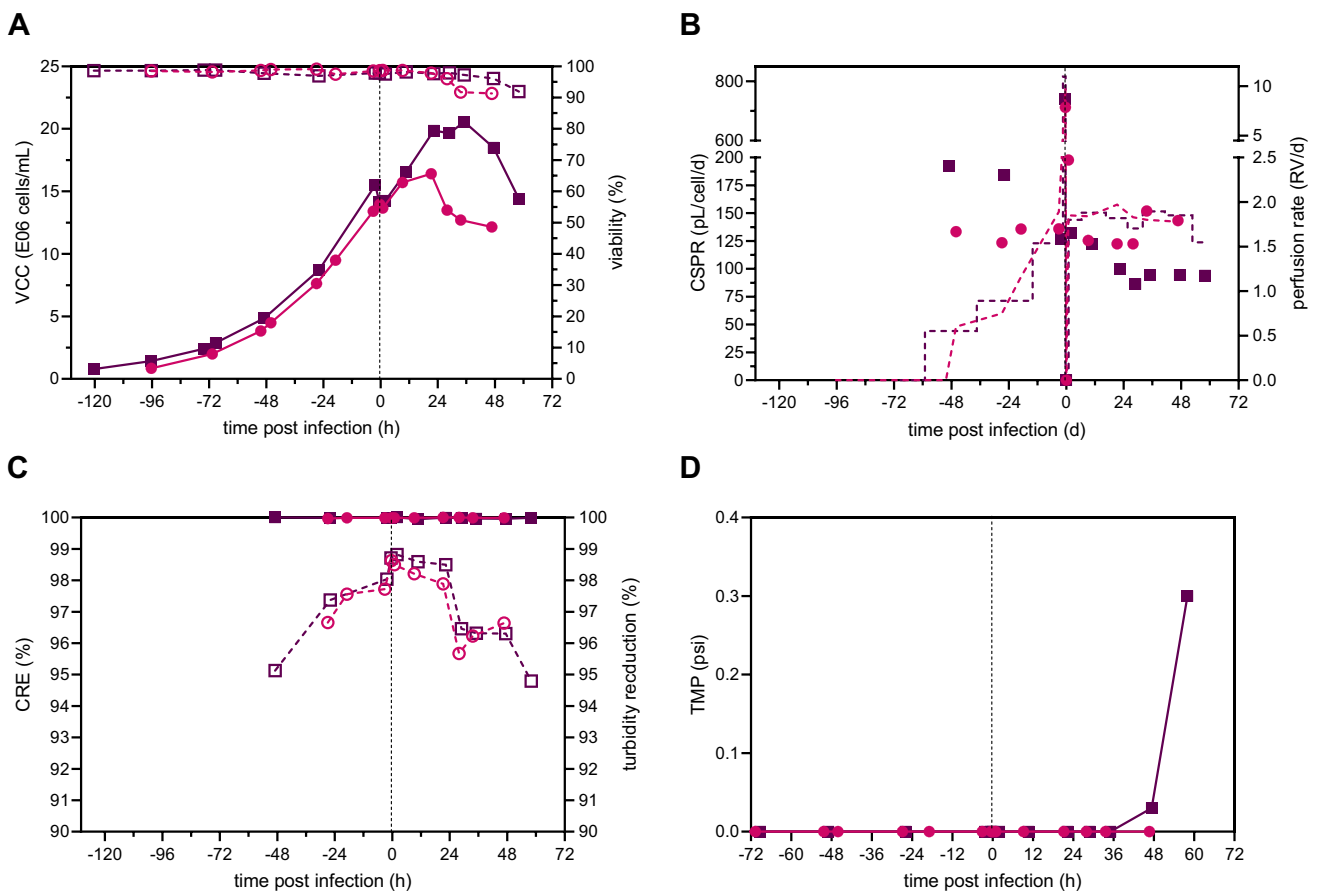


Fig. 3 Critical process parameters of rVSV-NDV production in BHK-21 cells in perfusion mode using a 3-L STR coupled to a TFDF system. BHK-21 cells were inoculated at 0.8×10^6 cells/mL, and perfusion was started 46–51 h after batch growth phase by utilizing a TFDF cartridge (pore size 2–5 μm). The first TFDF run (TFDF1, purple squares) was adjusted manually, while the second TFDF run (TFDF2, pink circles) was controlled based on the biovolume measured by a capacitance probe. Infection was carried out once a VCC

of 14×10^6 cells/mL was reached (MOI of $1\text{E-}4$), temperature was reduced to 34 °C, and perfusion was paused for 1–2 h. **A** Viable cell concentration (full) and viability (empty). **B** Cell-specific perfusion rate (full) and perfusion rate (dashed lined, weight of collected permeate divided by WV). **C** Cell retention efficiency (full) and turbidity reduction (empty) of TFDF membrane during growth and infection. **D** Transmembrane pressure (TMP) during cell growth and infection phase. The dashed line indicates the time of infection

only paused for 1–2 h (compared to 4 h) before setting the perfusion rate to a constant rate of 1.8 RV/day, as no loss of infectious virus particles into the permeate was observed. For both runs, cells continued to grow for 24–36 hpi up to a VCC of 20.5×10^6 cells/mL and 16.4×10^6 cells/mL displaying high viabilities above 96%. By sampling the bioreactor and permeate line, virus retention by the TFDF membrane can be assessed. For both runs, maximum titers of 7.5×10^9 TCID₅₀/mL and 5.6×10^9 TCID₅₀/mL were reached in the permeate at 29–34 hpi, respectively (Fig. 4A). Overall, infectious titers were very similar between the bioreactor and permeate line, indicating that rVSV-NDV was not retained by the TFDF membrane. On average, the percentage of infectious virus passing through the membrane was calculated as 124% and 118% for TFDF1 and TFDF2, respectively. Determination of the actual recovery was made by integration of the permeate line samples over the collected volume, considering the

changing concentrations within the permeate line and collected volume (Figure S3). Here, the area under the curve represents the maximum available amount of infectious virus particles that can be recovered. Maximum theoretical values were compared to the sum of the actual empirical values for the collected fractions (“Accumulated” Fig. 4B). For both runs, recoveries of 78% were obtained, most likely due to the partial loss of functionality while storing at RT. As expected due to the large pore sizes, impurity concentrations were very similar between the bioreactor and permeate line (Fig. 4C and E) and gradually increased during the infection, reaching maximum values at the time of final harvest, when viabilities were reaching 90% (Fig. 4D and F).

Interestingly, monitoring the bioreactor samples by bright field microscopy showed limited syncytia formation, reaching sizes of 25–38 μm in diameter, for 29 hpi onwards for TFDF1. In contrast, more pronounced syncytia formation

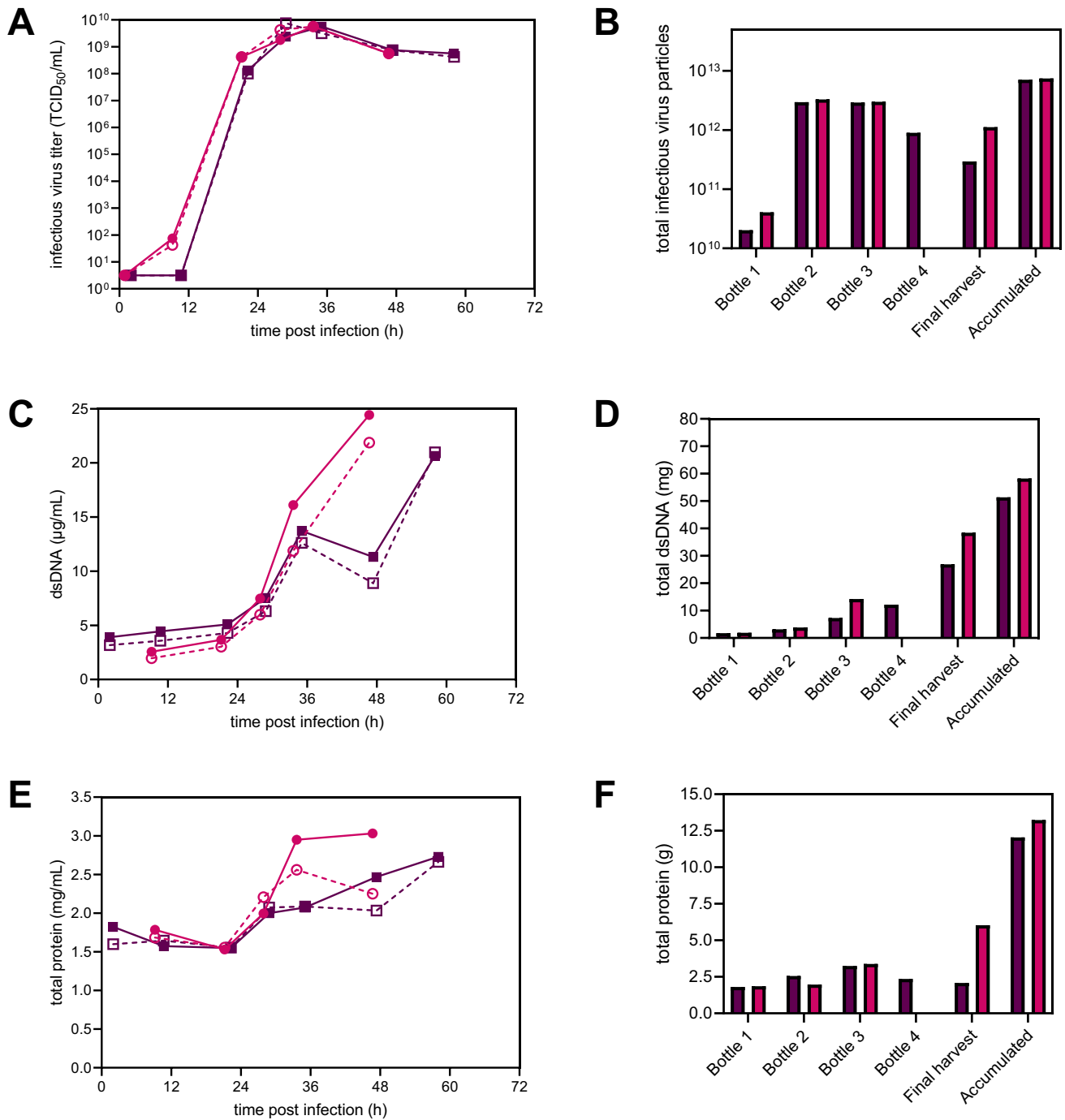


Fig. 4 rVSV-NDV production in BHK-21 cells in perfusion mode for TFDF1 (purple squares) and TFDF2 (pink circles). Time course of **A** infectious virus titer (TCID₅₀/mL), **C** double-stranded DNA (μg/mL), and **E** total protein (mg/mL) measured both in the reactor (full symbols) and permeate line (empty symbols). The TFDF membrane allowed a continuous harvesting of rVSV-NDV via the permeate. **B, D, F** The permeate was collected in multiple fractions (“Harvest

bottle 1-4”), which were exchanged every 12–24 h to prevent loss of virus infectivity. Bottle 1 refers to permeate collected from 0 to 24 hpi, Bottle 2 24–36 hpi, Bottle 3 36–48 hpi, and bottle 4 48–60 hpi. “Final harvest” refers to material recovered in the final harvest step (concentration 1, diafiltration; final concentration, 2). “Accumulated” refers to the accumulated yields from all bottles and the final harvest

was found for TFDF2, where scattered clusters of fused cells appeared between 18 and 33 hpi, reaching sizes of 50–100 μm in diameter (Figure S4). For the final one-step

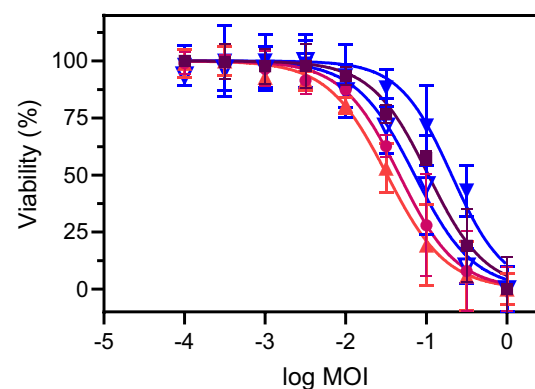
harvest, a modified C1-DF-C2 process was utilized using the same TFDF membrane as for cell growth and infection. For TFDF1, filter fouling was observed for the harvest at 60

hpi, using sterile PBS for diafiltration, and the membrane was completely blocked during the second concentration step after removal of 1100 mL (Figure S5). By carrying out the harvest 12 h earlier at 48 hpi, further increasing the recirculation rate to promote self-cleaning of the membrane while simultaneously reducing the permeate flow, and using medium for diafiltration, filter fouling was prevented, and the TMP was kept below 2 psi for the majority of the harvest for TFDF2 (Figure S5).

Finally, the TFDF production was compared with the ATF perfusion run using the mATF and a previously described optimized batch process and perfusion process using an acoustic settler (AS) as the cell retention device (Table 1). All perfusion systems achieved a higher infectious virus concentration compared to an optimized batch process infected at 2×10^6 cells/mL, with both TFDF runs being more than ten times higher compared to batch and more than 3.5 times higher compared to AS (Table 1). CSVY's of 342–365 TCID₅₀/cell were obtained in TFDF cultures, corresponding to a >twofold improvement compared to ATF and previous batch and AS cultivations. As both ATF and AS perfusion systems were infected at higher VCC's, this might indicate the presence of a cell density effect. In terms of VVP, TFDF cultures were comparable to batch cultivations; however, all perfusion systems had an increased STYs, with TFDF cultures showing an increase of >460% compared to batch cultivations.

In a final step, we evaluated whether sporadic formation of syncytia in TFDF mode (Figure S4) had an impact on the oncolytic properties in target Huh7 cells. Crude samples for both TFDF runs were compared to previously produced STR samples using optimized batch processes and AS perfusions. As expected, all samples displayed a similar oncolytic potential in Huh7 cells (Fig. 5). Regardless of the production mode or production system, the produced virus still maintained the ability to induce adequate oncolysis.

Fig. 5 Comparison of oncolytic viral potency values for rVSV-NDV using different production modes and processes. Viabilities of Huh7 cancer cells were determined 48 hpi for crude rVSV-NDV samples generated in batch mode (red triangle), acoustic settler perfusions (AS1, blue full triangle; AS2, hollow blue triangle), and TFDF perfusions (TFDF1, purple square; TFDF2, pink circle). Following non-linear regression analysis, IC₅₀ and log IC₅₀ values were determined from dose-response curves. All values are reported as the mean of technical triplicates with *n*=3



	Batch	AS1	AS2	TFDF1	TFDF2
Log IC ₅₀	-1.49	-0.69	-1.15	-0.98	-1.33
IC ₅₀	0.03	0.21	0.07	0.11	0.05

Production of rVSV-GFP in batch mode

Initially, a high-yield production process for rVSV-GFP in batch mode in shake flasks (SF) was developed (Fig. 6). Next, the process was transferred to two STRs of different sizes (STR 1, 700 mL WV; STR 2, 2100 mL WV). For this, HEK293-SF cells were inoculated at about 0.3×10^6 cells/mL and grown to 1.3×10^6 cells/mL (STR 1 and 2) or 1.1×10^6 cells/mL (SF) with viabilities above 95% (Fig. 6A). For the three cultivations, very similar cell growth and viability patterns were observed. Cell-specific growth rates ranged between 0.026 and 0.034 1/h (Table 2). As optimized in two recent studies for rVSV-based constructs, cells were infected at an MOI of 1E-3 after a temperature reduction to 34 °C. (Elahi et al. 2019; Gélinas et al. 2019). Maximum VCCs of 1.9×10^6 cells/mL were reached at 11 hpi for SF and STR 1 cultures, before virus-induced cell death occurred (Fig. 6A, for STR 2 data are not available). Virus production dynamics were very comparable between the three productions (Fig. 6B). Slightly higher maximum infectious virus titers were achieved for production in SF (8.8×10^{10} TCID₅₀/mL, 24 hpi) relative to STR 1 (3.2×10^{10} TCID₅₀/mL, 33 hpi) and STR 2 (5.3×10^{10} TCID₅₀/mL, 31 hpi). Thus, higher CSVY and STY/VVP were obtained for SF production (Table 2). Both STR runs showed high infectious virus titers for more than 36 h indicating a high stability of the virus.

Production of rVSV-GFP in perfusion mode using a TFDF system

To further support our proof-of-concept study of a TFDF system, we evaluated the production process for rVSV-GFP cultivating HEK293-SF cells in perfusion mode to reach higher VCC and infectious virus titers (Fig. 7). For this, as for the TFDF runs for rVSV-NDV, a 30-cm² TFDF cartridge

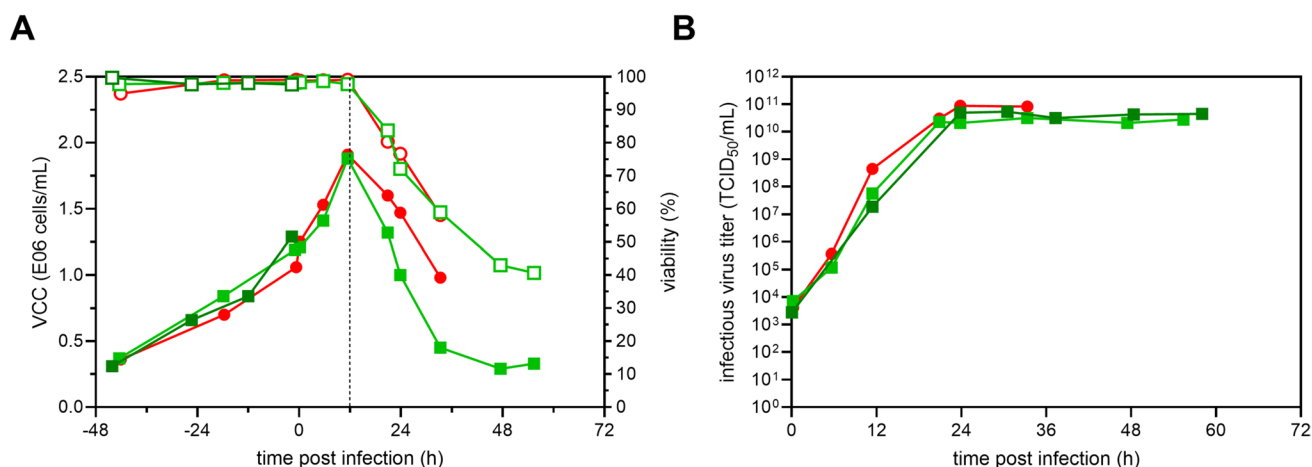


Fig. 6 rVSV-GFP production in HEK293-SF cells in batch mode. Three batch production runs were conducted using one shake flask (SF 1, 50 mL WV, red circles), one 1 L STR (STR 1, 700 mL WV, light green squares), and one 3 L STR (STR 2, 2100 mL, dark green squares). Cells were inoculated at $0.3\text{--}0.4 \times 10^6$ cells/mL and culti-

ated to $1.1\text{--}1.3 \times 10^6$ cells/mL. Prior to infection, temperature was lowered from 37 to 34 °C. Cells were infected at an MOI of 1E-3. **A** VCC (full symbols) and viability (hollow symbols). **B** Infectious virus titer (TCID₅₀/mL)

Table 2 Comparison of rVSV-GFP production in HEK293-SF cells for different production modes. Cell growth parameters were determined before infection.

	Batch			Perfusion
	STR 1 (1 L)	STR 2 (3 L)	SF	TFDF STR (3 L)
Cell-specific growth rate (1/h)	0.028	0.034	0.026	0.022
Doubling time (h)	24.6	20.7	26.6	31.0
Max. VCC p.i. (10^6 cells/mL)	1.9	n.d.	1.9	11.3
Max. infectious virus titer (10^{10} TCID ₅₀ /mL)	3.2	5.3	8.8	7.1
CSVY (TCID ₅₀ /cell)	16,865	n.d.	45,948	10,338
STY (10^{13} TCID ₅₀ /L/d)	1.0	1.7	2.8	1.9
VVP (10^{13} TCID ₅₀ /L/d)	1.0	1.7	2.8	0.2
Used medium (L)	0.67	2.10	4.60	13.93

max., maximum; *VCC*, viable cell concentration; *p.i.*, post infection; *n.d.*, not determined. Optimal harvest time point was defined as time point when the maximum infectious virus titer was reached in the supernatant. For the perfusion run, the calculations were based on infectious virus particles of the collected permeate in the harvest (stored at 4 °C) and final harvest

(pore size 2–5 μm), connected to a Krosflo TFDF system (Repligen), was coupled to the 3 L STR. Recirculation was already started before cell inoculation with a recirculation rate of 1.0 L/min corresponding to a shear rate of 1830 1/s. HEK293-SF cells were inoculated at 0.8×10^6 cells/mL into the 3 L STR (2100 mL WV) (Fig. 7A). After a batch growth phase for 24 h, perfusion mode was started (Fig. 7B). Cells grew at a slightly lower cell-specific growth rate of 0.022 1/h relative to the batch cultivation in STR 2 (0.028 to 0.034 1/h) (Table 2) during the total cell growth phase, while viabilities remained above 95% (Fig. 7A). The perfusion rate was manually adjusted based on a CSPR of 115 pL/cell/day (Fig. 7B). Due to an initial permeate flow rate of 0.9 mL/min (0.6 RV/day) (Fig. 7B), the actual CSPR was higher at the beginning of the cultivation. Before infection, one RV with

fresh medium was exchanged (10–33 mL/min) (Fig. 7B), and temperature was lowered from 37 to 34 °C. Cells were infected at 10.3×10^6 cells/mL at an MOI of 1E-3. After infection, perfusion was stopped for 1 h and, subsequently, the perfusion rate was kept constant at 1.4 RV/day (Fig. 7B). During the perfusion cultivation, no glucose or glutamine limitation was observed (Figure S6). Moreover, no toxic maximum levels of lactate (22.4 mM) or ammonium (1.4 mM) were found. After infection, cells continued to grow slightly until 11.3×10^6 cells/mL (12 hpi) with viabilities above 94% (Fig. 7A). Throughout the whole cultivation, the cell retention efficiency of the membrane was maintained above 99.6% (Fig. 7C). A maximum infectious virus titer of 7.1×10^{10} TCID₅₀/mL at 18 hpi was detected in the permeate line relative to 10.4×10^{10} TCID₅₀/mL at 24 hpi in the

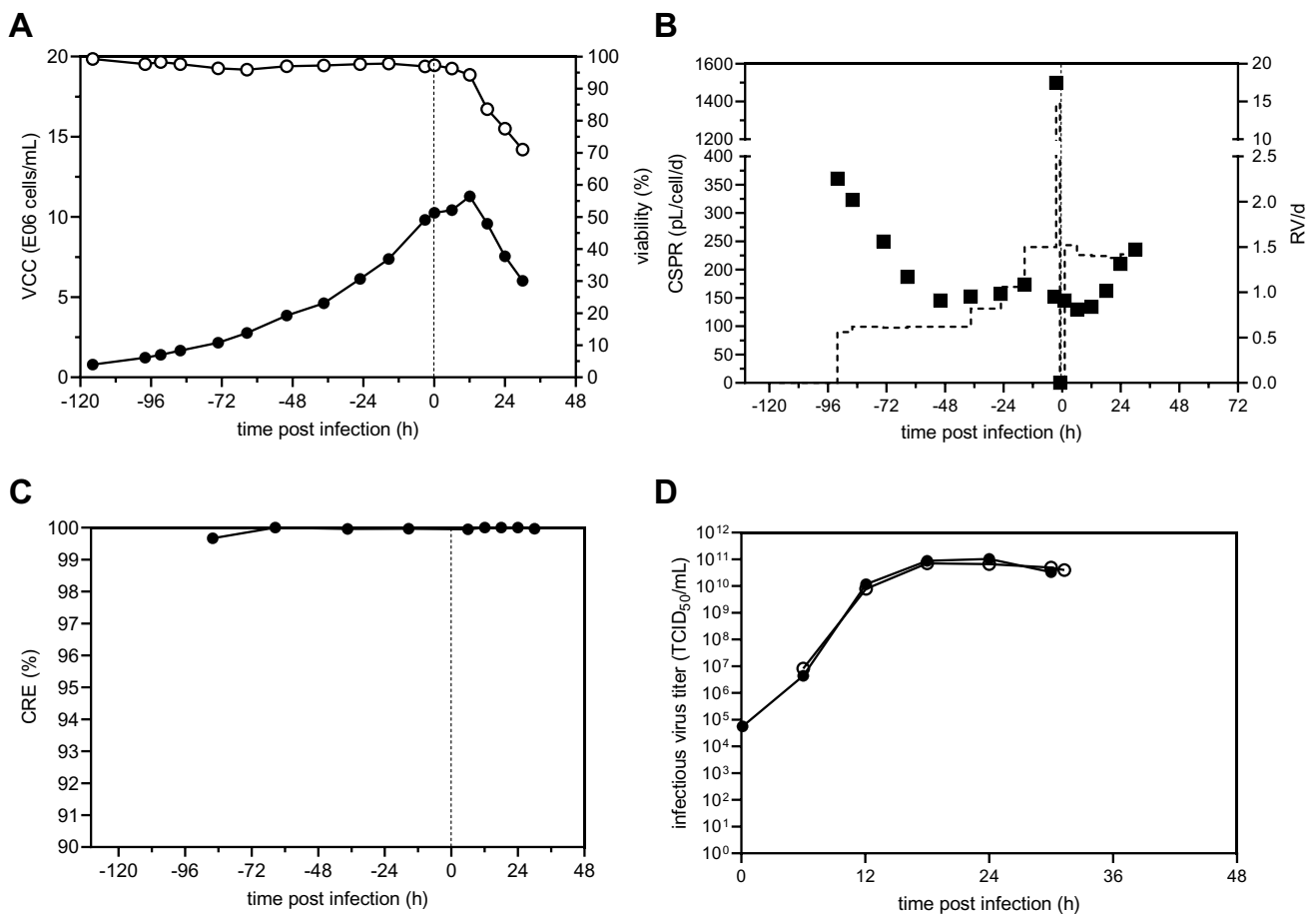


Fig. 7 rVSV-GFP production in HEK293-SF cells in perfusion mode using a 3-L STR coupled to a TFDF system. Recirculation was started prior to inoculation. HEK293-SF cells were inoculated at 0.8×10^6 cells/mL, and perfusion was started after 24 h of batch growth by utilizing a TFDF cartridge (pore size 2–5 μm). The perfusion rate was adjusted manually over time. Prior to infection, temperature was reduced to 34 °C. Cells (10×10^6 cells/mL) were infected at an MOI of 1E-3, and perfusion was paused for 1 h. **A** Viable cell con-

centration (full) and viability (empty). **B** Cell-specific perfusion rate (full) and perfusion rate (dashed lined, weight of collected permeate divided by WV). **C** Cell retention efficiency (full) of TFDF membrane during growth and infection. **D** Infectious virus titer (TCID₅₀/mL) in the reactor (full symbols) and permeate line (empty symbols) are plotted against the time post infection (h). Last time point shown for the permeate line (31 hpi) refers to the final harvest step

bioreactor vessel. Very similar infectious virus titers were observed by comparing the bioreactor vessel and permeate line during the virus production phase (Fig. 7D). On average, the percentage of infectious virus passing through the TFDF membrane was calculated to be 112%. In addition, the infectious virus titer of the final harvest step (4.0×10^{10} TCID₅₀/mL) starting at 31 hpi using the same TFDF membrane was similar to the last permeate sample time point of the production phase (4.9×10^{10} TCID₅₀/mL, 30 hpi), confirming that all infectious virus particles passed through the membrane even in the final harvest step with a significantly higher permeate flow rate that could cause membrane clogging. Comparing the theoretical maximum values of the amount of infectious virus particles in the permeate line (Figure S7) with the empirical values of the virus in the harvest bulk (collected permeate stored at 4 °C and final harvest, sampled

individually) resulted in a recovery of 103.5%, indicating no loss of virus infectivity during storage in the virus production phase. Next, we compared important production coefficients of the batch and perfusion run (Table 2). The perfusion process showed increased STY (1.9-fold (STR 1) and 1.1-fold (STR 2)); however, VVP and CSVY were lower.

Discussion

The first vaccine based on rVSV, the Ebola virus vaccine Ervebo[®], has been approved in 2019 (EMA 2019; FDA 2019). Moreover, multiple rVSV-based constructs for vaccine and oncolytic applications are currently undergoing clinical trials. Therefore, the development of a high-yield production platform is essential to meet clinical trial and

market demand regardless of the intended use. Compared to traditional vector platforms, induction of syncytia by rVSV-NDV introduces additional challenges to manufacturing processes. In this proof-of-concept study, we evaluated the versatility of the TFDF system for intensified high-cell density production for two different rVSV-based constructs (rVSV-NDV and rVSV-GFP) to allow continuous virus harvest and clarification.

rVSV-NDV production using mATF

Product retention of hollow-fiber membranes is a well-known challenge of ATF-based cell culture productions, preventing continuous harvest of, e.g., viral particles (Genzel et al. 2014; Hadpe et al. 2017; Nikolay et al. 2020; Nikolay et al. 2018; Tona et al. 2023; Vázquez-Ramírez et al. 2019). To evaluate the applicability of hollow-fiber membranes for the production of fusogenic oncolytic viruses forming large multi-nucleated syncytia, a commercially available 0.65- μm mPES membrane with a lumen size bigger than previously observed syncytia (120–140 μm) was selected, connected to a mATF, and characterized for virus retention. Impact of the membrane material on product retention is still not fully elaborated. While some studies found a more pronounced retention rate of antibodies using polysulfone (PS) membranes compared to polyethersulfone (PES) and mPES due to the higher negative charge densities (Su et al. 2021), others reported more favorable physiochemical and structural properties (open pore structure, high porosity) of PS membranes enabling virus harvest of yellow fever virus particles (~50 nm) even at low cut-offs of 0.34 μm (Nikolay et al. 2020). Beside membrane material, pore size plays a critical role regarding product retention. Surprisingly, membranes with higher cut-offs, e.g., 0.65 μm often display higher product retention rates compared to lower cut-offs, e.g., 0.2 μm (Nikolay et al. 2020; Su et al. 2021; Vázquez-Ramírez et al. 2019). More pronounced heterogeneous pore distributions for larger cut-offs can increase the susceptibility of fouling as variation in filtrate flux along the membrane makes larger pores prone to deposition of particles and concentration polarization (Nikolay et al. 2020). Moreover small-size cell debris (0.2–0.5 μm), caused by virus induced cell lysis, can enter larger pores causing membrane clogging and product retention, but can be rejected by smaller pores (Su et al. 2021). Usage of a 0.2- μm PES hollow fiber membrane for a rVSV-NDV ATF production using HEK293 cells resulted in a complete membrane blocking at 18 hpi, after first syncytia formation was observed (data not shown). Therefore, the choice of membrane was primarily based on internal fiber lumen rather than pore size or material. A higher flow rate inside the hollow fibers (1.5 L/min) was chosen compared to the initial ATF run using a 0.2- μm PES membrane (0.8 L/min) to increase the backflush over the membrane

and prevent or hamper the formation of syncytia due to increased shear stress. Surprisingly, the resulting shear rate of 5490 1/s neither impacted cell growth, as high VCCs of 44.5×10^6 cells/mL with high cell-specific growth rates of 0.031 1/h (Table 1) were reached, nor did it prevent the formation of syncytia (Figure S4). However, formed syncytia were smaller (up to 75- μm diameter) as previously observed with an acoustic settler (up to 140 μm (Göbel et al. 2023a)), allowing entrance into the larger fibers, which likely prevented complete blockage. Nevertheless, combination of high hollow fiber flow rates with low permeate flux rates of 1.91 L/h/m² did not prevent rVSV-NDV retention by the membrane. Already at 18 hpi, 97% of all infectious virus was retained, further underlining the challenge of using hollow fiber membranes for continuous harvest of viral particles.

rVSV-NDV production using TFDF

As a proof-of-concept, we set out to utilize the TFDF system as a cell retention device for perfusion and subsequent continuous harvest filtration. Performance was characterized by cell growth, TMP, and quantification of bioreactor and permeate turbidities, as well as virus permeability. The use of the TFDF system allowed BHK-21 cells to achieve high VCCs, with similar growth behavior compared to the mATF system despite the drastically lower shear stress there. Due to the lower CSVY obtained at very high VCCs in the previous experiment, the targeted cell concentration for infection was lowered drastically. The metabolic uptake rates for all perfusion cultures were slightly increased compared to those previously reported for batch cultivations ((Göbel et al. 2023a), Table 1). Increased shear stress, particularly in ATF and TFF systems, has been identified as one cause of increased substrate uptake rates (Zhan et al. 2020). Control of the perfusion rate via a capacitance probe did not improve overall process performance, but robustly maintained stable CSPR values over the entire growth phase (Fig. 3), reducing medium consumption by 15%. Compared to the manual perfusion control for TFDF1, where CSPR values were higher due to partial overfeeding, glucose levels were not stably maintained and fell below 5 mM prior to infection (Figure S2). The slightly increased growth rate of TFDF2 most likely resulted in an increased uptake of glucose and thus increased lactate formation. To support even higher VCCs, the set point of the CSPR should be increased for future capacitance-controlled runs.

The combination of DF with tangential cross filtration provides several benefits such as shearing of the membrane surface, minimizing deposition of particles within the filter, while simultaneously allowing some particles to be captured within channels of the DF without blocking the liquid flow through that same channel (Williams et al. 2020). Low TMP values (below 0.3 psi) for both TFDF runs, even after virus

infection, high cell retention efficiencies (>99%), and a low turbidity in the permeate (>95% reduction) indicated minimal particle breakthrough. Previous studies already demonstrated the applicability of the TFDF system for continuous harvest of AAV and LV (Mendes et al. 2022; Tona et al. 2023; Tran and Kamen 2022). As expected, we also achieved equal concentrations of infectious virus in both the bioreactor and permeate sample, taken at the same time. Calculated percentages of infectious virus passing through the membrane above 100% for both runs are not possible and were only achieved as the measured titer in the permeate sample was higher than the bioreactor sample. While comparison to theoretical yields only resulted in a total recovery of 78%, this is most likely due to partial losses of functionality while storing the harvest bulks at RT, as well as the quite large error of the TCID₅₀ assay itself (± 0.3 log (Göbel et al. 2022b)). Stabilizing effects of sucrose on proteins and enveloped viral vectors are well known (Croyle et al. 2001; Cruz et al. 2006; Evans et al. 2004); however, it acts mainly as a cryoprotectant or is only a small part of a complex storage formulation. Therefore, premature addition of sucrose was probably not sufficient to prevent degradation, and direct cooling of the harvest bulk at 4 °C should be preferred.

In terms of virus production, our intensified TFDF processes achieved the highest reported infectious virus titers of $5.6\text{--}7.5 \times 10^9$ TCID₅₀/mL in the permeate so far. Compared to optimized batch processes, VCCs were increased by five- to six-fold, but infectious virus titers were even more than 11-fold higher. Moreover, CSVYs were improved by twofold, STY by 460% (5.6-fold), and similar VVPs were reached. Lastly, the TFDF runs were compared to other perfusion cultivations using the same cell line but different cell retention devices. Compared to AS and ATF perfusions, maximum titers reached in TFDF systems were >threefold and >1.5-fold higher. This was also reflected in terms of VVP and STY, which were always more than twofold higher for TFDF runs. Surprisingly, CSVYs strongly decreased with increasing VCCs for the respective systems. For the ATF cultivation, where the highest VCC of 44.5×10^6 cells/mL was reached, the lowest CSVY was obtained, clearly indicating the presence of a “high cell density effect” (Bock et al. 2011; Nadeau and Kamen 2003). One major reason for this effect is typically the scarcity in nutrients or the accumulation of inhibitory ammonium and glucose. One study showed that ammonium and lactate concentrations at 2–3 mM and above 20–30 mM, respectively, can have negative effects on virus productivity and cell growth (Schneider et al. 1996). However, neither a nutrient limitation nor an accumulation of lactate and ammonium to excessively high concentrations was observed for any run ((Göbel et al. 2023a), Figure S2, data not shown for ATF). This suggests that other reasons, including the limitation or accumulation

of non-monitored metabolites or unknown cellular factors may play a role and are subject to further investigation. Another reason could be the formation of syncytia, which was observed to occur to differential extents, depending on the system used (Figure S4). Virus replication is possibly more efficient if the cells do not fuse, as we have observed the production of higher titers in oncolytic applications when a non-fusogenic VSV is used, despite similar levels of oncolysis (Abdullahi et al. 2018); however, whether or not this is also true in suspension culture systems which is not entirely clear and would warrant further investigation. Regardless, the direct comparison of the three perfusion systems should be considered very carefully, as various production parameters were different. For a fair comparison, re-evaluation should include the same bioreactor set-up and similar infection cell concentrations. For our proof-of-concept study this was, however, out of scope.

Fusogenic oncolytic viruses and the formation of syncytia introduce novel challenges for process controls and scale-up of manufacturing processes. We hypothesize that fusion of cells is dependent on three factors: high VCC, low shear stress, and long cell-to-cell contact time. Combination of all three factors most likely facilitates the formation of large multi-nucleated syncytia. Production in batch mode is associated with low VCC (up to 3.2×10^6 cells/mL), low shear stress, and short cell-to-cell contact times and does not lead to the formation of syncytia. Productions using ATF or TFDF systems allow for high VCCs (up to 44.5×10^6 cells/mL); however, shear rates are drastically increased (up to 5490 1/s), and cell-to-cell contact times are short, leading to the formation of small sized syncytia. Retention systems such as AS, combine high VCCs (up to 29.7×10^6 cells/mL), low shear rates (~340 1/s (Gränicher et al. 2020)), and long cell-to-cell contact times within the acoustic field and recirculation loop (3–12 min (Gränicher et al. 2020)), facilitating the formation of large multi-nucleated syncytia. Increased cell-to-cell contact by induction of aggregation by CaCl₂ supplementation at low VCC in batch mode did not result in the formation of syncytia, highlighting the complex interplay of all three factors (Göbel et al. 2022a). Future studies investigating the actual cause of syncytia formation in suspension cultures could be considered to better control their formation. However, whether or not syncytia are formed in suspension cultures during production is independent of the inherent fusogenicity of the virus, as the fusion proteins are encoded within its genome and need to be expressed in order to carry out an infection (Abdullahi et al. 2018). Nonetheless, a potency assay was carried out to assess potential effects of mode of production, as well as formation or non-formation of syncytia during production, on the ability of the virus to induce oncolysis. As expected, oncolytic potency was not affected by production mode or occurrence of syncytia (Fig. 5).

rVSV-GFP production in batch and perfusion mode

To take our proof-of-concept study one step further, we also wanted to evaluate the TFDF performance for a high-yield virus production process for rVSV-based vectors for a possible application as vaccine using the model vector rVSV-GFP. Process intensification using perfusion mode and the TFDF module led to a sixfold higher VCC of 11.3×10^6 cells/mL with an up to 1.9-fold higher STY compared to the STR 1 process in batch mode, allowing for a smaller footprint of the bioreactor. However, a more than 3.3-fold lower VVP and 1.6-fold reduced CSVY were observed compared to the STR batch process. As described before, this decline is most likely due to the “high cell density effect.” As neither limitation of monitored nutrients, nor accumulation of inhibitory byproducts was observed, it is clear that there is certainly room for optimization for this perfusion process, hopefully targeting even higher VCCs. For now, this perfusion run was a proof-of-concept run only to evaluate the TFDF system. Testing different feeding schemes (Vázquez-Ramírez et al. 2019), media compositions (Göbel et al. 2023a), or additives could be envisaged as next steps.

Using the TFDF module, we were able to directly harvest rVSV-GFP particles with a simultaneous clarification by depth filtration with a full recovery. Our proof-of-concept study together with the data on LV (Tona et al. 2023; Tran and Kamen 2022) and AAV (Mendes et al. 2022) seems to indicate that TFDF for continuous virus harvest in perfusion will play a big role in next generation processes and might be applicable for other viruses as well. Moreover, all HEK293-SF cells were retained inside the bioreactor enabling full production capacity. Perfusion cultivation with the TFDF module showed a slightly lower cell-specific growth rate (0.022 1/h) relative to the batch production (0.034 to 0.028 1/h), indicating that there is also room for improvement here and a need for further optimization. As previously discussed, cooling the harvest bulk to 4 °C increases virus stability. Indeed, we found a recovery of 103.5% in the final harvest bulk.

Overall, the TFDF module showed very good performance as a perfusion system for our tested rVSV-based vectors and cell lines. In addition, the continuous virus harvest, together with the clarification through the TFDF module in one step can simplify process operations and help to develop an integrated, scalable (up to 2000 L), and economical process for the future.

Supplementary Information The online version contains supplementary material available at <https://doi.org/10.1007/s00253-024-13078-6>.

Acknowledgements The authors would like to thank Gene Therapy Repligen for providing a KrosFlo TFDF lab unit as well as the custom TFDF membranes as part of the collaborative effort. Special thanks to Rachel Legmann (Gene Therapy Repligen) and Barbara Paes (Kamen

lab) for their active technical support and participation in fruitful discussions. We also want to thank Kühner AG, in particular, Tibor Anderlei and Tim Bürgin, for providing the 3-L modular adapter as well as the 3-L single-use bags. The excellent technical support of Ilona Behrendt is equally acknowledged.

Author contribution Conceptualization: S.G., L.P., U.R., and Y.G. Methodology: S.G., L.P., C.A.S.T, and Y.G. Investigation: S.G., L.P, C.A.S.T, and J.A. Writing—original draft: S.G. and L.P. Writing—review and editing: S.G., L.P., C.A.S.T, J.A., A.K., U.R., and Y.G. Supervision: A.K., U.R., and Y.G. Project administration: S.G., L.P., and Y.G.

Funding Open Access funding enabled and organized by Projekt DEAL.

Data availability Data available in article supplementary material. Additional data is available on request from the authors. The data that support the findings of this study are available from the corresponding author, Yvonne Genzel, upon reasonable request.

Declarations

Ethics approval This article does not contain any studies with human participants or animals performed by any of the authors.

Consent to participate Not applicable.

Consent for publication Not applicable.

Conflict of interest J. Altomonte (WO 2017/198779) holds a patent for the development and use of rVSV-NDV as an oncolytic therapy of cancer and is co-founder of Fusix Biotech GmbH, which is developing the rVSV-NDV technology for clinical use. B. Brühlmann and C.Hill are employees of Repligen where the Krosflo TFDF system has been developed.

Open Access This article is licensed under a Creative Commons Attribution 4.0 International License, which permits use, sharing, adaptation, distribution and reproduction in any medium or format, as long as you give appropriate credit to the original author(s) and the source, provide a link to the Creative Commons licence, and indicate if changes were made. The images or other third party material in this article are included in the article's Creative Commons licence, unless indicated otherwise in a credit line to the material. If material is not included in the article's Creative Commons licence and your intended use is not permitted by statutory regulation or exceeds the permitted use, you will need to obtain permission directly from the copyright holder. To view a copy of this licence, visit <http://creativecommons.org/licenses/by/4.0/>.

References

- Abdullahi S, Jäkel M, Behrend SJ, Steiger K, Topping G, Krabbe T, Colombo A, Sandig V, Schiergens TS, Thasler WE, Werner J, Lichtenthaler SF, Schmid RM, Ebert O, Altomonte J (2018) A novel chimeric oncolytic virus vector for improved safety and efficacy as a platform for the treatment of hepatocellular carcinoma. *J Virol* 92(23). <https://doi.org/10.1128/jvi.01386-18>
- Aunins JG (2003) Viral vaccine production in cell culture. In: Spier RE (ed) *Encyclopedia of cell technology*. <https://doi.org/10.1002/0471250570.spi105>

- Bock A, Schulze-Horsel J, Schwarzer J, Rapp E, Genzel Y, Reichl U (2011) High-density microcarrier cell cultures for influenza virus production. *Biotechnol Progr* 27(1):241–250. <https://doi.org/10.1002/btpr.539>
- Brown KS, Safronetz D, Marzi A, Ebihara H, Feldmann H (2011) Vesicular stomatitis virus-based vaccine protects hamsters against lethal challenge with Andes virus. *J Virol* 85(23):12781–12791. <https://doi.org/10.1128/jvi.00794-11>
- Cobleigh MA, Buonocore L, Uprichard SL, Rose JK, Robek MD (2010) A vesicular stomatitis virus-based hepatitis B virus vaccine vector provides protection against challenge in a single dose. *J Virol* 84(15):7513–7522. <https://doi.org/10.1128/jvi.00200-10>
- Coronel J, Behrendt I, Bürgin T, Anderlei T, Sandig V, Reichl U, Genzel Y (2019) Influenza A virus production in a single-use orbital shaken bioreactor with ATF or TFF perfusion systems. *Vaccine* 37(47):7011–7018. <https://doi.org/10.1016/j.vaccine.2019.06.005>
- Coronel J, Gränicher G, Sandig V, Noll T, Genzel Y, Reichl U (2020) Application of an inclined settler for cell culture-based influenza A virus production in perfusion mode. *Front Bioeng Biotechnol* 8:672–672. <https://doi.org/10.3389/fbioe.2020.00672>
- Croyle MA, Cheng X, Wilson JM (2001) Development of formulations that enhance physical stability of viral vectors for gene therapy. *Gene Ther* 8(17):1281–1290. <https://doi.org/10.1038/sj.gt.3301527>
- Cruz PE, Silva AC, Roldão A, Carmo M, Carrondo MJ, Alves PM (2006) Screening of novel excipients for improving the stability of retroviral and adenoviral vectors. *Biotechnol Prog* 22(2):568–576. <https://doi.org/10.1021/bp050294y>
- DeBuysscher BL, Scott D, Thomas T, Feldmann H, Prescott J (2016) Peri-exposure protection against Nipah virus disease using a single-dose recombinant vesicular stomatitis virus-based vaccine. *NPJ Vaccines* 1:16002. <https://doi.org/10.1038/npjvaccines.2016.2>
- Eccles R (2021) Why is temperature sensitivity important for the success of common respiratory viruses? *Rev Med Virol* 31(1):1–8. <https://doi.org/10.1002/rmv.2153>
- Elahi SM, Shen CF, Gilbert R (2019) Optimization of production of vesicular stomatitis virus (VSV) in suspension serum-free culture medium at high cell density. *J Biotechnol* 289:144–149
- EMA (2019) Ervebo: Ebola vaccine (rVSVΔG-ZEBOV-GP, live). European Medicines Agency. <https://www.ema.europa.eu/en/medicines/human/EPAR/ervebo>
- Emanuel J, Callison J, Dowd KA, Pierson TC, Feldmann H, Marzi A (2018) A VSV-based Zika virus vaccine protects mice from lethal challenge. *Sci Rep* 8(1):11043. <https://doi.org/10.1038/s41598-018-29401-x>
- Evans RK, Nawrocki DK, Isopi LA, Williams DM, Casimiro DR, Chin S, Chen M, Zhu DM, Shiver JW, Volkin DB (2004) Development of stable liquid formulations for adenovirus-based vaccines. *J Pharm Sci* 93(10):2458–2475. <https://doi.org/10.1002/jps.20157>
- FDA (2019) First FDA-approved vaccine for the prevention of Ebola virus disease: marking a critical milestone for public health. FDA. <https://www.fda.gov/news-events/press-announcements/first-fda-approved-vaccine-prevention-ebola-virus-disease-marking-critical-milestone-public-health>
- Geisbert TW, Jones S, Fritz EA, Shurtleff AC, Geisbert JB, Liebscher R, Grolla A, Ströher U, Fernando L, Daddario KM, Guttieri MC, Mothé BR, Larsen T, Hensley LE, Jahrling PB, Feldmann H (2005) Development of a new vaccine for the prevention of Lassa fever. *PLoS Med* 2(6):e183. <https://doi.org/10.1371/journal.pmed.0020183>
- Gélinas J-F, Azizi H, Kiesslich S, Lanthier S, Perderson J, Chahal PS, Ansoorge S, Kobinger G, Gilbert R, Kamen AA (2019) Production of rVSV-ZEBOV in serum-free suspension culture of HEK 293SF cells. *Vaccine* 37(44):6624–6632. <https://doi.org/10.1016/j.vaccine.2019.09.044>
- Genzel Y, Dietzsch C, Rapp E, Schwarzer J, Reichl U (2010) MDCK and Vero cells for influenza virus vaccine production: a one-to-one comparison up to lab-scale bioreactor cultivation. *Appl Microbiol Biotechnol* 88(2):461–475. <https://doi.org/10.1007/s00253-010-2742-9>
- Genzel Y, Vogel T, Buck J, Behrendt I, Ramirez DV, Schiedner G, Jordan I, Reichl U (2014) High cell density cultivations by alternating tangential flow (ATF) perfusion for influenza A virus production using suspension cells. *Vaccine* 32(24):2770–2781. <https://doi.org/10.1016/j.vaccine.2014.02.016>
- Göbel S, Jaén KE, Dorn M, Neumeyer V, Jordan I, Sandig V, Reichl U, Altomonte J, Genzel Y (2023a) Process intensification strategies towards cell culture-based high-yield production of a fusogenic oncolytic virus. *Biotechnol Bioeng*. <https://doi.org/10.1002/bit.28353>
- Göbel S, Jaén KE, Fernandes RP, Reiter M, Altomonte J, Reichl U, Genzel Y (2023b) Characterization of a quail suspension cell line for production of a fusogenic oncolytic virus. *Biotechnol Bioeng*. <https://doi.org/10.1002/bit.28530>
- Göbel S, Kortum F, Chavez KJ, Jordan I, Sandig V, Reichl U, Altomonte J, Genzel Y (2022a) Cell-line screening and process development for a fusogenic oncolytic virus in small-scale suspension cultures. *Appl Microbiol Biotechnol* 106(13–16):4945–4961. <https://doi.org/10.1007/s00253-022-12027-5>
- Göbel S, Pelz L, Reichl U, Genzel Y (2022b) Chapter 5 Upstream processing for viral vaccines—Process intensification. In: Amine Kamen LC (ed) *Bioprocessing of viral vaccines*, vol 1. Taylor & Francis Group. <https://www.routledge.com/Bioprocessing-of-Viral-Vaccines/Kamen-Cervera/p/book/9781032132112>, pp 79–137
- Gränicher G, Babakhani M, Göbel S, Jordan I, Marichal-Gallardo P, Genzel Y, Reichl U (2021a) A high cell density perfusion process for modified Vaccinia virus Ankara production: process integration with inline DNA digestion and cost analysis. *Biotechnol Bioeng*. <https://doi.org/10.1002/bit.27937>
- Gränicher G, Coronel J, Trampler F, Jordan I, Genzel Y, Reichl U (2020) Performance of an acoustic settler versus a hollow fiber-based ATF technology for influenza virus production in perfusion. *Appl Microbiol Biotechnol* 104(11):4877–4888. <https://doi.org/10.1007/s00253-020-10596-x>
- Gränicher G, Tapia F, Behrendt I, Jordan I, Genzel Y, Reichl U (2021b) Production of modified Vaccinia Ankara virus by intensified cell cultures: a comparison of platform technologies for viral vector production. *Biotechnol J* 16(1):e2000024. <https://doi.org/10.1002/biot.202000024>
- Hadpe SR, Sharma AK, Mohite VV, Rathore AS (2017) ATF for cell culture harvest clarification: mechanistic modelling and comparison with TFF. *J Chem Technol Biotechnol* 92(4):732–740. <https://doi.org/10.1002/jctb.5165>
- Hein MD, Chawla A, Cattaneo M, Kupke SY, Genzel Y, Reichl U (2021) Cell culture-based production of defective interfering influenza A virus particles in perfusion mode using an alternating tangential flow filtration system. *bioRxiv* 2021.06.07.446880. <https://doi.org/10.1101/2021.06.07.446880>
- Jones SM, Feldmann H, Ströher U, Geisbert JB, Fernando L, Grolla A, Klenk HD, Sullivan NJ, Volchkov VE, Fritz EA, Daddario KM, Hensley LE, Jahrling PB, Geisbert TW (2005) Live attenuated recombinant vaccine protects nonhuman primates against Ebola and Marburg viruses. *Nat Med* 11(7):786–790. <https://doi.org/10.1038/nm1258>
- Kahn JS, Roberts A, Weibel C, Buonocore L, Rose JK (2001) Replication-competent or attenuated, nonpropagating vesicular stomatitis viruses expressing respiratory syncytial virus (RSV) antigens protect mice against RSV challenge. *J Virol*

- 75(22):11079–11087. <https://doi.org/10.1128/jvi.75.22.11079-11087.2001>
- Krabbe T, Marek J, Groll T, Steiger K, Schmid RM, Krackhardt AM, Altomonte J (2021) Adoptive T cell therapy is complemented by oncolytic virotherapy with fusogenic VSV-NDV in combination treatment of murine melanoma. *Cancers* 13(5):1044
- Lauretti F, Chattopadhyay A, de Oliveira França RF, Castro-Jorge L, Rose J, Fonseca BA (2016) Recombinant vesicular stomatitis virus-based dengue-2 vaccine candidate induces humoral response and protects mice against lethal infection. *Human Vaccines Immunother* 12(9):2327–2333. <https://doi.org/10.1080/21645515.2016.1183857>
- Liao JB, Publicover J, Rose JK, DiMaio D (2008) Single-dose, therapeutic vaccination of mice with vesicular stomatitis virus expressing human papillomavirus type 16 E7 protein. *Clin Vaccine Immunol: CVI* 15(5):817–824. <https://doi.org/10.1128/cvi.00343-07>
- Manceur AP, Kim H, Misic V, Andreev N, Dorion-Thibaudeau J, Lanthier S, Bernier A, Tremblay S, Gélinas A-M, Broussau S, Gilbert R, Ansoorge S (2017) Scalable lentiviral vector production using stable HEK293SF producer cell lines. *Hum Gene Ther Methods* 28(6):330–339. <https://doi.org/10.1089/hgtb.2017.086>
- Mendes JP, Fernandes B, Pineda E, Kudugunti S, Bransby M, Gantier R, Peixoto C, Alves PM, Roldão A, Silva RJS (2022) AAV process intensification by perfusion bioreaction and integrated clarification. *Front Bioeng Biotechnol* 10:1020174. <https://doi.org/10.3389/fbioe.2022.1020174>
- Mendonça SA, Lorincz R, Boucher P, Curiel DT (2021) Adenoviral vector vaccine platforms in the SARS-CoV-2 pandemic. *NPJ Vaccines* 6(1):97. <https://doi.org/10.1038/s41541-021-00356-x>
- Moleirinho MG, Silva RJS, Alves PM, Carrondo MJT, Peixoto C (2020) Current challenges in biotherapeutic particles manufacturing. *Expert Opin Biol Ther* 20(5):451–465. <https://doi.org/10.1080/14712598.2020.1693541>
- Nadeau I, Kamen A (2003) Production of adenovirus vector for gene therapy. *Biotechnol Adv* 20(7-8):475–489
- Nikolay A, de Grooth J, Genzel Y, Wood JA, Reichl U (2020) Virus harvesting in perfusion culture: choosing the right type of hollow fiber membrane. *Biotechnol Bioeng* 117(10):3040–3052. <https://doi.org/10.1002/bit.27470>
- Nikolay A, Léon A, Schwamborn K, Genzel Y, Reichl U (2018) Process intensification of EB66® cell cultivations leads to high-yield yellow fever and Zika virus production. *Appl Microbiol Biotechnol* 102(20):8725–8737. <https://doi.org/10.1007/s00253-018-9275-z>
- Palin A, Chattopadhyay A, Park S, Delmas G, Suresh R, Senina S, Perlin DS, Rose JK (2007) An optimized vaccine vector based on recombinant vesicular stomatitis virus gives high-level, long-term protection against *Yersinia pestis* challenge. *Vaccine* 25(4):741–750. <https://doi.org/10.1016/j.vaccine.2006.08.010>
- Pelz L, Göbel S, Chavez K, Reichl U, Genzel Y (2022) Chapter 5 Upstream processing for viral vaccines—general aspects. In: Amine Kamen LC (ed) *Bioprocessing of viral vaccines*, vol 1. Taylor & Francis Group, <https://www.routledge.com/Bioprocessing-of-Viral-Vaccines/Kamen-Cervera/p/book/9781032132112>, pp 79–137
- Roberts A, Kretzschmar E, Perkins AS, Forman J, Price R, Buonocore L, Kawaoka Y, Rose JK (1998) Vaccination with a recombinant vesicular stomatitis virus expressing an influenza virus hemagglutinin provides complete protection from influenza virus challenge. *J Virol* 72(6):4704–4711. <https://doi.org/10.1128/jvi.72.6.4704-4711.1998>
- Schneider M, Marison IW, von Stockar U (1996) The importance of ammonia in mammalian cell culture. *J Biotechnol* 46(3):161–185. [https://doi.org/10.1016/0168-1656\(95\)00196-4](https://doi.org/10.1016/0168-1656(95)00196-4)
- Su Y, Wei Z, Miao Y, Sun L, Shen Y, Tang Z, Li L, Quan Y, Yu H, Wang W-C, Zhou W, Tian J (2021) Optimized process operations reduce product retention and column clogging in ATF-based perfusion cell cultures. *Appl Microbiol Biotechnol* 105(24):9125–9136. <https://doi.org/10.1007/s00253-021-11662-8>
- Suder E, Furuyama W, Feldmann H, Marzi A, de Wit E (2018) The vesicular stomatitis virus-based Ebola virus vaccine: from concept to clinical trials. *Human Vaccines Immunother* 14(9):2107–2113. <https://doi.org/10.1080/21645515.2018.1473698>
- Tona RM, Shah R, Middaugh K, Steve J, Marques J, Roszell BR, Jung C (2023) Process intensification for lentiviral vector manufacturing using tangential flow depth filtration. *Mol Ther- Methods Clin Dev* 29:93–107. <https://doi.org/10.1016/j.omtm.2023.02.017>
- Tran MY, Kamen AA (2022) Production of lentiviral vectors using a HEK-293 producer cell line and advanced perfusion processing. *Front Bioeng Biotechnol* 10:887716. <https://doi.org/10.3389/fbioe.2022.887716>
- Ura T, Okuda K, Shimada M (2014) Developments in viral vector-based vaccines. *Vaccines (Basel)* 2(3):624–641. <https://doi.org/10.3390/vaccines2030624>
- Ura T, Yamashita A, Mizuki N, Okuda K, Shimada M (2021) New vaccine production platforms used in developing SARS-CoV-2 vaccine candidates. *Vaccine* 39(2):197–201. <https://doi.org/10.1016/j.vaccine.2020.11.054>
- van den Pol AN, Mao G, Chattopadhyay A, Rose JK, Davis JN (2017) Chikungunya, influenza, Nipah, and Semliki forest chimeric viruses with vesicular stomatitis virus: actions in the brain. *J Virol* 91(6). <https://doi.org/10.1128/jvi.02154-16>
- Vázquez-Ramírez D, Jordan I, Sandig V, Genzel Y, Reichl U (2019) High titer MVA and influenza A virus production using a hybrid fed-batch/perfusion strategy with an ATF system. *Appl Microbiol Biotechnol* 103(7):3025–3035
- Williams T., Goodyear O., Davies L., Knevelman C., Bransby M., Mitrophanous K., J. M (2020) Lentiviral vector manufacturing process enhancement utilizing TDF™ technology. *Cell Gene Ther Insights*;6:455–467 doi:<https://doi.org/10.18609/cgti.2020.053>
- Wu Y, Bissinger T, Genzel Y, Liu X, Reichl U, Tan W-S (2021) High cell density perfusion process for high yield of influenza A virus production using MDCK suspension cells. *Appl Microbiol Biotechnol* 105(4):1421–1434. <https://doi.org/10.1007/s00253-020-11050-8>
- Yang Z, Paes B, Fulber JPC, Tran MY, Farnós O, Kamen AA (2023) Development of an integrated continuous manufacturing process for the rVSV-Vectored SARS-CoV-2 candidate vaccine. *Vaccines (Basel)* 11(4). <https://doi.org/10.3390/vaccines11040841>
- Yue J, Liu Y, Zhao M, Bi X, Li G, Liang W (2023) The R&D landscape for infectious disease vaccines. *Nat Rev Drug Discov*. <https://doi.org/10.1038/d41573-023-00119-4>
- Zhan C, Bidkhorji G, Schwarz H, Malm M, Mebrahtu A, Field R, Sellick C, Hatton D, Varley P, Mardinoglu A, Rockberg J, Chotteau V (2020) Low shear stress increases recombinant protein production and high shear stress increases apoptosis in human cells. *iScience* 23(11):101653. <https://doi.org/10.1016/j.isci.2020.101653>
- Zhang Y, Nagalo BM (2022) Immunovirotherapy based on recombinant vesicular stomatitis virus: where are we? *Front Immunol* 13. <https://doi.org/10.3389/fimmu.2022.898631>

Publisher's note Springer Nature remains neutral with regard to jurisdictional claims in published maps and institutional affiliations.

4. Conclusions

In the early development stages of novel VBBs, the primary focus is on designing new constructs, exploring their therapeutic potential, and assessing their safety profiles. Establishment of optimal production systems is often neglected until development progresses and moves towards (pre)clinical use. Until now, the rapid onset of syncytia formation following infection of host cells was a limiting factor in the efficient production and release of fusogenic viruses. In this work, chronological steps towards the establishment of easily transferrable, scalable and highly efficient production processes for a novel chimeric fusogenic oncolytic virus using suspension cells are outlined. Screening a wide range of potential host cell lines and production conditions allowed the generation of highly concentrated OV stocks in batch mode (first manuscript). By inclusion of a novel host cell line and thorough evaluation of various production vessels at scales spanning 3 orders of magnitude, the robustness and applicability of simple batch processes for highly concentrated OV production (third manuscript) was confirmed. Moreover, process intensification was realized by transfer of optimized production conditions, first carried out in small-scale semi-perfusion cultures, then transferred to perfusion cultures using an AS for cell retention (second manuscript). Finally, a membrane-based TFDF perfusion system was evaluated as a cell retention device for continuous virus harvesting and clarification to reduce the number of unit operations and enable the seamless integration of upstream and downstream processing to a complete rVSV-NDV manufacturing process (fourth manuscript).

Cell-line screening and process development in batch mode

In this study advantages of using suspension cell cultures for high titer production of a fusogenic OV in batch production processes were investigated. To achieve this, four suspension cell lines of various origins (avian, canine, rodent, and human) in various media were screened for their ability to replicate rVSV-NDV. Not only the cell line, but also the culture medium played a pivotal role for the peak virus titer and the stability of virus particles in the supernatant. As expected, the identification of an optimal MOI for each cell line was critical to achieve high infectious virus titers, while increased cell-to-

cell contact had no detectable effect on OV yield in suspension cultures. Serial adaptations of rVSV-NDV to the respective host cell line resulted in similar virus yields, however, onset of virus release was drastically reduced. From a production perspective, it appeared favorable to achieve a continuously increasing population of OV-infected cells rather than losing the cell substrate due to fast oncolysis before high titers are reached. Therefore, selection of a suitable cell line, media composition, virus adaptation, and MOI were identified as critical process parameters for rVSV-NDV production. Further studies to identify the specific adaptations at the genomic level by next-generation sequencing and to understand the exact mechanisms of syncytia formation and viral spread could allow targeted improvements to optimize viral replication. Next, as a proof of concept, scalability was evaluated by transfer of optimized processes for two cell lines to 1 L STRs. Here, lower virus yields were achieved for both cell lines after media dilution at TOI compared to full exchange of the medium in shake flask experiments. An unfavorable metabolic state of BHK-21 cells, combined with the occurrence of the so-called HCD effect [172] for HEK293 cells were considered as the primary reasons for reduced titers. To overcome these metabolic challenges, implementation of perfusion mode and further optimizations of batch infections were carried out in the following studies. Nevertheless, increases of infectious virus titers by 100-fold compared to adherent pIX cells were reached for the first time. Moreover, in collaboration with Fabian Kortum and Jennifer Altomonte (TU Munich), it was demonstrated that *in vitro* oncolytic potency was not affected during suspension production. Further studies in mouse and rat tumor models and serum stability investigations should be carried out to confirm this.

Characterization of a GMP-compliant quail cell line for rVSV-NDV production

As highlighted in the first manuscript, high yield virus production is dependent on the host cell line and the virus and requires thoughtful balancing of process parameters. Thus, a production process cannot be merely adapted to a different host cell line, but instead requires the re-characterization of specific production parameters. In this study, we established an easily transferrable batch process for production of rVSV-NDV in various cultivation systems, using a novel host cell line, which would qualify for production under GMP regulations. Therefore, CCX.E10 cells were transferred to

orbitally shaken systems (originally cultivated in spinner flasks) and demonstrated very robust growth to high cell concentrations over 180 days (40 passages) as well as a quick and successful scale-up using mixing time as a scaling parameter (>100-fold) up to 6 L in the single-use bioreactor SB10-X. Subsequent scale-up to SB-50X would already allow the production of sufficient material for conducting phase 1 clinical trials. Versatility of CCX.E10 cells was demonstrated by a direct transfer of the production process to STRs at different scales. Scale-down into the ambr15 system enabled testing multiple pH set-points in duplicate. To the best of my knowledge, there aren't any other published studies showing a direct transfer of virus processes from OSB bioreactors to STRs and the applicability in different virus production systems at different scales. Regardless of the production system, process impurity levels at the time-point of maximum virus titer (e.g. protein and DNA) were comparable to other virus production processes and should be easy to handle by a suitable purification train [173]. Despite the historical implementation of BHK-21 cells for large-scale manufacturing of veterinary vaccines (e.g. rabies and foot and mouth disease vaccines) as well as recombinant biopharmaceuticals (e.g. human FVIIa and FVIII), their use for human vaccine applications is highly controversial as they are known to harbor endogenous retroviruses and have been classified as tumorigenic [174-176]. Although the achieved production yields were slightly lower to those obtained with BHK-21 cells, CCX.E10 cells seem favorable for commercial production. To allow for even higher virus yields, process intensification by transition from batch to perfusion mode needs to be addressed [10, 80, 103, 108].

Steps towards high cell density cultivation in perfusion mode

To overcome the lower virus titers obtained after scale-up from shake flasks to 1 L STRs in batch mode, several process parameters known to influence virus production were investigated. Induction of hypoxia, addition of trypsin, or reduction of temperature after infection had no effect or allowed only a modest increase in titers (~0.5 log). As media dilution previously impaired total virus yields, additional medium supplementation with glucose and glutamine was tested. This provided a 2-fold increase in total virus yields compared to the initial process, confirming the hypothesis of a limitation of nonquantified metabolites or an accumulation of inhibiting compounds

to be the reason for the reduction in total virus yields [177]. Next, process intensification methods were evaluated by increasing cell concentrations in perfusion mode. Initial optimization studies were carried out in shake flasks (MOI, cell concentration, media, supplements) using a semi-perfusion strategy. Improved yields (43-56-fold), CSVY (5-28-fold), and VVP (6-18-fold) for both low producing AGE1.CR and HEK293 cells were observed after infection at $>20 \times 10^6$ cells/mL in semi-perfusion mode. Finally, findings were applied to establish a full perfusion system at VCCs ranging from $15\text{--}30 \times 10^6$ cells/mL using an AS for cell retention. The perfusion processes involved either a manually adjusted perfusion rate or a closed-loop control using a capacitance probe [15, 80, 108, 158]. The AS allowed continuous harvesting of rVSV-NDV particles with high cell retention efficiencies (above 97%) and more than 4–100 times higher infectious virus titers than for optimized batch processes for all cell lines. Moreover, no decrease in CSVY was observed at HCD, regardless of the cell line. Combined with a 15–30 fold increased VVP for AGE1.CR and HEK293SF cells compared to batch processes, this highlights the possibility to use STRs with a smaller footprint. In contrast to all previous findings, formation of syncytia was observed at HCD for BHK 21 cells and HEK293SF cells but not AGE1.CR cells. Further investigations to check whether syncytia formation had an effect on the production of the rVSV-NDV need to be conducted. Oncolytic potency was not affected compared to production in batch mode, however, this still needs to be confirmed in preclinical tumor models.

In summary, the transition to perfusion emerged as the most promising solution to overcome the limitations of production in batch mode and achieve high-yielding manufacturing processes. Increased VVPs allow the reduction of production footprints, thereby reducing initial capital investments and operations expenditures. Additional adoption of single-use technology would further propel this development, particularly for GMP-compliant manufacturing.

Evaluation of tangential flow depth filtration for continuous virus harvesting and clarification

For HCD cultivations, membrane-based systems utilizing HF modules are widely employed and preferred for GMP manufacturing. However, these systems are prone to filter fouling and retention of virus particles, which leads to unwanted accumulation

of virus inside the bioreactor until full harvest of the cultivation broth is possible [10, 14, 16, 103, 124, 178]. In particular for fusogenic OV production the formation of large multi-nucleated syncytia (>100 μm) in perfusion cultures resulted in the complete blockage of the commonly used 0.2 μm PES HF membranes with small lumen sizes [96]. Here, a scalable TFDF perfusion system that allows production, continuous virus harvesting, and clarification in one unit operation was investigated. The intensified production of two different rVSV-based vectors, one which induces classical cytopathic effects (rVSV-GFP; conducted by Lars Pelz at the McGill University, Canada) and one that mediates cell fusion reactions (rVSV-NDV) were compared to optimized batch processes. Using HEK293-SF cells and rVSV-GFP, TFDF perfusion cultivations resulted in a maximum VCC of 11.3×10^6 cells/mL, high cell retention efficiency (>99.6%), and continuous virus harvesting and clarification. Although the CSVY decreased relative to a batch process established as a control, an increased STY was obtained. Modification of a traditional ATF set-up by utilization of a HF membrane with a large internal lumen (0.75 mm; pore size 0.65 μm) combined with a high flow rate (1.5 L/min) hampered syncytia formation and prevented complete blockage. However, rVSV-NDV was retained by the membrane (>97% at 18 hpi). Transition to TFDF perfusion allowed achievement of HCD ($16.4\text{-}20.6 \times 10^6$ cells/mL), high reduction of solution turbidity (>95%), continuous virus harvesting, and clarification, despite occurrence of syncytia. Compared to optimized batch processes, VCCs were increased by 6-fold, but infectious virus titers were more than 11-fold higher. Moreover, CSVYs were improved by 2-fold, STY by 460% (5.6-fold), and similar VVPs were reached. These results align with previous investigations that have demonstrated the successful application of TFDF as a perfusion system for continuous virus harvesting and clarification for different viruses such as adeno-associated virus, lentivirus, and influenza A virus [101, 102, 138, 139]. Although perfusion runs using TFDF for cell retention outperformed both AS and ATF perfusions in terms of maximum yield, CSVY, VVP, and STY, a direct comparison should be drawn very carefully as production parameters differed significantly between the runs. Re-evaluation should include the same bioreactor set-up and similar infection cell concentrations. Compared to AS perfusions, the main benefit of TFDF includes scalability, decreased complexity, and reduction of unit operations after the final harvest. Compared to ATF perfusions,

continuous virus harvesting would allow for integrated continuous bioprocessing, directly linking upstream to downstream unit operations.

5. Outlook

Throughout the last 30 years, batch and fed-batch cell cultures were the dominant bioprocessing paradigm, both in upstream and downstream processes. For production facilities with separated upstream and downstream productions this will unlikely change. However, transition to continuous manufacturing by perfusion and direct integration of upstream and downstream processes are reshaping the historical production landscape. The main drivers for adoption of new technologies are economics and expansion of production sites outside the western world. Manufacturing in perfusion mode is generally cheaper, as smaller facility footprints can be utilized to achieve the same product output, leading to reduced expenses for both goods and capital investments [97, 179]. Historical concerns about the challenges associated with lot/batch definition and quality assurance/control are overshadowed by the encouragement and guidance provided by the regulatory authorities. In monoclonal antibody manufacturing, utilization of perfusion systems is already widely adopted by many companies including Bayer (Kogenate; factor VIII), Janssen/J&J (ReoPro; anti-platelet monoclonal antibody (mAb), and Remicade; tumor necrosis factor mAb), Genzyme/Sanofi (Campath; CD52 mAb), and Pfizer (Xyntha; modified factor VIII) [179]. While the same benefits could be translated to the field of VBBs, perfusion and process integration do not yet play a significant part of today's commercial manufacturing landscape. In particular, vaccine manufacturing is confined to outdated and low-yielding methodologies: Egg-based production and adherent cell-cultures are still the dominant production platforms for most viral vaccines. Although switching to perfusion cultivations involving suspension cells could greatly improve any currently used vaccine production process, the adaptation of this technology is mainly found in the scientific environment. Clearly economic benefits have already enabled a shift to perfusion processes in the field of mAbs, while vaccine manufacturers unfortunately still adhere to outdated methods. Paid-off production facilities, approved cell lines, established CMC protocols, low input doses that can be met with low yield processes, and the fear that significant process changes will require re-characterization of safety and efficacy in clinical trials are the main reasons why pharmaceutical companies are reluctant to embrace new technologies and changes. Even the more flexible options

offered by emergency use authorizations in the context of global pandemics such as COVID-19, have not enabled the adoption of perfusion technologies for conventional vaccines. Unfortunately, pharmaceutical companies failed to use this opportunity and expand their repertoire of established production processes for inactivated vaccines or viral vector vaccines using adherent cell cultures or batch processes with suspension cells. However, the pressure from alternative vaccine manufacturing options e.g. mRNA might be a new incentive to rethink old dogmas. Especially price pressure demanding vaccines at 1\$ per dose and new fields of application such as gene and cancer therapy, which require enormous input doses and have a large target population, are forcing companies to rethink their current production systems. High doses in large numbers can no longer be achieved by out-scaling low-yielding processes.

In this thesis, critical steps have been addressed to allow industrial-relevant high titer OV production in suspension cells. Such production processes are rarely touched, as they harbor unique production challenges that have been overcome for production of other vectors, like lentivirus or adeno-associated virus, which both can be manufactured using off-the-shelf platforms that are readily available and require minimal process optimization. Compared to the initial production using adherent AGE1.CR.pIX cells, the production processes established in the scope of this thesis either in batch or perfusion mode enabled >560-fold and >7500-fold higher virus yields. This serves as basis for the development of a GMP-compliant manufacturing process. Quantities obtained should provide sufficient amounts of highly potent virus material to enter a phase I clinical trial in cancer patients. In cooperation with iBET (Portugal) we developed a GMP-compatible downstream process based on anion exchange chromatography for the purification and concentration of rVSV-NDV produced in batch mode with CCX.E10 cells, resulting in an overall product recovery of ~50% (submitted to Separation and Purification Technology journal). In parallel, rVSV-NDV production in CCX.E10 cells was shifted to HCD using a TFDF perfusion system, achieving infectious virus titers above 10^9 TCID₅₀/mL. Both studies resulted in a final joint effort to develop a fully integrated production process combining high titer rVSV-NDV production in perfusion, continuous clarification through the TFDF membrane and

subsequent downstream operations with all three academic partners working together in the MPI Magdeburg laboratories.

Bibliography

1. Kelly, E. and S.J. Russell, *History of oncolytic viruses: genesis to genetic engineering*. Mol Ther, 2007. **15**(4): p. 651-9.
2. Russell, S.J., K.W. Peng, and J.C. Bell, *Oncolytic virotherapy*. Nat Biotechnol, 2012. **30**(7): p. 658-70.
3. EMA, *Assessment report Imlygic*, C.f.M.P.f.H.U. (CHMP), Editor. 2015.
4. Abdullahi, S., et al., *A Novel Chimeric Oncolytic Virus Vector for Improved Safety and Efficacy as a Platform for the Treatment of Hepatocellular Carcinoma*. J Virol, 2018. **92**(23).
5. Ungerechts, G., et al., *Moving oncolytic viruses into the clinic: clinical-grade production, purification, and characterization of diverse oncolytic viruses*. Molecular Therapy - Methods & Clinical Development, 2016. **3**: p. 16018.
6. Gallo-Ramírez, L.E., et al., *Bioreactor concepts for cell culture-based viral vaccine production*. Expert Rev Vaccines, 2015. **14**(9): p. 1181-95.
7. Grein, T.A., et al., *Screening different host cell lines for the dynamic production of measles virus*. Biotechnology Progress, 2017. **33**(4): p. 989-997.
8. Göbel, S., et al., *Cell-line screening and process development for a fusogenic oncolytic virus in small-scale suspension cultures*. Appl Microbiol Biotechnol, 2022. **106**(13-16): p. 4945-4961.
9. Caron, A.L., R.T. Biaggio, and K. Swiech, *Strategies to Suspension Serum-Free Adaptation of Mammalian Cell Lines for Recombinant Glycoprotein Production*. Methods Mol Biol, 2018. **1674**: p. 75-85.
10. Genzel, Y., et al., *High cell density cultivations by alternating tangential flow (ATF) perfusion for influenza A virus production using suspension cells*. Vaccine, 2014. **32**(24): p. 2770-2781.
11. Gränicher, G., et al., *Efficient influenza A virus production in high cell density using the novel porcine suspension cell line PBG.PK2.1*. Vaccine, 2019. **37**(47): p. 7019-7028.
12. Tapia, F., et al., *Bioreactors for high cell density and continuous multi-stage cultivations: options for process intensification in cell culture-based viral vaccine production*. Applied microbiology and biotechnology, 2016. **100**(5): p. 2121-2132.
13. Vázquez-Ramírez, D., et al., *High-cell-density cultivations to increase MVA virus production*. Vaccine, 2018. **36**(22): p. 3124-3133.
14. Vázquez-Ramírez, D., et al., *High titer MVA and influenza A virus production using a hybrid fed-batch/perfusion strategy with an ATF system*. Applied microbiology and biotechnology, 2019. **103**(7): p. 3025-3035.
15. Hein, M.D., et al., *Cell culture-based production of defective interfering influenza A virus particles in perfusion mode using an alternating tangential flow filtration system*. bioRxiv, 2021: p. 2021.06.07.446880.
16. Pelz, L., et al., *Production of antiviral "OP7 chimera" defective interfering particles free of infectious virus*. Applied Microbiology and Biotechnology, 2024. **108**(1): p. 97.
17. Chotteau, V., *Perfusion Processes*, in *Animal Cell Culture*, M. Al-Rubeai, Editor. 2015, Springer. p. 407-443.
18. Göbel, S., et al., *Chapter 5 Upstream processing for viral vaccines– Process intensification*, in *Bioprocessing of Viral Vaccines* L.C. Amine Kamen, Editor. 2022, Taylor & Francis Group: <https://www.routledge.com/Bioprocessing-of-Viral-Vaccines/Kamen-Cervera/p/book/9781032132112>. p. 79-137.
19. Flint, S.J., et al., *Principles of virology, Volume 2: pathogenesis and control*. 2020: John Wiley & Sons.
20. Miest, T.S. and R. Cattaneo, *New viruses for cancer therapy: meeting clinical needs*. Nature Reviews Microbiology, 2014. **12**(1): p. 23-34.
21. Hoster, H.A., R.P. Zanes, Jr., and E. Von Haam, *Studies in Hodgkin's syndrome; the association of viral hepatitis and Hodgkin's disease; a preliminary report*. Cancer Res, 1949. **9**(8): p. 473-80.
22. Southam, C.M. and A.E. Moore, *Clinical studies of viruses as antineoplastic agents with particular reference to Egypt 101 virus*. Cancer, 1952. **5**(5): p. 1025-34.
23. Georgiades, J., et al., *Research on the oncolytic effect of APC viruses in cancer of the cervix uteri; preliminary report*. Biul Inst Med Morsk Gdansk, 1959. **10**: p. 49-57.
24. Asada, T., *Treatment of human cancer with mumps virus*. Cancer, 1974. **34**(6): p. 1907-1928.

25. Lin, D., Y. Shen, and T. Liang, *Oncolytic virotherapy: basic principles, recent advances and future directions*. Signal Transduction and Targeted Therapy, 2023. **8**(1): p. 156.
26. Eager, R.M. and J. Nemunaitis, *Clinical development directions in oncolytic viral therapy*. Cancer Gene Therapy, 2011. **18**(5): p. 305-317.
27. Macedo, N., et al., *Clinical landscape of oncolytic virus research in 2020*. J Immunother Cancer, 2020. **8**(2).
28. Doniņa, S., et al., *Adapted ECHO-7 virus Rigvir immunotherapy (oncolytic virotherapy) prolongs survival in melanoma patients after surgical excision of the tumour in a retrospective study*. Melanoma Res, 2015. **25**(5): p. 421-6.
29. Liang, M., *Oncorine, the World First Oncolytic Virus Medicine and its Update in China*. Curr Cancer Drug Targets, 2018. **18**(2): p. 171-176.
30. Pol, J., G. Kroemer, and L. Galluzzi, *First oncolytic virus approved for melanoma immunotherapy*. Oncoimmunology, 2016. **5**(1): p. e1115641.
31. Frampton, J.E., *Teserpaturev/G47Δ: First Approval*. BioDrugs, 2022. **36**(5): p. 667-672.
32. Ma, R., et al., *The emerging field of oncolytic virus-based cancer immunotherapy*. Trends Cancer, 2023. **9**(2): p. 122-139.
33. Hanahan, D. and Robert A. Weinberg, *Hallmarks of Cancer: The Next Generation*. Cell, 2011. **144**(5): p. 646-674.
34. Chiocca, E.A., *Oncolytic viruses*. Nat Rev Cancer, 2002. **2**(12): p. 938-50.
35. Goradel, N.H., et al., *Oncolytic virotherapy as promising immunotherapy against cancer: mechanisms of resistance to oncolytic viruses*. Future Oncol, 2022. **18**(2): p. 245-259.
36. Kaufman, H.L., F.J. Kohlhapp, and A. Zloza, *Oncolytic viruses: a new class of immunotherapy drugs*. Nature Reviews Drug Discovery, 2015. **14**(9): p. 642-662.
37. Ma, J., et al., *Characterization of virus-mediated immunogenic cancer cell death and the consequences for oncolytic virus-based immunotherapy of cancer*. Cell Death & Disease, 2020. **11**(1): p. 48.
38. Podbilewicz, B., *Virus and Cell Fusion Mechanisms*. Annual Review of Cell and Developmental Biology, 2014. **30**(Volume 30, 2014): p. 111-139.
39. Krabbe, T. and J. Altomonte, *Fusogenic Viruses in Oncolytic Immunotherapy*. Cancers, 2018. **10**(7): p. 216.
40. Salsman, J., et al., *Extensive syncytium formation mediated by the reovirus FAST proteins triggers apoptosis-induced membrane instability*. J Virol, 2005. **79**(13): p. 8090-100.
41. Higuchi, H., et al., *Viral fusogenic membrane glycoprotein expression causes syncytia formation with bioenergetic cell death: implications for gene therapy*. Cancer Res, 2000. **60**(22): p. 6396-402.
42. Galanis, E., *Therapeutic potential of oncolytic measles virus: promises and challenges*. Clin Pharmacol Ther, 2010. **88**(5): p. 620-5.
43. Cuadrado-Castano, S., et al., *The therapeutic effect of death: Newcastle disease virus and its antitumor potential*. Virus Res, 2015. **209**: p. 56-66.
44. Donnelly, O.G., et al., *Measles virus causes immunogenic cell death in human melanoma*. Gene Ther, 2013. **20**(1): p. 7-15.
45. Matveeva, O.V., et al., *Oncolysis by paramyxoviruses: multiple mechanisms contribute to therapeutic efficiency*. Mol Ther Oncolytics, 2015. **2**: p. 15011-.
46. Galluzzi, L., et al., *Essential versus accessory aspects of cell death: recommendations of the NCCD 2015*. Cell Death Differ, 2015. **22**(1): p. 58-73.
47. Delpeut, S., et al., *Membrane fusion-mediated autophagy induction enhances morbillivirus cell-to-cell spread*. J Virol, 2012. **86**(16): p. 8527-35.
48. Bateman, A.R., et al., *Viral fusogenic membrane glycoproteins kill solid tumor cells by nonapoptotic mechanisms that promote cross presentation of tumor antigens by dendritic cells*. Cancer Res, 2002. **62**(22): p. 6566-78.
49. Pedersen, J.C., et al., *Phylogenetic relationships among virulent Newcastle disease virus isolates from the 2002-2003 outbreak in California and other recent outbreaks in North America*. J Clin Microbiol, 2004. **42**(5): p. 2329-34.
50. Emmerson, P.T., *NEWCASTLE DISEASE VIRUS (PARAMYXOVIRIDAE)*, in *Encyclopedia of Virology (Second Edition)*, A. Granoff and R.G. Webster, Editors. 1999, Elsevier: Oxford. p. 1020-1026.
51. Peebles, M.E., *Newcastle Disease Virus Replication*, in *Newcastle Disease*, D.J. Alexander, Editor. 1988, Springer US: Boston, MA. p. 45-78.

52. Peeters, B.P., et al., *Genome replication of Newcastle disease virus: involvement of the rule-of-six*. Arch Virol, 2000. **145**(9): p. 1829-45.
53. Dortmans, J.C.F.M., et al., *The Viral Replication Complex Is Associated with the Virulence of Newcastle Disease Virus*. Journal of Virology, 2010. **84**(19): p. 10113-10120.
54. Elankumaran, S., et al., *Type I interferon-sensitive recombinant newcastle disease virus for oncolytic virotherapy*. J Virol, 2010. **84**(8): p. 3835-44.
55. Mueller, S.N. and B.T. Rouse, *27 - Immune responses to viruses*, in *Clinical Immunology (Third Edition)*, R.R. Rich, et al., Editors. 2008, Mosby: Edinburgh. p. 421-431.
56. Altomonte, J., et al., *Engineered newcastle disease virus as an improved oncolytic agent against hepatocellular carcinoma*. Mol Ther, 2010. **18**(2): p. 275-84.
57. Walker, P.J., et al., *ICTV Virus Taxonomy Profile: Rhabdoviridae 2022*. J Gen Virol, 2022. **103**(6).
58. Whelan, S.P.J., *Vesicular Stomatitis Virus*, in *Encyclopedia of Virology (Third Edition)*, B.W.J. Mahy and M.H.V. Van Regenmortel, Editors. 2008, Academic Press: Oxford. p. 291-299.
59. Ahmed, M., et al., *Ability of the matrix protein of vesicular stomatitis virus to suppress beta interferon gene expression is genetically correlated with the inhibition of host RNA and protein synthesis*. J Virol, 2003. **77**(8): p. 4646-57.
60. Stillman, E.A., J.K. Rose, and M.A. Whitt, *Replication and amplification of novel vesicular stomatitis virus minigenomes encoding viral structural proteins*. J Virol, 1995. **69**(5): p. 2946-53.
61. Follett, E.A.C., et al., *Virus Replication in Enucleate Cells: Vesicular Stomatitis Virus and Influenza Virus*. Journal of Virology, 1974. **13**(2): p. 394-399.
62. von Messling, V. and R. Cattaneo, *Toward novel vaccines and therapies based on negative-strand RNA viruses*. Curr Top Microbiol Immunol, 2004. **283**: p. 281-312.
63. Murphy Andrea, M., et al., *Vesicular Stomatitis Virus as an Oncolytic Agent against Pancreatic Ductal Adenocarcinoma*. Journal of Virology, 2012. **86**(6): p. 3073-3087.
64. Barber, G.N., *Vesicular stomatitis virus as an oncolytic vector*. Viral Immunol, 2004. **17**(4): p. 516-27.
65. Wollmann, G., et al., *Attenuation of vesicular stomatitis virus infection of brain using antiviral drugs and an adeno-associated virus-interferon vector*. Virology, 2015. **475**: p. 1-14.
66. EMA, *Ervebo*. 2019.
67. FDA, *First FDA-approved vaccine for the prevention of Ebola virus disease, marking a critical milestone in public health preparedness and response*. 2019.
68. Case, J.B., et al., *Replication-Competent Vesicular Stomatitis Virus Vaccine Vector Protects against SARS-CoV-2-Mediated Pathogenesis in Mice*. Cell Host Microbe, 2020. **28**(3): p. 465-474.e4.
69. Rose, N.F., et al., *An effective AIDS vaccine based on live attenuated vesicular stomatitis virus recombinants*. Cell, 2001. **106**(5): p. 539-49.
70. Emanuel, J., et al., *A VSV-based Zika virus vaccine protects mice from lethal challenge*. Sci Rep, 2018. **8**(1): p. 11043.
71. Jones, S.M., et al., *Live attenuated recombinant vaccine protects nonhuman primates against Ebola and Marburg viruses*. Nat Med, 2005. **11**(7): p. 786-90.
72. Geisbert, T.W., et al., *Development of a new vaccine for the prevention of Lassa fever*. PLoS Med, 2005. **2**(6): p. e183.
73. Lauretti, F., et al., *Recombinant vesicular stomatitis virus-based dengue-2 vaccine candidate induces humoral response and protects mice against lethal infection*. Hum Vaccin Immunother, 2016. **12**(9): p. 2327-33.
74. Ezelle, H.J., D. Markovic, and G.N. Barber, *Generation of hepatitis C virus-like particles by use of a recombinant vesicular stomatitis virus vector*. J Virol, 2002. **76**(23): p. 12325-34.
75. Kahn, J.S., et al., *Replication-competent or attenuated, nonpropagating vesicular stomatitis viruses expressing respiratory syncytial virus (RSV) antigens protect mice against RSV challenge*. J Virol, 2001. **75**(22): p. 11079-87.
76. Furuyama, W., et al., *A single dose of a vesicular stomatitis virus-based influenza vaccine confers rapid protection against H5 viruses from different clades*. npj Vaccines, 2020. **5**(1): p. 4.
77. Schlereth, B., et al., *Successful vaccine-induced seroconversion by single-dose immunization in the presence of measles virus-specific maternal antibodies*. J Virol, 2000. **74**(10): p. 4652-7.

78. Ebert, O., et al., *Syncytia induction enhances the oncolytic potential of vesicular stomatitis virus in virotherapy for cancer*. *Cancer Res*, 2004. **64**(9): p. 3265-70.
79. Pelz, L., et al., *Chapter 5 Upstream processing for viral vaccines—General aspects*, in *Bioprocessing of Viral Vaccines* L.C. Amine Kamen, Editor. 2022, Taylor & Francis Group: <https://www.routledge.com/Bioprocessing-of-Viral-Vaccines/Kamen-Cervera/p/book/9781032132112>. p. 79-137.
80. Gränicher, G., et al., *A high cell density perfusion process for Modified Vaccinia virus Ankara production: Process integration with inline DNA digestion and cost analysis*. *Biotechnol Bioeng*, 2021.
81. Nadeau, I. and A. Kamen, *Production of adenovirus vector for gene therapy*. *Biotechnology advances*, 2003. **20**(7-8): p. 475-489.
82. Fedosyuk, S., et al., *Simian adenovirus vector production for early-phase clinical trials: A simple method applicable to multiple serotypes and using entirely disposable product-contact components*. *Vaccine*, 2019. **37**(47): p. 6951-6961.
83. Joe, C.C.D., et al., *Accelerated and intensified manufacturing of an adenovirus-vectored vaccine to enable rapid outbreak response*. *Biotechnology and Bioengineering*, 2024. **121**(1): p. 176-191.
84. Southam, C.M., *DIVISION OF MICROBIOLOGY: PRESENT STATUS OF ONCOLYTIC VIRUS STUDIES**. *Transactions of the New York Academy of Sciences*, 1960. **22**(8 Series II): p. 657-673.
85. ICH, *Quality of biotechnological products: derivation and characterisation of cell substrates used for production of biotechnological/biological products. ICH Harmonised Tripartite Guideline*. *Dev Biol Stand*, 1998. **93**: p. 223-34.
86. FDA, *Guidance for Industry, Characterization and Qualification of Cell Substrates and Other Biological Materials Used in the Production of Viral Vaccines for Infectious Disease Indications*. 2010, U.S. Department of Health and Human Services, Food and Drug Administration, Center for Biologics Evaluation and Research.
87. Sugawara, K., et al., *Efficacy of a Third-Generation Oncolytic Herpes Virus G47Δ in Advanced Stage Models of Human Gastric Cancer*. *Mol Ther Oncolytics*, 2020. **17**: p. 205-215.
88. Santry, L.A., et al., *Production and Purification of High-Titer Newcastle Disease Virus for Use in Preclinical Mouse Models of Cancer*. *Mol Ther Methods Clin Dev*, 2018. **9**: p. 181-191.
89. McGinnes, L.W., et al., *Newcastle Disease Virus: Propagation, Quantification, and Storage*. *Current Protocols in Microbiology*, 2006. **1**(1): p. 15F.2.1-15F.2.18.
90. Arifin, M.A., et al., *Production of Newcastle disease virus by Vero cells grown on cytodex 1 microcarriers in a 2-litre stirred tank bioreactor*. *J Biomed Biotechnol*, 2010. **2010**: p. 586363.
91. Lee, D.Y., et al., *Review of the Current Research on Fetal Bovine Serum and the Development of Cultured Meat*. *Food Sci Anim Resour*, 2022. **42**(5): p. 775-799.
92. Lesch, H.P., et al., *Process Development of Adenoviral Vector Production in Fixed Bed Bioreactor: From Bench to Commercial Scale*. *Hum Gene Ther*, 2015. **26**(8): p. 560-71.
93. Wulff, N.H., M. Tzatzaris, and P.J. Young, *Monte Carlo simulation of the Spearman-Kaerber TCID50*. *J Clin Bioinforma*, 2012. **2**(1): p. 5.
94. Radhakrishnan, D., E.A. Wells, and A.S. Robinson, *Strategies to enhance productivity and modify product quality in therapeutic proteins*. *Current Opinion in Chemical Engineering*, 2018. **22**: p. 81-88.
95. Göbel, S., et al., *Characterization of a quail suspension cell line for production of a fusogenic oncolytic virus*. *Biotechnol Bioeng*, 2023.
96. Göbel, S., et al., *Process intensification strategies towards cell culture-based high-yield production of a fusogenic oncolytic virus*. *Biotechnol Bioeng*, 2023.
97. Konstantinov, K.B. and C.L. Cooney, *White paper on continuous bioprocessing. May 20-21, 2014 Continuous Manufacturing Symposium*. *J Pharm Sci*, 2015. **104**(3): p. 813-20.
98. Elahi, S.M., C.F. Shen, and R. Gilbert, *Optimization of production of vesicular stomatitis virus (VSV) in suspension serum-free culture medium at high cell density*. *Journal of biotechnology*, 2019. **289**: p. 144-149.
99. Merchuk, J.C., et al., *Studies of mixing in a concentric tube airlift bioreactor with different spargers*. *Chemical Engineering Science*, 1998. **53**(4): p. 709-719.
100. Ozturk, S.S., *Engineering challenges in high density cell culture systems*. *Cytotechnology*, 1996. **22**(1): p. 3-16.

101. Silva, C.A.T., A.A. Kamen, and O. Henry, *Intensified Influenza Virus Production in Suspension HEK293SF Cell Cultures Operated in Fed-Batch or Perfusion with Continuous Harvest*. Vaccines, 2023. **11**(12): p. 1819.
102. Mendes, J.P., et al., *AAV process intensification by perfusion bioreaction and integrated clarification*. Front Bioeng Biotechnol, 2022. **10**: p. 1020174.
103. Wu, Y., et al., *High cell density perfusion process for high yield of influenza A virus production using MDCK suspension cells*. Applied Microbiology and Biotechnology, 2021. **105**(4): p. 1421-1434.
104. Coronel, J., et al., *Application of an Inclined Settler for Cell Culture-Based Influenza A Virus Production in Perfusion Mode*. Frontiers in bioengineering and biotechnology, 2020. **8**: p. 672-672.
105. Coronel, J., et al., *Influenza A virus production in a single-use orbital shaken bioreactor with ATF or TFF perfusion systems*. Vaccine, 2019. **37**(47): p. 7011-7018.
106. Gränicher, G., et al., *Performance of an acoustic settler versus a hollow fiber-based ATF technology for influenza virus production in perfusion*. Applied Microbiology and Biotechnology, 2020. **104**(11): p. 4877-4888.
107. Gränicher, G., et al., *Production of Modified Vaccinia Ankara Virus by Intensified Cell Cultures: A Comparison of Platform Technologies for Viral Vector Production*. Biotechnol J, 2021. **16**(1): p. e2000024.
108. Nikolay, A., et al., *Process intensification of EB66® cell cultivations leads to high-yield yellow fever and Zika virus production*. Appl Microbiol Biotechnol, 2018. **102**(20): p. 8725-8737.
109. Göbel, S., et al., *Production of recombinant vesicular stomatitis virus-based vectors by tangential flow depth filtration*. Appl Microbiol Biotechnol, 2024. **108**(1): p. 240.
110. Petiot, E., et al., *Metabolic and kinetic analyses of influenza production in perfusion HEK293 cell culture*. BMC Biotechnol, 2011. **11**: p. 84.
111. Nie, J., et al., *The efficient development of a novel recombinant adenovirus zoster vaccine perfusion production process*. Vaccine, 2022. **40**(13): p. 2036-2043.
112. Alvim, R.G.F., I. Itabiana, Jr., and L.R. Castilho, *Zika virus-like particles (VLPs): Stable cell lines and continuous perfusion processes as a new potential vaccine manufacturing platform*. Vaccine, 2019. **37**(47): p. 6970-6977.
113. Bleckwenn, N.A., et al., *Production of recombinant proteins by vaccinia virus in a microcarrier based mammalian cell perfusion bioreactor*. Biotechnol Bioeng, 2005. **90**(6): p. 663-74.
114. Cortin, V., et al., *High-Titer Adenovirus Vector Production in 293S Cell Perfusion Culture*. Biotechnology Progress, 2004. **20**(3): p. 858-863.
115. Valkama, A.J., et al., *Optimization of lentiviral vector production for scale-up in fixed-bed bioreactor*. Gene Ther, 2018. **25**(1): p. 39-46.
116. Tao, Y., et al., *Development and implementation of a perfusion-based high cell density cell banking process*. Biotechnol Prog, 2011. **27**(3): p. 824-9.
117. Müller, D., et al., *Process intensification in the biopharma industry: Improving efficiency of protein manufacturing processes from development to production scale using synergistic approaches*. Chemical Engineering and Processing - Process Intensification, 2022. **171**: p. 108727.
118. Bielser, J.M., et al., *Perfusion mammalian cell culture for recombinant protein manufacturing - A critical review*. Biotechnol Adv, 2018. **36**(4): p. 1328-1340.
119. Shevitz, J., *Fluid filtration system patent 6544424*. 2000.
120. Warnock, J. and M. Al-Rubeai, *Production of Biologics from Animal Cell Cultures*, in *Applications of Cell Immobilisation Biotechnology*, V. Nedović and R. Willaert, Editors. 2005, Springer Netherlands: Dordrecht. p. 423-438.
121. Zhan, C., et al., *Low Shear Stress Increases Recombinant Protein Production and High Shear Stress Increases Apoptosis in Human Cells*. iScience, 2020. **23**(11): p. 101653.
122. Radoniqi, F., et al., *Computational fluid dynamic modeling of alternating tangential flow filtration for perfusion cell culture*. Biotechnol Bioeng, 2018. **115**(11): p. 2751-2759.
123. Zydny, A.L., *Continuous downstream processing for high value biological products: A Review*. Biotechnol Bioeng, 2016. **113**(3): p. 465-75.
124. Hadpe, S.R., et al., *ATF for cell culture harvest clarification: mechanistic modelling and comparison with TFF*. Journal of Chemical Technology & Biotechnology, 2017. **92**(4): p. 732-740.

125. Clincke, M.F., et al., *Very high density of CHO cells in perfusion by ATF or TFF in WAVE bioreactor™. Part I. Effect of the cell density on the process.* Biotechnol Prog, 2013. **29**(3): p. 754-67.
126. Voisard, D., et al., *Potential of cell retention techniques for large-scale high-density perfusion culture of suspended mammalian cells.* Biotechnol Bioeng, 2003. **82**(7): p. 751-65.
127. Shirgaonkar, I.Z., S. Lanthier, and A. Kamen, *Acoustic cell filter: a proven cell retention technology for perfusion of animal cell cultures.* Biotechnology Advances, 2004. **22**(6): p. 433-444.
128. Hwang, S.-H. and Y.-M. Koo, *Design of acoustic cell settler for filtering and recycling microbial cells.* Biotechnology Letters, 2003. **25**(4): p. 345-348.
129. Gaida, T., et al., *Selective retention of viable cells in ultrasonic resonance field devices.* Biotechnol Prog, 1996. **12**(1): p. 73-6.
130. Doblhoff-Dier, O., et al., *A novel ultrasonic resonance field device for the retention of animal cells.* Biotechnol Prog, 1994. **10**(4): p. 428-32.
131. Henzler, H.-J., *Kontinuierliche Fermentation mit tierischen Zellen. Teil 2. Techniken und Methoden der Zellrückhaltung.* Chemie Ingenieur Technik, 2012. **84**(9): p. 1482-1496.
132. Gorenflo, V.M., et al., *Scale-up and optimization of an acoustic filter for 200 L/day perfusion of a CHO cell culture.* Biotechnology and Bioengineering, 2002. **80**(4): p. 438-444.
133. Ryll, T., et al., *Performance of small-scale CHO perfusion cultures using an acoustic cell filtration device for cell retention: Characterization of separation efficiency and impact of perfusion on product quality.* Biotechnology and Bioengineering, 2000. **69**(4): p. 440-449.
134. Zhang, J., et al., *High-density perfusion culture of insect cells with a biosep ultrasonic filter.* Biotechnol Bioeng, 1998. **59**(3): p. 351-9.
135. Dalm, M.C., et al., *Stable hybridoma cultivation in a pilot-scale acoustic perfusion system: long-term process performance and effect of recirculation rate.* Biotechnol Bioeng, 2005. **91**(7): p. 894-900.
136. Bielser, J.-M., et al., *Continuous bleed recycling significantly increases recombinant protein production yield in perfusion cell cultures.* Biochemical Engineering Journal, 2021. **169**: p. 107966.
137. Moleirinho, M.G., et al., *Current challenges in biotherapeutic particles manufacturing.* Expert Opin Biol Ther, 2020. **20**(5): p. 451-465.
138. Tona, R.M., et al., *Process intensification for lentiviral vector manufacturing using tangential flow depth filtration.* Molecular Therapy - Methods & Clinical Development, 2023. **29**: p. 93-107.
139. Tran, M.Y. and A.A. Kamen, *Production of Lentiviral Vectors Using a HEK-293 Producer Cell Line and Advanced Perfusion Processing.* Front Bioeng Biotechnol, 2022. **10**: p. 887716.
140. Strober, W., *Trypan Blue Exclusion Test of Cell Viability.* Curr Protoc Immunol, 2015. **111**: p. A3.B.1-a3.B.3.
141. Bergin, A., J. Carvell, and M. Butler, *Applications of bio-capacitance to cell culture manufacturing.* Biotechnology Advances, 2022. **61**: p. 108048.
142. Pelletier, F., et al., *Software sensors for the monitoring of perfusion cultures: evaluation of the hybridoma density and the medium composition from glucose concentration measurements.* Cytotechnology, 1994. **15**(1-3): p. 291-9.
143. Kyung, Y.S., et al., *High density culture of mammalian cells with dynamic perfusion based on on-line oxygen uptake rate measurements.* Cytotechnology, 1994. **14**(3): p. 183-90.
144. Whelan, J., et al., *Use of focussed beam reflectance measurement (FBRM) for monitoring changes in biomass concentration.* Bioprocess Biosyst Eng, 2012. **35**(6): p. 963-75.
145. Buckley, K. and A.G. Ryder, *Applications of Raman Spectroscopy in Biopharmaceutical Manufacturing: A Short Review.* Applied Spectroscopy, 2017. **71**(6): p. 1085-1116.
146. Suhr, H., et al., *In situ microscopy for on-line characterization of cell-populations in bioreactors, including cell-concentration measurements by depth from focus.* Biotechnol Bioeng, 1995. **47**(1): p. 106-16.
147. Marose, S., C. Lindemann, and T. Scheper, *Two-dimensional fluorescence spectroscopy: a new tool for on-line bioprocess monitoring.* Biotechnol Prog, 1998. **14**(1): p. 63-74.
148. Davey, C.L., et al., *Introduction to the dielectric estimation of cellular biomass in real time, with special emphasis on measurements at high volume fractions.* Analytica Chimica Acta, 1993. **279**(1): p. 155-161.

149. Eggleton, M.J. and A.A. Sharp, *Platelet counting using the Coulter electronic counter*. J Clin Pathol, 1963. **16**(2): p. 164-7.
150. Salimi, E., et al., *Dielectric model for Chinese hamster ovary cells obtained by dielectrophoresis cytometry*. Biomicrofluidics, 2016. **10**(1): p. 014111.
151. Asami, K., et al., *Dielectric spectroscopy of biological cells*. Bioelectrochemistry and Bioenergetics, 1996. **40**(2): p. 141-145.
152. Asami, K., E. Gheorghiu, and T. Yonezawa, *Real-time monitoring of yeast cell division by dielectric spectroscopy*. Biophys J, 1999. **76**(6): p. 3345-8.
153. Schwan, H.P., *Electrical Properties of Tissue and Cell Suspensions** *This work was supported in part by grants from the United States Public Health Service, H-1253(c2-4) and in part by the Office of Naval Research, 119-289, in *Advances in Biological and Medical Physics*, J.H. Lawrence and C.A. Tobias, Editors. 1957, Elsevier. p. 147-209.
154. Carvell, J.P. and J.E. Dowd, *On-line Measurements and Control of Viable Cell Density in Cell Culture Manufacturing Processes using Radio-frequency Impedance*. Cytotechnology, 2006. **50**(1-3): p. 35-48.
155. Moore, B., R. Sanford, and A. Zhang, *Case study: The characterization and implementation of dielectric spectroscopy (biocapacitance) for process control in a commercial GMP CHO manufacturing process*. Biotechnol Prog, 2019. **35**(3): p. e2782.
156. Justice, C., et al., *Process control in cell culture technology using dielectric spectroscopy*. Biotechnol Adv, 2011. **29**(4): p. 391-401.
157. Metze, S., et al., *Multivariate data analysis of capacitance frequency scanning for online monitoring of viable cell concentrations in small-scale bioreactors*. Anal Bioanal Chem, 2020. **412**(9): p. 2089-2102.
158. Nikolay, A., et al., *Perfusion Control for High Cell Density Cultivation and Viral Vaccine Production*. Methods Mol Biol, 2020. **2095**: p. 141-168.
159. Braasch, K., et al., *The changing dielectric properties of CHO cells can be used to determine early apoptotic events in a bioprocess*. Biotechnol Bioeng, 2013. **110**(11): p. 2902-14.
160. Dowd, J.E., et al., *Optimization and control of perfusion cultures using a viable cell probe and cell specific perfusion rates*. Cytotechnology, 2003. **42**(1): p. 35-45.
161. Petiot, E. and A. Kamen, *Real-time monitoring of influenza virus production kinetics in HEK293 cell cultures*. Biotechnology Progress, 2013. **29**(1): p. 275-284.
162. Monica, T.J., et al., *Monitoring adenovirus infections with on-line and off-line methods*. Biotechnol Prog, 2000. **16**(5): p. 866-71.
163. Ansorge, S., G. Esteban, and G. Schmid, *On-line monitoring of infected Sf-9 insect cell cultures by scanning permittivity measurements and comparison with off-line biovolume measurements*. Cytotechnology, 2007. **55**(2-3): p. 115-24.
164. Pais, D.A.M., et al., *Dielectric Spectroscopy to Improve the Production of rAAV Used in Gene Therapy*. Processes, 2020. **8**(11): p. 1456.
165. Ansorge, S., et al., *Monitoring lentiviral vector production kinetics using online permittivity measurements*. Biochemical Engineering Journal, 2011. **54**(1): p. 16-25.
166. Petiot, E., et al., *Critical phases of viral production processes monitored by capacitance*. J Biotechnol, 2017. **242**: p. 19-29.
167. Negrete, A., G. Esteban, and R.M. Kotin, *Process optimization of large-scale production of recombinant adeno-associated vectors using dielectric spectroscopy*. Appl Microbiol Biotechnol, 2007. **76**(4): p. 761-72.
168. Joshi, P.R.H., et al., *Achieving High-Yield Production of Functional AAV5 Gene Delivery Vectors via Fedbatch in an Insect Cell-One Baculovirus System*. Mol Ther Methods Clin Dev, 2019. **13**: p. 279-289.
169. Walther, J., et al., *The business impact of an integrated continuous biomanufacturing platform for recombinant protein production*. J Biotechnol, 2015. **213**: p. 3-12.
170. Olin, M., et al., *An automated high inoculation density fed-batch bioreactor, enabled through N-1 perfusion, accommodates clonal diversity and doubles titers*. Biotechnology Progress, 2024. **40**(2): p. e3410.
171. Carvell, J.P., et al., *Developments in Using Off-Line Radio Frequency Impedance Methods for Measuring the Viable Cell Concentration in the Brewery*. Journal of the American Society of Brewing Chemists, 2000. **58**(2): p. 57-62.

172. Kamen, A. and O. Henry, *Development and optimization of an adenovirus production process*. The Journal of Gene Medicine: A cross-disciplinary journal for research on the science of gene transfer and its clinical applications, 2004. **6**(S1): p. S184-S192.
173. Marichal-Gallardo, P., et al., *Steric exclusion chromatography for purification of cell culture-derived influenza A virus using regenerated cellulose membranes and polyethylene glycol*. J Chromatogr A, 2017. **1483**: p. 110-119.
174. Pay, T.W., et al., *Production of rabies vaccine by an industrial scale BHK 21 suspension cell culture process*. Dev Biol Stand, 1985. **60**: p. 171-4.
175. Radlett, P.J. *The use of BHK suspension cells for the production of foot and mouth disease vaccines*. in *Vertebrate Cell Culture I*. 1987. Berlin, Heidelberg: Springer Berlin Heidelberg.
176. Reid, L.M., C.L. Jones, and J. Holland, *Virus carrier state suppresses tumorigenicity of tumor cells in athymic (nude) mice*. J Gen Virol, 1979. **42**(3): p. 609-14.
177. Lavado-García, J., et al., *The cell density effect in animal cell-based bioprocessing: Questions, insights and perspectives*. Biotechnol Adv, 2022. **60**: p. 108017.
178. Nikolay, A., et al., *Virus harvesting in perfusion culture: Choosing the right type of hollow fiber membrane*. Biotechnology and Bioengineering, 2020. **117**(10): p. 3040-3052.
179. Langer, E.S. and R.A. Rader, *Continuous bioprocessing and perfusion: wider adoption coming as bioprocessing matures*. Bioprocess J, 2014. **13**(1).

List of publications

Research articles

Gränicher G, Babakhani M, **Göbel S**, Jordan I, Marichal-Gallardo P, Genzel Y, Reichl U. A high cell density perfusion process for Modified Vaccinia virus Ankara production: Process integration with inline DNA digestion and cost analysis. *Biotechnol Bioeng.* **2021**. doi: 10.1002/bit.27937

Contribution: Methodology, Writing – review & editing

Publications included in this cumulative dissertation:

Göbel S*, Kortum F, Chavez KJ, Jordan I, Sandig V, Reichl U, Altomonte J, Genzel Y. Cell-line screening and process development for a fusogenic oncolytic virus in small-scale suspension cultures. *Appl Microbiol Biotechnol.* **2022**. doi: 10.1007/s00253-022-12027-5

Contribution: Conceptualization, Formal analysis, Investigation, Methodology, Project Administration, Writing – Original draft, Writing – Review & Editing

Göbel S*, Jaén KE*, Dorn M, Neumeyer V, Jordan I, Sandig V, Reichl U, Altomonte J, Genzel Y. Process intensification strategies toward cell culture-based high-yield production of a fusogenic oncolytic virus. *Biotechnol Bioeng.* **2023**. doi: 10.1002/bit.28353.

Contribution: Conceptualization, Formal analysis, Investigation, Methodology, Project Administration, Writing – Original draft, Writing – Review & Editing

Göbel S*, Jaén KE, Fernandes RP, Reiter M, Altomonte J, Reichl U, Genzel Y. Characterization of a quail suspension cell line for production of a fusogenic oncolytic virus. *Biotechnol Bioeng.* **2023**. doi: 10.1002/bit.28530.

Contribution: Conceptualization, Formal analysis, Investigation, Methodology, Project Administration, Writing – Original draft, Writing – Review & Editing

Göbel S*, Pelz L*, Silva C, Brühlmann B, Hill C, Altomonte J, Kamen A, Reichl U, Genzel Y. Production of recombinant vesicular stomatitis virus-based vectors by tangential flow depth filtration. *Appl Microbiol Biotechnol.* **2024**. doi: 10.1007/s00253-024-13078-6.

Contribution: Conceptualization, Formal analysis, Investigation, Methodology, Project Administration, Writing – Original draft, Writing – Review & Editing

Book chapters

Göbel S*, Pelz L, Reichl U, & Genzel Y (2022). Chapter 5b upstream processing for viral vaccines—Process intensification. In L. C. Amine Kamen (Ed.), *Bioprocessing of Viral Vaccines* (Vol. 1, pp. 79–137). Taylor & Francis Group.

Pelz L, **Göbel S**, Reichl U, & Genzel Y (2022). Chapter 5a upstream processing for viral vaccines—General aspects . In L. C. Amine Kamen (Ed.), *Bioprocessing of Viral Vaccines* (Vol. 1, pp. 79–137). Taylor & Francis Group.

** first author*

Supervised theses

Max-Leopold Rössig. Stability analysis of a chimeric yellow fever-Zika vaccine construct. Bachelor Thesis. Faculty of Process- and Systems Engineering, Otto-von-Guericke University. 2022.

Carolin Heinemann. Evaluation of the FiberCell-bioreactor system for cultivation of MDCK-PB2 suspension cells and production of Influenza „defective interfering particles. Bachelor Thesis. Faculty of Process- and Systems Engineering, Otto-von-Guericke University. 2022.

Marie Dorn. Process Intensification of a fusogenic oncolytic virus production in suspension cell culture. Master Thesis. Faculty of Process- and Systems Engineering, Otto-von-Guericke University. 2021.

Talks

Göbel S, Genzel Y, Reichl U. Perfusion with shaken bioreactors. 4th Large Scale Meeting: Orbital Shaken Bioreactors (from 10L up to 2500L). Girona, Spain (2021).

Göbel S, Pelz L, Behrendt I, Prömmel M, Altomonte J, Anderlei T, Bürgin T, Genzel Y, Reichl U. Scale-Down of an Orbital Shaken Bioreactor: High Cell Density Cultivation in Perfusion Mode and Virus production. ECI Single-Use Technologies V: Building the Future, Marseille, France (2022).

Gränicher G, **Göbel S**, Marichal-Gallardo P, Jordan I, Sandig V, Genzel Y, Reichl U. Integrated cell-culture based MVA virus production process with perfusion mode for vaccines or gene therapy. 27th ESACT Meeting, Lisbon, Portugal (2022).

Gränicher G, **Göbel S**, Marichal-Gallardo P, Jordan I, Sandig V, Genzel Y, Reichl U. Integrated cell-culture based MVA virus production process with perfusion mode for vaccines or gene therapy. Value through intensified bioprocessing II. Oxford, United Kingdom (2022).

Göbel S, Dallmeier K, Jordan I, Jong JD, Reichl U, Genzel Y. Intensified production for a yellow fever-ZIKA virus vaccine candidate. Democratization of biotherapies: new manufacturing modalities and intensifications. Oxford, United Kingdom (2023).

Göbel S, Chavez KJ, Altomonte J, Genzel Y, Reichl U. Intensifying OSBs for high titer virus production. 5th Large Scale Meeting: Orbital Shaken Bioreactors (from 10L up to 2500L), Girona, Spain (2023).

Genzel Y, Zinnecker T, **Göbel S**, Reichl U. Intensified cell-based virus production: A process development challenge for multiple cell-virus combinations!, PEACe conference, Sitges, Spain (2023).

Genzel Y, Zinnecker T, **Göbel S**, Reichl U. Next-Generation Virus Production: From Clone, to AMBR, to Perfusion and Very High Virus Yield, ISV conference, Lausanne, Switzerland (2023).

Genzel Y, Zinnecker T, **Göbel S**, Reichl U. Increase in supply through use of new technologies for high yield vaccines, Flanders Vaccine, Brussels, Belgium (2023).

Göbel S, Pineda E, Keebler M, Reichl U, Genzel Y, Lehrer A. Process optimization for recombinant Marburg virus glycoprotein production using *Drosophila* S2 cells. ECI Vaccine Technology IX. Cabo San Lucas, Mexico (2024).

Genzel Y, **Göbel S**, Reichl U. Shaking to very high cell densities- perfusion for virus production. 6th Large Scale Meeting: Orbital Shaken Bioreactors (from 10L up to 2500L), Girona, Spain (2024).

Göbel S, Legmann R, Altomonte J, Kamen A, Reichl U, Genzel Y. Intensified production of a fusogenic oncolytic virus by tangential flow depth filtration. Levitronix Bioprocessing Conference. Cambridge, MA, United States (2024).

Genzel Y, Zinnecker T, **Göbel S**, Reichl U. Next-generation virus production: from clone, to AMBR, to perfusion and very high virus yield, 8th International Symposium on Immunobiologicals, Rio de Janeiro, Brasil (2024).

Posters

Göbel S, Kortum F, Chavez KJ, Dorn M, Altomonte J, Genzel Y, Reichl U. Production of a fusogenic oncolytic rVSV-NDV virus: cell line screening and establishment of a small scale production process. ECI Advancing Manufacture of cell and gene therapy VIII, San Diego, US (2022).

Göbel S, Chavez KJ, Dorn M, Jordan I, Sandig V, Altomonte J, Genzel Y, Reichl U. Production of a fusogenic oncolytic rVSV-NDV virus in perfusion processes. ECI Vaccine Technology VIII. Sitges, Spain (2022).

Göbel S, Chavez KJ, Dorn M, Jordan I, Sandig V, Altomonte J, Genzel Y, Reichl U. Towards the production of a fusogenic oncolytic rVSV-NDV virus in perfusion mode. 27th ESACT Meeting, Lisbon, Portugal (2022).

Göbel S, Kazemi O, Jordan I, Dallmeier K, Reichl U, Genzel Y. Multifactorial high-throughput process screening for a yellow-fever virus vectored Zika vaccine candidate. ECI Vaccine Technology IX. Cabo San Lucas, Mexico (2024).

Göbel S, Pelz L, Silva C, Brühlmann B, Hill C, Altomonte J, Kamen A, Reichl U, Genzel Y. Intensified production of recombinant vesicular stomatitis virus-based vectors by tangential flow depth filtration. 28th ESACT Meeting, Edinburgh, Scotland (2024).

Göbel S, Brühlmann B. Intensified production of recombinant vesicular stomatitis virus-based vectors by tangential flow depth filtration. Cell & Gene Therapy Insights (2024). DOI: 10.18609/cgti.2024.062

Anderlei T, **Göbel S**, Genzel Y, Lehrer A. A New Alternative Single Use Cultivation System Covering the Scale Range from mL to 2500L Working Volume. Latin American Symposium on Cell Culture Technology. Viña del Mar, Chile (2024).

Declaration of Honor

I hereby declare that I produced this thesis without prohibited external assistance and that none other than the listed references and tools have been used.

In the case of co-authorship, especially in the context of a cumulative dissertation, the own contribution is correctly and completely stated. I did not make use of any commercial consultant concerning graduation. A third party did not receive any nonmonetary perquisites neither directly nor indirectly for activities which are connected with the contents of the presented thesis. All sources of information are clearly marked, including my own publications.

In particular I have not consciously:

- Fabricated data or rejected undesired results,
- Misused statistical methods with the aim of drawing other conclusions than those warranted by the available data,
- Plagiarized data or publications,
- Presented the results of other researchers in a distorted way.

I do know that violations of copyright may lead to injunction and damage claims of the author and also to prosecution by the law enforcement authorities.

I hereby agree that the thesis may need to be reviewed with an electronic data processing for plagiarism.

This work has not yet been submitted as a doctoral thesis in the same or a similar form in Germany or in any other country. It has not yet been published as a whole.

Magdeburg, 17.06.2024

Sven Göbel